Protein nanomechanics: from fast-folding proteins to microbial infections

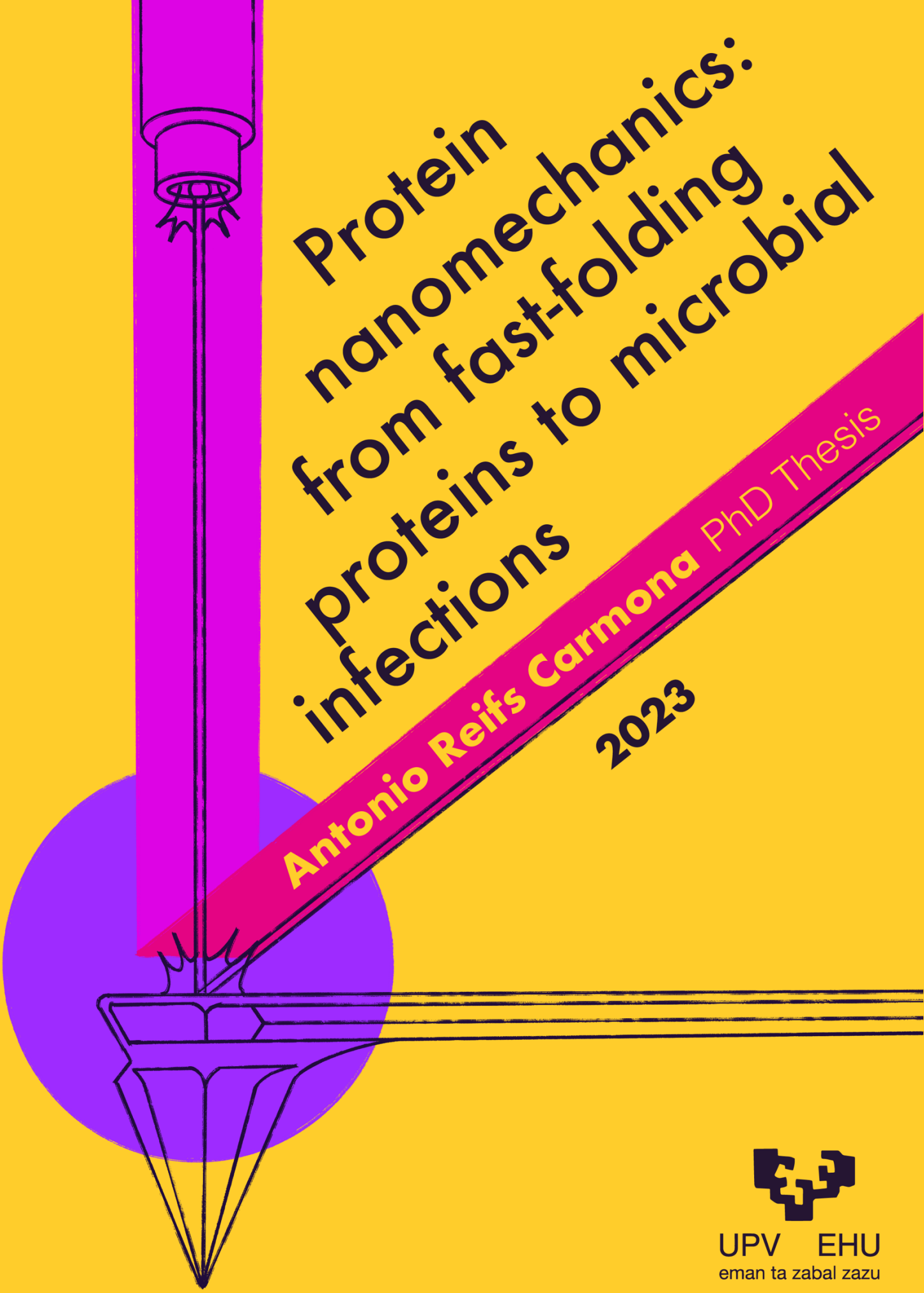

Antonio Reifs Carmona PhD Thesis

2023

UPV EHU
eman ta zabal zazu

(c)2023 ANTONIO REIFS CARMONA

Protein nanomechanics: *from fast-folding proteins to microbial infections*

Antonio Reifs Carmona

PhD Thesis

Thesis supervisors:

Dr. Raúl Pérez Jiménez

Dr. David de Sancho Sánchez

"Nature uses only
the longest threads
to weave her patterns,
so that each small piece
of her fabric
reveals the organization
of the entire tapestry"

Interstellar

Abstract

The end of the 20th century saw the birth of single-molecule techniques allowing for the first time to study one molecule at a time. The beginning of the 21st century has witnessed the implementation and establishment of such techniques, especially to study proteins and DNA with single-molecule resolution. In the past two decades, a myriad of works has been published demonstrating the capabilities of single-molecule techniques to study physical, chemical, and biological phenomena.

There are fundamentally two types of single-molecule techniques, those that use optical phenomena to observe single molecules, such as Fluorescence Resonance Energy Transfer (FRET), and those using physical phenomena to study single molecules, such as Optical and Magnetic Tweezers (OT and MT) and Atomic Force Spectroscopy. The later ones permit the direct manipulation of molecules such as proteins and DNA, which adds a physical component to the study of these biomolecules.

These protein nanomechanics studies are today a fundamental branch in Biophysics. OT and MT use an optical trap and a magnetic field, respectively, to apply mechanical forces to biomolecules, whereas AFS uses a cantilever tip to do so. Although the amount of information reported using the single-molecules technique is enormous, the overwhelming majority of experiments explore proteins and DNA from a physical perspective leaving the biological significance apart.

Another problem of single-molecule techniques is that scientists have mainly focused on fundamental problems with little or no applicability. In this thesis, I have explored the limits of AFS techniques by studying proteins in a broad range of mechanical stability, from a few picoNewtons to the nanoNewtons scale. This has allowed me to understand how proteins that fold without an energy barrier, the so-

called fast-folding proteins, behave under the effect of force, but also to provide answers to a complex biological phenomenon such as the initial steps of microbial infections.

I have used all this knowledge to design the first protocol based on similar high-throughput methods used by the pharmaceutical industry to search for small molecules in chemical libraries that act as mechano-regulators, altering the mechanical stability and folding pattern of proteins; and the first assay that connects in a quantitative manner protein and cell mechanics using a combination of MT and protein biochemistry to generate magnetic-sensing bacteria to study the very initial steps of bacterial infection.

I have studied a total of four proteins that go from the very labile engrailed homeodomain transcription factor to the much more mechanically resistant Caf-1 from *Yersinia pestis. This agent* causes black death and FnBPA from *Staphylococcus aureus,* a bacterium behind many infections such as endocarditis. I have also studied the mechanics of CD4. This cell surface protein plays a role in the immune system but also serves as an anchoring point of the HIV-1 receptor, which has been the target used to find small molecules that change the mechanics of CD4 with potential applications as viral entry inhibitors.

Thus, I consider my work in this thesis a tour de force that covers fundamental aspects of protein nanomechanics and connects them to biological questions such as how microbial infections start or how we can alter the mechanical stability of proteins.

Resumen

A finales del siglo XX, se presenció el nacimiento de las técnicas de Singlemolecule, lo que permitió que por primera vez se estudiaran moléculas de forma individualizada. A continuación, durante el siglo XXI, dichas técnicas se consolidaron y establecieron, especialmente para el estudio de ADN y proteínas. De hecho, en las dos últimas décadas, se han publicado innumerables artículos empleando técnicas de single-molecule, estudiando fenómenos tanto físicos, químicos y biológicos, lo que pone de manifiesto las capacidades de dichas técnicas.

Las técnicas de single-molecule se pueden diferenciar en dos grupos fundamentales: aquellas técnicas que emplean fenómenos ópticos para observar moléculas individuales, aquellas que hacen uso de transferencia de energía de resonancia Föster (FRET) (del inglés Föster resonance energy transfer) para estudiar las moléculas y, finalmente, aquellas que se sirven de fenómenos físicos, como son el caso de las pinzas magnéticas y ópticas (MT, OT) (del inglés magnetic tweezers y optical tweezers), así como la espectroscopia de fuerza atómica (AFS) (del inglés atomic force spectroscopy). Estas últimas permiten la manipulación directa de proteínas y ADN estudiando sus propiedades físicas.

El estudio de la nanomecánica de proteínas es una de las ramas fundamentales de la Biofísica. Técnicas como OT y MT hacen uso de una trampa óptica o un campo magnético respectivamente para aplicar y monitorear fuerzas mecánicas a biomoléculas, como es el caso de las proteínas, mientras que la técnica de AFS emplea una punta de cantiléver ultra afilada, la cual llega al rango de los nm de grosor, para estudiar la nanomecánica de biomoléculas. A pesar que la cantidad de estudios de single-molecule es enorme, la inmensa mayoría de trabajos exploran las propiedades físicas de ADN y proteínas dejando completamente a un lado su

contexto e importancia biológica, centrándose en problemas básicos con poca o ninguna aplicabilidad.

En la presente tesis hemos explorado los límites de la técnica de AFS estudiando proteínas en un amplio rango de estabilidades mecánicas, desde los pocos piconewtons hasta el rango de los nanonewtons. Esto nos ha permitido comprender desde el comportamiento bajo estrés mecánico de proteínas que se pliegan sin barreras energéticas aparentes, como son las fast-folder (del inglés de plegamiento rápido), hasta complejos procesos biológicos, como son las fases iniciales de las infecciones microbianas.

Hemos usado todo lo aprendido durante la realización de la presente tesis para desarrollar el primer protocolo en la búsqueda de pequeñas moléculas con potencial mecano regulador, es decir, que puedan modular la estabilidad mecánica y el proceso de plegamiento-desplegamiento de proteínas ya expresadas y funcionales. Para ello, nos hemos basado en metodologías ya existentes y usadas habitualmente en la industria farmacéutica, como son los protocolos de high throughput methods y molecular docking (del inglés métodos de alto rendimiento y acoplamiento molecular respectivamente).

También hemos desarrollado las bases de una metodología que estudia cuantitativamente y conecta por primera vez la mecánica de proteínas y la adhesión celular. Para ello, hemos empleado una combinación de MT con ingeniería y bioquímica de proteínas para generar bacterias magneto sensibles. Dicha tecnología la hemos usado para estudiar la adhesión bacteriana de la cual dependen las primeras fases de la infección microbiana.

En esta tesis se han estudiado un total de cuatro proteínas, las cuales van desde la lábil engrailed homeodomain (EnHD), un factor de transcripción presente en el organismo *Drosophila melanogaster*, poniendo el foco en su resistencia mecánica y más en especial en su dinámica de plegamiento-desplegamiento. La proteína EnHD

es considerada una ultrafast folder (del inglés de plegado ultrarrápido) esto es debido a que se pliega en el rango de los pocos micro segundos. Esta velocidad de plegamiento es debida a varios motivos, uno a su pequeño tamaño, EnHD está compuesta por 54 aminoácidos, los cuales se pliegan en un núcleo compacto formado por 3 alfa hélices. Otro de los motivos es la prácticamente ausencia de barreras energéticas en su proceso de plegamiento. Por todo ello EnHD es una proteína muy lábil, presentando una estabilidad mecánica de entorno a 8 pN, una característica que comparten el resto de proteínas fast folder (del inglés plegado rápido).

En la presente tesis, también hemos explorado y estudiado proteínas mucho más resistentes mecánicamente, como es el caso de la Caf1 de *Yersinia pestis*. Dicho organismo es el responsable de la peste negra, epidemia que devastó Europa causando entre 80 y 200 millones de muertes entre Europa, Asia y África del norte.

Entre todos los genes de virulencia que convierten a esta bacteria en una tan letal, nos hemos centrado en la Caf1, una proteína con capacidad auto asociativa, debido principalmente a una lámina beta expuesta que puede introducirse en un bolsillo hidrofóbico, presente en otra subunidad de Caf1 próxima. Esta capacidad le permite generar largos polímeros, los cuales presentan una estabilidad mecánica sorprendente y, una vez más, es debido a su estructura tridimensional. La proteína Caf1 posee una estructura tipo inmunoglobulina compuesta principalmente por láminas betas.

La proteína Caf1 presenta una estabilidad mecánica de entorno a 400 pN, lo que le confiere al polímero, el cual conforma una estabilidad mecánica determinante para su función. El polímero compuesto por subunidades de proteínas Caf1 forma una especie de escudo o caparazón, el cual envuelve a toda la bacteria. Este polímero presenta una cualidad crítica, además de su alta estabilidad mecánica y esta es una elevada anti adherencia. Ambas cualidades unidas le confieren a la bacteria una coraza, la cual el sistema inmune innato no es capaz de sobrepasar, impidiendo a

los macrófagos fagocitar a la bacteria *Y. pestis*. Los años han moldeado dicho mecanismo para sobrepasar las fuerzas ejercidas por la interacción con los macrófagos de forma marginal, ya que modificando y disminuyendo la estabilidad mecánica de Caf1 solo en un 20% dicho organismo pierde por completo su capacidad de evasión del sistema inmune, en cuanto a lo que el mecanismo de virulencia de Caf1 se refiere. Este hecho pone de manifiesto el alto interés que puede presentar la nanomecánica de proteínas, como herramienta a la hora de desarrollar fármacos y terapias efectivas contra las infecciones microbianas.

Continuando con los procesos de infección bacterianos en esta tesis, también hemos estudiado el mecanismo de adhesión de la bacteria *Staphylococcus aureus*, la cual se sirve de numerosas proteínas de adhesión para anclarse en diversos tipos de tejidos y matrices extracelulares, pasando incluso por biomateriales y prótesis.

En esta tesis nos hemos centrado en una de estas proteínas de adhesión, la fibronectin binding protein A (FnBPA) (del inglés proteína A de unión a fibronectina). Dicha proteína puede adherirse a la proteína humana fibronectina, concretamente a las subunidades tipo 1 presentes en la fibronectina, formando una unión de láminas beta de forma antiparalela con los Fibronectin binding repeats 1 (FBR1) (del inglés repeticiones tipo 1 de unión a fibronectina) presentes en la proteína FnBPA. Las regiones de FBR presentes en la FnBPA son regiones intrínsecamente desestructuradas de la proteína, las cuales se ven estabilizadas y adoptan una forma estructurada cuando se unen a la fibronectina humana.

Dicha adhesión la hemos estudiado desde el punto de vista de molécula única pero también de célula única. Hemos comenzado el desarrollo de una tecnología, la cual permitirá medir la adhesión de una bacteria a su tejido diana de forma cuantitativa, que conseguirá avances importantes en la industria biomédica, ya que permitirá la búsqueda de fármacos que modulen o inhabiliten la adhesión bacteria, inhabilitando por tanto el proceso de infección.

Finalmente, también hemos estudiado la proteína humana CD4. Esta proteína de superficie celular tiene un papel crucial en el sistema inmune, interaccionando con el complejo mayor de histocompatibilidad II (CMHII), pero, además sirve como punto de anclaje para el virus de la inmunodeficiencia humana tipo 1 (VIH-1). En el proceso de anclaje y de infección, el virus debe de desplegar parcialmente la proteína CD4 para poder realizar todos los anclajes necesarios con el resto de proteínas presentes en la superficie celular que le permiten la invaginación y entrada a la célula.

Por lo tanto, hemos estudiado la estabilidad mecánica de dicha proteína y hemos desarrollado una metodología de búsqueda de compuestos o moléculas pequeñas que nos ha permitido regular mecánicamente la estabilidad de la proteína CD4 aumentándola y así potencialmente inhibir la entrada del virus.

Por todo lo expuesto, consideramos el trabajo realizado en la presente tesis un “tour de forcé”, el cual cubre todos los aspectos básicos de la nanomecánica de proteínas y que además los conecta con preguntas de relevancia biológica como son los inicios de las infecciones microbianas o como alterar la estabilidad mecánica de proteínas ya expresadas y funcionales.

Table of contents

Chapter I:
Introduction

I.I. Building blocks of life: *from amino acids to protein polymers*

Introduction to proteins

Proteins are one of the most abundant biological macromolecules in every organism, from the simplest virus to the most complex multicellular creature. (Dill and MacCallum 2012) Proteins are a very important part of the cell's dry mass, and this is because proteins are molecular instruments. Almost every function in living cells is mediated or performed by proteins, acting as enzymes, antibodies, transporters, hormones, feathers, muscle fibers, eye lenses, antibiotics, mushroom poisons, and a myriad of other biological functions. (Alberts, A, and Lewis J 2002)

The uncountable number of functions that proteins show is due to their structure complexity and versatility. Protein versatility is a result of evolution. As in many other biomolecules, proteins have been shaped by evolutionary processes across billions of years, modeling this wide range of protein roles from the smallest peptide to the largest polymer. (Dill and MacCallum 2012)

How can proteins, being the same type of biomolecule, perform an endless number of different functions? This is a result of their structural nature. Proteins are composed of relatively simple monomeric subunits called amino acids. Amino acids are like the alphabet in which the language of proteins is written, allowing to write small words like peptides or enormous paragraphs like the most complex polymers. Twenty different amino acids compose proteins, also called α-amino acids, because of their structure.

Every amino acid comprises a central α carbon bonded to carboxyl and amino groups. This feature is common for every amino acid. They differ in their side chain or R groups which is characteristic of each amino acid and provides distinctive qualities. (see Fig. I.1.) Due to their nature, the amino acids can be grouped into nonpolar, polar, aromatic, positively charged, and negatively charged. (Anfinsen 1973)

Nonpolar amino acids like glycine, alanine, or proline are hydrophobic and tend to bury together in the core of the protein, stabilizing it. In this group can be found

glycine, the simplest amino acid. The glycine side chain is a hydrogen atom. For this reason, glycine is the only amino acid, not enantiomer. (Nelson and Cox 2017) Polar amino acids like serine, threonine, or cysteine have greater hydrophilicity and better solubility in water because they contain functional groups that can form hydrogen bonds with water. In this group can be found cysteine, which is readily oxidized to form a covalent bond with another cysteine performing a disulfide bond and playing a crucial role in the structure of many proteins. (Nelson and Cox 2017)

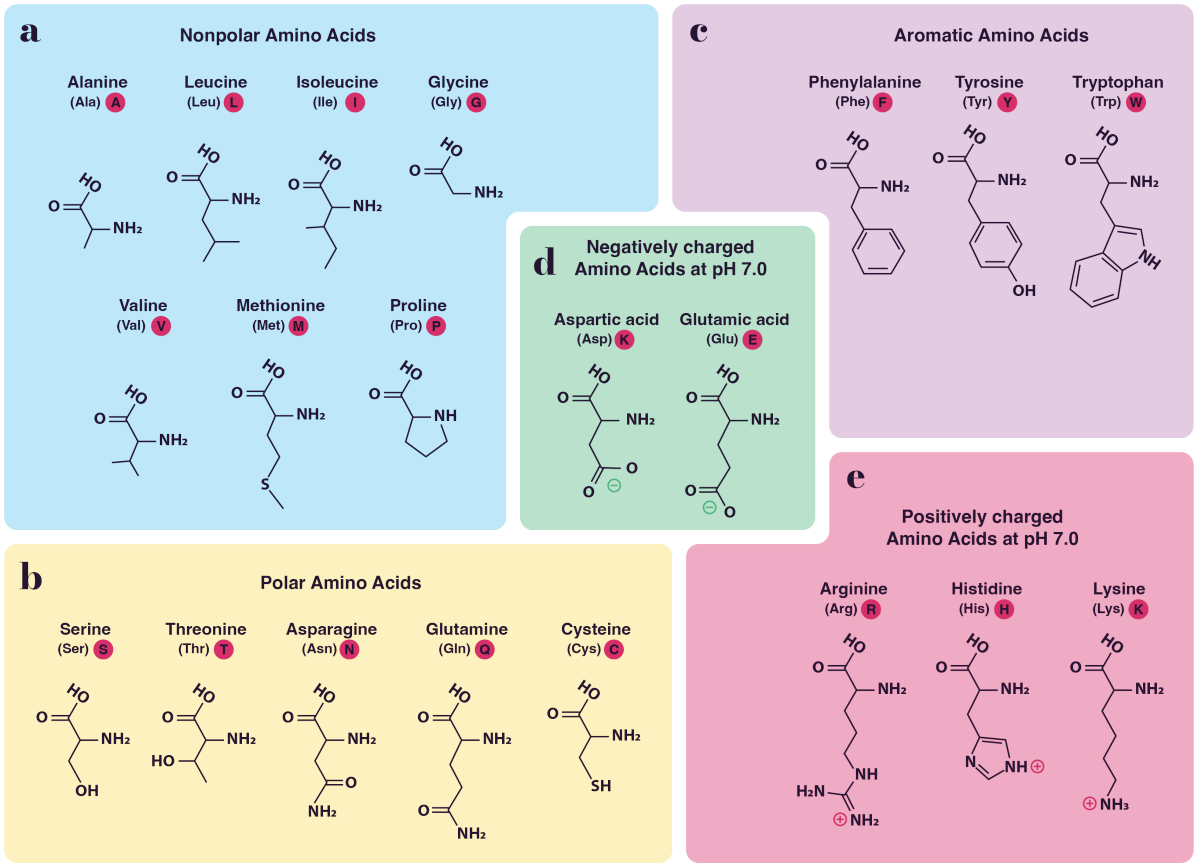

Fig. I.1. The 20 common amino acids of proteins. a. nonpolar amino acids b. polar amino acids c. aromatic amino acids d. negatively charged amino acids at pH 7.0 e. positively charged amino acids at pH 7.0.

Aromatic amino acids like phenylalanine, tyrosine, or tryptophan are relatively nonpolar or hydrophobic, and all of them can participate in hydrophobic interactions.

Tyrosine and tryptophan are significantly more polar than phenylalanine. The three of them can absorb ultraviolet light at 280 nm. (Nelson and Cox 2017) Positively charged amino acids like lysine arginine or histidine and negatively charged ones are the most hydrophilic amino acids. Aspartate and glutamate are the only two amino acids to have negatively charged groups. (Krupyanko 2000)

The 20 different amino acids can form polymers of various sizes, from two or three to thousands of linked amino acids, through a special covalent bond called peptide bond. This bond is formed by dehydration from the carboxyl group (COOH) of the first amino acid and the amino group (NH2) of the following amino acid. Within the polypeptide chain, each amino acid is also called “residue”, Indicating the loss of water during peptide bond formation. The structure formed by all the consecutive peptide bonds in a polypeptide chain is called the backbone or main chain and always begins with an amino (N) terminus and ends with a carboxyl (C) terminus. (see Fig. I.2.) (Nelson and Cox 2017)

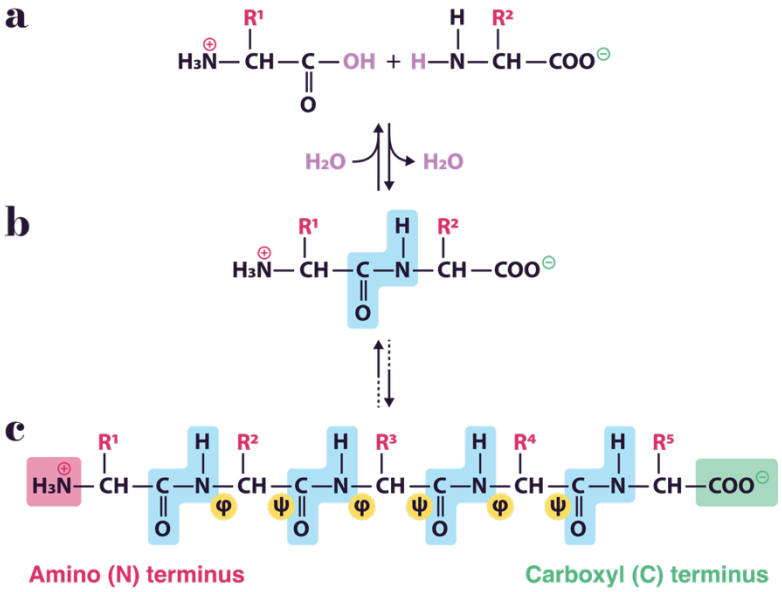

Fig. I.2. Peptide bond and backbone polypeptide. a. Two different amino acids with R1 and R2 sidechains, respectively. b. A peptide bond is formed (shaded in blue) when the amino group of one amino acid (with R2 group) acts as a nucleophile to displace the hydroxyl group of another amino acid (with R1 group). c. Following multiple repetitions of the same reaction, a pentapeptide is formed. The amino terminus is shaded in red), and the C-terminus is shaded in green. Phi (φ), and Psi (ψ) torsion angles are shaded in yellow.

Protein structure

The sequence of amino acids forms the primary structure and should always be read from the (N) terminus to the (C) terminus. Every peptide bond present in the polypeptide has two different dihedral angles, also known as backbone torsion angles, which apport flexibility to the chain. These angles are formed between (N-Cα) and (Cα-C), called phi (φ) and psi (ψ), respectively (see Fig. I.2.) These torsion angles are crucial in the final three-dimensional structure of a protein, because consecutive residues typically adopt similar dihedral angle values, resulting in the formation of α helices and β strands. The assembly of two or more β strands is called β sheet. Those motifs are called secondary structures. (Nelson and Cox 2017) (see Fig. I.3.)

β sheets can be either parallel or antiparallel. In addition to the torsion angle, the secondary structure is stabilized by inter and intra-peptide weak interactions, which involve hydrogen bonds, electrostatics, van der Waals, and hydrophobic interactions. Each motif shows distinctive qualities. For example, α helices present higher flexibility, while β sheets offer higher rigidity and more considerable mechanical stability. Finally, a third structural motif called loop regions is commonly less structured and apport high flexibility. Loop regions usually connect several α helices or two consecutively β strands. (Nelson and Cox 2017)

The different secondary structure motifs interacted spatially to form the so-called tertiary structure of the protein, the interaction that leads to this tertiary structure is composed mainly of hydrophobic interactions, salt bridges, and disulfide bonds. (see Fig. I.3.)

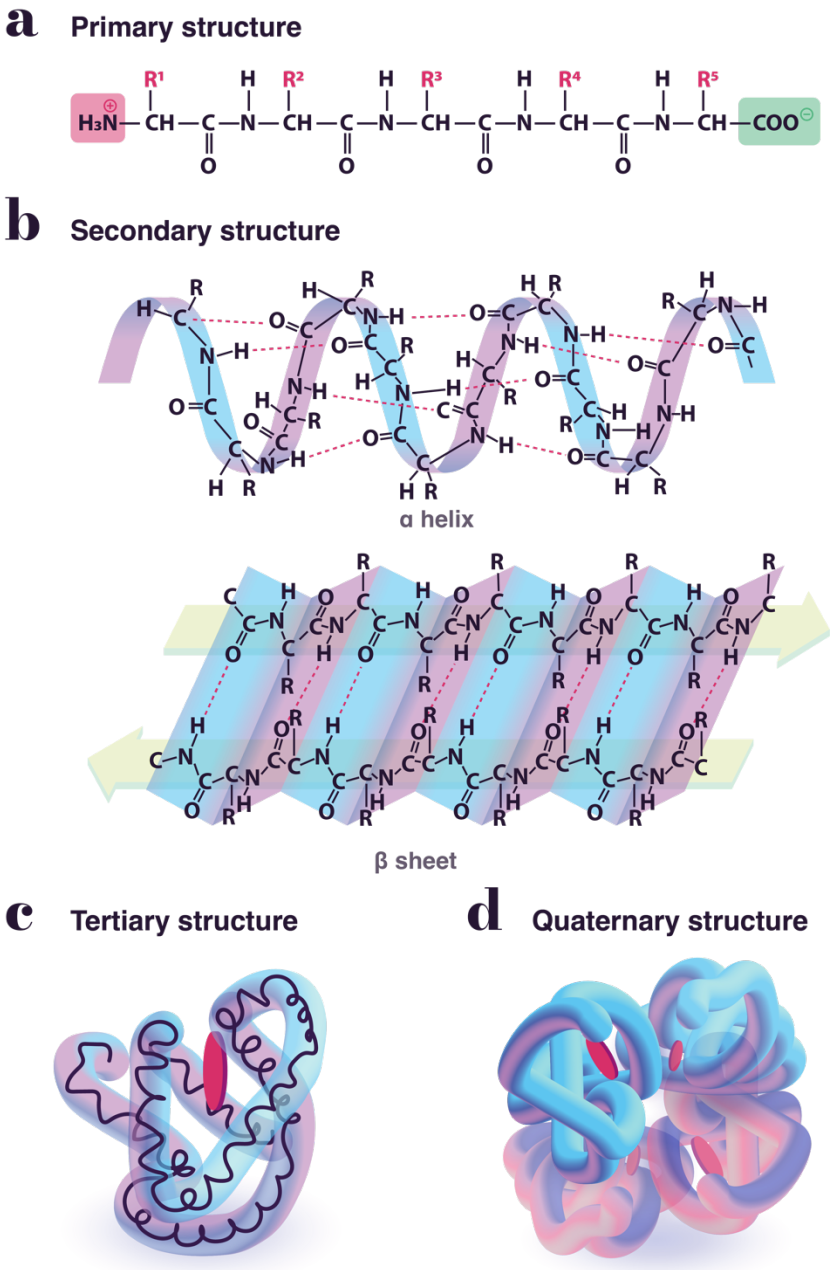

Fig. I.3. Protein structure, from primary structure to quaternary. a. Primary structure, sequence of amino acids. b. secondary structure, alpha helix, and antiparallel beta-sheet (red dash line) represent hydrogen bonds between amino acids at different locations in the polypeptide chain. c. tertiary structure, formed mainly hydrophobic interactions, salt bridges, and disulfide bonds from different secondary structure motifs. d. quaternary structure, an assembly of two or more polypeptides leads by weak interactions.

Additionally, when two or more polypeptides with their tertiary structures assemble into a new and more complex system. This new level of architecture is called a quaternary structure (see Fig. I.3.) Finally, the tridimensional structure and properties of a specific protein are determined by the exact location of each amino acid in the polypeptide sequence. This defined structure, native structure, confers to this protein its functionality and qualities. (Nelson and Cox 2017)

Historical introduction to protein folding

Protein folding is the process whereby a polypeptide sequence with a given primary structure adopts a well-defined 3-dimensional native tertiary. Scientists began to recognize the significance of proteins in biological systems in the early 20th century, but the structure of these molecules remained an enigma. In the 1920s and 1930s, there were great developments in X-ray crystallography and other analytical techniques, which in the following decades enabled scientists to determine the structures of basic proteins, such as myoglobin and hemoglobin, for whose structures John Kendrew and Max Perutz were awarded the Nobel Prize in Chemistry. Not until the 1950s and 1960s did scientists begin to comprehend the complexities of protein folding. (Dill and MacCallum 2012; Kendrew JC. 1961)

1959's Anfinsen experiment was a significant early discovery in the field of protein folding. Christian Anfinsen demonstrated that ribonuclease could be denatured by disrupting its disulfide bonds with a reducing agent and refolded by removing the reducing agent. This demonstrated that a protein's amino acid sequence contains all of the information required for it to fold into its native configuration. (Anfinsen 1973)

In the 1960s and 1970s, scientists developed new methods for investigating protein folding, such as circular dichroism and nuclear magnetic resonance (NMR) spectroscopy. These techniques enabled scientists to observe the folding process in real time, yielding new insights into the folding mechanisms and kinetics of proteins. (Van Mierlo and Steensma 2000)

In the 1980s and 1990s, advancements in computer modeling and simulation techniques allowed scientists to investigate the energy landscape of protein folding in greater detail. These studies demonstrated that the folding of proteins is a complex process involving the exploration of a vast energy landscape with numerous potential pathways and intermediates. (Onuchic, Luthey-Schulten, and Peter G Wolynes 1997; Wooley and Ye 2007)

The study of protein folding continues to be an important area of biochemistry, molecular biology, and biophysics research today. New techniques and technologies, such as cryo-electron microscopy and deep learning algorithms, have opened up new avenues for understanding the complexities of protein folding and structure prediction. (Noé, De Fabritiis, and Clementi 2020; Jumper et al. 2021)

In addition, in recent years, the field of protein folding and structure prediction has witnessed a revolutionary breakthrough with the introduction of the AlphaFold 2 program. AlphaFold 2 is an artificial intelligence system developed by DeepMind that has demonstrated remarkable accuracy in predicting protein structures from their amino acid sequences. This discovery has revolutionized our understanding of protein folding (Jumper et al. 2021) AlphaFold 2 utilizes deep learning algorithms and enormous quantities of protein sequence and structure data to predict the three-dimensional structures of proteins with outstanding precision. The ability to precisely predict protein structures has profound implications for numerous fields of biological research, including drug discovery, enzyme design, and the understanding of the mechanisms of disease. (Jumper et al. 2021)

Energy landscape and protein folding

A complete description of the protein folding energy landscape involves determining the energies of all possible configurations or conformations a protein can adopt. The energy landscape can be visualized as a three-dimensional funnel-shaped surface, where the vertical dimension represents the energy and the width is the entropy. At the bottom of the funnel, we find the native state of the protein, which is the lowest

in energy and also in entropy. As we go up in energy in the landscape, we find partially folded and ultimately at the very top the unfolded state, which has the greatest degeneracy. The landscape is rugged, with multiple hills and valleys. (Bartlett, structural & molecular biology, and undefined 2009 n.d.; Onuchic, Luthey-Schulten, and Wolynes 1997) (see Fig. I.4.)

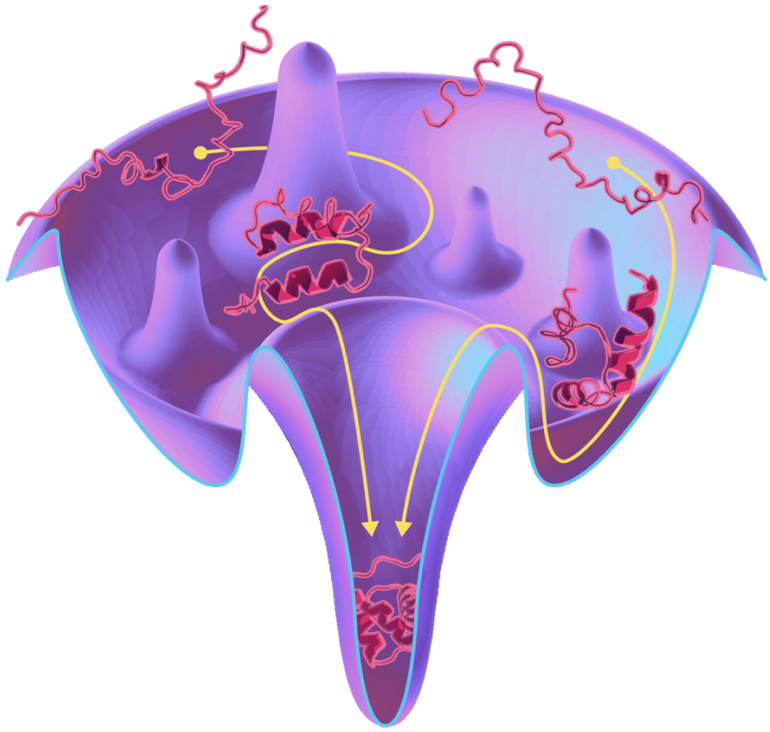

Fig. I.4. Funnel-shaped energy landscape. The energy landscape is the set of all possible configurations or conformations a protein can adopt.

During protein folding, the polypeptide chain must navigate this energy landscape in order to locate its most stable or least energetic conformation. Various factors, such as the attractive and repulsive forces between amino acid residues, the solvent environment, and the temperature and pressure of the system, shape the energy landscape. As the polypeptide chain traverses the environment, it may encounter a number of energy barriers or traps that impede or prevent folding. (Bartlett et al. n.d.) Energy landscape theory proposes that there exist multiple routes or pathways down the funnel (Onuchic, Luthey-Schulten, and Peter G. Wolynes 1997)

In order to overcome these obstacles, the protein may undergo a conformational search, in which it tries out various conformations until it discovers a stable configuration. Chaperone proteins aid in guiding the folding process and preventing the formation of nonfunctional or misfolded structures. (Stefan Walter and Johannes Buchner 2002; Schonfelder et al. 2018a)

Once a protein has attained its conformation with the lowest energy, it is said to be in its native state. This structure is typically compact and ordered, with hydrophobic amino acids buried in the protein core and hydrophilic amino acids on the surface. Some proteins require additional factors, such as molecular chaperones or post-translational modifications, to achieve their native state. (Brockwell and Radford 2007; Bryngelson et al. 1995; Ferreiro et al. 2007)

In conclusion, protein folding is a complex process involving the navigation of a vast energy landscape in search of the most stable conformation. To unravel the mysteries of protein folding and its role in biological function, it is essential to comprehend the energy landscape and the factors that shape it. (Bartlett et al. n.d.)

I.II. Unfolding the mystery: *mechanics of protein denaturation from native state to primary structure*

Mechanical forces in biology

Mechanical forces play an essential role in protein biology by regulating protein folding, stability, function, and interaction with other biomolecules. In vivo, proteins are subjected to diverse mechanical stresses, including stretching, compression, shear, and bending, which can modify their conformation, activity, and signaling. (Li and Xu 2007; Traub and Berk 1998; Zou et al. 1998; Yamazaki, Komuro, and Yazaki 1996; Marszalek et al. 1999; Schonfelder et al. 2018b) Tension force in the unfolding and refolding of proteins is one of the best-known examples of mechanical forces in protein biology. The non-covalent interactions that maintain the folded state of a protein can be disrupted by mechanical force, leading to its unfolding. (Marszalek et al. 1999; Strick et al. 2003; Erickson 1994) (see Fig. I.5.) In contrast, the release of mechanical force can induce the refolding of a partially unfolded protein, which can have significant effects on the function and stability of the protein. (Haldar et al. 2017; Shtilerman, Lorimer, and Englander 1999; Schönfelder, Alonso-Caballero, et al. 2018) The paradigmatic case of unfolding and refolding transitions in biology is the massive muscle protein titin, which is essential for muscle contraction and relaxation. (Marszalek et al. 1999; Schönfelder, Alonso-Caballero, et al. 2018)

The attachment process of viruses and bacteria is another example of the significance of mechanical forces in protein biology; the application of mechanical forces on proteins is essential for successful infection. The attachment process involves a series of interactions that can be disrupted by mechanical forces between the pathogen's proteins and the host cell receptors. (Alonso-Caballero, Echelman, et al. 2021; Alonso-Caballero et al. 2018; Peters et al. 2022; Perez-Jimenez et al. 2014). The attachment of viruses entails the binding of viral proteins to specific receptors on the surface of the host cell. Mechanical forces enable viral proteins to achieve the correct conformation for binding to the host cell receptor, thereby facilitating the binding process. Once the binding has occurred, additional mechanical forces are applied to permit the virus to penetrate the host cell via fusion or endocytosis. (Perez-Jimenez et al. 2014; Hu et al. 2021; Gefen 2010)

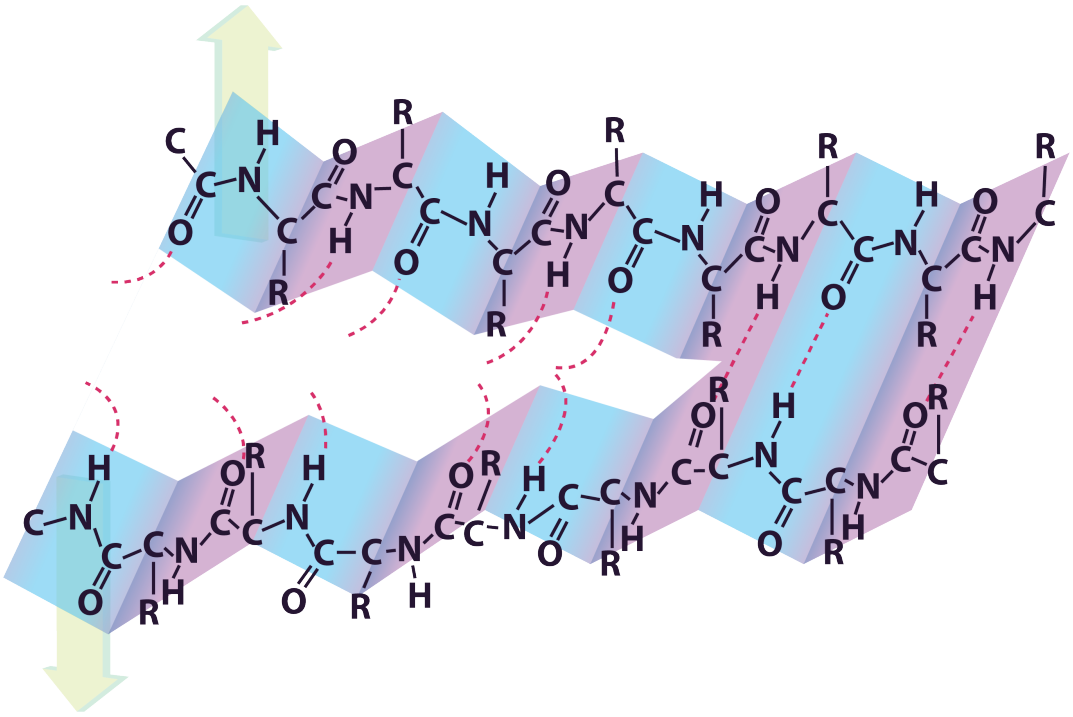

Fig. I.5. Mechanical force breaks weak chemical interactions. Representation of the disruption of hydrogen bonds (red dash line) in a beta sheet when it is subjected to a stretching force. The green arrows mark the direction of the force vector.

The bacterial attachment also requires mechanical forces to be applied to bacterial proteins. Mechanical forces are essential for stabilizing the interaction between bacterial proteins and host cell receptors. Once the stable binding has occurred, the bacteria can invade the host cell and manipulate its replication, and spread machinery. (Herman-Bausier et al. 2018; Geoghegan and Dufrêne 2018; Huang et al. 2022)

To develop effective treatments for viral and bacterial infections, one promising possibility is to interfere with the mechanics of the attachment process. Targeting the proteins involved in the attachment process with medications or other interventions that inhibit protein binding or modify the mechanical forces associated with this binding may be useful to prevent pathogen attachment and entry into the host cell. (Perez-Jimenez et al. 2014)

Mechanical unfolding of proteins

Mechanical unfolding is the process by which a protein is stretched by an external force, such as that applied by an atomic force microscope (AFM) or a laser trap, among others. (Hoffmann and Dougan 2012; Neuman and Nagy 2008) Mechanical unfolding offers a unique perspective on the structure and stability of proteins, as it permits researchers to investigate the strength of individual chemical bonds and the protein's response to external forces. (Neuman and Nagy 2008)

The mechanical unfolding of proteins is a complex process that depends on many variables, including the applied force, the unfolding speed, and the stability of the protein structure. When a protein is pulled apart, the applied forces cause it to elongate and deform, thereby breaking weak chemical bonds such as hydrogen bonds and van der Waals forces. As the force increases, stronger bonds, such as covalent bonds, may also break, resulting in an irreversible unfolding. (Schönfelder, Alonso-Caballero, et al. 2018)

Important insights into the structure and function of proteins, as well as their response to mechanical stress, have been discovered from the mechanical unfolding of proteins. Experiments involving mechanical unfolding have demonstrated, for instance, that certain proteins, such as titin, are extraordinarily resilient and can withstand very large forces without unfolding. (Oberhauser et al. 2001; Rief et al. 1997) Other proteins, such as dystrophin, are essential for maintaining the structural integrity of tissues and their mechanical disruption can lead to disease.(Singh et al. 2014). Studying unfolding mechanics may cast light on an extensive variety of biological processes, from muscle contraction to cell adhesion, and may eventually lead to the development of new therapeutic strategies for treating protein-related diseases. (Schönfelder, Alonso-Caballero, et al. 2018; Neuman and Nagy 2008)

Single Molecule Force Spectroscopy Experiments

Single-molecule force spectroscopy (SMFS) is a technique used to investigate the mechanical properties of single molecules, such as proteins and nucleic acids. (Neuman and Nagy 2008; Schönfelder, De Sancho, and Perez-Jimenez 2016)
Experiments employing SMFS involve imparting mechanical force to a single molecule while monitoring its response. There are a variety of SMFS techniques, including, optical tweezers (OT) (Moffitt et al. 2008), magnetic tweezers (MT) (Alonso-Caballero, Tapia-Rojo, et al. 2021), and atomic force spectroscopy (AFM) (Garcia-Manyes et al. 2007).

▪ Optical and magnetic tweezers

Optical Tweezers (OT) and Magnetic Tweezers (MT) are two single-molecule techniques used for studying molecular-level biological processes.

Optical Tweezers work according to the principle of radiation pressure, in which electromagnetic radiation exerts pressure on any surface. Ashkin built the first optical trap in 1986 using an Argon LASER and a high numerical aperture lens. (Ashkin et al. 2016; Chu et al. 1986) In a fluid chamber, the trap exerts forces of the order of picoNewtons on dielectric nanoparticles. In a typical experimental configuration, one face of the target molecule is attached to a micron-sized dielectric bead particle, which is then captured in an optical trap. The opposite side of the molecule is immobilized on a fixed surface or another bead particle held by a micropipette or another optical trap. This apparatus permits a variety of methods for applying a mechanical force to the molecule of interest. With sub-nanometer precision, optical tweezers can apply mechanical forces in the low pN range (0.1-100pN). The current time resolution is in the sub-millisecond range.(Moffitt et al. 2008; Svoboda and Block 1994; Lang et al. 2002)

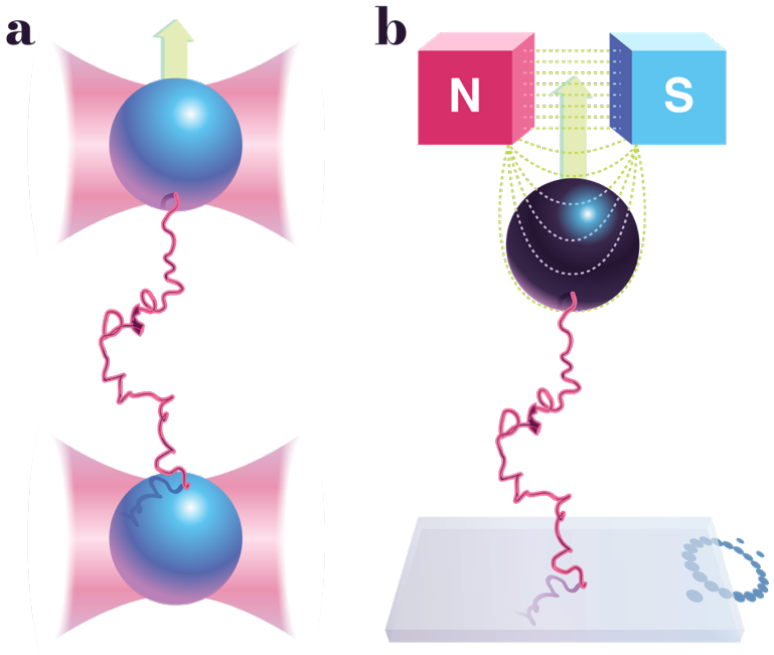

Fig. I.6. Optical tweezer and magnetic tweezer. a. Schematic illustration of optical, at both extremities, the studied protein is attached to two polystyrene beads captured in a laser beam. The movement of the top trap stretches the protein. b. magnetic tweezers, the studied protein is attached to a magnetic bead and anchored to a glass slide. The particle is attracted to the external magnets that generate the strongest magnetic field gradient. Reducing the height of the magnets increases the tension applied force.

Magnetic Tweezers operate on the premise that a magnetic particle with a magnetic dipole moment experiences a force when positioned inside the magnetic field of a pair of permanent or electromagnets. In a typical setup, the molecule of interest is bound specifically to the magnetic bead and the glass surface. Magnetic tweezers can impart mechanical forces including torque in the range of femtonewtons (0.0001-100pN). Typically, the obtained length and time resolution is on the order of several tens of nanometers (displacement) and milliseconds (time). (Alonso-Caballero, Tapia-Rojo, et al. 2021; Gosse and Croquette 2002) (see Fig. I.6.)

Atomic Force spectroscopy

A variation of the atomic force microscope (AFM) is used to manipulate and stretch single molecules such as DNA and proteins that are adsorbed to a surface. The AFM technique employs an ultrasharp tip situated on a cantilever (tip radius: tens of nanometers; material: silicon nitride). The surface on which the protein sample is adsorbed is moved in the x, y, and z directions by a piezoelectric actuator (PZA) in the sub-nanometer range. (Rief et al. 1997)

For single-molecule force microscopy measurements, the PZA is moved towards the cantilever in the z-direction. After contacting the surface and retracting the cantilever, a mechanical force is applied to the protein, if it was indeed adsorbed to the tip. This force resistance will cause the cantilever to bend, and the laser beam reflected on the cantilever's back will vary based on the tip's bending. When a protein is unfolded, broken, or detached from the tip, the cantilever will release its bending. However, the cantilever tip may also produce non-specific bending signals when in contact with the surface. For this reason, a polyprotein construct is typically utilized, which must be composed of several 6-12 domains of the studied protein, or the presence of 4-6 or more monomers of a model domain as a fingerprint. Applying a mechanical force to the polyprotein construct will result in a distinctive repetitive pattern, which helps in the identification of the investigated protein's signal. (Hinterdorfer and Dufrêne 2006)

AFM measurements usually depend on the non-specific binding of the protein sample to the substrate. One strategy is to add one or two isolated cysteine residues to the polyprotein construct. Cysteine residues create a gold-sulfur bond with the substrate, gold is a frequently employed substrate. On the opposite side, the polyprotein construct binds non-specifically to the cantilever via a poorly understood mechanism.

It has been proposed that the non-specific binding to the cantilever is due to the high amount of pressure exerted by the sharp tip on a nanometer-sized region. All the components and operation modes of the AFS are described in greater detail in Materials and methods section of this thesis. (Popa et al. 2013) (see Fig. I.7.)

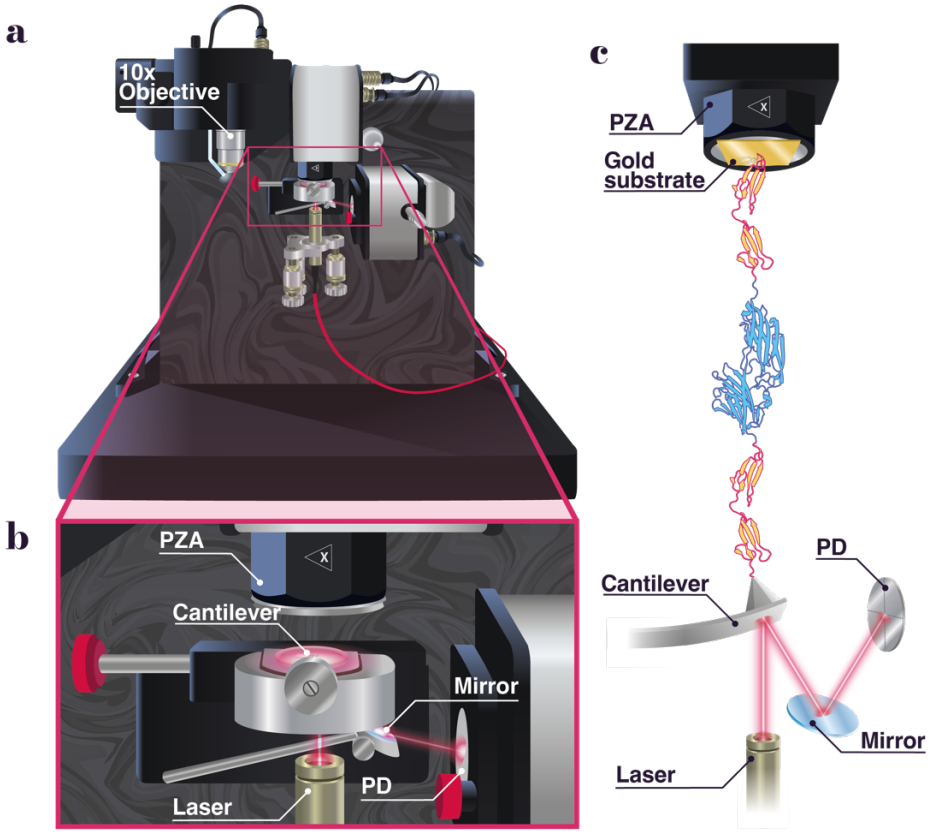

Fig. I.7. AFM set-up and key parts. a. Main AFM. b. Zoom showing the key parts of AFM set-up, these parts are PZA, cantilever, laser, mirror, and PD. c. Scheme of the AFM, laser beam is reflexed in the back part of cantilever and reach the PD through the mirror, in the tip of the cantilever is bonding our protein construct and being stretched from the gold substrate which is placed in the PZA.

Several scientists, including Carlos Bustamante, Julio Fernandez, Hermann Gaub, and Daniel Müller, among many others, have made significant contributions to the development of Atomic Force Microscopy (AFM) as a technique for investigating protein mechanics. AFM was first introduced by Binnig, Quate, and Gerber (Binnig

et al. n.d.; Binnig et al. 1987) in the 1980s. Carlos Bustamante extended the knowledge of how mechanical forces affect different biomolecules using AFM and combined it with optical trapping. Measuring the forces involved in protein folding and unfolding, thereby shedding light on the mechanics of proteins. (Carlos Bustamante et al. 2000) Julio Fernandez combined AFM with other biophysical techniques to simultaneously measure protein mechanics and structural changes, thereby expanding our knowledge of protein function. (Carrion-Vazquez, Andres F Oberhauser, et al. 2000) Hermann Gaub (Michel Grandbois et al. 1999) and Daniel Müller (Müller and Dufrêne 2008) made significant contributions to single-molecule manipulation techniques based on AFM. These scientists have advanced the field of AFM-based protein mechanics, advancing our understanding of the mechanical behavior of biological molecules and determining the future of research in this field.

The effect of force on the free energy landscape

Understanding the forces and interactions that maintain proteins in their folded state is the first step in studying protein mechanical unfolding using smFS techniques.

Protein folding is driven by enthalpic and entropic contributions, resulting in a specific structure held together by many weak enthalpic interactions. Short-range interactions are responsible for resistance when a protein is mechanically stretched until at sufficient force the protein yields and transitions from the native to an extended state. In the simplest case, a two-state model, the energy landscape of a protein consists of two energy wells separated by a barrier, with the folded state at an energy minimum and the unfolded state at a shallower, less favorable well. The height of the energy barrier in the unfolding direction is due to enthalpic interactions that maintain the protein folded, and when force is applied, both the barrier height and the energy of the unfolded state are tilted and reduced. (Bustamante et al. 2004; Tinoco and Bustamante 2002) Bell's model has traditionally been used to examine the effect of mechanical forces on protein kinetics. (Bell 1978) The bond rupture rate is exponentially dependent on the applied force. Theoretical advances in smFS techniques have made it possible the correction of the experimental setup's effect

on unfolding/folding rates and the accurate acquisition of valuable data. (Bustamante et al. 2004) (see Fig. I.8.)

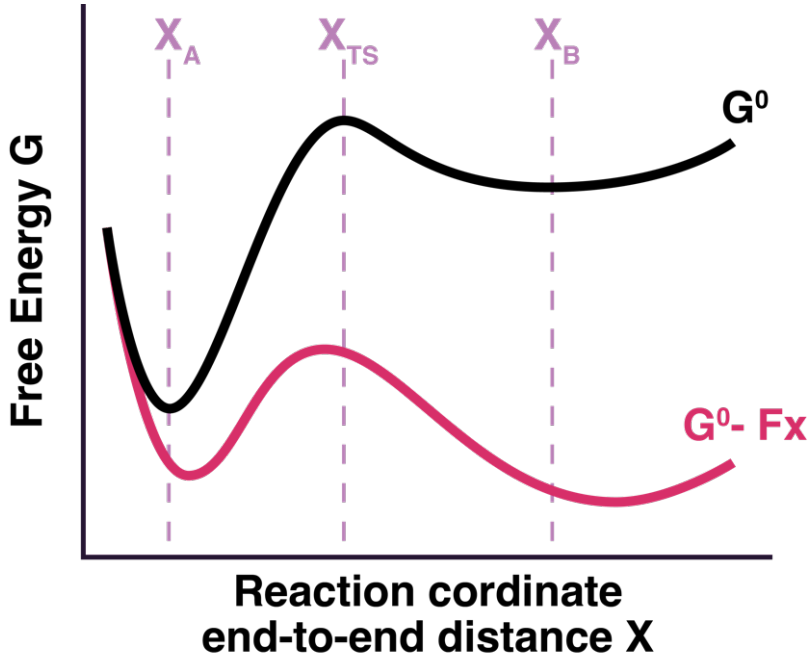

Fig. I.8. Folding free energy landscape of a two-state protein under mechanical stress. Sketch depicting how a mechanical force (red) in the direction of x tilts the surface of free energy G (black). The position of the states folded X_A,unfolded X_B, and transition state X_{TS}, will be affected by the mechanical force.

I.III. From chaos to order: *understanding mechanisms of protein folding*

Protein mechanics spectrum

Understanding the mechanical properties of proteins, such as their mechanical stability and force-dependent (un)folding kinetics, is crucial for their characterization. Extensive research has been conducted over the years to unravel the protein mechanics spectrum, which encompasses a wide range of protein behaviors, including labile proteins that undergo conformational changes in response to mechanical perturbation, as is the case of ultra fast folders, that fold or unfold instantly in response to external forces, and resistant proteins that exhibit two-state or multi-state behavior in mechanical unfolding. (West et al. 2006; Rief et al. 1999; Paci and Karplus 2000; Carrion-Vazquez, Andres F. Oberhauser, et al. 2000)

Labile proteins are susceptible to mechanical perturbations, such as stretching and compression forces. In response to mechanical stress, these proteins undergo structural modifications, which can result in altered protein function, for example, the exposure of buried binding sites. (Del Rio et al. 2009) Some labile proteins, such as intrinsically disordered proteins, suffer disorder-to-order transitions upon mechanical stretching, enabling them to adopt a particular structure and perform their function. (Brucale, Schuler, and Samorì 2014; Bondos, Dunker, and Uversky 2022) Other labile proteins, such as mechanosensitive ion channels, undergo conformational changes in response to mechanical deformation (Wang and Ha 2013), leading to alterations in ion permeability and cellular signaling. Understanding the mechanical properties of labile proteins is essential for elucidating their functional mechanisms and how they respond to mechanical stresses in vivo.

A fascinating class of labile proteins is ultra fast folders, which fold or unfold immediately in response to mechanical forces. The transition between the folded and unfolded states of these proteins can occur within microseconds. Low activation energy barriers and efficient energy dissipation pathways enable ultra fast folders to rapidly adapt their conformational states in response to mechanical perturbations. (Muñoz and Cerminara 2016; Ghosh, Ozkan, and Dill 2007) As molecular motors and molecular switches, these proteins play crucial roles in cellular processes requiring rapid conformational changes. Investigating the mechanical properties and folding kinetics of ultra fast folders provides important insights into the physical

mechanisms underlying the rapid folding and unfolding of proteins. (Muñoz and Cerminara 2016) (see Fig. I.9a.)

On the opposite extreme of the spectrum are proteins that exhibit a two-state behavior during unfolding. These proteins are robust and resistant to mechanical deformation, and they retain their folded conformation even when subjected to substantial mechanical stress. (Schönfelder, Perez-Jimenez, and Muñoz 2016) Typically, resistant proteins have a high activation energy barrier for unfolding and a cooperative and reversible unfolding transition. Enzymes (Sacquin-Mora, Laforet, and Lavery 2007) and structural proteins (Manteca et al. 2017; Alonso-Caballero et al. 2018) are examples of resistant proteins with well-defined tertiary structures and globular shapes. Understanding the mechanical properties of resistant proteins is essential for elucidating the physical principles that govern protein stability and resistance to mechanical forces. (see Fig. I.9b.)

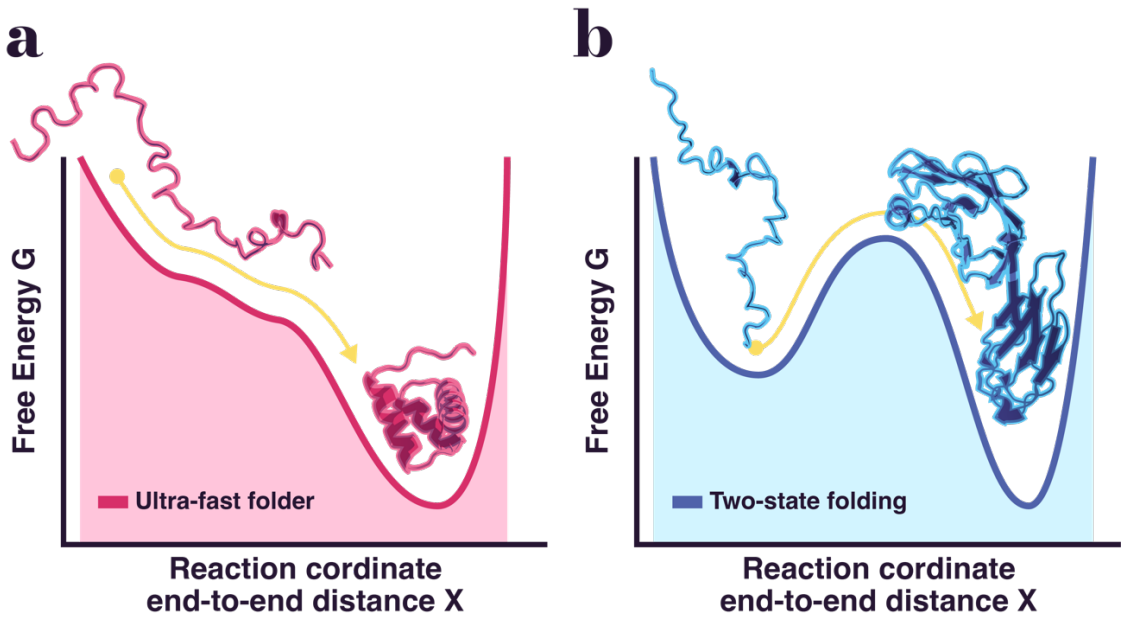

Fig. I.9. Folding free energy landscape of protein spectrum from ultra-fast folder to two-state protein folding. Free energy surface for a. an ultra-fast folder and b. a two-state protein folding reaction. The x-axis is the reaction coordinate describing the progress of the folding reaction and the y-axis shows the free energy G_0.

Two state protein unfolding

Proteins are dynamic entities that experience conformational changes in response to environmental stimuli such as temperature, pH, and chemical denaturants. The behavior of some proteins to undergo a two-state unfolding transition, in which they transition directly from a folded to an unfolded state without detectable intermediates, is an intriguing property. This peculiar behavior has generated considerable interest in the field of protein mechanics, as it challenges our understanding of the mechanisms underlying protein folding and unfolding. (Schönfelder, Perez-Jimenez, et al. 2016)

Two-state protein unfolding is characterized by a rapid and cooperative transition from a folded to an unfolded state with no detectable intermediates. This indicates that the protein unfolds in a single, determined step, without exhibiting any detectable intermediate states. Typically, this behavior is observed in proteins with a stable native state (see Fig. I.10.) a well-defined folding pathway, and a high energy barrier between the folded and unfolded states. Typically, the unfolding transition is reversible, with the protein refolding back into its native state when denaturing conditions are removed. (Bakk et al. 2000; Mayne and Englander 2000; Zwanzig 1997)

The presence of a well-defined melting temperature (T_m), which is the temperature at which 50% of the protein is unfolded, is an essential characteristic of two-state protein unfolding. The T_m is a measure of the stability of the folded state and is affected by a number of factors, including protein size, the stability of secondary and tertiary structures, and the presence of stabilizing or destabilizing mutations. Typically, proteins with two-state unfolding behavior exhibit a sharp, cooperative transition at the T_m, indicating that the unfolding transition occurs simultaneously in every single part of the protein. (Bakk et al. 2000; Nelson and Cox 2017; C.N. 1986)

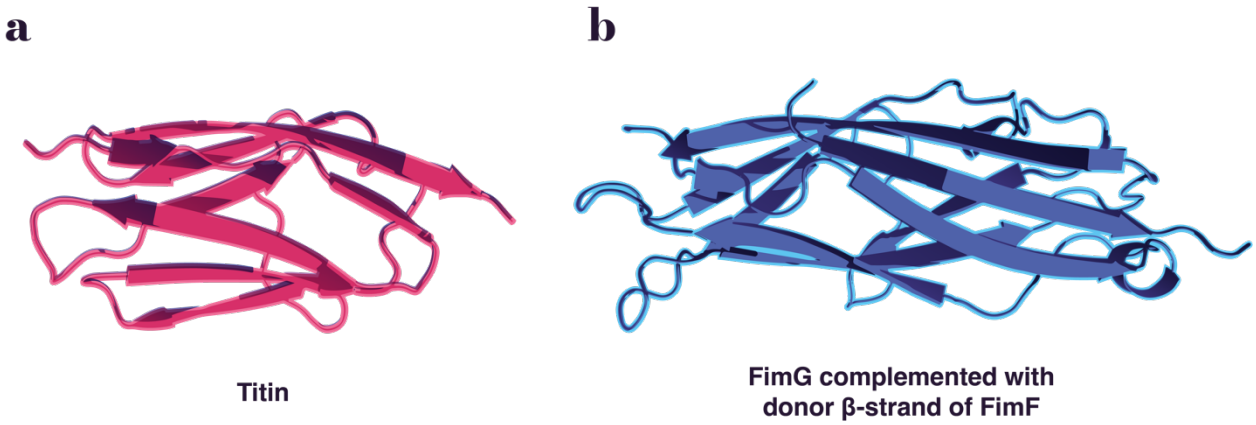

Fig. I.10. 3D structure of mechanical resistant proteins which follow a two-state folding. a. Titin subdomain (Marszalek et al. 1999). b. FimG (Alonso-Caballero et al. 2018) self-complemented with a donor β strand form FimF.

The mechanisms underlying the unfolding of two-state proteins are still the subject of ongoing research and debate. The "global unfolding" paradigm proposes that the entire protein unfolds simultaneously without any detectable intermediates or local unfolding events. This model suggests that all secondary and tertiary structures collapse simultaneously, resulting in the formation of the unfolded state. Experimental evidence from numerous biophysical techniques, such as protein unfolding studies using spectroscopic methods, as well as computer simulations and theoretical models, support the global unfolding model. (Schönfelder, Perez-Jimenez, et al. 2016; Bakk et al. 2000)

The "local unfolding" model proposes that the protein endures local unfolding events in specific regions previous to the unfolding of the entire protein. This model proposes that the protein unfolds in stages, with local unfolding events occurring in specific regions of the protein followed by the unfolding of the entire protein, following a pre-defined pathway. (Englander and Mayne 2014) Experimental evidence from techniques such as hydrogen-deuterium exchange mass spectrometry, which can detect local unfolding events in specific regions of the protein, supports the local unfolding model. (Bai et al. 1993)

Additionally, knowledge about mechanical resistant proteins is crucial for engineering and design. Understanding the principles governing protein mechanical resistance facilitates the rational design of proteins with the desired stability and folding properties. For instance, proteins used in biotechnological applications, such as enzymes, antibodies, and other biotherapeutics, must be stable and retain their functional conformation under different conditions. Knowledge of the properties and mechanisms of two-state protein unfolding can aid in the development of more stable and functional proteins for these applications. (Carrion-Vazquez, Andres F. Oberhauser, et al. 2000; Hoffmann et al. 2013)

In addition, the study of two-state protein unfolding contributes to the comprehension of the evolutionary aspects of protein folding and stability. Evolutionarily, the mutations that increase or compensate the protein's mechanical stability may be advantageous in terms of protein function, and regulation. On the other hand, destabilizing mutations may introduce novel protein functions, despite the fact that they are typically deleterious mutations. At the level of evolution, the global stability of proteins appears to be compromised by stabilizing and destabilizing mutations; depending on the protein and its evolutionary process, some mutations will predominate more than others. (Tokuriki and Tawfik 2009; Bloom and Arnold 2009)

Ultra fast folder proteins

Ultra fast folder proteins are typically small in size and possess particular structural characteristics. Usually are conformed by helical structure (Reifs et al. 2023; Schönfelder, De Sancho, et al. 2018) but also can be found ultrafast folder proteins compose by β sheets structures (Schönfelder, De Sancho, et al. 2018; Wu and Shea 2010), (see Fig. I.11.) but the most important characteristics of fast folding proteins are a negligible (<3kBT) free-energy barriers and (un)folding timescales between millisecons and microseconds by these reasons fast folding proteins reside in the other side of the cooperativity spectrum compared to two-state proteins. (Garcia-Mira et al. 2002)

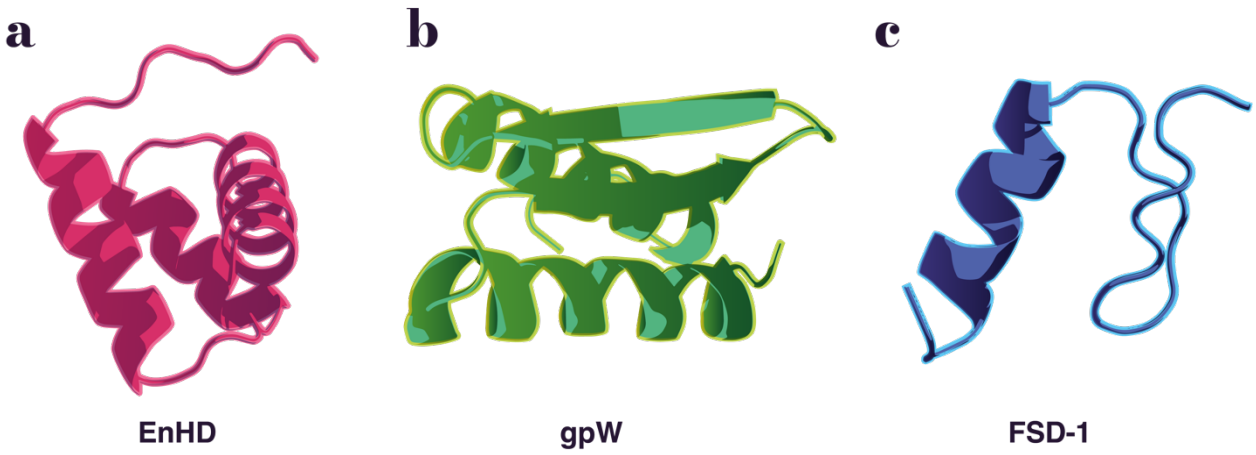

Fig. I.11. 3D structure of ultra fast folder proteins. a. EnHD (Reifs et al. 2023) complete α helices secondary structure. b. gpW (Schönfelder, De Sancho, et al. 2018) mix of α helices and β sheets secondary motifs. c. FSD-1 (Wu and Shea 2010) majority of β sheets secondary motifs.

The T_m represents the temperature at which ultrafast folder proteins experience a rapid unfolding transition from a folded to an unfolded state. Ultrafast folder proteins may exhibit more complex folding pathways, with the presence of intermediate states during the unfolding process. In contrast, two-state proteins suffer a direct and cooperative unfolding transition without intermediate states. These intermediate states are experimentally detectable by spectroscopy and contribute to the folding kinetics as a whole.

It can be difficult to precisely calculate the melting temperature of ultra fast folder proteins. They lack the conventional two-state unfolding transition with a well-defined T_m. The (un)folding processes of ultra fast folder proteins are commonly characterized by a downhill energy landscape with a very broad melting transition.

The folding mechanisms of ultra fast folder proteins continue to be a topic of investigation and debate. The "zipping and assembly" model proposes that proteins fold by sequentially assembling secondary structure elements around the folding nucleus under the influence of hydrophobic interactions and hydrogen bonding. This model suggests that the folding process involves a series of discrete intermediate states, with the protein transitioning rapidly from one intermediate state to the next

until it reaches the folded state. (Mok et al. 2007; Dyer 2007) The zipping and assembly model is a plausible explanation for the rapid folding kinetics observed in ultra fast folder proteins, as it permits the rapid assembly of secondary structure elements around the folding nucleus, resulting in the formation of the native state. (Voelz and Dill 2007)

The "conformational diffusion" model proposes that during the folding process, the protein explores a large conformational space and simultaneously examines multiple conformations. This model proposes that the folding process is not strictly hierarchical and implies the protein dynamically samples a range of conformations, the native state being one of the many conformations sampled. The conformational diffusion model offers an alternative explanation for the rapid folding kinetics observed in ultra fast folder proteins, as it permits the exploration of a large conformational space in a brief period of time, resulting in the rapid formation of the native state. (Ghosh et al. 2007; Sullivan and Kuntz 2002)

These proteins' ultra fast folding kinetics have significant functional implications for numerous biological processes. In molecular recognition and binding events, the rapid folding and unfolding behaviors of ultra fast folder proteins enable them to rapidly adapt to changing environmental conditions and interact with their binding partners. Many signaling proteins and receptors, for instance, experience rapid conformational changes upon ligand binding; the ultra fast folding kinetics of these proteins allow them to rapidly respond to the binding event and transmit the signal downstream. (Muñoz and Cerminara 2016)

In addition, ultra fast folder proteins play a role in protein folding and quality control within cells. In order to rapidly interact with unfolded or misfolded proteins and prevent their aggregation or degradation, molecular chaperones frequently exhibit extremely rapid folding kinetics. To prevent the accumulation of misfolded proteins, these chaperones must rapidly recognize and bind to them, and their ultra fast folding and unfolding behaviors allow them to carry out their functions effectively. (Hartl 2009; Park and Rapoport 2012)

I.IV. Decoding protein mechanics: *understanding protein mechanics modulation for mechanomedicine*

Mechano-regulators

During their biological functions, such as enzyme catalysis, molecular recognition, and signal transduction, proteins are dynamic entities that suffer mechanical forces and deformations. Understanding and modulating the mechanical stability and resistance of proteins is of great interest in the field of protein engineering, as it has major implications for their structural integrity, functional performance, and biological activity.

Genetic modifications are potent instruments for modifying the mechanical resistance of proteins because they permit precise control over the amino acid sequence and, by extension, the structural and mechanical properties of the protein. Several genetic modification strategies can be utilized to modify the mechanical resistance of proteins:

- Site-directed mutagenesis involves introducing specific mutations into the amino acid sequence of a protein in order to alter its mechanical properties. By substituting amino acids with different characteristics, such as size, charge, or hydrophobicity, for instance, the protein's mechanical stability can be altered. Mutations in critical structural regions, such as alpha helices or beta sheets, can also have an effect on the mechanical resistance of proteins by altering their folding/unfolding pathways or stability. (Perez-Jimenez et al. 2006; Li et al. 2000; Peters et al. 2022) (see Fig. I.12a.)

- De novo protein design involves the creation of entirely new proteins from scratch by designing their amino acid sequences in accordance with their intended structural and functional properties. This method permits the production of proteins with customized mechanical properties, such as increased mechanical stability or resistance. In de novo protein design, computational methods such as molecular modeling and simulations are frequently used to predict and optimize the mechanical properties of the designed proteins. (Floudas et al. 2006; Khoury et al. 2014; Kuhlman and Bradley 2019) (see Fig. I.12b.)

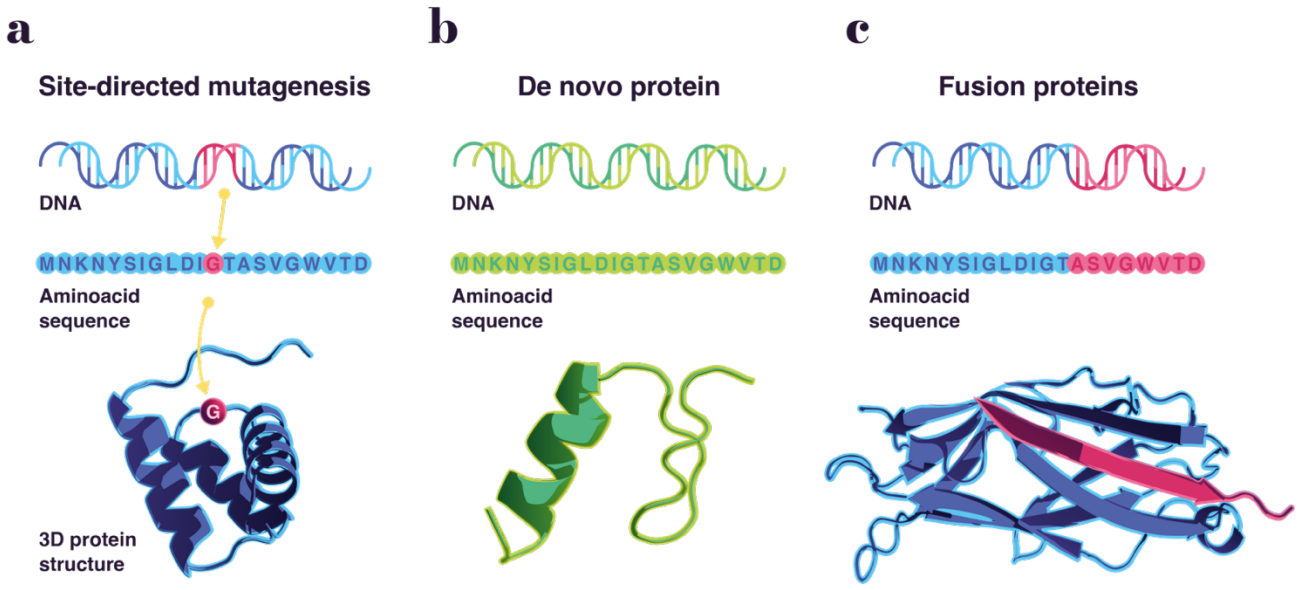

Fig. I,12. Types of genetic modifications. a. Site-directed mutagenesis. b. De novo proteins. c. Fusion proteins.

- Fusion proteins include the combination of two or more proteins with distinct mechanical properties to produce hybrid proteins with the desired mechanical properties. By fusing distinct protein domains or motifs, it is possible to modify the mechanical resistance of proteins. Fusion of a rigid protein domain with a flexible protein domain, for example, can produce proteins with intermediate mechanical properties. (Infante et al. 2019) (see Fig. I.12c.)

Molecular interactions, such as ligand binding, small molecule interactions, and post-translational modifications, can be used to modify the mechanical resistance of proteins. By inducing conformational changes, altering folding/unfolding pathways, or stabilizing specific structural motifs, these interactions can affect the mechanical stability of proteins. Many common strategies for modulating mechanical resistance via molecule interactions include:

- Ligand binding can affect the mechanical stability of proteins by inducing conformational changes or stabilizing particular structural motifs. For

instance, the binding of antibodies (Perez-Jimenez et al. 2014), peptides (Rivas-Pardo et al. 2018), or small molecules such as metal ions, and cofactors (Beedle et al. 2015), between others, to particular binding sites in proteins can modify their mechanical properties. The ability of ligand binding to induce mechanical unfolding or stretching of proteins has been exploited in the design of mechanosensitive proteins with tunable mechanical properties. (see Fig. I.13a.)

- Interactions between small molecules: small molecules, such as chemical denaturants or stabilizers, can interact with proteins and modulate their mechanical stability. Urea and guanidine hydrochloride, for instance, are commonly employed denaturants that can impair the noncovalent interactions in proteins, resulting in their mechanical unfolding. (Cao and Li 2008) By stabilizing their folded states, small molecule stabilizers, such as osmolytes or osmoregulatory solutes, can increase the mechanical resistance of proteins. (Schneck, Horinek, and Netz 2013) (see Fig. I.13b.)

- Protein mechanical resistance can also be modulated by post-translational modifications such as phosphorylation, acetylation, and glycosylation. These modifications may affect the conformation, stability, or interactions of a protein with other molecules, thereby altering its mechanical properties. For instance, phosphorylation of specific residues in a protein can modulate its mechanical stability by introducing electrostatic repulsion or altering the hydrogen bonding patterns, resulting in modifications to the protein's conformation and mechanical properties. (Grützner et al. 2009; Solís and Russell 2021; Bär et al. 2022) (see Fig. I.13c.)

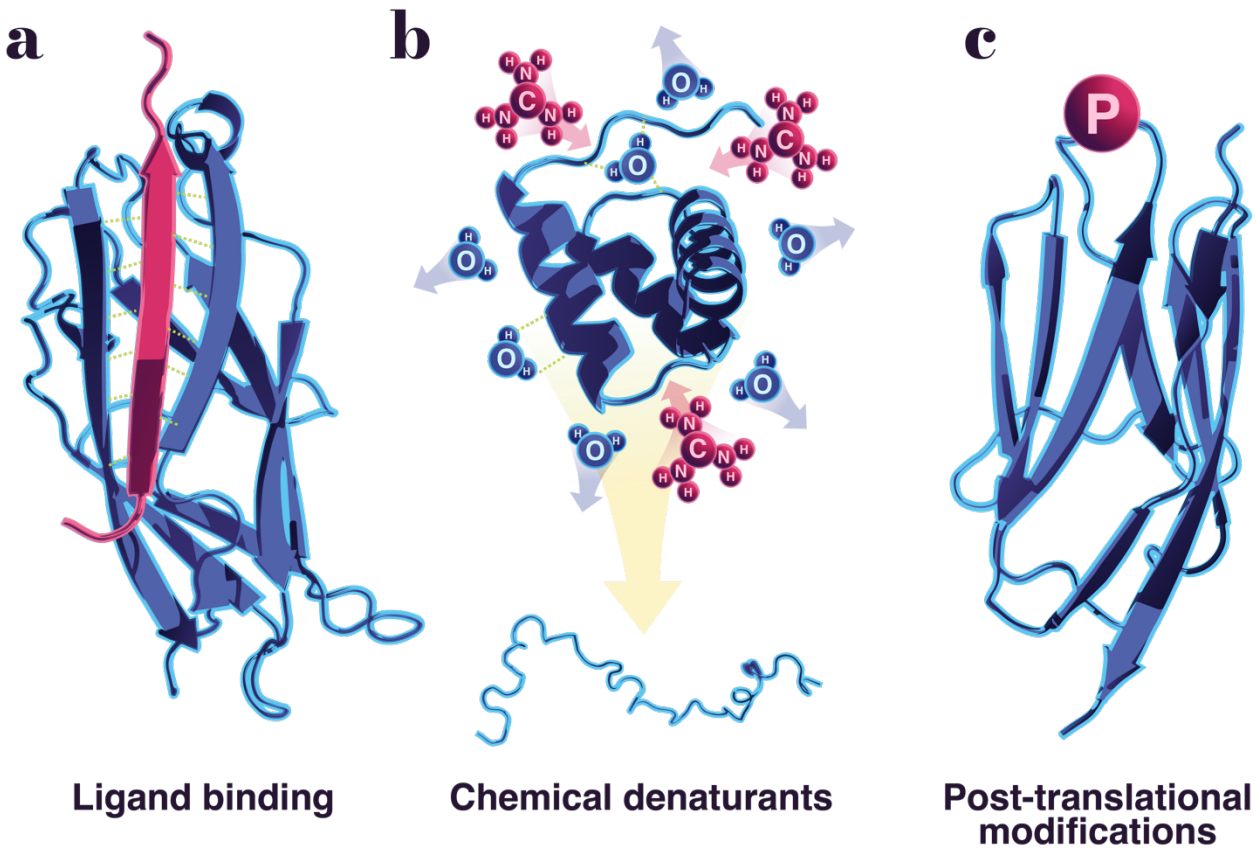

Fig. I.13. Types of molecular interactions that can be affected by mechano-regulators. a. Ligand binding. b. chemical denaturants. c. post-translational modifications.

It can be difficult to predict the effects of genetic modifications or molecule interactions on the mechanical properties of proteins. Computational methods, such as molecular modeling and simulations, can provide valuable insights, but they may not always accurately predict the mechanical properties of modified proteins. Additionally, the reproducibility of the desired mechanical properties may be difficult to obtain due to the fact that small variations in the amino acid sequence or molecule interactions can result in totally different mechanical behaviors. To guarantee the predictability and reproducibility of the mechanical properties of engineered proteins, rigorous experimental characterization and validation are required.

High-throughput methods and molecular docking

In recent years, molecular docking and high-throughput methods have arisen as powerful tools for identifying small molecules with the potential to modulate the mechanical stability of proteins. These methods provide a systematic and effective means for screening a large number of small molecules and predicting their binding affinities to particular target proteins. (Lavecchia and Giovanni 2013; Ke et al. 2014) By targeting specific regions of the protein associated with its mechanical stability (Perez-Jimenez et al. 2014; Rivas-Pardo et al. 2018), these small molecules may be able to influence the protein's mechanical properties, such as its resistance to mechanical stress or unfolding.

Molecular docking is a computational technique for predicting the binding mode and affinity of a small molecule to a particular target protein. It involves calculating the energetics of the protein-ligand interaction and predicting the binding conformation with the highest affinity. Molecular docking methods employ algorithms to search for and evaluate the potential binding positions of small molecules within the target protein's binding site. These methods rely on a variety of scoring functions that estimate the binding free energy and evaluate the complementarity between the protein and ligand in terms of shape, electrostatics, and other molecular properties. (Guedes, de Magalhães, and Dardenne 2014; Fan, Fu, and Zhang 2019) (see Fig. I.14.)

Molecular docking can be used to identify small molecules that interact with particular regions of a protein that contribute to its mechanical stability. For instance, if it is known that a particular region of the protein is crucial for its mechanical stability (Rivas-Pardo et al. 2018; Perez-Jimenez et al. 2014), molecular docking can be used to scan a large database of small molecules to identify those that have favorable interactions with this region. The identified small molecules can then be experimentally evaluated to determine their effects on the mechanical stability of the protein. (Guedes et al. 2014)

Large chemical libraries can be screened with HTS techniques for small molecules that modulate the mechanical stability of proteins. Using optical tweezers, atomic force microscopy (AFM), or mechanical spectroscopy. Once the molecular docking and HTS have been done, those results can be measured experimentally using SMFS techniques to measure the effect of small molecules on the mechanical stability of a protein. By applying mechanical stress to the protein in the presence of small molecules, HTS methods can identify molecules that, depending on the desired outcome, either increase or decrease the protein's mechanical stability.

The benefits of molecular docking and HTS techniques are several, including a rapid and effective screening, allowing the screening of a large number of small molecules in a relatively short amount of time, making them highly effective for identifying potential modulators of protein mechanical stability. The prediction of binding affinities can provide estimates of the binding affinities between small molecules and target proteins, which helps in the prioritization and selection of the most promising candidates for further experimental validation. Finally, a target-specific screening permits to focus on specific regions of the protein associated with its mechanical stability, enabling the screening of small molecules that interact with these regions. (Guedes et al. 2014; Fan et al. 2019)

Despite their benefits, molecular docking and high-throughput methods present a constraint despite being able to efficiently identify potential mechano-modulators of protein mechanical stability, experimental validation is still necessary to confirm the effects of these small molecules on protein stability. Biophysical techniques such as SMFS assays are required to validate the predicted effects of small molecules on the mechanical stability of proteins.

Fig. I.14. Molecular docking and high throughput screening workflow. Sketch of the systematic and efficient method for screening a large number of small molecules and predicting their binding affinities to specific target proteins.

I.V. Understanding the whole: *systems characterized in this thesis*

Engrailed Homeodomain (EnHD)

Engrailed Homeodomain (EnHD) from *Drosophila melanogaster* is a highly conserved protein that plays a crucial role in embryonic cell development, specifically in the differentiation of posterior half of the fly. (Ray, Acharyya, and Chatterjee 2001) EnHD is expressed in a segmental pattern along the anterior-posterior axis of the embryo, with increased levels of expression in the posterior segments. (Ray et al. 2001) This protein is a member of the homeodomain family of transcription factors, which regulate gene expression by binding to specific DNA sequences.(Ray et al. 2001; Religa et al. 2007)

EnHD is a small protein with only 54 amino acids, and its three-dimensional structure is composed of three alpha helice. Its compact structure is critical for binding to DNA and regulating gene expression. (Stollar et al. 2003; Religa et al. 2007)

Engrailed family is highly conserved across evolution, in vertebrated species has been implicated in many other biological processes, in addition to its role in embryonic development. (Kornberg 1993; Simon, Thuret, and Alberi 2004) Two transcription factors called Engrailed-1 (en1) and Engrailed-2 (En2) It has been shown to play a role in neuronal differentiation and the development of the nervous system, for instance. (Simon et al. 2004) In addition, it has been shown to be involved in the regulation of cell proliferation and apoptosis and to play a key role in the development of certain types of cancer. (Simon et al. 2004)

EnHD structure

EnHD is composed of three helices organized in a "helix-turn-helix" motif, (Religa et al. 2007; Stollar et al. 2003) a structural feature shared by many DNA-binding proteins. (see Fig. I.15.) EnHD contains a number of highly conserved amino acid residues that are essential to its function. (Kornberg 1993) These residues are located on the protein's surface and are responsible for DNA binding and protein-protein interactions. The residue with the highest degree of conservation is

asparagine 51 (Asn 51) in the third helix (the "recognition" helix). Asn 51 forms a series of hydrogen bonds with adenine in the binding site, and together with the series of backbone contacts made by other concatenated residues, it is believed that Asn 51 positions conform the recognition helix on the DNA. (Kornberg 1993) Other key residues, such as glutamine 50 (Gln50) and arginine 53 (Arg53), also located in the third helix, are important to EnHD's ability to interact with DNA. (Kornberg 1993)

EnHD is highly dynamic, its fold stabilities are typically inferior to those of other proteins of comparable size. (Stollar et al. 2003) In solution, the termini of EnHD are disordered, and the structures of the free and DNA-bound forms reveal that DNA binding is accompanied by a structural condensation of the termini. Upon DNA binding, the EnHD core may also suffer subtle structural changes. Thus, it would appear that the EnHD adapts to the surface of specific DNA through induced fit. (Stollar et al. 2003) Despite the abundance of current stereochemical and functional data for EnHD, the reason for their relatively low stability and its relationship, if any, to their induced fit have yet to be determined.

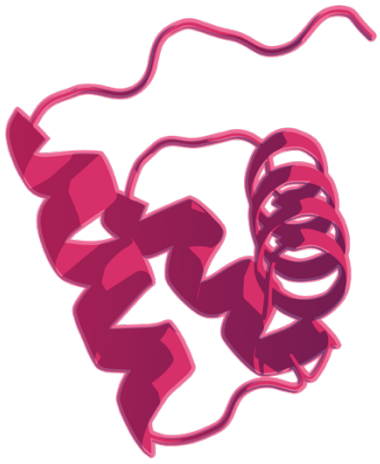

Fig. I.15. Engrailed homeodomain 3D structure. EnHD consists of an extraordinarily compact structure of alpha helices. The helices are structured in a "helix-turn-helix" motif.

EnHD folding

EnHD is an exceptional example of ultra fast folder. Folding times are on the order of microseconds, making it one of the fastest-folding proteins known to date. The highly compact structure of EnHD, (Stollar et al. 2003) which is stabilized by a network of hydrogen bonds and hydrophobic interactions, (Stollar et al. 2003) is believed to be responsible for this ultra rapid folding behavior.

Studies on the kinetics of EnHD folding have revealed that the folding process presents low cooperativity and negligible folding energy barrier. (Religa et al. 2007; Mayor et al. 2003) Extensive experimental and computational research has been conducted on the folding transition state, which corresponds to the point of maximal free energy along the folding pathway. These investigations have provided crucial insights into the structural characteristics and dynamics of EnHD, which are essential for its rapid folding. (Religa et al. 2007; Mayor et al. 2003; Mayor et al. 2000)

In relation to this system, we have included Chapter III: *compliant mechanical response of the ultrafast folding protein EnHD under force* which has been published in Communications physics.

Caf1 from *Yersinia pestis*

Yersinia pestis is a gram-negative bacterium responsible for one of the deadliest pandemics in human history, the bubonic plague also known as Black Death. It is estimated that between 75 and 200 million people died by the Black Death, which devastated Europe in the 14th century. Worldwide outbreaks of *Yersinia pestis* remain a significant hazard to public health in the present day, (Perry and Fetherston 1997) although fortunately today it can be treated with antibiotics.

Yersinia pestis is a highly virulent bacterium that has evolved a variety of sophisticated mechanisms to evade the immune system of its host and establish infection. The ability of Yersinia pestis to resist phagocytosis, the process by which

immune cells engulf and destroy invading pathogens, is one of its main virulence factors. (Li and Yang 2008)

Yersinia pestis present this resistance producing a variety of virulence factors that interfere with different aspects of the phagocytosis process. Using a type III secretion system, the bacterium produces a range of virulence factors, such as the Yop proteins. that are injected into host cells. These proteins have a variety of effects on the immune cells of the host, including inhibition of phagocytosis, induction of apoptosis, modulation of cytokine signaling, inhibition of the production of reactive oxygen species and other immune defenses by interfering with host cell signaling pathways. (Perry and Fetherston 1997; Li and Yang 2008)

The capsule of *Yersinia pestis*, which is composed of a polymer of the Caf1 protein, is a crucial virulence factor. Caf1 polymer is essential for preventing *Yersinia pestis* from being recognized and attacked by the host immune system. The polymer is extremely stable and resistant to degradation, enabling it to persist in the host for extended time periods. (Perry and Fetherston 1997; Li and Yang 2008) (see Fig. I.16.) Due to its capacity to elude the host immune system and cause disease, *Yersinia pestis* poses a significant threat to public health. (Perry and Fetherston 1997; Li and Yang 2008)

Caf1 polymer

Caf1 is the key element of the capsule that covers *Yersinia pestis*. The protein consists of a repeating unit that forms β-helix structure, the ability of the Caf1 protein to undergo auto-self association, which results in the formation of high-molecular-weight polymers, is one of its remarkable properties. This self-assembly phenomenon is known as beta strand complementation. (Alonso-Caballero et al. 2018; Zavialov et al. 2001) (see Fig. I.17.) This process entails the antiparallel pairing of individual Caf1 monomers so that the β strands of one monomer are complemented by those of its neighbor. It is believed that the resulting structure, a

highly stable, extended β sheet, is essential for the formation of the *Yersinia pestis* capsule. (Alonso-Caballero et al. 2018; Du, Rosqvist, and Forsberg 2002)

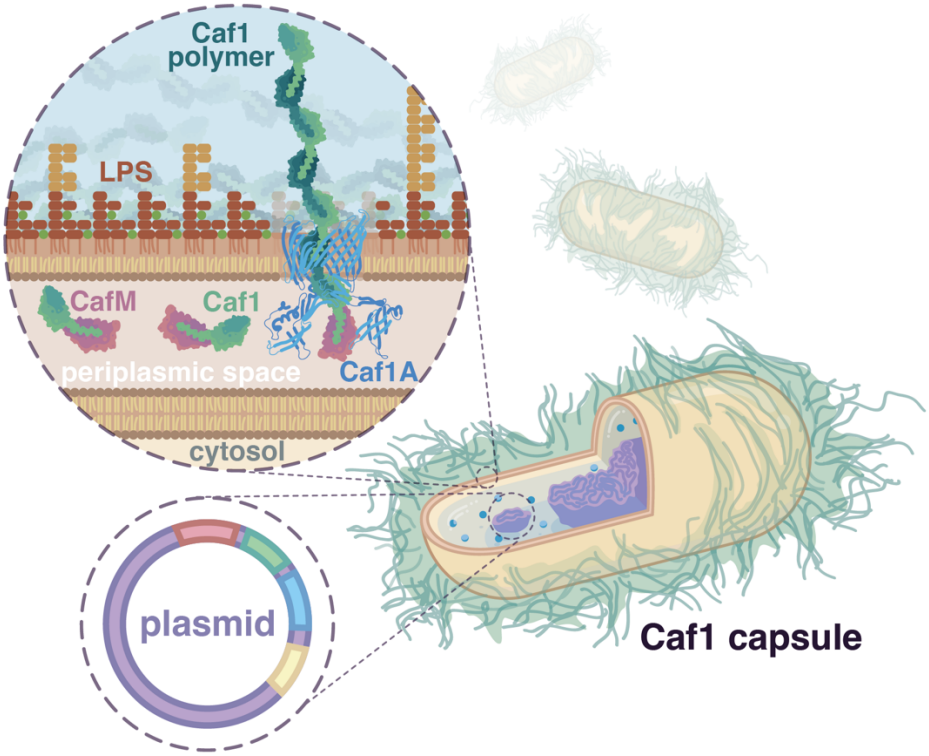

Fig. I.16. *Yersinia pestis* Caf1 cloak. A crucial virulence factor is the Caf1 capsule, which is made up of a polymer of the Caf1 protein. Caf1 polymer is essential for preventing the host immune system from recognizing and attacking Yersinia pestis. The presence of the chaperone Caf1M directs the folding of Caf1 monomers. Caf1M chaperone aids in periplasmic folding and prevents aggregation of newly translocated Caf1 subunits, thereby facilitating the correct assembly of the polymer.

The folding of one Caf1 monomer is directed by the presence of a chaperone called Caf1M. Caf1M chaperone assists in the periplasmic folding and prevents the aggregation of newly translocated Caf1 subunits (Zavialov et al. 2001), leading the correct assembly of the polymer. This mechanism is believed to facilitate the efficient assembly of the Caf1 polymer, as it aligns each monomer with its neighbor. (Zavialov et al. 2001; Du et al. 2002)

It is believed that the mechanism of beta strand complementation contributes to the remarkable stability of the Caf1 polymer. (Du et al. 2002) The extended β sheet structure formed by the complemented β strands is highly resistant to proteolytic degradation because it lacks the vulnerable loops and turns found in globular proteins. It is believed that this stability is essential for the Caf1 polymer to persist in the host for protracted periods of time. (Zavialov et al. 2001; Ulusu et al. 2017)

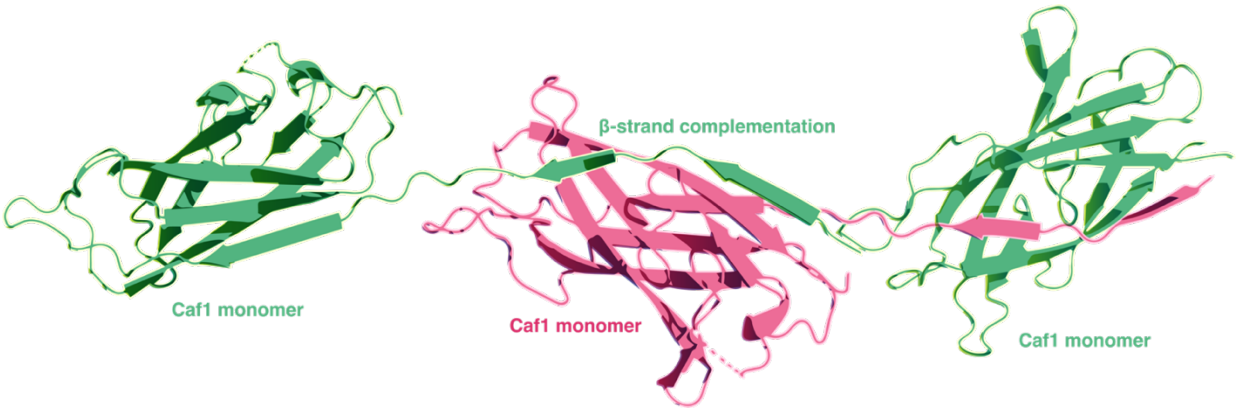

Fig. I.17. Caf1 polymer and β strand complementation. This process involves the antiparallel pairing of Caf1 monomers so that the β strands of one monomer complement those of its neighbor.

Caf1 polymer mechanical stability

The mechanical stability of the Caf1 protein polymer is an additional remarkable characteristic that contributes to *Yersinia pestis* persistence in the host. It has been demonstrated that the Caf1 polymer is highly resistant to mechanical disruption, such as that caused by blood flow or the migration of phagocytic immune cells. (Ulusu et al. 2017; Zavialov et al. 2003)

Studies have demonstrated that the mechanical stability of the Caf1 polymer is partially attributable to its extended β sheet structure, which provides a large surface area for intermolecular interactions and results in a high degree of cooperativity in the self-assembly process. (Ulusu et al. 2017; Zavialov et al. 2003)

It is believed that the mechanical stability of the Caf1 polymer is a crucial factor in Yersinia pestis' ability to elude host immune defenses and establish infection. Caf1 polymer's resistance to mechanical disruption ensures that it remains intact in the host, providing a protective capsule for the bacteria and preventing immune system recognition. (Alonso-Caballero et al. 2018; Ulusu et al. 2017; Roque et al. 2014)

Caf1 and its self-assembly process are fascinating examples of the remarkable properties of proteins and their function in the biology of pathogenic microorganisms. Extensive research into the structure, self-assembly, and stability of the Caf1 protein polymer has yielded important insights into the mechanisms that drives *Yersinia pestis* infection and opened up new avenues for the development of therapeutics against this lethal pathogen.

In relation to this system, we have included Chapter IV: *evasion of phagocytosis by the plague bacterium Yersinia pestis requires exceptional protein mechanostability* which has been published in PLOS pathogens.

Adhesion proteins from *Staphylococcus aureus* and Endocarditis

Endocarditis is a life-threatening infection of the heart's membrane and valves caused by bacteria. *Staphylococcus aureus* is one of the most common bacterial agents responsible for this disease. (Lower et al. 2011) Numerous virulence factors in *S. aureus* enable the bacteria to adhere to host tissues and avoid host immune defenses. The ability of *S. aureus* to form biofilms on the heart valves is one of the most crucial factors in endocarditis. Biofilms are complex bacterial communities covered by a protective extracellular matrix. Once *S. aureus* adheres to the surface of a heart valve, it can form an antibiotic and immune-resistant biofilm. (Lower et al. 2011; Josse, Laurent, and Diot 2017)

Several virulence factors of *S. aureus* are crucial to the pathogenesis of endocarditis. These include surface proteins that facilitate adhesion, tissue-degrading enzymes, and toxins that injure host cells and tissues. (Josse et al. 2017; Foster et al. 2014)

The production of the secreted toxin alpha-toxin is one of the most dangerous virulence factors in *S. aureus* endocarditis. This toxin is known to injure host cells and contribute to the formation of a fibrin clot on the surface of the heart valve, which promotes bacterial colonization. (Josse et al. 2017)

The complex immune response of the host to *S. aureus* endocarditis involves innate and adaptive immune mechanisms. Neutrophils play a crucial role in the control of S. aureus infections, but the bacteria have evolved mechanisms to evade and even subvert neutrophils. In addition, *S. aureus* is capable of activating complement pathways, resulting in the deposition of complement factors on the surface of the heart valve, which can promote further bacterial colonization. (Josse et al. 2017; Foster et al. 2014)

Therapeutic interventions for *S. aureus* endocarditis are challenging due to the formation of biofilm and the bacteria's antibiotic resistance. The need for long-term treatment and the possibility of adverse effects can complicate the use of combination antibiotic therapy. Novel therapeutic approaches are needed that target the bacterial biofilm or the virulence factors that contribute to the pathogenesis of endocarditis. (Lower et al. 2011)

FnBPA and *S. aureus* attachment

But the very first step of the infection process is the attachment. *S. aureus* uses several virulence factors to attach to host tissues and evade immune responses called cell-wall anchored proteins (CWA). (Geoghegan and Foster 2017) One of the most significant mechanisms for attachment is the interaction between bacterial CWA proteins and host extracellular matrix components. A special class of CWA involved in endocarditis are MSCRAMM (Microbial Surface Components Recognizing Adhesive Matrix Molecules) For example two of the most important MSCRAMM are fibronectin-binding proteins A and B (FnBPA and FnBPB), which are known to mediate bacterial attachment to host cells and extracellular matrix proteins. (Lower et al. 2011; Geoghegan and Foster 2017) (see Fig. I.18a.)

Of these, FnBPA is the most extensively studied. It is a surface protein that contains an N-terminal domain, which is responsible for binding to host fibronectin, and a C-terminal domain, which is responsible for binding to the bacterial cell wall. The binding of FnBPA to host fibronectin is a key step in the pathogenesis of *S. aureus* infections, including endocarditis. (Lower et al. 2011)

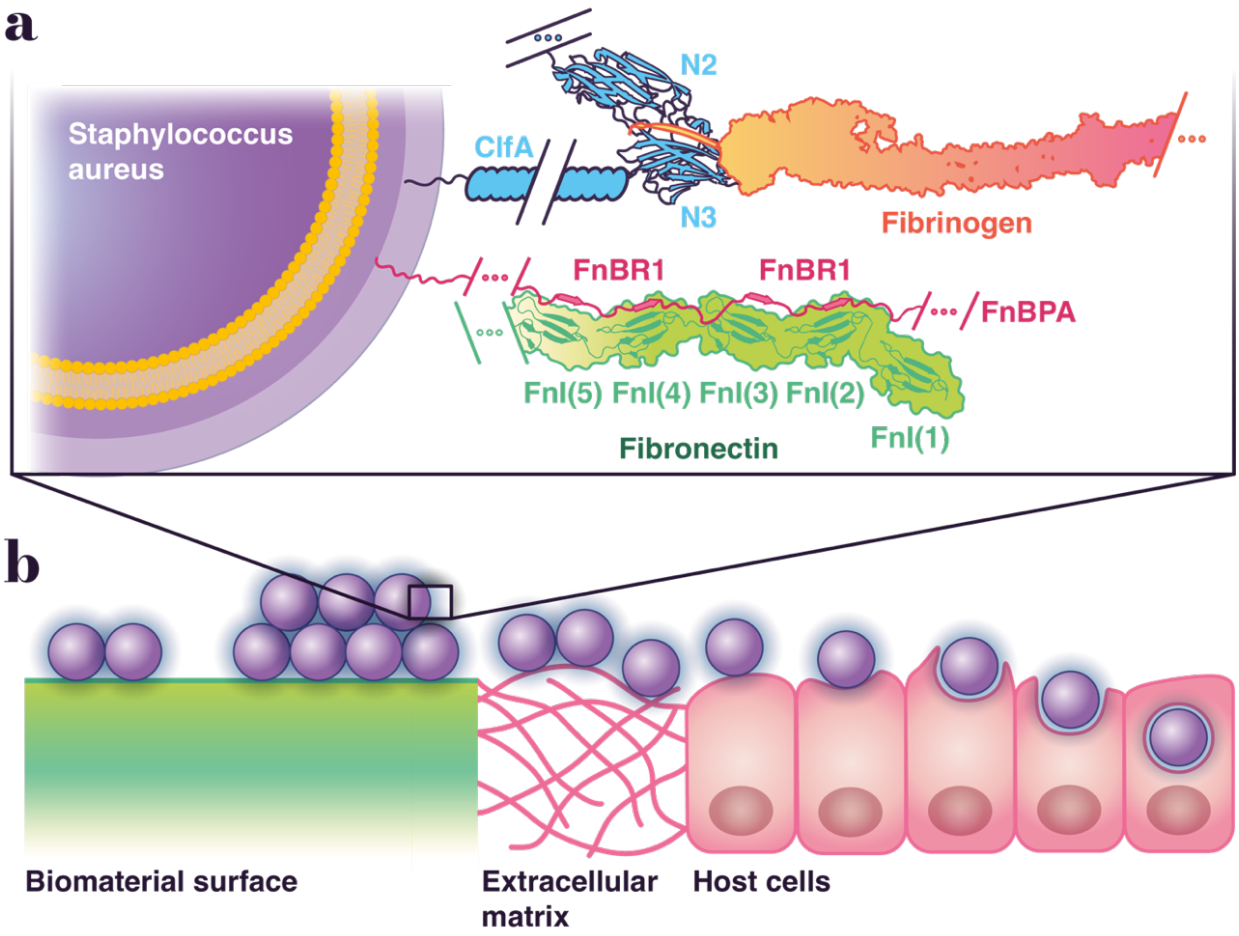

Fig. I.18. Microbial surface components recognizing adhesive matrix molecules (MSCRAMM) attachment. a. example of two cell wall anchored proteins, clumping factor A (ClfA) and Fibronectin binding protein A (FnBPA) attached to their target proteins. b. examples of different surfaces and tissues that *S. aureus* can colonize.

The attachment mechanism of FnBPA involves several stages. First, the protein bonds to the extracellular matrix protein fibronectin, which is present on the host cell surface. (see Fig. I.18b.) The binding of FnBPA to fibronectin is mediated by a specific region of the protein known as the fibronectin binding repeats (FnBRs). (Lower et al. 2011; Speziale and Pietrocola 2020) This domain contains 11 different types of tandem repeats or FnBRs which are considered intrinsically disordered proteins. Each FnBR forms antiparallel stands along a triple β strand of up to six Fibronectin type I domains connected by a tandem β zipper mechanism. (Speziale and Pietrocola 2020; O'Neill et al. 2008)

In conclusion, the attachment of *S. aureus* to host tissues is a critical phase in the pathogenesis of endocarditis. The interaction between bacterial surface proteins and host extracellular matrix components, such as fibronectin, is a key mechanism by which S. aureus attaches to host tissues and evades immune responses. The fibronectin-binding protein A (FnBPA) is a critical virulence factor for attachment and a potential target for therapeutic inhibitors such as small molecules or antibodies. Further research is needed to completely understand the attachment mechanisms of *S. aureus* and to develop effective treatments for endocarditis and other *S. aureus* infections.

In relation to this system, we have included Chapter VI: *nanomechanics of microbial infection, from single molecule to single bacterium* in which we are still working

Magnetosome and Magnetic-sensing bacteria

Magnetic-sensing bacteria are a unique category of microorganisms with the ability to sense magnetic fields and utilize them for navigation. This remarkable ability is due to the presence of magnetosomes, specialized organelles within these bacteria.(Balkwill, Maratea, and Blakemore 1980) Magnetosomes are membrane-bound vesicles containing magnetic nanoparticles of iron oxide or iron sulfide that help microbes to orient themselves in the Earth's magnetic field. (Balkwill et al. 1980; Gorby, Beveridge, and Blakemore 1988)

Magnetosome formation is a complex process that requires the expression of numerous genes and the coordination of multiple cellular processes. The genes responsible for magnetosome formation are organized in large clusters known as magnetosome gene islands, which are found in a variety of magnetic-sensing bacteria. (Gorby et al. 1988; Komeili et al. 2004)

Magnetospirillum magneticum is one of the most extensively studied magnetosome-producing bacteria. It is commonly found in aquatic environments. The process of magnetosome formation and the function of these organelles in magnetic sensing have been significantly elucidated by research on *M. magneticum.* (Balkwill et al. 1980) A number of proteins in the magnetosome membrane are involved in the transport and mineralization of iron, as well as the formation of magnetic nanoparticles. (Komeili et al. 2004) MamJ, a structural protein that works interacting with its parnet MamK, both creates the scaffold and assembly of magnetosomes chains, both are indispensable for the proper formation of magnetosome membranes and the production of functional magnetosomes, in experiments where these genes were knockout the magnetosomes resultant suffered a collapse by magnetic attraction. (Uebe and Schüler 2016) (see Fig. I.19.)

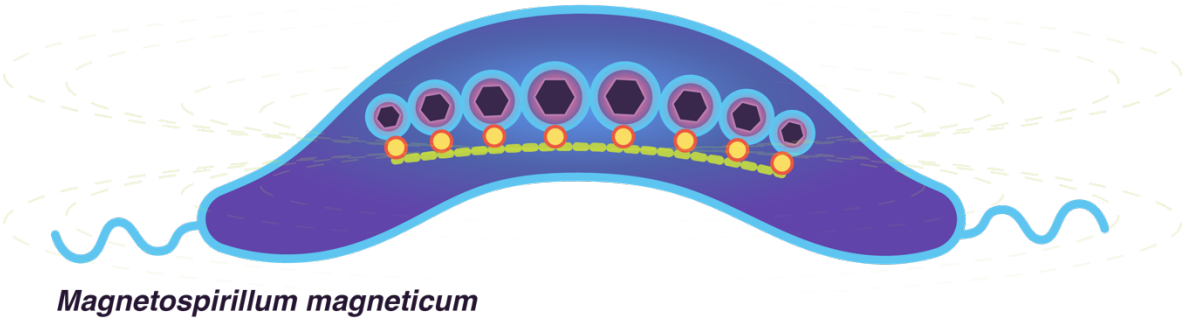

Fig. I.19. Magnetospirillum magneticum. The magnetosome is composed of vesicles which contain magnetite nanoparticles arranged in a line parallel to the longitudinal axis of the bacterium. MamK and MamJ are represented in green and yellow respectively.

Magnetosomes have several potential biotechnological applications in addition to their function in magnetic sensing. The magnetic nanoparticles generated by magnetosomes have been utilized in a number of biomedical and environmental applications, such as drug delivery and magnetic hyperthermia (Jabalera et al. 2020; Jabalera et al. 2019), antibacterial-directed chemotherapy, (Jabalera et al. 2021) biosensors, and removal from wastewater. (Peigneux et al. 2020)

This system has served as an inspiration for the development of the methodology described in chapter Chapter VI: *nanomechanics of microbial infection, from single molecule to single bacterium* in which we are still working

Gp120 and CD4 interaction, HIV-1 infection mechanism

HIV-1 is the virus responsible for acquired immunodeficiency syndrome (AIDS), a disease that has affected millions of individuals worldwide. (Greene 2007) The virus targets CD4+ T cells, macrophages, and other immune cells, resulting in a progressive deterioration of the immune system and increased vulnerability to opportunistic infections and cancers. (Greene 2007; Schüpbach et al. 1984)

HIV-1 infection begins with the binding of gp120 to CD4 receptors on the surface of target cells. (Westby and Dalgleish 1998; Wilen, Tilton, and Doms 2012) This interaction induces a conformational change in gp120, allowing it to bind to a CCR5 or CXCR4 co-receptor on the surface of the target cell. The exposure of the viral transmembrane protein gp41, which mediates the fusion of the viral and target cell membranes, is caused by the binding of gp120 to the co-receptor. (Wilen et al. 2012; Checkley, Luttge, and Freed 2011)

The viral capsid is released into the cytoplasm of the target cell as a result of the fusion of the viral and target cell membranes. (Wilen et al. 2012) The capsid contains the viral RNA genome, reverse transcriptase, integrase, and other replication-essential viral proteins. Once inside the target cell, the viral reverse transcriptase enzyme converts the viral RNA genome into DNA, and the viral integrase enzyme

integrates the resultant DNA into the host cell genome. (Westby and Dalgleish 1998; Wilen et al. 2012)

The proviral DNA functions as a template for the transcription of viral RNA and production of viral proteins. The viral proteins are assembled into new viral particles, which emerge from the infected cell's surface and infect new cells. HIV-1's replication cycle is intricate and comprises multiple stages, making it a difficult target for antiviral therapy. (Wilen et al. 2012; Checkley et al. 2011)

The high mutation rate of the HIV-1 virus is one of the major obstacles to the development of effective treatments for HIV-1 infection. The error-prone nature of the viral reverse transcriptase enzyme results in the production of antiviral-resistant viral variants. (Westby and Dalgleish 1998) In addition, the virus's high replication rate and the presence of viral reservoirs, such as latently infected cells, make it difficult to eradicate the virus completely from the body. (Westby and Dalgleish 1998)

CD4 relevance in the HIV-1 infection

As was mentioned before, the binding of the viral envelope glycoprotein gp120 to CD4 receptors on the surface of target cells is a key step of HIV-1 entry, since it is the first step to complete in order to achieve a successful infection. (Wilen et al. 2012)

CD4 is a transmembrane protein that aids T cells in recognizing and responding to antigens, thereby playing an essential role in the immune response. It is expressed on the surface of T helper cells, macrophages, and dendritic cells, all of which are potential targets for HIV-1 infection. (HARRIS et al. 1990)

The interaction between gp120 and CD4 is required for HIV-1 entry into target cells, as it initiates a series of conformational changes in Env that allow it to bind to co-receptors CCR5 or CXCR4 and mediate the fusion of the viral and target cell membranes. (Wilen et al. 2012) Nonetheless, the mechanical resistance of the CD4

receptor is also crucial in determining the susceptibility of target cells to HIV-1 infection. (see Fig. I20.)

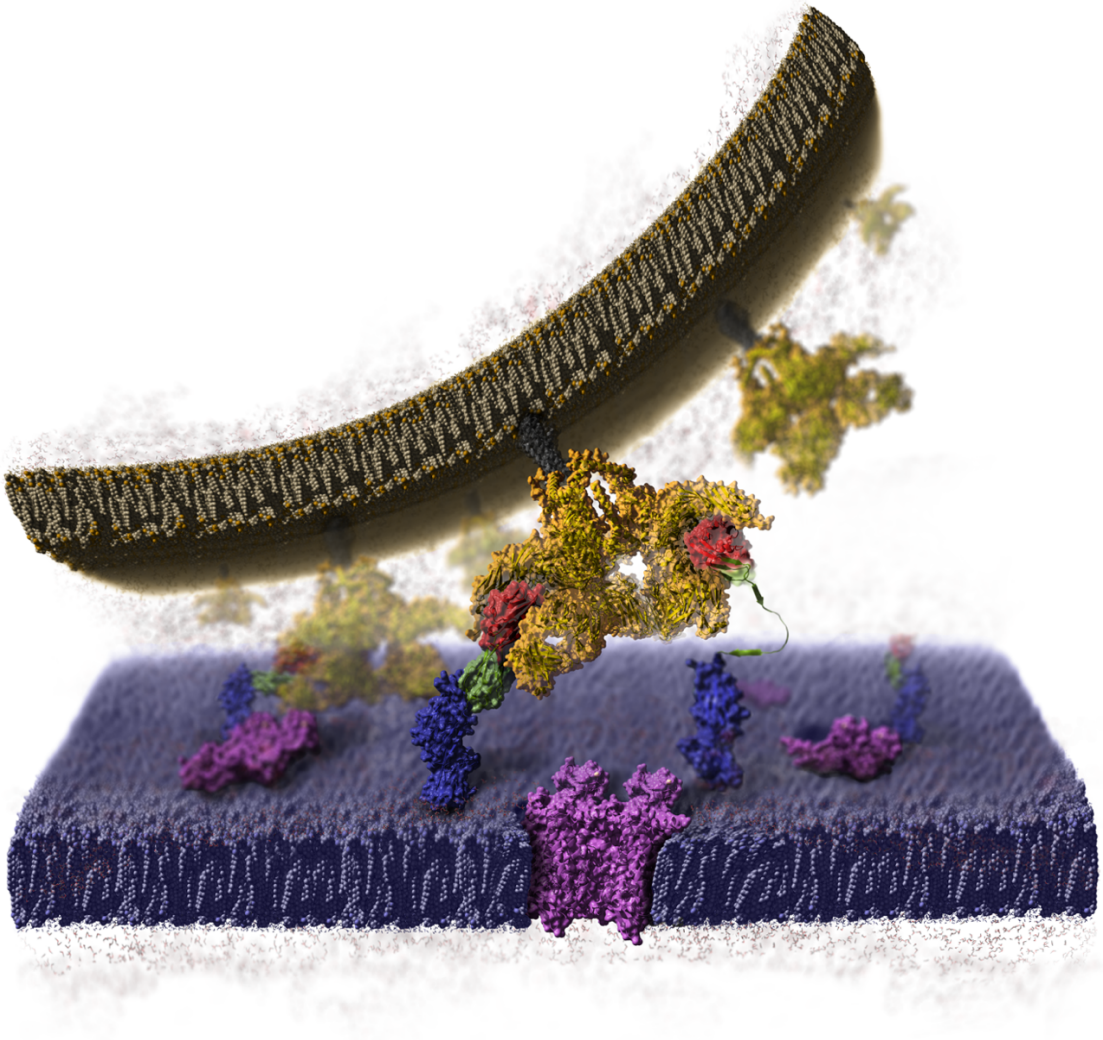

Fig. I.20. HIV-1 attachment. The interaction between gp120 (yellow) and CD4D1D2 (red and green) receptors on the surface of target cells. This interaction induces a conformational change in gp120 that allows it to bind to a CCR5 or CXCR4 co-receptor (purple) on the target cell's surface. One CD4 is partially unfolded.

CD4 undergoes significant conformational changes upon binding to gp120 (Yin, Wang, and Mariuzza 2012; Wyatt et al. 1998), which can influence its mechanical stability and sensitivity to mechanical force, according to research. Studies using

atomic force microscopy have demonstrated, for instance, that the binding of gp120 to CD4 can destabilize the CD4 protein unfolding it. (Wyatt et al. 1998)

In addition, it has been hypothesized that the unfolding of CD4 by gp120 may play a role in the assembly of the final, stable Env-CD4 complex, which is required for HIV-1 entry. Since the unfolding of the CD4 protein leads to an increase in the scanning surface in which gp120 can make contacts. (see Fig. I.21.) Increasing the probability of finding the necessary CCR5 or CXCR4 coreceptors to complete their infection mechanism. (Perez-Jimenez et al. 2014; Haqqani and Tilton 2013)

Recent studies have demonstrated that ibalizumab, a monoclonal antibody that targets the CD4 receptor, can increase the mechanical stability of CD4 and inhibit HIV-1 infection. Ibalizumab binds to a distinct site on CD4 from the site where gp120 binds, and it has been shown to induce conformational changes in CD4 that stabilize the protein and increase its resistance to mechanical force. (Perez-Jimenez et al. 2014)

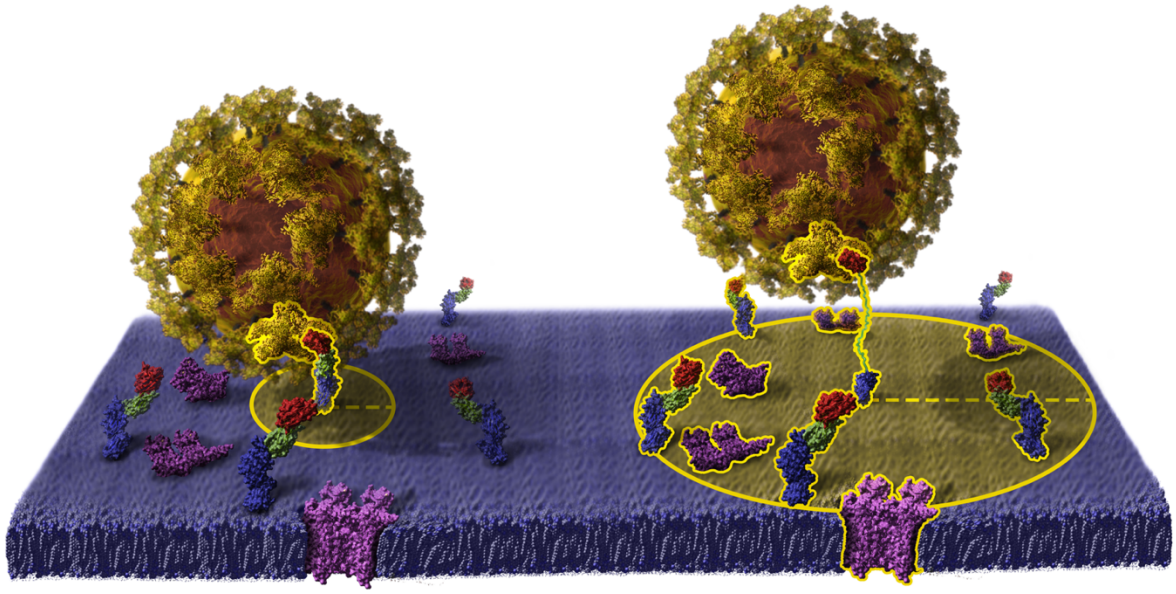

Fig. I.21. CD4-HIV tethering. HIV is attached to CD4. The unfolding of the D2 domain as a result of the force exerted by the virus on CD4 increases the length of the tether, allowing the virus to explore a larger surface area of the cell, thereby increasing the probability of locating a coreceptor. D2 is able to refold when the forces are reduced, functioning as a spring.

One study investigated the mechanical stability of CD4 in the presence of ibalizumab using atomic force microscopy. The results demonstrated that ibalizumab binding significantly increased the mechanical stability of CD4, while decreasing the receptor's susceptibility to mechanical deformation. These results suggest that ibalizumab may be capable of protecting CD4 from the mechanical stress caused by viral entry. (Perez-Jimenez et al. 2014)

In relation to this system, we have included Chapter V: *high throughput search of small molecules for controlling the mechanical stability of proteins* which is under review in Communications chemistry

Chapter II: *Materials & Methods*

Protein design

In order to measure the mechanical stability of any protein, we will need to produce that specific protein. But, due to the nature of the smFS technique, we must consider two important features.

First, we need to introduce a fingerprint as a control in our sample and second, our polyprotein should be continuous from beginning to end, without any interruption. (see Fig. II.1a.)

Because of how the AFS technique works it is extremely important to introduce in our polyprotein a quality control which could help us to make a proper selection of correct traces, due to this reason we cannot use the protein as we can find it in nature, we must design a construct in which our studied protein will be flanked by four I91 subunits from Human titin protein. Why I91? Because it is a model protein in mechano-field and its mechanical properties are well described. This subunit will allow us to select and validate the correct traces properly, only accepting traces that present 3 or 4 unfolding steps of this model subdomain.

But why it is so important the presence of these fingerprints? The AFS technique consists of stretching the desired protein from one extreme to the other, how we can achieve this? as is described in AFM preparation and sample calibration in this chapter, thanks to fixing our construct by its C-terminal extreme to a gold substrate thanks to cysteine binding and in the N-terminal due to a more unspecific binding from amino peptide bond and silicon nitride which coated the very sharp cantilever tip. Because of the second one biding could happen in any amino acid present in our construct, this could happen on one hand in the N-terminal extreme as we are looking for, or on other hand in any other point of our protein, obtaining a partially unfolded state. For this reason, it is very important to Introduce two pairs of fingerprints on both sides of our studied protein, if we select only traces where we can observe the unfolding of 3 or more fingerprints, we can strongly affirm that our protein is completely unfolded, as long as we have reached its unfolding force.
(see Fig. II.1b.)

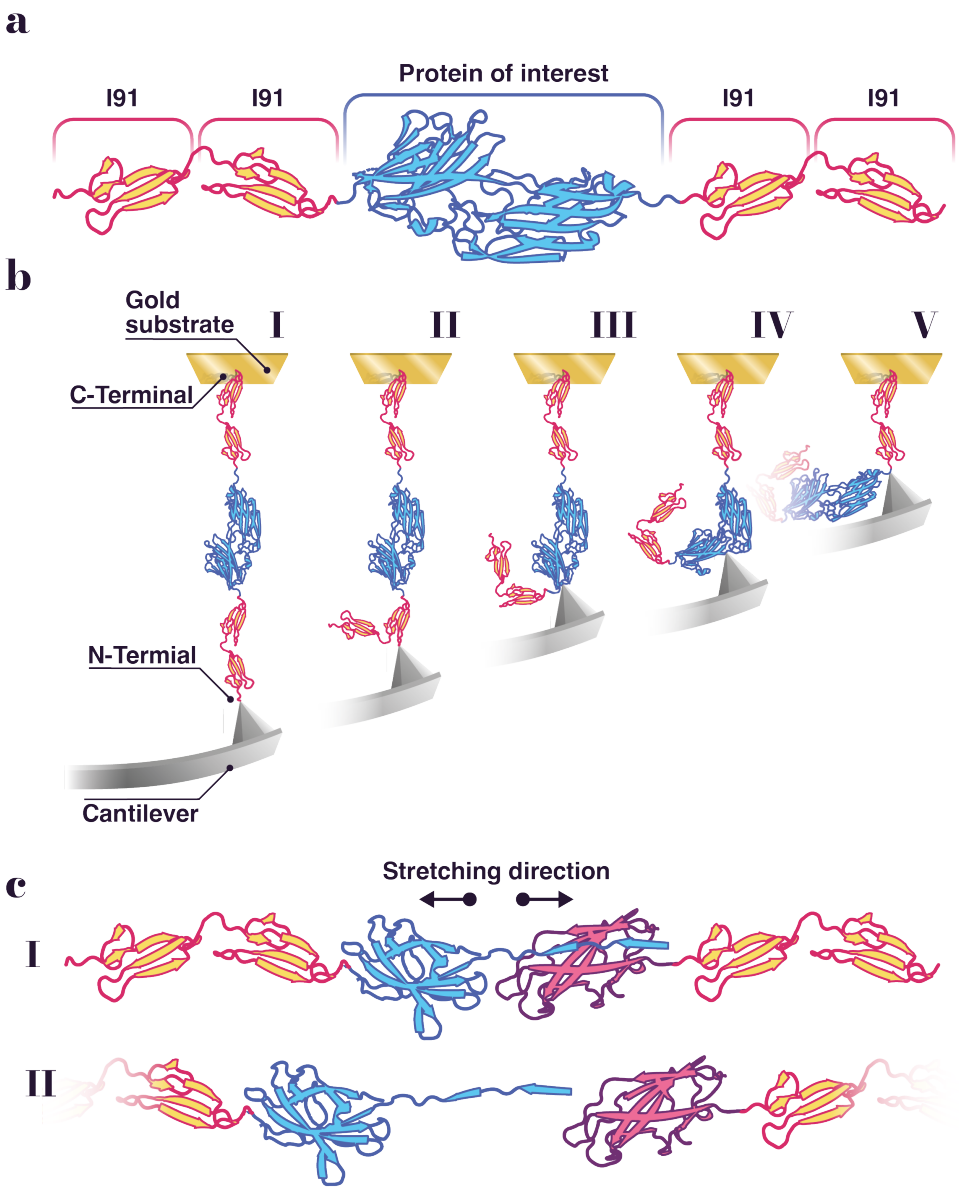

Fig. II.1. Key elements in protein design for SMFS experiments. a. typical AFS construct flanked by two I91 titin subunits on both sides of our protein of interest. b. Due to unspecific binding between protein and cantilever, the stretching of our protein could happen from extreme to extreme I, or in any other point of our construct, the only proper traces to work with is the case of I and II, where we can observe the unfolding of three or more I91, in the rest of cases (III, IV, V) we cannot ensure the proper and complete unfolding of our protein of interest. c. If our protein of interest does not present continuity in its sequence, when unbinding between chains happens the tension force in the equipment drop to zero, like when detachment happens between our protein and cantilever or gold substrate.

Also, our polyprotein must be uninterrupted from extreme to extreme, and this could be obvious if we have a gap in our amino acid sequence even if these two sequences are bonded due to interactions present in tertiary and quaternary structures during folding when the unfolding of that subdomains happen, the continuity of the polyprotein will be compromised. (see Fig. II.1c.)

But how can we measure the binding of two different proteins using the AFS technique? We need to design a circular permutant. A circular permutant is a fusion polyprotein that merges and remodels two different proteins into an unique one. Following this technique, in this thesis we have designed circular permutants for proteins: Caf-1, different Caf-1 mutants, and Fibronectin binding protein A (FnBPA). To join these different proteins, we must introduce a linker to connect their sequences.

In another way, we cannot differentiate the rupture of both proteins binding from the detachment of our construct from the cantilever or the gold substrate, because when this rupture happens the continuity of our construct will be broken, and this will drop the tension force of the system to zero.

In the case of Caf-1 as it is explained in Chapter I: I.V. Understanding the whole: *systems characterized in this thesis* the polymer formed by Caf-1 proteins follows an auto-complementation phenomenon called β-strand complementation, in which an exposed beta strand from one caf-1 protein is stabilized by internalization into a hydrophobic pocket present in the next caf-1 protein across the polymer. To measure the binding formed by the beta-strand I and I' with their neighbor beta strands A and H present in the pocket, we must redesign this protein by introducing a small flexible linker, with the sequence "GSGNG", which connects the beta-strand H with the beta strands I and I'. We have done remodeling of the natural sequence of this protein because in nature the beta-strand that we called I and I' is present in the N-terminal of the protein instead of connected to the C-terminal as we have redesigned. (see Fig. II.2.)

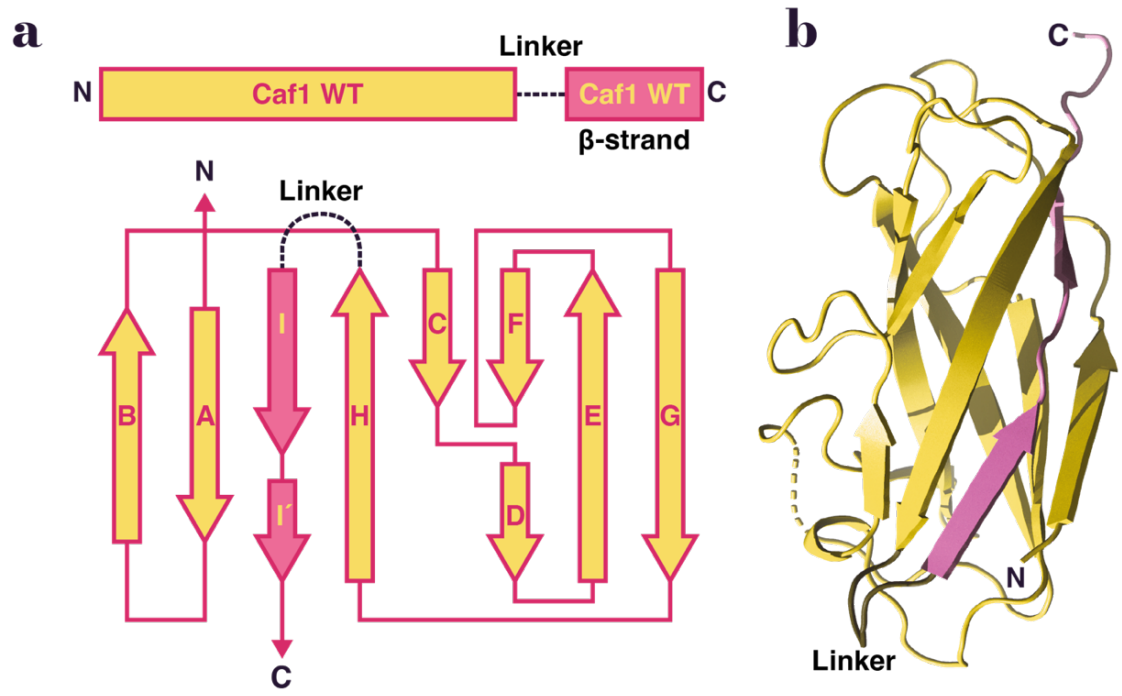

Fig. II.2. Caf-1 circular permutant design. a. Scheme of Caf-1 circular permutant in which donor beta strands position and interaction can be observed. b. Cartoon structure representation of same caf-1 circular permutant.

The case of the protein FnBPA is slightly different and easier because we do not need to rebuild our protein, we only need to link both proteins. We have joined the subunits that intervene in the attachment process, being these repetitions two to five subunit type I from human fibronectin and fibronectin binding repeat 1 from FnBPA. To achieve this, we have introduced a small flexible linker formed by the sequence "GGGSGGGS". (see Fig. II.3.)

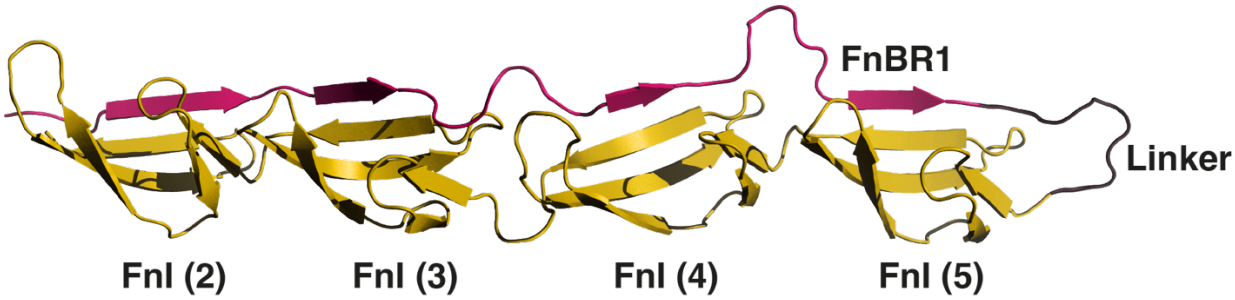

Fig. II.3. Fibronectin binding protein A zipper design. Cartoon structure representation of Human Fibronectin type I (2-5) yellow linked to FnBR1 magenta.

It is very common to use linkers with a high concentration of glycine residues because glycine is the amino acid that shows the highest flexibility, this feature is due to its side chain. The side chain of glycine is just hydrogen being the simplest one in comparison with the rest of the amino acids found in nature. The smaller the side chain is, the less of steric hindrances that provokes, allowing this amino acid to occupy a higher number of different torsional angles in the Ramachandran plot than the rest of the amino acids. (see Fig. II.4.)

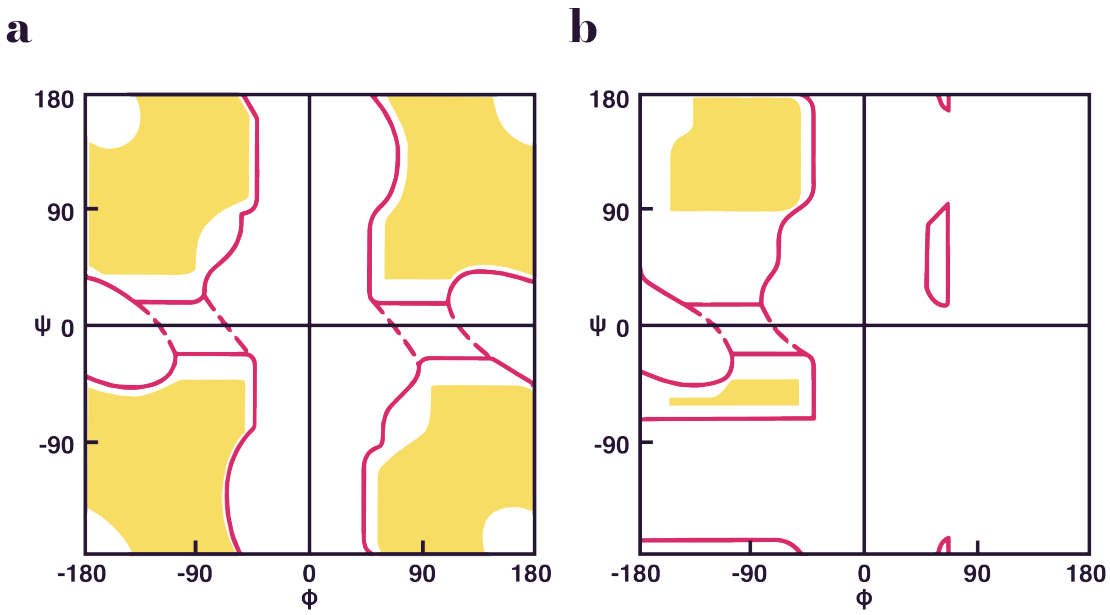

Fig. II.4. Glycine and Alanine Ramachandran plot. The classical version of the Ramachandran plot for a. glycine and b. alanine according to Ramachandran & Sasisekharan (1968).

Following those premises, during the development of this thesis, the design of eight proteins was carried out, the sequence of these proteins is present in the sequence appendix.

Protein expression and purification

Now that we have the sequence of our proteins, we must express and obtain them. First, we must synthesize the DNA sequence, every protein used in this thesis was synthesized by the company GeneScript Biotech, giving us our desired gene

inserted into the expression plasmid PQE80, between the restriction sites BamHI and KpNI.

PQE-80L expression plasmid

In this plasmid the gene of interest is regulated by lac promotor which is constitutively downregulated by LacI. The presence of lactose or its analogous Isopropyl-β-D-thiogalactoside (IPTG, Sigma) in media represses LacI, lac promotor repressor, activating the expression of our gene of interest.

This plasmid also contains a Multiple Cloning Site (MCS) which inserted our gene of interest upon this site we find the sequence necessary to produce six histidines (histidine tag) which is critical for purification.

At the end of our gen of interest, we have added a codon stop, necessary for interrupting the translation process, even though downstream of MCS already are a codon stop.

Another important gene in this plasmid is the Ampicillin resistance gene (AmpR) and the Chloramphenicol resistance gene (CmR) which confer to carrier bacteria the resistance to this antibiotic. This is very important to be able to select bacteria that had incorporate our plasmid properly.

Finally, this plasmid contains an origin of replication which is necessary for the DNA replication of this plasmid during the division process into the bacteria. (see Fig. II.5.)

Competent bacteria transformation

Once we have our expression plasmid with our gene of interest inside, we must introduce this plasmid into a proper bacterium, we have two different purposes, the first of them is to amplify our commercial plasmid quantity, for usage and storage, and the second one is to use the plasmid to produce our desired protein. As we have

different purposes, we must use two different bacteria, one for each objective. To apply the plasmid, we have used Escherichia coli XL1-Blue on the other hand for protein expression we have used Escherichia coli C41.

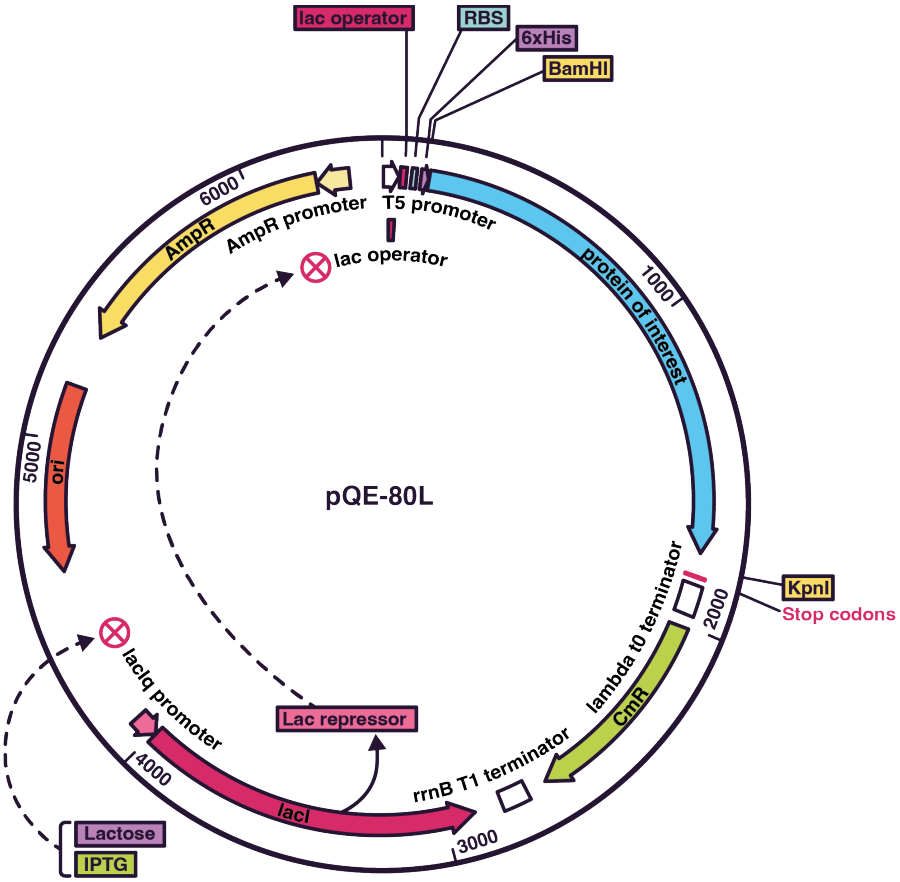

Fig. II.5. pQE-80L plasmid. pQE-80L expression plasmid scheme, our protein of interest is inserted between BamHI and KpnI restriction sites, also the lactose induction pathway mediated by Lac repressor is highlighted.

E. coli XL1-Blue is an excellent host strain for routine cloning applications ideally for amply any gene material. [I]

E. coli C41 is an overexpression strain that is effective in expressing toxic proteins from all classes of organisms. [II]

But first, to introduce any plasmid inside of any bacteria, we must alter the bacteria membrane, conferring the ability to absorb DNA from the media. This is what is called a competent bacteria or competent cell. To achieve that we have to use Mix & Go! Transformation Kit [III] Following the manufacturer protocol we prepared competent E. coli for simple and highly efficient DNA transformation.

Once we had both competent strains, we transformed both with our plasmid of interest. To do that, competent bacteria were incubated for 30 min with 50 ng of plasmid DNA in ice, after this time a heat shock was made, incubating our samples at 42ºC for 30-35 s, next another incubation step in ice was made for 5 min, then we let bacteria incubate during 1 h in SOC media [IV] at 37ºC with a strong agitation (250 RPM). Finally, 200 μL of bacteria culture was plated over LB agar plates containing carbenicillin antibiotic [V] to select only colonies with our plasmid which confer resistance to this antibiotic, we let grow those plates overnight (O.N.) at 37ºC. (see Fig. II.6.)

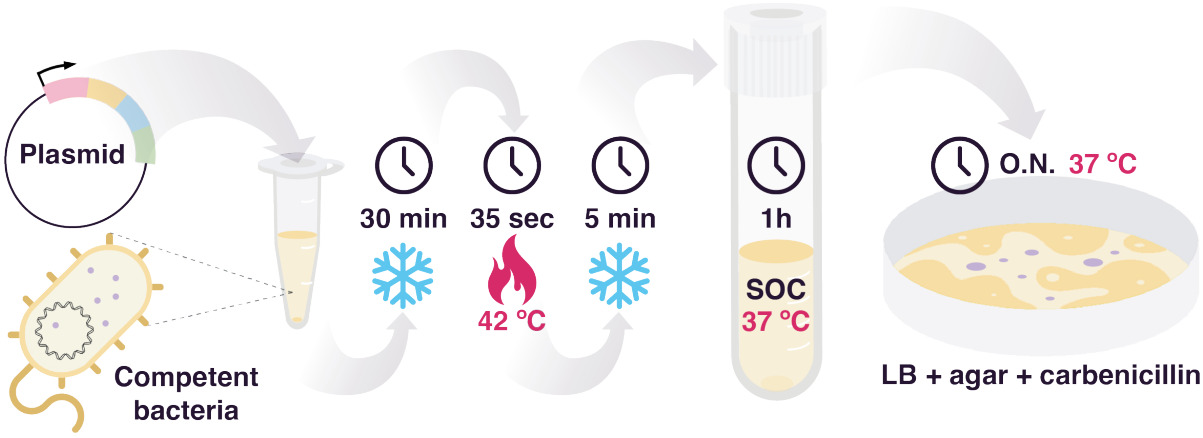

Fig. II.6. Competent bacteria transformation protocol. Competent bacteria were mixed with 50 ng of plasmid and exposed to a heat shock, then were incubated in SOC medium for 1h and palleted O.N. in agar.

Commercial plasmid amplification

When colonies were observed on plates, one single colony was picked and incubated in LB with 0.1 ug/mL of carbenicillin with a strong agitation (250 RPM) until reaching an optical density (O.D.) at 600 nm of at least 0.6 after this incubation bacteria were pelleted centrifugation at 4000xG for 20 min at 4ºC, once we have bacteria pellet GeneJET miniprep kit [VI] was used to extract DNA from bacteria. Finally, DNA was eluted in DEPC nuclease-free water, and its concentration was measured using Nanodrop 2000L spectrophotometer [XX].

Protein expression screening

Once that we had enough quantity of the plasmid DNA, we repeated the same transformation protocol explained before, with E. coli C41 and proceeded to look for the optimal induction condition to maximize the yield of protein obtained, exploring different temperatures and induction times. For example, room temperature (R.T.), 37ºC, 4 h, and O.N.

To do that, we incubate one colony of transformed bacteria per condition into 10 mL of LB media with 0.1 μg/mL of carbenicillin, at 37ºC in the agitation of 250 RPM. Just after culture, O.D. reached a value of 0.6, Then every volume condition was split into two, one of them without inductor (control), meanwhile in the other 1 μM of IPTG was added. When every condition was complete, 1 mL of culture was centrifugated at 4000xG for 20 min to pelleted bacteria, the 4 mL remaining was reserved for glycerol stock preparation. Every pellet was resuspended in 10 μL of extraction buffer [XXVI] and 10 μL of Laemmli sample buffer [VIII] was added. To continue, every condition was boiled at 95ºC for 5 min and centrifugated for 40 min at 12000 xG, to make lysis and release their cell content to the medium.

Once the lysis was completed 10-20 μL of supernatant was loaded into a Polyacrylamide Gel Electrophoresis (SDS-PAGE) to differentiate every protein in the sample by its size. The gel was done with a polyacrylamide percentage of 4% for stacking and 8-12% for resolving, depending on the protein of interest size. The

Electrophoresis gel and samples were running immersed into running buffer solution [XXVIII] using the Bio-rad electrophoresis system [XIX] at 120 V for 70 min. After this time the electrophoresis gel was washed two times with Milli-Q water and then was stained in Staining buffer [XXIX] for 5-10 min. Once the gel was stained, we proceed to wash it using washing buffer [XXX] to fade every part of the gel where there is not any protein or band. We washed as many times as was necessary.

Finally, we looked for the condition in which our protein band was most intense, that is the optimal conditions for producing our protein on a large scale. Additionally using the 4 mL of culture reserved in previous steps, from these selected conditions. We prepared a frozen bacteria aliquot, to do that we mixed 500 μL from this culture with 500 μL of glycerol 50% v/v. Then, we did a flash frozen into liquid nitrogen and kept our aliquots at -80ºC. (see Fig. II.7.)

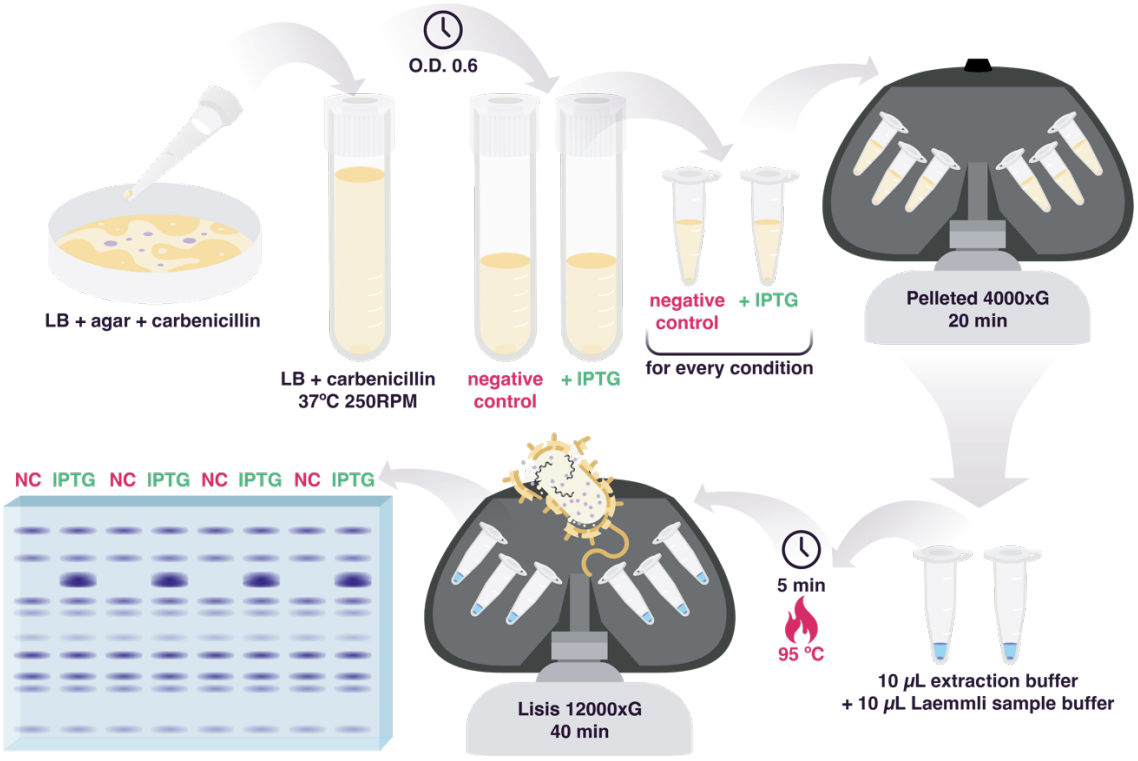

Fig II.7. Protein expression screening. C41 bacteria containing our expression plasmid were tested to different expression conditions with and without IPTG, finally, every lysate was run in an SDS-PAGE electrophoresis gel, our protein of interest only should be visible in that conditions which IPTG.

Large-scale protein expression

We started by diluent a frozen aliquot prepared in previous steps into 50 mL of LB media with 0,1 μg/mL of carbenicillin, this culture was incubated at 37ºC with a strong agitation (250 RPM). When an increase in culture turbidity was observed, we increased total culture volume to 4-6 L, splitting this volume in different Erlenmeyer (2 L) using a total volume per Erlenmeyer (2 L) of no more than 800 mL. In this step, the incubation condition remains the same except for the agitation, which was decreased to 180 RPM, because of the risk of leaking due to the bigger total volume. When O.D. at 600 nm of those cultures reached a value of 0.6, then our cultures were ready for induction. The necessary volume of IPTG [VII] to reach a concentration of 1 μM was added and let express our protein O.N. at 37ºC and 180 RPM of agitation.

These expression conditions were the same for the production of every protein in this thesis except for the CD4 construct, in which we started with a new bacteria transformation instead of frozen bacteria aliquot, also induction conditions were at 20ºC for 4 h.

Protein extraction

When induction was completed, bacteria were pelleted by centrifugation at 4000 xG for 20 min at 4ºC. After this, every pellet was resuspended in a total volume of 20 mL of Extraction buffer [XXVI] in presence of 200 μL of protease inhibitor [XI]. Then we proceeded with mechanical lysis of bacteria thanks to a French press (G. Heinemann HTU DIGI-F Press) this tool can disrupt cell walls and bacteria membranes by application of high shear forces generated by a huge level of pressure (15000 Pa) into a very small duct with a very low flow (around 0.5 mL/min) controlled by a valve connected with this mentioned duct. We performed three steps of French Press rupture to maximize the yield of bacterial lysis. The resulting lysate contains our proteins which were released into the medium from bacteria cytosol. But we had a mixture of proteome, genome, and cellular debris between other biomolecules. As the first step of purification, we centrifuged our lysate at 33000 xG for 30 min at 4ºC.

We conserved the soluble portion which contains bacterial proteome, for further purification steps.

Protein purification

From the beginning to the end of the protein purification protocol, every single step should be performed on ice or at 4ºC to minimize protein degradation. For exactly this reason, a protease inhibitor was added to the extraction buffer during the protein extraction. First, we started with a series of three filtration steps, using different pore diameters of 0.8, 0.45, and 0.22 μm respectively (Millipore). As we mentioned before in this filtered supernatant, we have a mixture of every protein produced by our expression bacteria, but our protein was designed with a significant difference from every other protein expressed. This distinction consists of a histidine tag which is formed by six consecutive histidine residues in the N-terminal extreme of our protein. This tag presents a significant affinity to metals like cobalt or nickel, for this reason, in the following step we mixed our filtered lysate with 5 mL of HisPur Cobalt Resin (Thermo scientific) previously washed and resuspended in extraction buffer with 5 mM Imidazole. We let incubate for at least 1 h with gentle agitation (5-10 RPM) at 4ºC. In the case of FnBPA HisPur Nickel Resin was used instead of Cobalt, because this one shows a better retention yield of our protein of interest.

Once our protein is supposedly attached to the resin, we washed by three centrifugation steps our resin to remove every possible protein present in the medium and not attached to the resin, those washed steps were performed with an extraction buffer with 5 mM of Imidazole. Why is necessary this low concentration of imidazole? Imidazole group is the side chain present in histidine residue and is the reason why his residue show affinity to metallic atoms. So, including concentrations of this group in the medium will generate a selective competition between every protein to the attachment of Cobalt or Nickel atoms present in the resin, only allowing attachment of proteins that show high affinity to the resin, in other words, proteins that show various consecutive histidines in their amino acid sequence.

After these washing steps, we proceeded with our protein elution adding small volumes (500 μL) of extraction buffer with 500 mM of Imidazole which will remove our protein from resin, we collected every aliquot of eluted and measured its protein concentration with nanodrop, we continued collection aliquots until observing extremely low protein concentration. Every aliquot was loaded in an electrophoresis polyacrylamide gel (SDS PAGE) to know which fractions contains our proteins of interest, we gathered those aliquots and concentrated until reached a total volume of 500 μL. In the case of CD4 purification after this step, the protein was incubated O.N. with a 3% concentration v/v of hydrogen peroxide to produce a disulfide bond oxidation between cysteines present in this protein.

Then we proceeded with an additional purification step, a size exclusion chromatography in which proteins were separated into different eluted fractions depending on their size, first proteins of bigger size were eluted followed by the smaller ones. A column of Sephadex 200pg [xxv] connected to an AKTA pure (GE Healthcare) fast protein liquid chromatography (FPLC) equipment was used for this purpose. To run this chromatography Hepes Buffer (pH 7.2, NaCl 150 mM, and EDTA 1 mM) [xxxi] was used. FPLC systems were measuring continuously buffer absorbance at 280 nm, when a rapid increase in this absorbance was detected, the system started to collect a fraction of a preestablished volume. These fractions contain eluted proteins.

To continue another Electrophoresis polyacrylamide gel (SDS-PAGE) was loaded with the different relevant aliquots depending on the chromatogram to know in which maximum from the chromatogram our protein was eluted. Finally, those fractions were collected, and flash frozen to be preserved at -80ºC. This flash frozen step into Liquid nitrogen is crucial because avoids the characteristics of water crystal formed by a slow freeze which could break proteins present in the medium. (see Fig. II.8.)

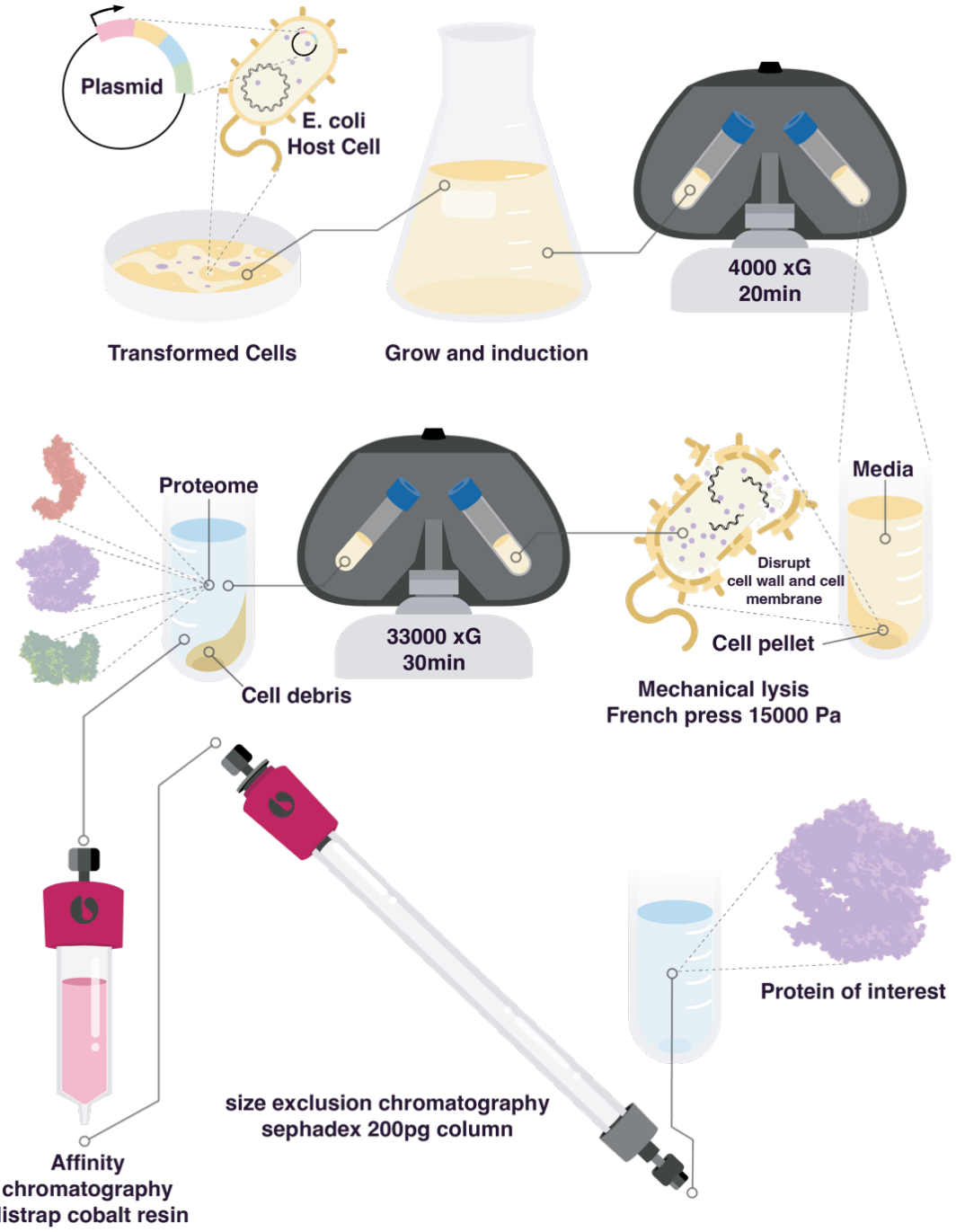

Fig. II.8. Protein expression, extraction, and purification. C41 bacteria containing our expression plasmid were grown and inducted, then its content was released by mechanical lysis using a French press. Finally, our protein of interest was purified using a series of chromatography steps.

Single-molecule Force Spectroscopy

Every protein produced as we mentioned before was designed expressly to be used in AFM equipment to measure its mechanical stability. In this section every important part of AFM set-up, how it works, and how we collected and analyzed data will be explained.

AFM set-up

AFM system is composed mainly of three crucial parts, being: piezoelectric actuator (PZA), cantilever, and four quadrants photodetector (PD). (see Fig. II.9.)

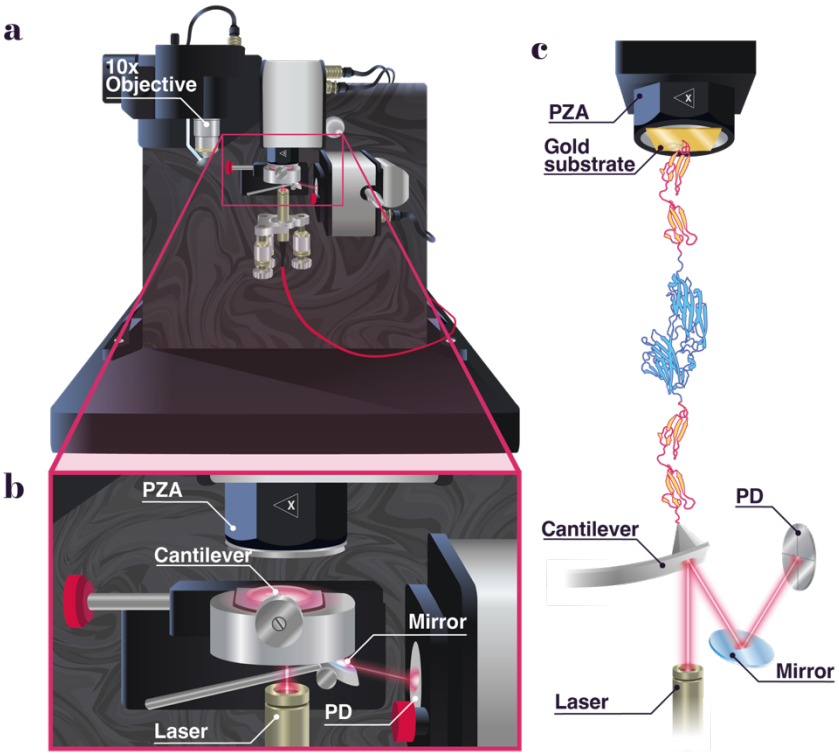

Fig. II.9. AFM set-up and key parts. a. Main AFM. b. Zoom showing the key parts of AFM set-up, these parts are PZA, cantilever, laser, mirror, and PD. c. Scheme of the AFM, laser beam is reflexed in the back part of cantilever and reach the PD through the mirror, in the tip of the cantilever is bonding our protein construct and being stretched from the gold substrate which is placed in the PZA.

PZA is composed of a material that shows piezoelectricity. What is piezoelectricity? Is the quality of certain materials, composed of electric dipoles in their crystal matrix, to generate an electric field when they are mechanically stressed. This property also works inversely, a piezoelectric material can be expanded or contracted depending on the different voltages applied to it. This expansion or contraction of material can be controlled at the sub-nanometer range, this property between others will determine the sensibility of equipment and it is crucial to measure the range of forces in which proteins unfold. (see Fig. II.10.)

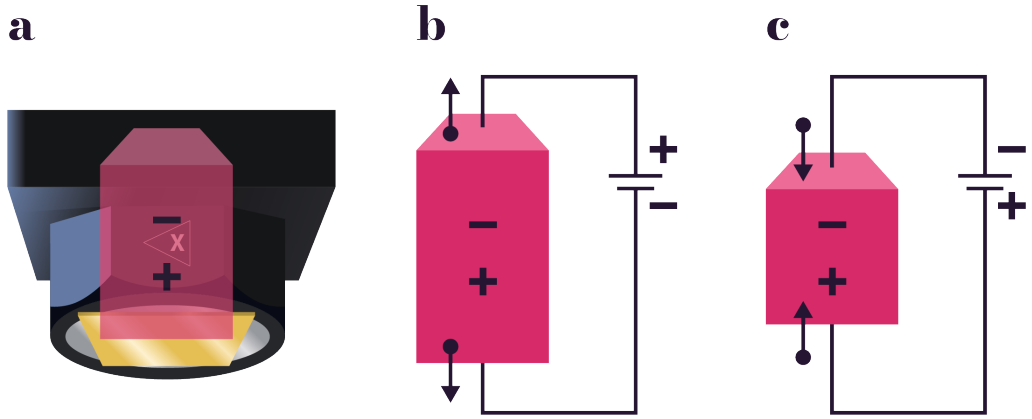

Fig. II.10. PZA piezoelectricity effect. a. Piezo-electric material present in PZA. b. and c. show this material deformation depending on the electrical potential applied.

Another essential element of AFM is the cantilever, composed of a series of flexible tips. In this thesis, we used OBL-10 cantilevers (Bruker) which are made of silicon nitride and coated with a 30nm layer of reflective gold on its top side, this coating is very important, because on this reflective surface is where the laser beam will be spotted, when cantilever tip bends its reflection angle will deflect and this is how the AFM can translate the force apply to our protein.

This OBL-10 cantilever shows two different types of tips with different lengths and more important spring constant (k) being these A: 30 $pN \cdot nm^{-1}$ B: 6 $pN \cdot nm^{-1}$. The Spring constant of a cantilever tip is a measure of how flexible this tip is, behaving like a spring. The sharpness of these tips is in the range of 20-30 nm. Thanks to this sharpness and very high pressure applied by this tip to our protein, previously fixed

into the gold substrate, is how the cantilever achieves this unspecific binding between cantilever tip and protein. (see Fig. II.11.)

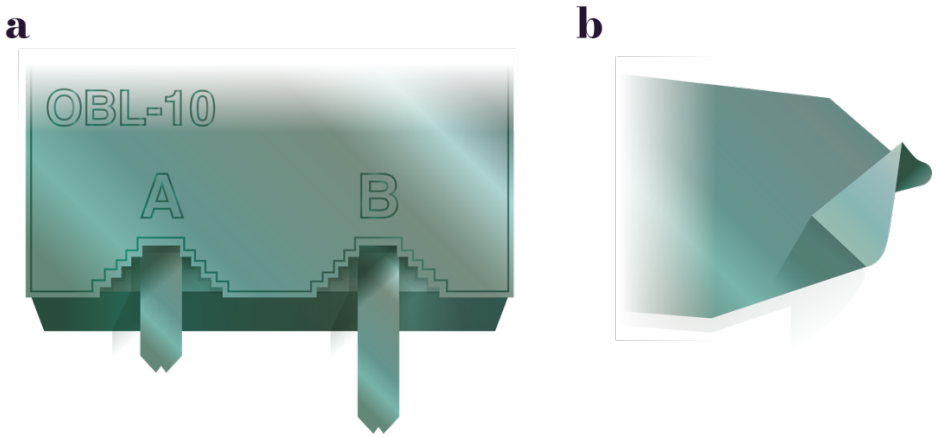

Fig. II.11. OBL-10 cantilevers. a. OBL-10 chip illustration (top side) showing both cantilevers A and B. b. (back side) showing the cantilevers tip proportions.

The final decisive part is PD, it is where the laser beam reflection will fall on. PD can translate the detected light into an electrical signal (V). PD is separated into four photodiodes, at beginning of any experiment we will spot the laser beam in the center of these four photodiodes, when a deflection of the reflection angle happens, due to the bending of the cantilever tip, the position of the laser beam into PD will change. Knowing the specific *k* of our cantilever tip, and the new position of the laser in the PD the exact force applied to our probe can be calculated. (see Fig. II.12.)

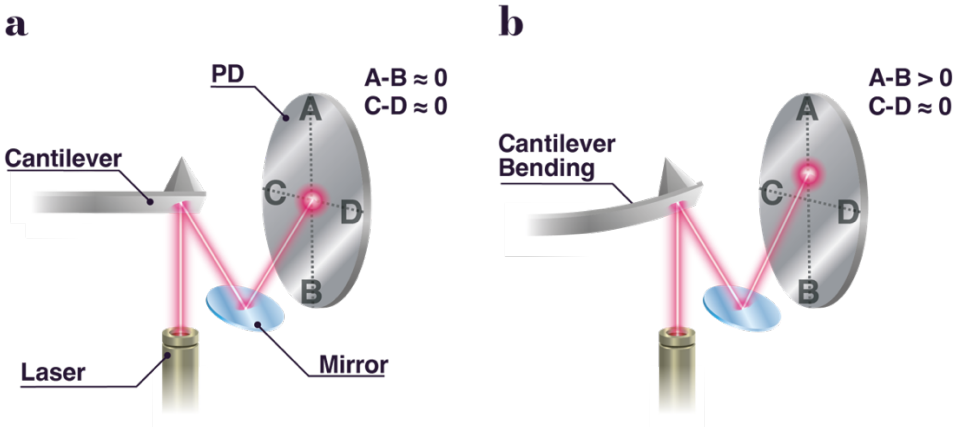

Fig. II.12. Four quadrant PD. Changing the position of the laser beam into de PD due to a bending of the cantilever provokes a deflection of the reflection angle. b. bent cantilever. a. relaxed cantilever.

AFM calibration and sample preparation

First, we prepared 14 x 14 mm gold substrates, by deposition of a 40 nm layer of gold into a 5 nm layer of titanium previously deposited in a 2 mm borosilicate substrate (Pi-Kem). Every deposition was made with an Oerlikon 450B Evaporation System (Leybold). The gold substrate was fixed on top of PZA thanks to vacuum grease (Dow Corning), next, we dropped 20 μL of our protein in a final concentration of around 20 μM and let it incubate for 20 min. As we explained in protein design apart, our protein has two cysteines in its C-terminal extreme which formed a covalent bonding with the gold present in the substrate, this is the reason for this incubation.

Meanwhile, we cleaned the liquid cell where the cantilever tip is accommodated and O-ring was filled with the same buffer in which our protein is dissolved, paying special attention to not introducing any air bubbles in this process. For this reason, a previous step of 10 min of buffer degasification is mandatory. To optimize AFM performance, it is desirable to filtrate buffers and samples, also to work with every buffer at RT.

Once we have our cantilever immersed in buffer, in this thesis we worked with Hepes buffer with every protein, we spotted the laser beam on the extreme of the reflective back cantilever tip, to achieve that we used a laser alignment function that controlled a cam connected with a 10x objective.

When protein adsorption time was completed, we washed using 100 μL of the same Hepes buffer and proceeded to face gold substrate with the O-ring present in the liquid cell to seal the chamber. Then the calibration of the experiment begins. (see Fig. II.13.)

To measure the force, as we mentioned before, the PD is a key part. The PD measures the cantilever deflection (Z_C) which behaves like a Hookean spring for small bending angles, then, following Hooke's law equation II.1. and knowing the cantilever deflection (Z_C) and its exact spring constant (k), the force applied (F) can be calculated:

$$F = -k \cdot Z_C \quad \text{(II.1.)}$$

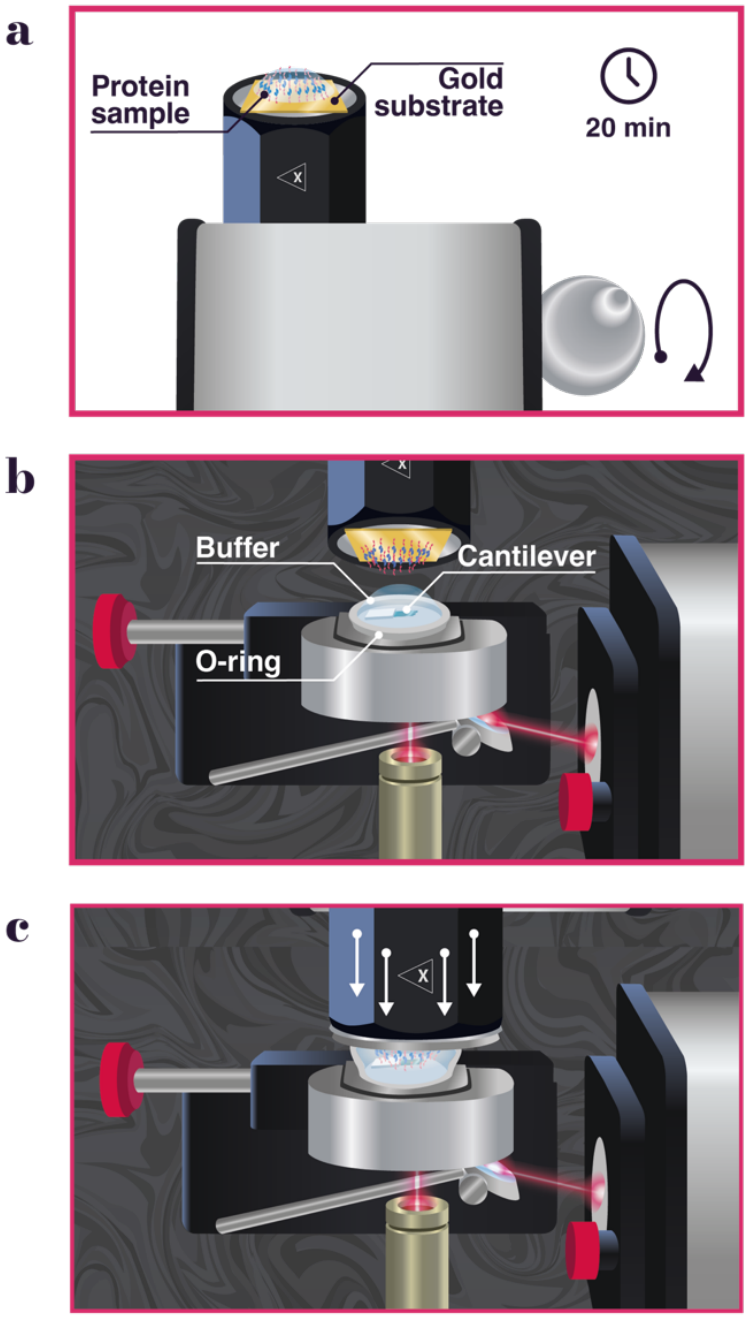

Fig. II.13. Sample adsorption, PZA, and liquid chamber sealing. a. adsorption of our sample into the gold substrate for 20 min, after this adsorption we washed the substrate with buffer and proceed to upside-down the PZA to face the liquid chamber. b. shows the O-ring rinsed with buffer where is immersed our cantilever. c. shows the sealing of the liquid chamber by approximation of the PZA.

The cantilever calibration comprises two steps to determine cantilever deflection and spring constant respectively. The first step consists in measure the thermal fluctuations of the cantilever when this one is far away from the PZA. Applying the Fourier-transformed to separate the main vibrational mode and integrating the area below this first resonance peak the first oscillation mode $\langle {Z_C}^2 \rangle$ can be calculated as $\langle V^2 \rangle$, being this the difference registered in voltage between the upper and lower quadrants in the PD.

For these calculations, the Equipartition theorem is applied in which (k) is the spring constant, (k_B) is the Boltzmann constant, (T) is the absolute temperature, and $\langle {Z_C}^2 \rangle$ is the first oscillation mode:

$$k = \frac{k_B \cdot T}{\langle {Z_C}^2 \rangle} \quad \text{(II.2.)}$$

In the second step, the cantilever must be approached to the PZA for the sake of measuring a deflection-extension curve. When both are in contact, cantilever bending in Z-direction (ΔZ_C) is the same as PZA Z-displacement (ΔZ_{PZA}). So, this slope correlates the change in the voltage (ΔV) measured by the PD and the cantilever bending (ΔZ_C) measured from the PZA movement:

$$s = \frac{\Delta Z_C}{\Delta V} \quad \text{(II.3.)}$$

Thanks to this slope correlation we can find out spring constant value from equation II.3., finally applying Hooke's law is possible to calculate how much force (F) is being applied to our protein:

$$k = \frac{k_B \cdot T}{\langle {Z_C}^2 \rangle \cdot s^2} \quad \text{(II.4.)}$$

At the beginning of every experiment the cantilever is calibrated, and its spring constant is calculated as explained before. (see Fig. II.14.)

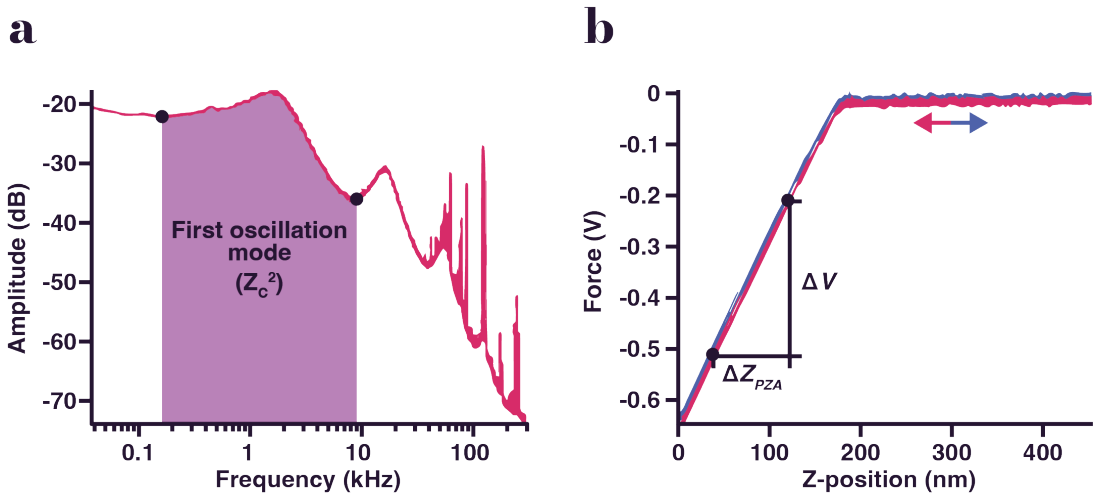

Fig. II.14. Cantilever two steps calibration. a. First oscillation mode b. slope

AFM operational modes

During this thesis 3 different operational modes were used for different purposes, being these: force extension (FX), force ramp (FR), and force clamp (FC).

Force extension

In this operational mode the PZA moves at a constant speed first approaching the cantilever and then going back, this result in stretching a single protein at a constant speed. The typical FX trace consists of a sawtooth pattern in which every peak corresponds to the unfolding event of each subdomain present in our protein construct. (see Fig. II.15.) depicts a typical FX experiment from the protein Caf-1.

First, the PZA exerts a force against the cantilever to pick up a single protein, being this one caught from end to end between the gold substrate present in PZA and the cantilever. Once the protein is trapped the PZA retracts continuously stretching our protein until its maximum length, where the cantilever begins to bend triggering a change in the angle of incidence light, reading this fact as a change in force by PD. The stretching force continuously increases until one domain from the protein

unfolds. In a homopolyprotein where every or some domains are the same, the mechanical unfolding of these domains is stochastic. The mechanical unfolding of one domain is produced by the disruption of contact present in its native structure, such as hydrogen bonding, salt bridges, or hydrophobic interactions.

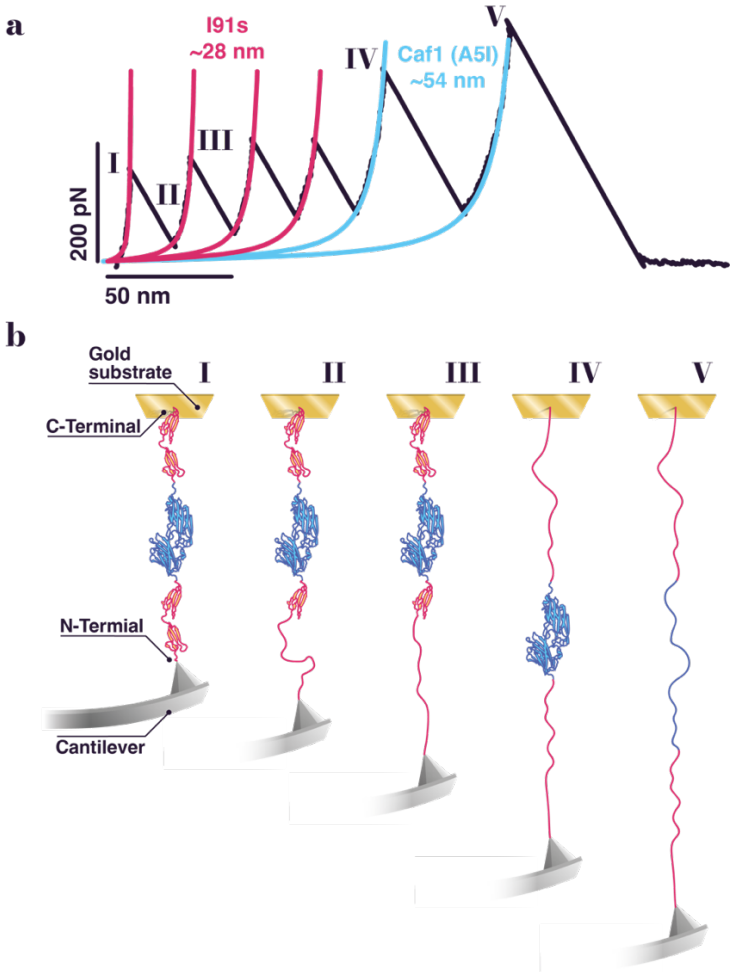

Fig. II.15. FX trace of (I91)2-Caf1(A5I)-(I91)2 mutant. a. red unfolding events correspond to four I91 subdomains used as a fingerprint, and the blue one corresponds to our protein of interest. b. depicted each step taken by the protein until its complete unfold I, the protein construct its complete stretch to its maximum length. II, stochastically one of the four I91 domains unfolds causing a drop in the tension force exerted on the construct. III, again the protein is stretched until its maximum length reaches a new maximum of tension force. IV, after three unfolding events we only have our protein of interest folded. V, Finally, when the system reaches the necessary force to unfold our protein of interest, it only remains the detachment event to happen.

When the unfolding of one domain happens the stretching force will drop due to the increase of the total length, returning the cantilever to its resting position until reaching the new protein total length, where force will increase progressively as far as a new unfolding event take place. Finally, when every domain is unfolded the force will rise until the protein detachment from the cantilever happens.

Force clamp

This operational mode consists in stretching a single protein at a constant force, to do that it is necessary a feedback loop that controls the PZA movement to constantly hold the predefined force. The feedback loop read the output force measured by PD and move the PZA to match with the input force, when any unfolding event happens the total length increase and for this reason the output force drop, then the feedback loop quickly, in a window of 5 milliseconds, correct PZA position to restore the force applied to the protein. The typical FC trace follows a staircase pattern in which every step corresponds with each unfolding event. The height of each step corresponds with the extension in length of each domain. An example of an FC trace is depicted in Fig. II.16. from a real measurement of $(I91)_2$-EnHD-$(I91)_2$.

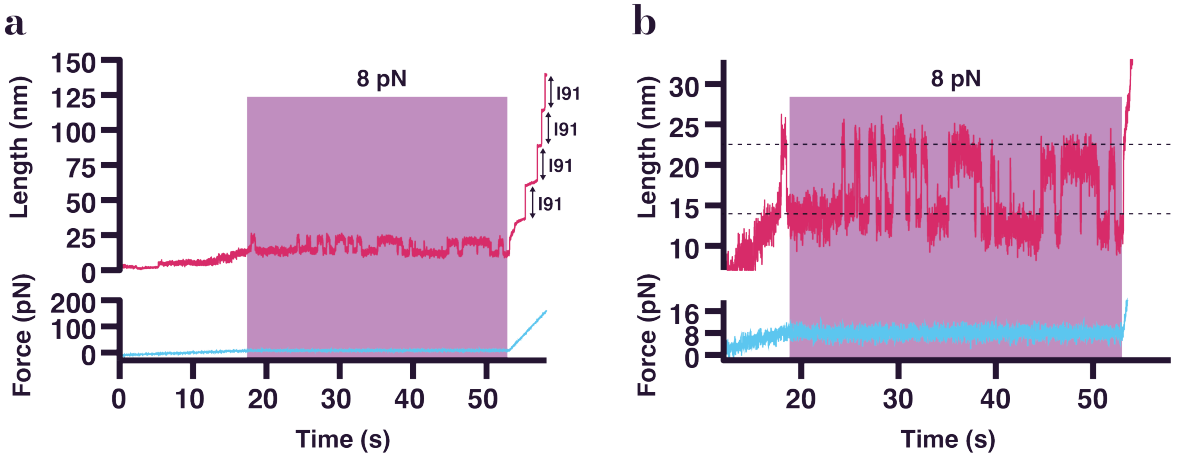

Fig. II.16. FC trace of (I91)2-EnHD-(I91)2. a. First, to reach the purple window at 8pN of constant force we applied a force ramp of 1pN/s, once that 8pN of force was reached this force was maintained for 35 seconds where a hopping behavior can be observed, the EnHD protein fluctuates between its unfolded and folded states with a total extension of approximately 10nm. Finally, another ramp was applied to unfold I91 domains. b. Zoom of hopping behavior from a.

Force ramp

In this operational mode the force applied to our protein change linearly with time. The work system is very similar to a force clamp, but instead of maintaining a constant force over time in this mode, the force will increase following a previously determined loading rate. An example of an FR trace is depicted in Fig. II.17. from a real measurement of $(I91)_2$-CD4D2D1-$(I91)_2$.

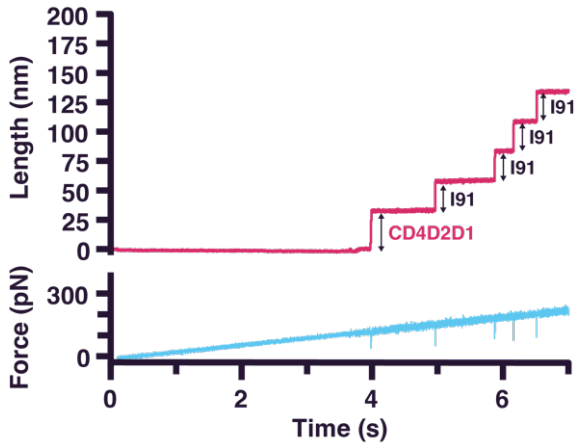

Fig. II.17. FR trace of (I91)2-CD4D2D1-(I91)2. A loading rate of 33 pN/s was applied to the protein CD4D2D1 in the presence of SUPROMER 1. Every step corresponds with the increase in extension of each domain in our polyprotein.

SmFS data analysis

The experimental data were analyzed with Igor pro software (Wavemetrics). The procedure was kindly provided by Prof. Julio M. Fernández laboratory (AFM_Analysis_V2.40.ipf). A modification of this procedure for force correction was kindly supplied by Mariano Carrión laboratory (LN_AFM_Analusis_V1.1_Filtering). In the case of FX data, each peak on the trace was fitted to the World-Like Chain (WLC) model for polymer elasticity equation II.5.

$$F(x) = \frac{K_B T}{p}\left[\frac{1}{4}\left(1 - \frac{x}{L_C}\right)^{-2} - \frac{1}{4} + \frac{x}{L_C}\right] \text{ (II.5.)}$$

Where (k_B) is the Boltzmann constant, (T) is the absolute temperature, (p) is the persistent length, (L_C) is the contour length, and (x) is the extension.

The difference of the estimated contour length of two consecutive unfolding peaks (ΔL_C) (see Fig. I.15.) corresponds to the released relative amount of amino acids during unfolding and is, therefore, a typical fingerprint of the protein sample used beside its unfolding force. I91 subdomains show ΔL_C of ~28 nm.

In the case of FC and FR, both show a staircase pattern in which every step corresponds with unfolding events of different domains in our polyprotein. Therefore the increase in length is measured as the difference in height before and after the step. I91 subdomains show ΔL_C of ~25 nm. Because of constant force, the protein is not stretched at its maximum as it is at a constant speed.

High-Throughput virtual screening Molecular Docking

To, find different molecules with the potential to mechano-modulate the protein CD4, a Molecular Docking was carried out. This High-Throughput virtual screening Molecular Docking includes the following steps.

Rational identification of CD4 surface receptor mechanical regulators:

Compound selection criteria

A virtual screening protocol was set up to identify small molecules that can modify the mechanical properties of CD4. In this sense, the critical properties of an ideal CD4 mechano-modulator were established in this work as follows:

- Should display a substantial (at least nanomolar) binding to CD4.
- Should not compete directly with MHCII or gp120 binding to CD4.
- Should have optimal ADMEt properties.
- Should enjoy complete freedom of operation at the industrial property level

In addition, the commercial availability and price of the compounds identified were also considered. (see Fig. II.18.)

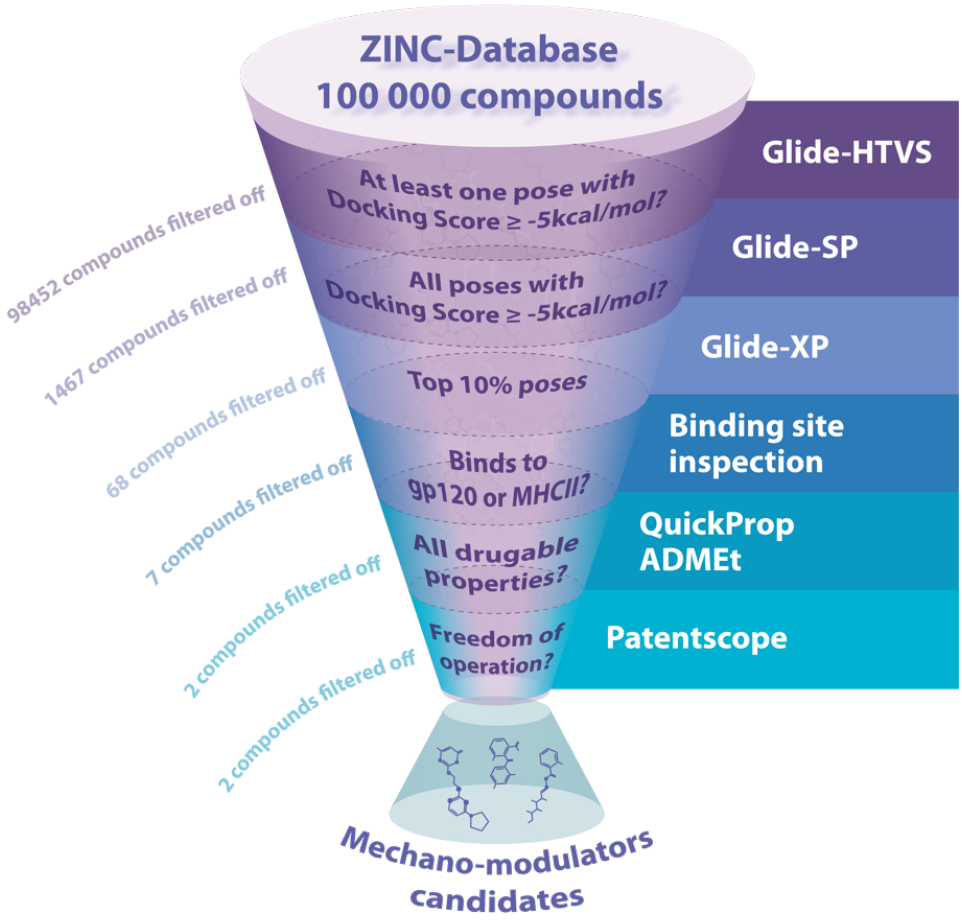

Fig. II.18. Workflow is used to identify protein mechano-modulators. The critical properties of an ideal mechano-modulator were established as follows: it should display a solid binding to the problem protein. To achieve this, we make use of Glide-HTVS, Glide-SP, and Glide-XP; they should not interfere with the protein binding site or any relevant epitope/active site, depending on the problem protein; they should have optimal ADMEt properties and should enjoy complete freedom of operation at the industrial property level.

Receptor preparation

The following procedure was followed to quantify the binding affinity of known molecules to CD4: The structure of residues 1-178 of the human T-Cell surface glycoprotein CD4 was downloaded from the protein data bank (PDB ID: 1WIP) and prepared with the Protein Preparation Wizard of Schrödinger suite. The pre-processing was done with default methods, and H-bond refinement was carried out with a default pH value of 7. Three Glide Grid files with an enclosing box of ca. 46 Å were created using the above structure, centered on Ser23, Leu95, and Val146, respectively (Supplementary figure 1), which adequately cover CD4-D1, CD4-D2, and the CD4-D1D2 interface, respectively.

Ligand preparation and docking

Molecules (ligands) to be screened were downloaded from the ZINC Database, a free database of commercially available compounds for virtual screening. Approximately 100.000 compounds of the lead-like subset of the ZINC database (add names to the SI) were prepared for docking using LigPrep 5 with the OPLS_2005 force field. To set compounds' ionization and tautomerization state at a pH range of 6–8, Epik v16207 was used, with a maximum number of 4 generated structures. The binding affinity of 100000 lead-like prepared compounds was estimated through a three steps docking protocol summarized as follows (Supplementary figure 1): a) a High Throughput Virtual Screening (HTVS) Glide procedure of all the compounds and a subsequent filtering-off of those that did not display a single pose with a binding affinity (docking score) above a predefined lower-limit value of -5 kcal/mol; b) a Standard Precision (SP) level Glide docking procedure applied to those compounds overcoming the HTVS filter and a subsequent selection of those compounds displaying consistent binding affinities (docking scores) above -5 kcal/mol in all their poses; c) an extra precision (XP) Glide docking and selection of top binders (10%).

Forbidden binding site

The compounds overcoming the mentioned energy barriers. We subjected to a second analysis focused on identifying their binding regions, aimed at discarding drug candidates that would competitively interfere with either MHCII or gp120 binding. In this line, two distinct regions with “forbidden residues” were defined in the CD4 structure (Supplementary figure 3), a part defined by residues 35-52, 55-60, and 164-165 (MHCII binding epitope) and an area around residues 29, 35, 43-47 and 59 in D1 tip (gp120 binding epitope). By discarding compounds that bind strongly to any of these two regions, experimental observations derived from AFS experiments, gp120 binding inhibition experiments, and HIV viral entry assays will be ascribed only to changes in the mechanical properties of CD4.

Final selection criteria

The ADMEt properties of the non-competitive and efficient CD4 binders identified so far were estimated using the Quick prop module of the Schrödinger software (Schrödinger Release 2017–4: Canvas, Schrödinger, LLC, New York, NY, 2017). Also, the conclusions derived from a deep analysis of these compounds' patentability, market price, and availability were crucial for selecting the final molecules to be tested as novel CD4 mechano-modulators.

Cell thawing

To, work with the TZM lb cell line. First, we must thaw an aliquot from the N2 tank. We started by warming the DMEM media and our TZM lb aliquot into a water bath at 37ºC. Once that media reached the desired temperature, we mixed 9mL of media with our aliquot content into a 15mL falcon under the hood. Then a centrifugation step (300xG for 5 minutes) was done to remove the DSMO content from the freezing buffer. After centrifugation, the supernatant was removed, and the pellet was gently resuspended in 1ml of media. Finally, a 75cm^2 flask was filled with 9mL of media,

and the 1 mL aliquot previously prepared, the Passage number, was written down on the flask.

Cell passage

Once we got our cell line from thawing, we must repeat some passages to achieve maximum performance in our cell experiments. First, we must detach our cells from the flask. To do this, we must aspirate the media, wash our cell culture in 15 ml of PBS at 37ºC and aspirate again. Then, 10 ml of diluted trypsin at 37ºC was added and incubated at 37ºC for 5 minutes. After this incubation time, the cell culture should be detached from the surface. In another case, the incubation time should be extended and gently hit the flask to remove the cells from the flask surface. The trypsin was equilibrated with the same amount of FBS-containing media (10 ml) and resuspended several times, finally filling the cell suspension into a 50 ml falcon. A centrifugation step (300xG for 5 minutes) was done, the supernatant was aspirated, and the pellet was resuspended into 1 ml of media, then diluted into the same amount of media that was before in the flask. To calculate the cell concentration, a dilution of 1:100 was done, and 10 µl was used to fill a KOVA Glasstic slide (REF 87144). The concentration was calculated using the following equation II.6. when counting nine small squares:

$$concentration\ (1/ml) = \frac{nº\ cells \cdot Dilution\ factor}{nº\ squares \cdot 1.1 \cdot 10^{-5}} \quad \text{(II.6.)}$$

When the concentration was calculated, the corresponding cell volume was added to the flask and then incubated at 37ºC.

MTT cytotoxicity assay

After two weeks of TZM lb passage, our cell cultures were ready to try a cytotoxicity assay using our SUPROMER. We used a colorimetric assay using MTT, which measures the metabolic activity by a reduction that takes place in the mitochondria

of viable cells. In those cells, this reactive change its color from yellow to purple, measured at 590 nm. To do that, our cell culture was grown in a P96 well plate. When cell coverage was optimum, the assay began. Every well was treated with different concentrations of SUPROMER and Ibalizumab, After the convenient incubation time, media from every well was discarded, and a 100 μl of a mixture of FBS-free media and MTT solution (ratio 1:1) was added to every well, we let incubate at 37ºC for 3 hours. After incubation, 150 μl of MTT solvent was added to each well, incubated, wrapped in foil, and shaken on an orbital shaker at RT for 15 minutes. Finally, absorbance at 590nm of each well was measured in Victor equipment.

Bacteria Magnetization

First, we must prepare and functionalize our magnetic beads (Dynabeads M-270; Invitrogen) with our desired protein. In this case, we functionalized our magnetic beads with human fibronectin protein. To do so, we must wash 5 mg of magnetic beads with PBS. Using a magnetic rack, we can pellet the beads and perform any washing step. To proceed, we must incubate our magnetic beads in MES solution containing 0.1M EDC and 0.7M NHS for one hour at 20ºC. Once incubation is complete, the magnetic beads must be washed twice with pH 6.5 PBS. Finally, we must add 150-250 μg of the desired protein (human fibronectin) and incubate at 20ºC overnight. Now, we must cease the functionalization with a saturated solution of glycine (20 mg) for 30 minutes. Following this, we must wash our functionalized magnetic beads twice in PBS and then resuspend them in 1 mL PBS.

Now that our magnetic beads are functionalized with human fibronectin, we must bind them to our desired bacteria, in this case, Staphylococcus aureus SH1000 FnBPA+. Strain SH1000 lacks most MSCRAMMS proteins, but strain SH1000 FnBPA+ has a fibronectin binding protein A plasmid that overexpresses the mentioned protein. First, we must grow these bacteria until reaching an O.D. of 0.2. Once this O.D. is reached, we mix 1mL of bacteria with 100 μL of functionalized magnetic bead (0.5 mg) and incubate at RT with agitation for no more than 2 minutes. It is important to not incubate for a long time in order to avoid unspecific binding, as we want to bind the bacteria to the bead through FnBPA present in the cell wall of the bacteria to human fibronectin protein present in the surface of the bead. We must gently wash our mixture of bacteria and magnetic beads three times in PBS. We must pipet slowly to be sure not to disrupt the bond between the bacteria

and magnetic beads. Finally, we must resuspend our bacteria and magnetic bead tandem in 1mL of PBS and we get our magnetic like bacteria.

Glass slide functionalization

In order to prepare the adequate surface needed for further we must begin by depositing the protein (human fibronectin) onto the surface of a NHS-glass slide (24x74mm) and allowing it to incubate overnight in a water-saturated atmosphere. The slide is then washed twice with PBS (phosphate-buffered saline) followed by a wash with PBS-T (PBS with Tween-20 0.5%). Next, the coverslip is blocked with 10% BSA (bovine serum albumin) in PBS-T for a duration of 2 hours. After the blocking step, the slide is washed three times with PBS-T.

Magnetic tip calibration

Before starting the measurement, the sample needs to be prepared. The sample holder consists on a glass slide (24x74mm) and a gasket (Sigma Aldrich).
Now put vacuum grease on the bottom of the gasket and press it on the glass slide. For the force calibration we must use the same magnetic beads that we are using in experiments (Dynabeads M-270; Invitrogen).

In order to start the magnetic tip force calibration, the magnetic tip has to be installed inside the confocal microscope LSM 710. As a reference liquid with high viscosity, we use DMPS Dimethylpolysiloxane. The DMPS has such a high viscosity that taking something out with the normal pipette is quite difficult, so you can also use a spatula. With that you fill the gasket. Now take 4µl of the dynabeads inside a small eppendorf. Proceed to Pelleted the magnetic beads using the magnetic rack and removing all the liquid and then mixing it with the DMPS inside the gasket. It has to be well mixed in order to separate some beads from each other.

The gasket can now be inserted into the sample holder. Then turn on the LSM/PC and the magnetic controller/PC. Now with using the magnetic tip controlling joystick move the tip into the DMPS liquid and bring it into the focus of the 10X objective.
Now center the magnetic tip, change the objective to the 63X objective and focus on the magnetic beads. Now Drive the tip up or down in order to be in the same focus

like the magnetic beads. Once you have beads and tip in focus use the Time Series option in the confocal microscope software to produce brightfield pictures with a certain time interval (minimum is 0.2s with the inserted camera). (see Fig. II.19.) Before applying any voltage to the circuit which provokes the magnetic field, click the Des- magnetize button in the software. Now the real signal can be applied.

In order to start the calibration first click the start button for the Time Series brightfield acquisition. Then click the manual button in the magnetic tip software, which applies a voltage of desired magnitude. With time the bead will get closer to the tip until it finally reaches it. Afterwards click again on the manual button and stop the acquisition of the Time Series images. Save the images as an .lsm file.

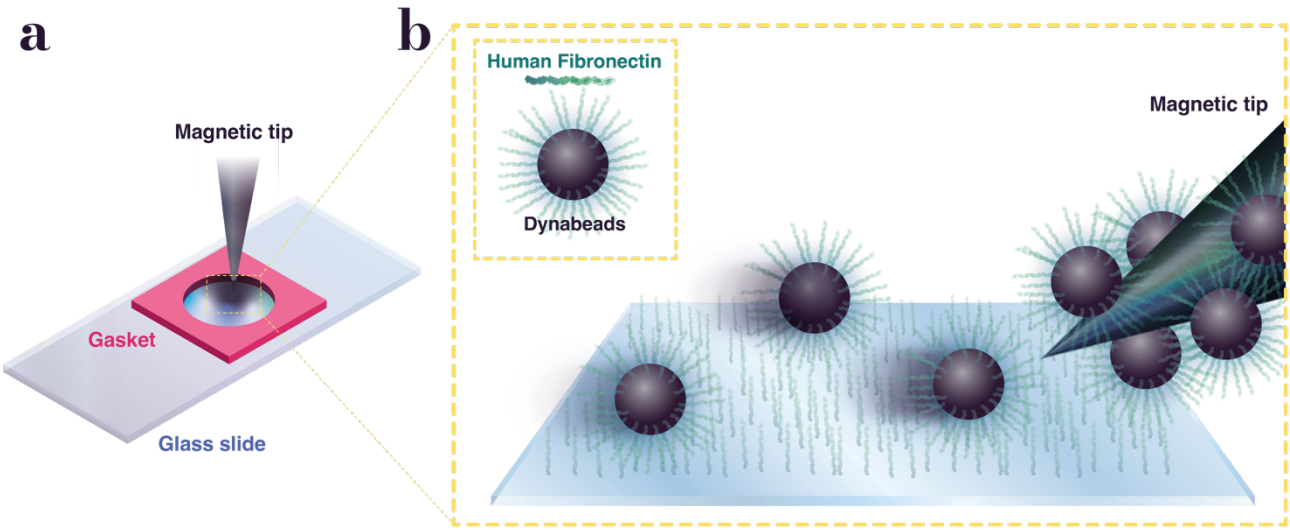

Fig. II.19. Schematic representation of the magnetic tip calibration process. Our magnetic beads (Dynabeads) are functionalized with the protein human fibronectin, which is critical for measuring our bacterial attachment force.

The Time Series .lsm file can now be analyzed using the free available ImageJ software with the Nano Tracking plugin. This plugin enables the estimation of the coordinates (which is directly converted into distance in µm) of the magnetic beads while reaching the magnetic tip. Load the .lsm file directly in the software and then go to Plugin → Analyze → Nano Tracking.

- Conversion factor from pixel size to µm; 0.1023810 · pixel when using a 63X objective
- Absolute viscosity (Pa*s), which is calculated by the kinetic viscosity (12500 · -6e(m^2)) s and the density 0.98 · 3e (kg)m^3
- The Magnetic bead radius r in (m) (2r is around 2.8µm for the used M270 beads).
- Sampling time dt, which is set with the Time Series option. (fixed to 0.25s)

When executing the Matlab file, you will have to choose now the first and then the last image. With the cursor click on the tip. The procedure file will estimate then the drift of the tip while taking the time series image.
Then the velocity of the bead is being calculated from the position coordinates and the sampling time dt.
The final distance d is calculated from the vector deriving from bead position minus the tip position and from $d^2 = d^2x + d^2y$.
For calculating the force F stokes equation is being used. The velocity vector is calculated from the velocity vector of the bead. Then again $v^2 = vx^2 + vy^2$. v need to be in m/s. Then the force is being calculated by $F = 6 * \pi * r * \mu * v$ with µ being the absolute viscosity.
Then the vector for distance d and force F is being saved also as a .csv file (.dat) And the F vs d curve will be plotted in (m vs µm). The curve should be fitted with a power function.

These measurements were conducted in triplicate for each voltage applied by the magnetic tip, ranging from 0.0V to 2.5V in 0.1V increments. With these measurements, we were able to construct a series of standard curves that relates the magnetic tip voltage, magnetic tip distance, and magnetic force applied to the magnetic bead. Using these standard curves, we are able to clarify the magnetic force applied to our sample during actual measurements, where we are measuring the attachment force of a specific bacteria.

Attachment force measurements

For taking real measurements in which, we are analyzing the bacterial attachment force we design the following methodology, in which our study bacteria is attached

to the glass slide surface through exactly the same binding that we have designed before with the magnetic bead. The bacterium is attached like a sandwich between the glass slide surface and the magnetic bead thanks to the same MSCRAMM protein binding to the same target, for this reason when we will measure the force necessary to break the bacterial attachment, we can take it as positive results both breaking when we detach the bacteria-magnetic bead tandem from the glass slide surface or when we detach the bacteria from the magnetic bead, both are valid. (see Fig. II.20.)

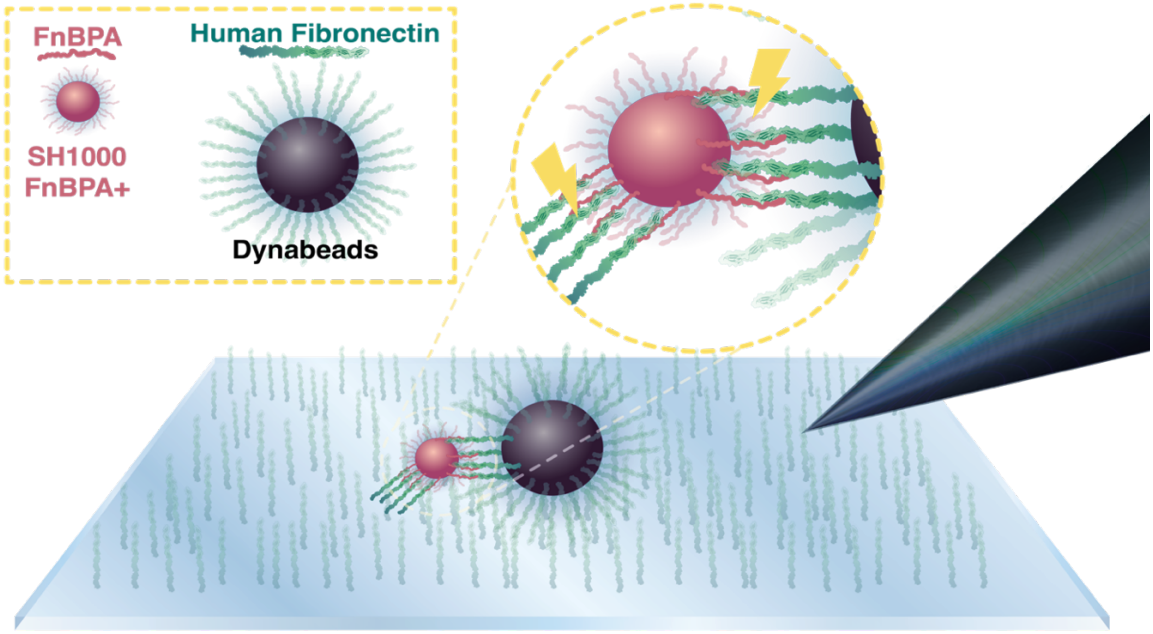

Fig. II.20. Schematic representation of bacterial attachment force measurements. Our magnetic like bacterium (SH1000 FnBPA+) is sandwiched between functionalized glass slide surface and magnetic beads (Dynabeads) both bonding is done through FnBPA present in the bacteria and human fibronectin present in the glass slide and the magnetic bead. Yellow lightning represents that both ruptures are exactly the same so, the measurement of both detach is valid for future analysis.

Once we have focused one magnetic bead with a single bacterium attached we must apply a ramp protocol to the magnetic tip in which the voltage applied to the tip will increase linearly with time, while the process is recorded in the precise time that the bacteria detach from the glass surface or from the magnetic bead the voltage applied can be calculated, and knowing the distance of the magnetic bead from the magnetic tip, the magnetic force applied to the bacteria can be extrapolated thanks to the previously elaborated standard curve.

Chapter III:
compliant mechanical response of the ultrafast folding protein EnHD under force

Antonio Reifs[1], Irene Ruiz Ortiz[2,3], Amaia Ochandorena Saa[1], Jörg Schönfelder[1], David De Sancho[2,3], Victor Muñoz[4,*], and Raul Perez-Jimenez[1,5,*]

1. *CIC nanoGUNE BRTA, Tolosa Hiribidea 76, 20018 San Sebastian, Spain.*
2. *Faculty of Chemistry, University of the Basque Country (UPV/EHU), Manuel Lardizabal Ibilbidea 3, 20018 San Sebastian, Spain.*
3. *Donostia International Physics Center (DIPC), Manuel Lardizabal Ibilbidea 4, 20018 San Sebastian, Spain.*
4. *Department of Bioengineering, University of California, 95343 Merced, California, USA*
5. *Ikerbasque Foundation for Science, Plaza Euskadi 5, 48009 Bilbao, Spain.*

*Corresponding Authors

Ultrafast folding proteins have become an important paradigm in the study of protein folding dynamics. Due to their low energetic barriers and fast kinetics, they are amenable for study by both experiment and simulation. However, single-molecule force spectroscopy experiments on these systems are challenging as these proteins do not provide the mechanical fingerprints characteristic of more brittle proteins, which makes it difficult to extract information about the folding dynamics of the molecule. Here, we investigate the unfolding of the ultrafast protein Engrailed Homeodomain (EnHD) by single-molecule atomic force microscopy experiments. Constant speed experiments on EnHD result in featureless transitions typical of compliant proteins. However, in the force-ramp mode we recover sigmoidal curves that we are able to interpret using a combination of a simple theoretical model and coarse-grained molecular simulations. Our results show the ability of force to modulate the unfolding dynamics of ultrafast folding proteins.

Introduction

Most single-domain proteins exhibit an all-or-none folding behavior due to the high energy barriers that need to be overcome during the (un)folding process. The (un)folding of this type of proteins is highly cooperative (Guinn et al. 2013), and equilibrium and kinetic experiments on this type of systems where the equilibrium is perturbed either by temperature or a chemical denaturant is easily interpretable. However, given that the molecular ensemble almost entirely distributes between the folded and unfolded state, it is not possible to extract information about the folding mechanism, i.e., the myriad of conformations that are visited as the protein evolves towards the native state (Carrion-Vazquez et al. 1999). This becomes possible for ultrafast folding proteins, which lie at the other side of the cooperativity spectrum. They fold in timescales between milliseconds and microseconds and are characterized by their small size, typically helical structure and low (<3kBT) free-energy barriers (Garcia-Mira et al. 2002). For this reason, there is measurable population in the intermediate states of the protein, which could in principle be resolved by spectroscopy and, potentially, even at the single-molecule level.

After their initial applications to protein folding three decades ago, single-molecule force spectroscopy (smFS) techniques are now established as a means of accessing details of the (un)folding process that are distinct of those derived from traditional methods reliant on ensemble averaging(Schönfelder, De Sancho, and Perez-Jimenez 2016). smFS techniques either using optical or magnetic tweezers or an atomic force microscope (AFM) allow direct manipulation of an (un)folding reaction coordinate throughout the application of controlled mechanical forces (Tapia-Rojo, Eckels, and Fernández 2019; Schönfelder, Perez-Jimenez, and Muñoz 2016; Bustamante et al. 2020). Two-state and multi-state proteins often have easily interpretable signals upon mechanical unfolding, e.g., a saw-tooth pattern characterized by well-defined contour lengths in constant speed mode, or discrete jumps of measurable extension in the force-ramp and force-clamp modes(Perales-Calvo et al. 2018; Alonso-Caballero et al. 2018; Perez-Jimenez et al. 2014). However, as the cooperativity of the protein decreases, proteins oppose less resistance to the external force and these fingerprints become less predictable or disappear altogether. For example, Rief and his co-workers studied the prototypical

ultrafast folder villin headpiece subdomain using optical tweezers (Zoldak et al. 2013) They obtained continuous hump-like equilibrium transitions at a range of pulling speeds and completely featureless constant force traces at the midpoint. More recently, Perkins and his co-workers studied the computationally designed, three helix bundle α3D (Edwards et al. 2017; Walder et al. 2017; Edwards, LeBlanc, and Perkins 2021a), which in bulk also folds in the microsecond regime (Zhu et al. 2003). α3D turned out to be extremely labile under force, resulting in a barely distinguishable peak of less than 12 pN. In previous work, we studied the reversible folding and unfolding protein gpW at constant force under the AFM (Schönfelder et al. 2018; De Sancho et al. 2018). We resolved hopping transitions in an energy landscape with a low free energy barrier induced by the external force.

Here we expand the realm of ultrafast folders studied using smFS examining the mechanical unfolding of the Engrailed Homeodomain (EnHD), a DNA binding domain of the transcription factor engrailed from Drosophila melanogaster. EnHD is a three helix bundle of 54 residues that folds close to the protein folding speed limit, in the range of a few microseconds, and has been extensively characterized in bulk (Mayor et al. 2000; Mayor et al. 2003; Religa et al. 2007). From the analysis of calorimetric and kinetic experiments, it has been predicted to have a marginal folding barrier (Naganathan, Sanchez-Ruiz, and Muñoz 2005; Naganathan, Doshi, and Munoz 2007). Remarkably, EnHD did not fold into its conformation in a set of long time-scale atomistic simulations, but another homeodomain exhibited a downhill free energy surface (Lindorff-Larsen et al. 2011). Our pulling experiments show that EnHD has a weak mechanical stability, as expected for a protein that folds over a marginal free energy barrier. When subjected to a gradually increasing mechanical force (i.e., a force-ramp) the observed signature is not stepwise but sigmoidal. We interpret these results using a simple theoretical model and molecular simulations using a coarse-grained simulation model. The emerging picture is that of a very compliant protein that folds and unfolds many times over a marginal barrier induced by the applied force.

Results

• Single-molecule force-extension experiments at constant speed

For our AFM experiments we engineered a polyprotein where the protein EnHD (PDB code:1enh), (see Fig. III.1a.) is sandwiched between two pairs of I91 domains of human cardiac titin, resulting in the $(I91)_2$-EnHD-$(I91)_2$ construct. The I91 domains serve as mechanical handles when the polyprotein is subjected to mechanical force. (see Fig. III.1b.) Importantly, the mechanical properties of I91 such as unfolding force and contour length (ΔLc), are well characterized and are clearly distinguishable in force spectroscopy measurements (Peters et al. 2022; Manteca et al. 2017).

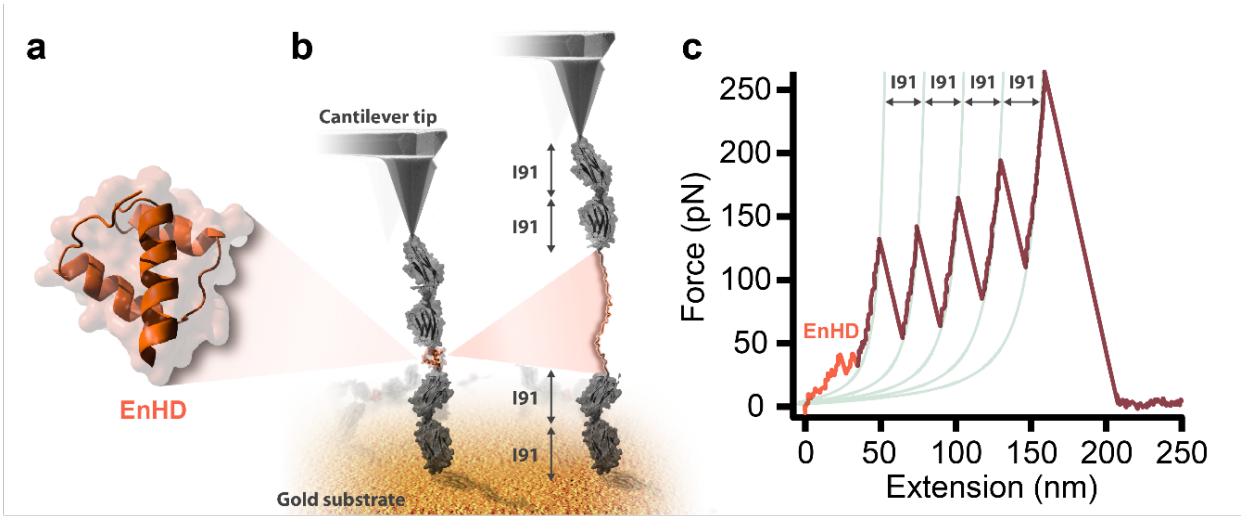

Fig. III.1. Single-molecule force-extension experiments. a. Representation of the crystal structure of the EnHD domain. b. Scheme of the experimental setup. The EnHD is sandwiched between two titin homodimers, deposited in solution over a gold surface and dragged by the AFM cantilever, resulting in the unfolding of the proteins. c. Force-extension trace including the characteristic sawtooth pattern for the titin domains, and the initial featureless signal for EnHD. Stretching is conducted at a speed of 40 nm s^{-1}.

Thus, I91 serves as a molecular fingerprint for an adequate trace selection when the mechanical properties of the protein of investigation are difficult to recognize. In the case of EnHD, this is particularly important given its weak cooperativity, which may result in a featureless signal under force.

Firstly, we conducted force-extension experiments where the EnHD polyprotein is forced to elongate at a constant velocity of 40 nm s^{-1}. The unfolding of the molecule typically creates a sawtooth pattern in these experiments because the unfolding of each domain is composed of a stage of building up force while the domain remains resistant to the applied tension followed by a sudden drop on the registered force due to the triggering of unfolding. Registered measurements show the characteristic sawtooth pattern for I91 domains, (see Fig. III.1c.) and the analysis with the worm like chain (WLC) model reveals a mechanical stability of approximately in the range of 181±8 pN, although it depends on the unfolding speed, and a ΔLc of 28±1 nm, in agreement with what is described in the literature (Perez-Jimenez et al. 2006). (see Fig. III.2.) Conversely, no clear sawtooth pattern is detected for the unfolding EnHD. This suggests that EnHD has a very low mechanical resistance and unfolds at very low forces, so it goes virtually undetected on force extension experiments.

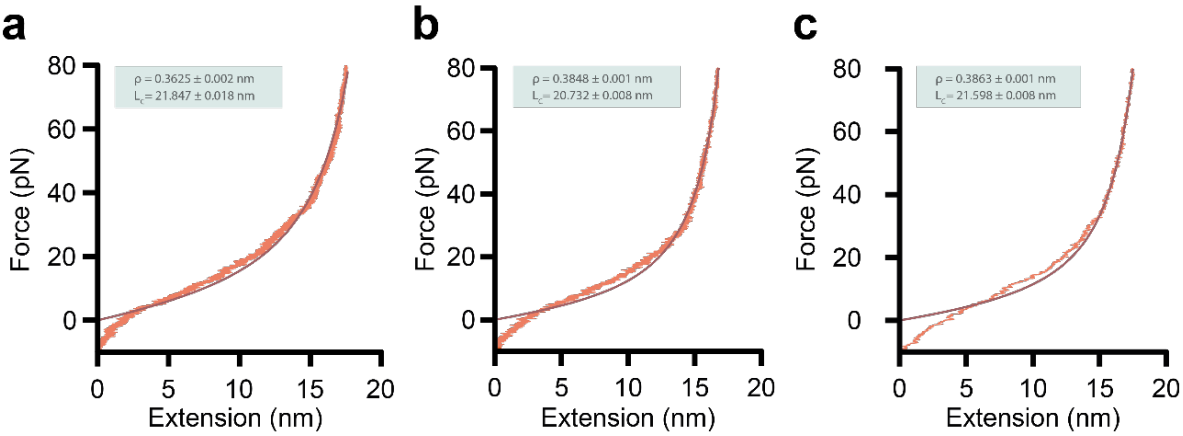

Fig. III.2. WLC model fitting to Force vs extension plot. a. Average plot from traces at 1 pNs-1. WLC model fit to unfolded state with a persistent length of 0.36 and a contour length of 21.84 nm. b. Average plot from traces at 10 pNs-1. WLC model fit to unfolded state with a persistent length of 0.38 and a contour length of 20.73 nm. c. Average plot from traces at 100 pNs-1. WLC model fit to unfolded state with a persistent length of 0.38 and a contour length of 20.73 nm.

• Coarse-grained molecular dynamics simulations

These experimental results are consistent with coarse-grained molecular simulations using a structure-based all-atom simulation model (see Methods).

First, in native conditions the protein exhibits a unimodal free energy surface derived from the projection on the relevant reaction coordinate for folding, the fraction of native contacts, Q. (see Fig. III.3a.) Upon the application of an external force that pulls from the protein ends at constant extension speed, EnHD is very compliant, resulting in a low force peak. (see Fig. III.3b.) Because the units in the model cannot be compared directly with those in the experiment, we show the same result for pulling simulations on an immunoglobulin-like domain of titin used as a fingerprint for reference.

The simulations recover the stark differences between a mechanically resistant protein and the featureless force-extension pattern for EnHD. We show snapshots of different conformations along the unfolding trajectory in Fig. III.3d.

The mechanical unfolding involves untangling the bundle, followed by the melting of the alpha helices. We have also run constant force simulations using our coarse-grained model. Like we found for protein gpW (Schönfelder et al. 2018), force induces a small free energy barrier of approximately ~2 kBT that separates two well defined minima in the protein landscape. (see Fig. III.3a. and Fig. III.3c.)

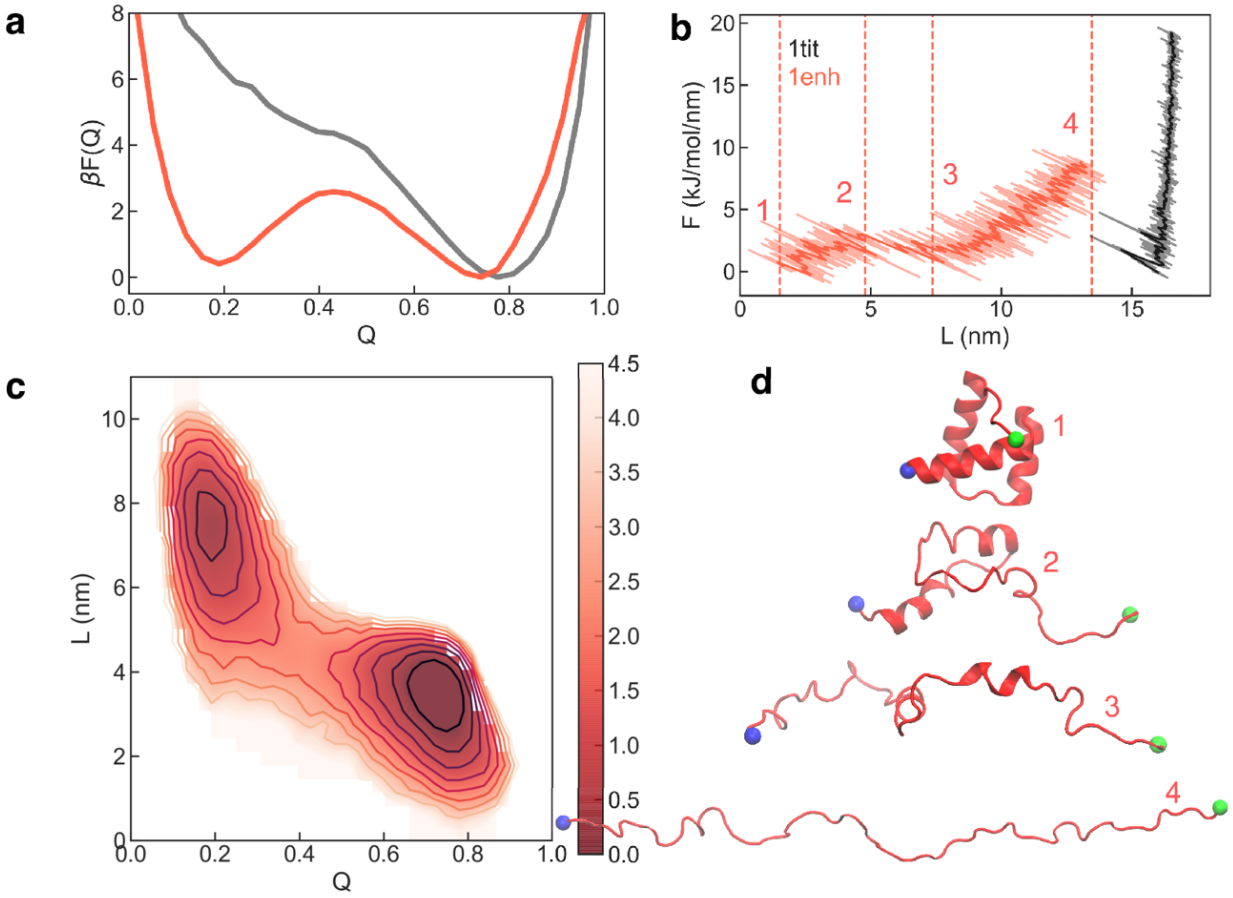

Fig III.3. Course-grained molecular dynamics simulations a. Potential of mean force for the projection of coarse-grained simulations on the fraction of native contacts, Q. The black curve corresponds to the simulations in native conditions and the red curve at the mechanical midpoint. b. Force-extension curves from simulations at constant pulling speed of 1e-3 nm/ps for EnHD (red) and titin (black). c. Free energy landscape for both the end-to-end extension, L, and Q. Contour lines mark 0.5 kBT. d. Cartoon representation of different conformations sampled during the mechanical unfolding, with timestamps relative to the numbering in. The green and blue beads correspond to the alpha carbons of the N and C-termini, respectively.

We note that a similar hopping pattern between the folded and unfolded states is observed in experiments performed at a constant force of 8 pN, (see Fig. III.4.) although we were able to measure only few of these events due to the complexity of low force experiments using our AFM.

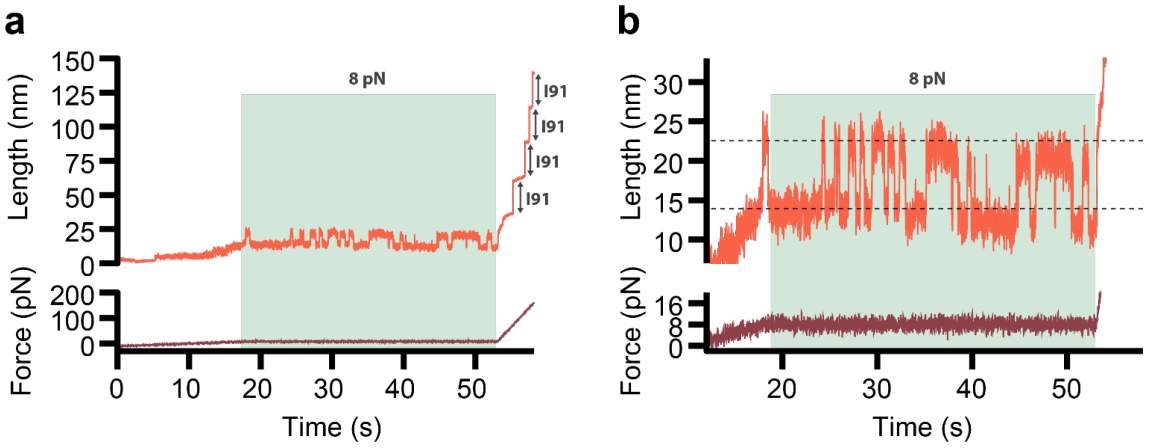

Fig. III.4. two states behaviour of EnHD under mechanical force (un)folding. a. Force clamp trace: first, we applied a force ramp of 1pNs-1 until reaching a force of 8pN, we maintained our protein at this force during 35 second and finally we applied a force ramp to unfold the I91 in our construct. During the 8pN constant force we observed a hopping transition. b. Hopping behaviour from a., the EnHD protein fluctuates between its unfolded and folded states with a total extension of approximately 10nm.

• Single-molecule force-ramp experiments

To further resolve the mechanical unfolding of the EnHD protein, we prepared force-ramp measurements at different values of the force loading rate. This approach gives an accurate control of the applied force due to the intervention of a feedback loop that compensates for changes at a window of time below 1 ms. Thus, this protocol permits scanning a broad range of unfolding forces while controlling the force applied. The force protocol starts by pushing the cantilever against the gold substrate with a 10 pN force. Then, the cantilever slowly pulls from the protein at the desired loading rate (we used values of 1, 10 and 100 pN s^{-1}), providing enough resolution to detect the unfolding response of our protein at both low and high forces. Finally, the rate is increased so that forces high enough to unfold I91 are reached more quickly. For two-state proteins, this type of experiments typically registers discrete jumps with lengths extensions that are force dependent and that can be explained by models of polymer elasticity such as the Worm-like chain or freely-jointed chain

(Oberhauser et al. 2001; Schlierf, Li, and Fernandez 2004). However, for EnHD we obtained an unexpected sigmoidal unfolding pattern at forces below 20 pN. (see Fig. III.5a. and Fig. III.6.) In the final force ramp at an increased loading rate, we observe the events corresponding to the four titin repeats with a characteristic 24.5 nm length. The initial change in the extension matches the extension of EnHD of 12 nm expected in this range of force, suggesting that this unexpected behavior corresponds to the unfolding.

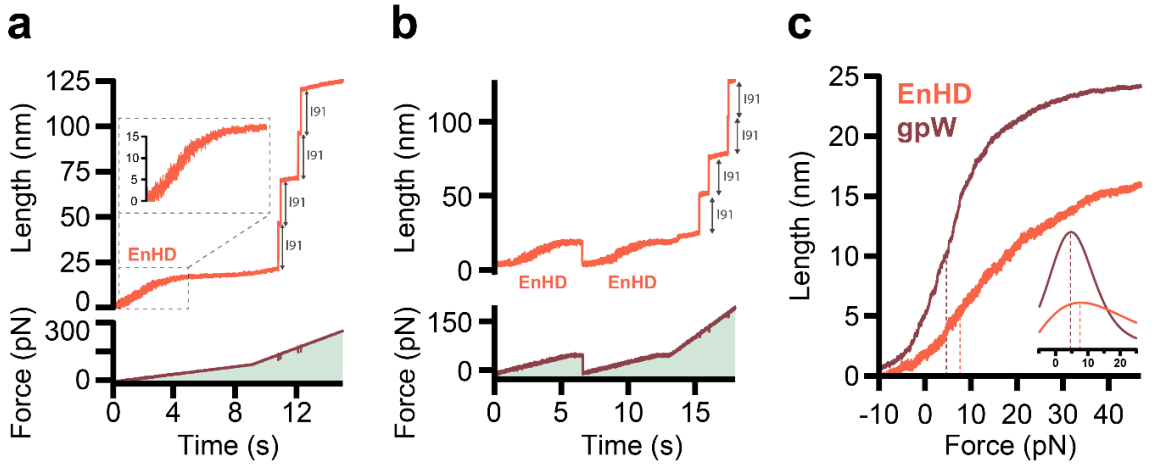

FigIII.5. Single-molecule force-ramp experiments. a. Time series for the measured extension (top) and force (bottom) in a force ramp experiment at 10 pN/s. The inset highlights the signal corresponding to EnHD unfolding. b. Same as a., but now including two consecutive low loading-rate force ramps separated by a force-quench. c. Average force extension curve from multiple traces for EnHD and protein gpW (n=29 for both). The inset is the first derivative of the sigmoidal fit.

To discard the possibility of any unspecific interactions between the protein construct and the surface, we repeat the cycle by quenching the force after the initial sigmoidal increase followed by another force-ramp at the same loading rate, which resulted in a similar sigmoidal increase very much like in the first event. (see Fig. III.5b.) This reproducibility in a single protein domain suggests that we are indeed looking at the mechanical unfolding of EnHD. The sigmoidal curves that we report have not been observed in the smFS literature before and must be interpreted with care. In Fig. III.5c. we show the average of several traces, from whose derivative we estimate a mid-unfolding force $F_{1/2}$ for this protein of 7.6 pN, which is close also to the value of

the force at which we observed the hopping in force-clamp experiments. (see Fig. III.4.) This value is comparable to that for gpW also measured at ramps of 10 pN/s (F1/2=4.6 pN; (see Fig. III.5c. inset) and is also consistent with the value of the mid-unfolding force recently determined for α3D ($F_{1/2}$=8.9 pN) (Edwards, LeBlanc, and Perkins 2021a). These results suggest that EnHD has a mechanical resistance which is intermediate those for gpW and α3D, demonstrating that the mid-unfolding force is a feature of ultrafast folding proteins, but, more importantly, show that force-ramp experiments are suitable for the characterization of compliant unfolding patterns and that the unfolding midpoint is unique to each protein.

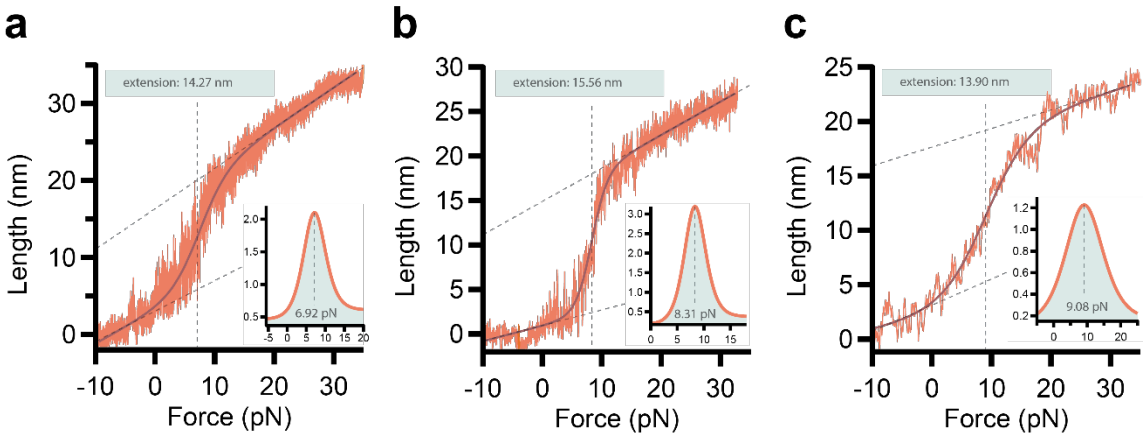

Fig. III.6. a. Length vs. force plot of a representative trace of EnHD at a force ramp of 1 pNs-1 with an extension of approximately 14 pN and a mid-unfolding force of 7 pN. b. Length vs. force plot of a representative trace of EnHD at a force ramp of 10 pNs-1 with an extension of approximately 15 pN and a mid-unfolding force of 8 pN. c. Length vs. force plot of a representative trace of EnHD at a force ramp of 100 pNs-1 with an extension of approximately 14 pN and a mid-unfolding force of 9 pN

• Theoretical Bell model

To better understand the molecular event responsible for the sigmoidal signal we have run stochastic simulations based on the Bell model at increasing force(Bell 1978; Edwards, LeBlanc, and Perkins 2021b). We set the model parameters using folding and unfolding rates in the order of the experimentally derived values for the in bulk at 25 ^{0}C(Mayor et al. 2000; Religa et al. 2007), and calibrate the position of the transition state to match the average experimental curve. (see Fig. III.5c.)

In Fig. III.7. we present the result of multiple stochastic simulations where folding and unfolding can occur multiple times in the timescale of the experiment. We represent the distance to the transition state (DTS) as a percentage of the total length. Using a transition state that is close to the unfolded state (i.e., at 90% the distance between folded and unfolded) allows us to recapitulate the sigmoidal curves observed in the experiments. (see Fig. III.7a.) Other DTS are represented in Fig. III.7b. for comparison.

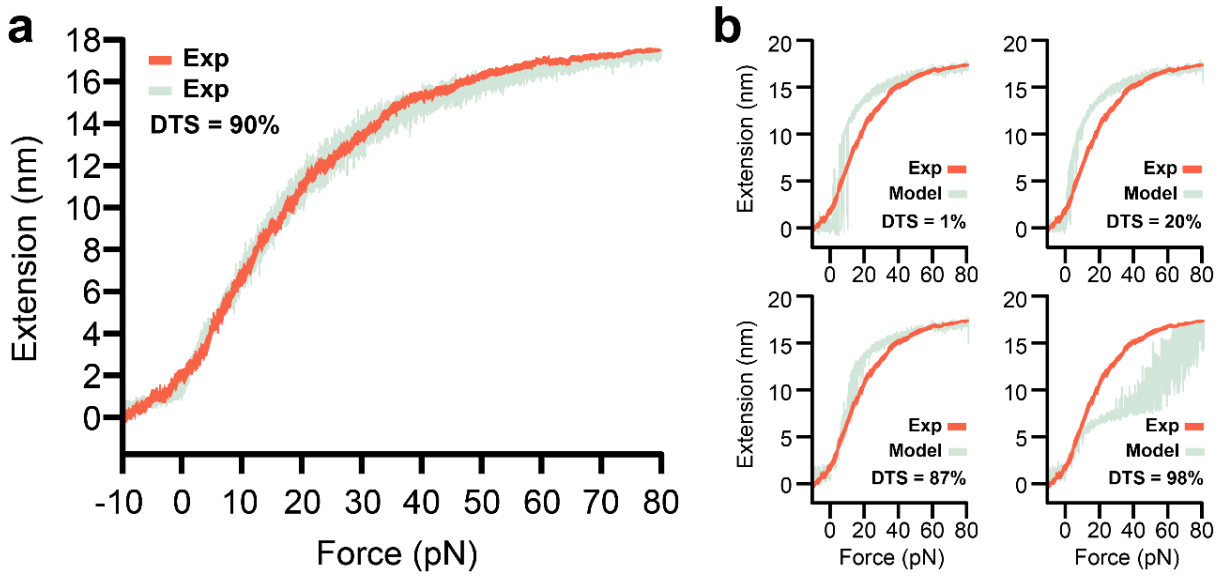

Fig. III.7. Data analysis using the Bell model. a. Force-extension plot from a simulation using the numerical Bell model with stochastic transitions (light green). Average experimental traces obtained at 1 pN/s (orange). b. Same Bell model are show in (green) using different transition state distances and the average experimental traces are superimposed (orange).

We note that a short distance to the transition state would result in stepwise transitions, as observed for brittle proteins like the titin domains, and a longer transition state would result in an almost linear unfolding. In our experiments we have occasionally observed both types of transitions, (see Fig. III.8.) suggesting a certain plasticity in the transition state of EnHD that would be consistent with its low free energy barrier. Using the atomistic coarse-grained model, we have run simulations gradually increasing the unfolding force (see Methods).

The timescale that we cover in the molecular simulations is shorter than that in the experiments and in the stochastic model. Still, it is sufficient to reproduce the repetitive folding and unfolding, supporting our interpretation of the results.

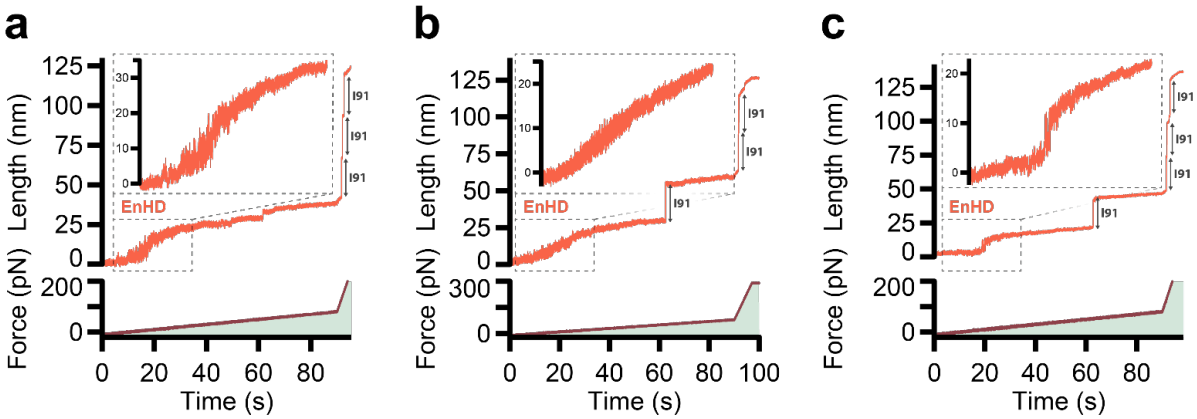

Fig. III.8. EnHD types of transitions a. EnHD sigmoid unfolding. b. Lineal unfolding. c. Step unfolding.

Discussion

In the past decade, the study of proteins by single-molecule force spectroscopy has revealed a variety of aspects in their folding dynamics that are mostly undetectable by traditional ensemble averaging methods. However, only recently have these methods been applied to proteins with low cooperativity, which are challenging due to their low unfolding forces and fast folding kinetics (Schönfelder et al. 2018). Here we have presented results on a protein with weak cooperativity, EnHD, using a combination of experiment, numerical modelling, and molecular simulations. Our results show that EnHD is a compliant protein that folds overcoming a marginal free energy barrier induced by mechanical force. The mid-unfolding force obtained from both constant force and force-ramp experiments for EnHD is in the same range of other labile proteins like gpW (Schönfelder et al. 2018) and α3D (Edwards, LeBlanc, and Perkins 2021a). From our force-ramp experiments, we obtain a novel sigmoidal signature that we interpret as multiple events of folding and unfolding of the protein, which occur repetitively in the timescale of the experiment.

In previous work we have investigated the instrumental effects in constant-force experiments on gpW (De Sancho et al. 2018; Schönfelder et al. 2018). Recent theoretical analysis indicates that folding and unfolding will be slowed down considerably both by the force probe and the in smFS experiments (Nam and Makarov 2016; Cossio, Hummer, and Szabo 2015). Although a detailed analysis of these effects is beyond the scope of the current work, we have the robustness of our results using folding and unfolding rates in the stochastic model up to two orders of magnitude slower than in bulk. Our previous analysis for gpW also indicated that despite introducing a slowdown in the dynamics, the apparent folding and unfolding measured by the instrument indeed trace the true molecular folding and unfolding events. We find that even in these conditions the force-ramp experiments with EnHD result in a sigmoidal curve with multiple folding and unfolding events, that could be reproduced using a simple Bell model. We have discovered that the plasticity of the mechanical transition state is a feature of EnHD that defines the low cooperativity of this protein, making the unfolding highly compliant. Thus, this work shows how force can be used as a tool to investigate low-cooperativity proteins creating a mechanical signature that reveals the plasticity and compliance of the unfolding process. We believe that with greater improvements both in the time resolution of the instruments and in the design of cantilevers (Edwards et al. 2017; Edwards et al. 2015), we anticipate that smFS experiments of folding and unfolding will continue revealing molecular details of weakly cooperative proteins.

Methods

Protein expression and purification. Gene encoding $(I91)_2$-EnHD-$(I91)_2$ chimeric polyprotein construct was designed and optimized for expression in E. coli (Life Technologies). Here two additional cysteine residues were added in the C-terminus, which helps for sample immobilization on the gold surface. Standard DNA manipulation protocols were used to clone the construct into the pQE80L expression plasmid (Qiagen). C41 strand competent cells E. coli (Novagen) were used for protein expression. Transformed competent cells were grown in 1L of LB media at 37°C until an OD600 of around 0.6 was reached. Then protein expression was

introduced by 1mM of IPTG and further incubation at 37°C for 4 hours. Cells were then centrifuged, and a gentle cell lysis protocol was used to avoid damage to the expressed polyproteins. The sample was then purified first by HisTag affinity chromatography using a gravity column filled with HisPur Cobalt resin (Thermo Fisher Scientific) and second by size exclusion chromatography using a Superdex 200 HR column (GE Healthcare). The final elution buffer was HEPES 10mM pH 7.0, NaCL 150mM and EDTA 1 mM. The sample was further concentrated using ultrafiltration Amicon 3k filters (Millipore). The final protein concentration was estimated to be around 1 mg mL^{-1} using a Nanodrop (Thermo Scientific). Then the samples were snap frozen in liquid nitrogen and stored at -80°C.

Single molecule force spectroscopy (smFS). All single-molecule force spectroscopy force extension, constant force and force ramp experiments were performed on an Atomic Force Spectrometer AFS-1 (Luigs Neumann). Biolever cantilevers from Olympus/Bruker were used with a spring constant of around 6 pN nm-1 for all constant force and force ramp measurements. The spring constant was measured before each experiment using the equipartition theorem within a software built-in procedure. Data was recorded between 0.5 to 4 kHz for the constant force and force ramp measurements. For those experiments that included quenching of force (Figure 2c), the force was ramped at 1pN s-1 until 45 pN (starting from 10 pN pushing $F < 0$). At this point it was restored back to 10 pN pushing and ramped with the same rate until 45 pN again. During combination of force-ramp and constant force experiments (Figure 3), the force was ramped at rate of 1pN s-1 until reaching the 8 pN constant force. Then the protein was held for 20-30 s at the constant force before the ramp at 1pN s-1 was continued. To reduce total experimental acquisition time, all traces include a rapid increase of the force rate to 30 pN s-1 at the end to quickly reach the high forces required to unfold Titin-I91 domains. All AFM experiments were carried out at room-temperature (~24 °C) in HEPES buffer at pH 7.0. Typically, 40 μl of the protein sample (~μM concentration) was left around 20 minutes for adsorption on a fresh gold coated surface, using gold evaporation (Oerlikon UNIVX350). After the adsorption time the sample was then rinsed of the gold surface by the HEPES buffer to remove unbounded protein sample just before starting the measurements.

Theoretical model. To interpret the force ramp experiments we use a simple model of two-state kinetics that allows for stochastic jumps between the folded and unfolded states depending on the force-dependent rates for folding and unfolding, kf(F) and ku(F). This dependence is described using the Bell model(Bell 1978), i.e. kf(F)=kf(0)exp(-βΔxfF) and ku(F)=ku(0)exp(βΔxuF), where kf/u(0) are the values of the folding and unfolding rates in bulk, Δxf/u is the distance to the from either state to the transition state and β is the inverse thermal energy. The extension of either the folded and the unfolded state at a given force are described using the worm-like chain model, using a contour length of 19 nm and a persistence length of 0.4 nm. Simulations were run using a Gillespie algorithm (Gillespie 1977).

Coarse Grained Molecular Dynamics Simulations. We run molecular simulations using an atomistic structure-based model(Whitford et al. 2009). Briefly, the model keeps all the heavy atoms of the protein and represents interactions via harmonic terms for bonds, angles, and dihedrals. For atom pairs that are in contact in the native conformation, a non-bonded interactions are represented by a Lennard-Jones potential. All other pairwise interactions are repulsive. Models were generated using the stand-alone version of the SMOG software package (Noel et al. 2016) and simulations were performed using the Gromacs software package (Abraham et al. 2015), using a leap-frog stochastic dynamics integrator with a timestep of 5e-4 fs and a coupling constant of 1 ps (we note that the timescales of the model do not correspond to physical times). We first run simulations at multiple temperatures to estimate the folding temperature in the model. Then we run pulling simulations at constant force and constant pulling speed using the pull code in Gromacs. Finally, we emulate the force-ramp mode by concatenating thousands of short simulations runs, each of which has an incrementally larger constant pulling force and starts from the last snapshot of the previous run. Results were analyzed using the MDtraj Python library (McGibbon et al. 2015).

Data availability

Data supporting the findings of this study are available from the corresponding author upon reasonable request.

Acknowledgements

This work has been supported by grants PID2019-109087RB-I00 to R.P.-J. and PGC2018-099321-B-I00 to DD from Spanish Ministry of Science and Innovation. This project has received funding from the European Union's Horizon 2020 research and innovation programme under grant agreement No 964764 to R.P.-J. A. R. is the recipient of a doctorate fellow from Spanish Ministry of Science and Innovation. I.R.-O. acknowledges financial support from Donostia International Physics Center (DIPC).

Competing financial interest

The authors declare no competing financial interest.

Author Contributions

R.P.-J., V.M, and D. D. conceived the project and designed research. A.R, A. O-S and J. S. cloned the protein and performed smFS experiments. A.R., D. D., V. M., and R. P.-J. analysed smFS experiments. I. R.-O. and D. D conducted computational molecular dynamics simulations. V. M. performed theoretical analysis. All authors contributed to writing and revising the manuscript.

Chapter IV: *evasion of phagocytosis by the plague bacterium Yersinia pestis requires exceptional protein mechanostability*

Daniel T. Peters[1], Antonio Reifs[2], Alvaro Alonso-Caballero[2], Azzeldin Madkour[1], Helen Waller[1], Brendan Kenny[1], Raul Perez-Jimenez[2,3], Jeremy H. Lakey[1]*

1. *Biosciences Institute, Faculty of Medical Sciences, Newcastle University, Newcastle upon Tyne, NE2 4HH, UK*
2. *CIC nanoGUNE, San Sebastian, Spain*
3. *Ikerbasque Foundation for Science, Bilbao, 48013, Spain*

* Corresponding Author

Macrophages employ both molecular recognition and mechanical force to engulf pathogens. Here we demonstrate how the polymeric protein, Caf1, protects bacteria from phagocytosis by inhibiting both mechanisms. First, we show that recombinant Caf1-producing *Escherichia coli* adhere poorly to macrophages, and those that do are not engulfed. Inserting either an RGDS integrin binding motif or destabilising point mutations into Caf1 did not change the adherence but significantly increased the fraction of bacteria engulfed. Therefore, phagocytic evasion relies upon (i) reduced cell adhesion, (ii) lack of specific receptor binding sites and (iii) Caf1 physical stability. Single-molecule force spectroscopy (SMFS) experiments reveal that wild-type Caf1 displays an extremely high mechanical stability of 400 pN. Surprisingly, the destabilised mutants that are fully engulfed are only 20% weaker. This exceptional tensile strength has therefore evolved to only marginally exceed the mechanical force applied to the Caf1 polymer.

Introduction

Macrophages recognise their targets through a wide variety of cell surface receptors (Flannagan, Jaumouillé, and Grinstein 2012; Gordon 2016; Swanson 2008), attacking foreign bodies such as bacterial cells by recognising either (i) particular molecules, present in these organisms but not the host, called pathogen associated molecular patterns (PAMPs) or (ii) opsonising molecules such as complement. Once recognised, the macrophage engages the actin cytoskeleton to draw the prey into the newly formed phagocytic cup, where it is engulfed by the macrophage and degraded in a specialised organelle called the phagosome. Elegant biophysical approaches have shown that macrophage filopodia exert forces in the pN-nN range as they attach to microparticles and draw them towards the cell body for engulfment (Vonna et al. 2007; Kress et al. 2007; Vorselen et al. 2020). Receptor binding has been shown to be essential for phagocytosis (Gordon 2016; Swanson 2008; Vorselen et al. 2020) but the biomechanics involved are still poorly understood (Jain, Moeller, and Vogel 2019; Barger, Gauthier, and Krendel 2020).

Bacterial pathogens can avoid destruction via a diverse array of strategies including subverting the phagosome to enable intracellular expansion within the macrophage (Connor et al. 2018) or through masking their distinctive surface by hiding behind a capsule to avoid detection by cells of the immune system (Finlay and McFadden 2006). *Yersinia pestis*, the causative agent of the plague, uses both strategies (Li and Yang 2008). Initially, following infection of the host via a flea bite, bacteria are readily engulfed by neutrophils and macrophages. Within the phagosome it inhibits the destructive pathway and expands in numbers whilst at the same time expressing genes such as *yop* and *caf* that will provide protection from engulfment following escape from the initial host macrophage (Li and Yang 2008; Connor et al. 2018; Spinner et al. 2014; Fukuto and Bliska 2014).

The Yop (*Yersinia* outer membrane protein) system injects phagocytosis inhibiting proteins into macrophages via a type III secretion system (T3SS) (Von Pawel-Rammingen et al. 2000; Grosdent et al. 2002; Fällman et al. 1995) whilst Caf1 (capsular antigen fraction 1) enables passive phagocytosis resistance by cloaking *Y. pestis* in a gel-like protein coat (Du, Rosqvist, and Forsberg 2002). Caf1 is a 15

kDa protein that assembles into long, non-covalent, extracellular polymers, via the chaperone-usher pathway (Zavialov et al. 2001), which surround the bacterium (Du, Rosqvist, and Forsberg 2002) and enable *Y. pestis* cells to avoid macrophage engulfment (Du, Rosqvist, and Forsberg 2002; Pujol and Bliska 2005; Cavanaugh and Randall 1959). Crucially, Caf1 does not inhibit the phagocytic activity of macrophages (Du, Rosqvist, and Forsberg 2002), and instead inhibits the association of *Y. pestis* bacteria with the macrophages, suggesting Caf1 is anti-adhesive (Du, Rosqvist, and Forsberg 2002). *In vitro* studies have shown that the "non-stick" phenotype of the Caf1 polymer extends to cell types other than macrophages, with a wide range of cells adhering very poorly to Caf1 treated surfaces in culture (Roque et al. 2014).

Here, we investigate the molecular determinants of Caf1's anti-phagocytic activity. We first determine that recombinant *E. coli* producing Caf1 polymers evade engulfment by macrophages through two methods. Firstly, far fewer bacteria attach to the surface of the macrophage and of those very few are phagocytosed. We then show that simple insertion of an integrin binding motif into Caf1 polymers enabled macrophages to engulf attached *E. coli,* reversing the second mechanism of the protective phenotype(Roque et al. 2014)[2121121]. Next, we investigate the effect of mutations affecting Caf1 polymer stability and find that single amino acid substitutions also abrogate Caf1's protection of adhered bacteria. Single-molecule force spectroscopy (SMFS) experiments then reveal not only that Caf1 has an exceptionally high tensile strength but also that the inactivating mutations cause a drop in strength of only ~20%, suggesting that the wild type strength is only just sufficient to prevent phagocytosis. The combined results suggest that three key properties of Caf1 " its low non- specific affinity for cells, its absence of ligands for macrophage receptors and its exceptional mechanostability" have co-evolved to generate the anti-phagocytic property of the protein, contributing significantly to the virulence of the plague pathogen. Furthermore, since there is still much to be learned about the biomechanics of engulfment, the data presented here offer a new insight by reporting directly from the pathogen-macrophage interface.

Results

• Expression of Caf1 in E. coli confers anti-phagocytic ability

Y. pestis produces a Caf1 coat upon transfer from a flea vector to a warm-blooded host, enabling it to evade phagocytosis (Du, Rosqvist, and Forsberg 2002). To determine if heterologous expression of *caf1* provides *E. coli* cells with a protective coat, BL21(DE3) cells were transformed with either empty pGEM-T vector or the pT7-COP plasmid, in which pGEM-T contains the entire *caf1* operon (*caf1R*, *caf1M, caf1A* and *caf1*). These cells were grown for 22 h at 35°C to induce *caf1* expression, and then imaged using transmission electron microscopy (TEM).

Compared to the cells transformed with the empty vector, cells expressing *caf1* appeared to be surrounded by an amorphous gel-like coat (see Fig. IV.1a. and Fig. IV.1b.) The images are similar to those of *Y. pestis* bacteria expressing *caf1* (Runco et al. 2008). Therefore, heterologous expression of the *caf1* operon results in the same morphological phenotype as in the natural system, providing *E. coli* with a Caf1 capsule.

Next, to determine whether this capsule possessed the same anti-phagocytic properties as those described for *Y. pestis*, we transformed *E. coli* with pGEM-T, pT7-COP and pT7-COPΔF1, where Caf1 translation is prematurely terminated through the introduction of a stop codon. Production of Caf1 polymers produces a flocculent layer which can be seen above the cell pellet after centrifugation (Miller et al. 1998).

Cells containing the pT7-COP plasmid produced a flocculent layer, and Caf1 polymers could be detected in the extracellular fraction of the culture using SDS-PAGE (see Fig. IV.1c.), whereas cells containing pGEM-T or pT7-COPΔF1 showed no detectable flocculent layer or Caf1 protein. Additionally, a Caf1 coat could not be observed by TEM on pT7-COPΔF1 transformed cells (see Fig. IV.1d.) These cell cultures were used to infect J774.A1 macrophages at a multiplicity of infection of 100:1 bacteria:macrophage before fixing.

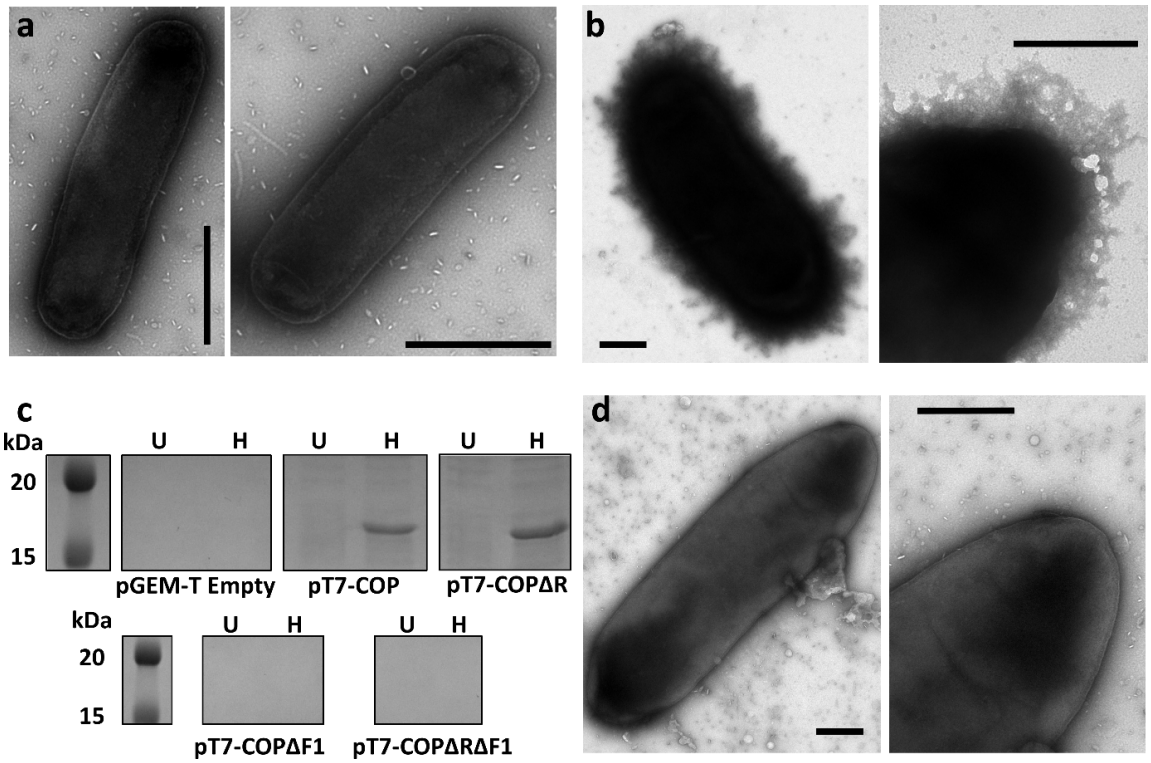

Fig. IV.1. Expression of caf1 in E. coli results in capsule formation. Transmission electron micrographs of E. coli transformed with either empty vector (pGEM-T) a. or pT7-COP b. c. SDS-PAGE analysis of the extracellular fraction (comprising flocculent and supernatant) of cultures of E. coli transformed with the indicated plasmids and grown for 22 h at 35°C. Samples were incubated at either room temperature (unheated, U) or 100°C (heated, H) for 5 min prior to loading on the gel. d. Transmission electron micrographs of E. coli transformed with pT7-COPΔF1. All scale bars represent 500 nm.

The number of *E. coli* engulfed by the macrophages was then determined by a previously described immunofluorescence assay (Quitard et al. 2006) where extracellular bacteria are labelled red and all bacteria (intra- and extracellular) are labelled green. Macrophages were then examined by fluorescence microscopy, and the ratio of green to red stained bacteria counted to determine the percentage of engulfed cells in Fig. IV.2a. and Fig. IV.2b. The comparisons were made using three biological replicates in a blind assay.

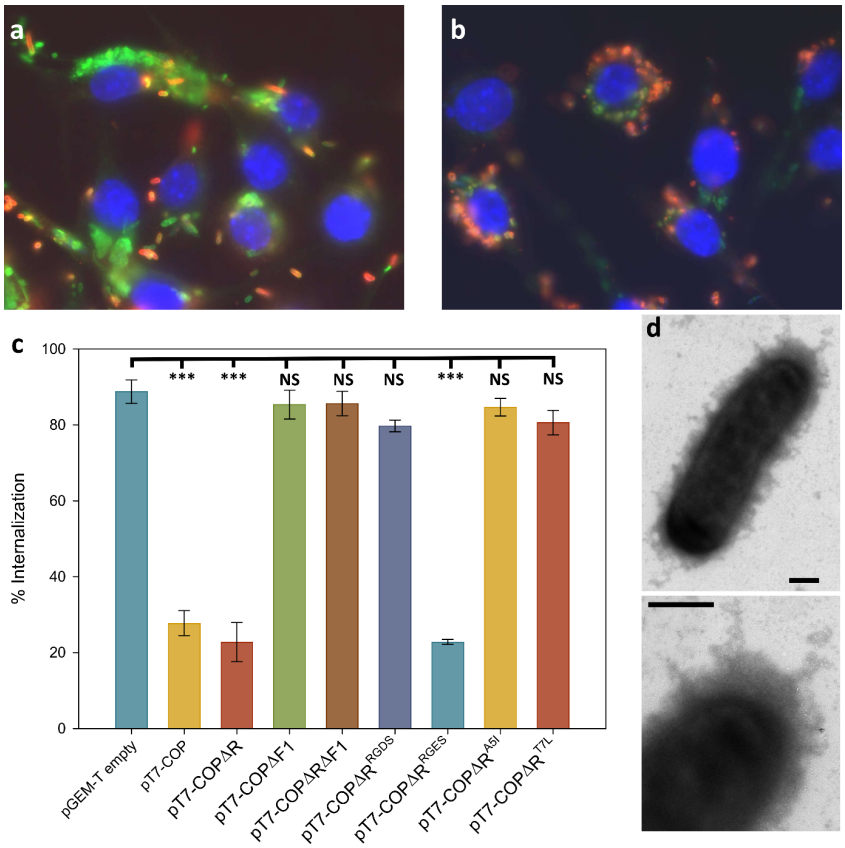

Fig. IV.2. Expression of caf1 protects E. coli from phagocytosis. BL21(DE3) E. coli cells transformed with the indicated plasmids were grown for 18 h and used to infect J774.A1 macrophages for 2 h. Bacteria external to the macrophages were labelled in red and all bacteria labelled green, with macrophage nuclei stained blue. Representative microscopy images are shown for bacteria transformed with pT7-COPΔRΔF1 a. and pT7-COPΔR b. Images were taken with a Zeiss Axioskop Epifluorescence microscope with a 100x oil objective. c. Percentage of bacterial cells internalised by J774.A1 macrophages. Percentages were calculated by determining the ratio of red:green cells counted post-infection. Error bars represent the S.E.M of three independent biological replicates. Data were analysed by one way ANOVA with a Holm-Sidak post-hoc test. NS – Not significant, *** - P<0.01. d. Transmission electron micrographs of E. coli transformed with pT7-COPΔR. All scale bars represent 500 nm.

These data gave three important results. Firstly, that Caf1's anti-phagocytic activity can be easily transferred to *E. coli.* Secondly, that the total number of cells associated with the macrophages is reduced by about 80% in Caf1 coated compared to uncoated bacteria and thirdly that even macrophage-bound bacteria were protected from subsequent engulfment when *caf1* was expressed (see Fig. IV.2c.)

The Caf1R protein regulates *caf1* expression as part of a complex thermosensitive system that responds to host body temperature (Al-Jawdah et al. 2019). To ensure reproducible Caf1 levels we simplified *caf1* expression in our assays by deleting *caf1R,* and so used only basal T7 expression from pT7-COPΔR. The cells transformed with this plasmid displayed the expected Caf1 coat when observed by TEM (**Fig. 2d**). The macrophage assay was thus repeated using pT7-COPΔR, with pT7-COPΔRΔF1 as a control. Expression of *caf1* from pT7-COPΔR allowed the *E. coli* to avoid phagocytosis, with a drop in internalisation similar to that seen in the presence of Caf1R, whereas prevention of *caf1* translation again reversed this effect and allowed the phagocytosis of the bacteria. (see Fig. IV.2c.) Therefore, the ability to evade phagocytosis by macrophages can be conferred to *E. coli* in a *caf1* dependent, *caf1R* independent, manner.

• Addition of a cell binding motif reverses anti-phagocytic activity of Caf1

Caf1 has previously been shown to possess “non-stick” properties, with mammalian cells in 2D cell culture adhering very poorly to Caf1 coated surfaces. This phenotype was reversed through the addition of the integrin binding motif, RGDS, which then facilitated cell attachment to the Caf1 surface (Roque et al. 2014).

To investigate whether this “non-stick” property of Caf1 has a role in its anti-phagocytic activity, *E. coli* cells were transformed with pT7-COPΔR^{RGDS} in which Caf1 contains the RGDS integrin binding motif inserted within loop 5 of the protein (between residues N106 and D111 in the mature sequence), or with pT7-COPΔR^{RGES}, which has the RGES motif at the same site. The RGES motif differs from the RGDS motif by a single -CH_2- group but does not support cell adhesion (Roque et al. 2014; Hersel, Dahmen, and Kessler 2003). When the bacteria containing these plasmids were grown for 22 h at 35°C, the cells were seen by TEM to be surrounded by a capsule (see Fig. IV.3a. and Fig. IV.3b.) Additionally, a flocculent layer was visible above a centrifuged cell pellet, and Caf1 polymers could be detected by SDS-PAGE.

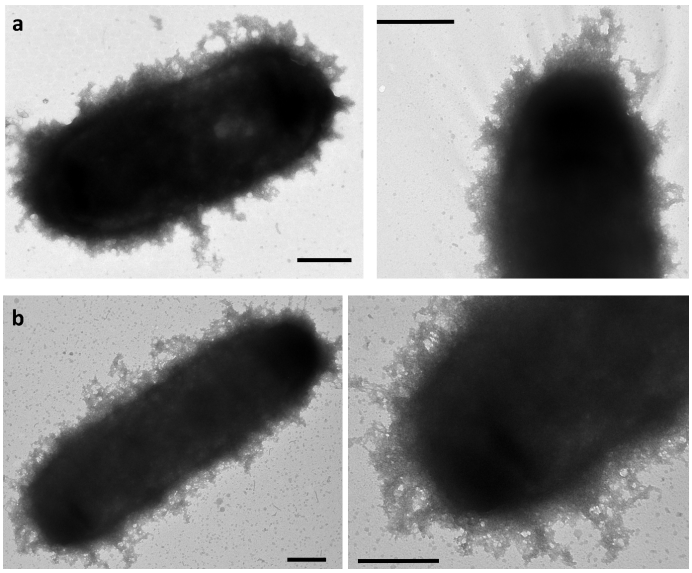

Fig. IV.3. Expression of Caf1^{RGDS} and Caf1^{RGES} result in capsule formation. Transmission electron micrographs of *E. coli* transformed with either pT7-COPΔR^{RGDS} a. or pT7-COPΔR^{RGES} b. All scale bars represent 500 nm.

The transformed cells were then used to infect cultures of macrophages in the phagocytosis assay. The results revealed that adding the integrin binding motif to Caf1 reversed the anti-phagocytic phenotype allowing engulfment of the majority of the bacteria adhered to the macrophages (see Fig. IV.2c.). The control RGES subunit retains the full anti-phagocytic effect of Caf1, showing that engulfment of the RGDS mutant occurs through specific integrin recognition. Interestingly, WT, RGDS and RGES Caf1 variants all reduced the total number of bacteria attached to the macrophages equally showing that the low non-specific adherence is unaffected by enhanced integrin binding. The results demonstrate that low non-specific cell adherence and lack of specific ligands for phagocytic cell receptors contribute separately to Caf1's protective phenotype.

- **Caf1's exceptional stability is essential for protection from phagocytosis**

Caf1 subunits assemble into polymers non-covalently through the process of donor strand complementation, where the N-terminal β-strand of one subunit completes the Ig-like fold of the next subunit in the polymer (Zavialov et al. 2003). This results in polymers with exceptionally high chemical and thermo-stability which can, however, be reduced simply by mutagenesis of single residues in the N-terminal strand to larger, hydrophobic residues (such as alanine to isoleucine) (Ulusu et al. 2017; Yu et al. 2012; Peters et al. 2019). We wanted to investigate the role of polymer stability in Caf1 function, and so examined the effect of two single amino acid substitutions that are known to lower the thermostability of Caf1 (Ala-5 to Ile [A5I] and Thr-7 to Leu [T7L]), with both substitutions causing a drop in protein melting temperature of ~7°C (Yu et al. 2012; Peters et al. 2019).

The macrophage assays were repeated using *E. coli* cells transformed with the pT7-COPΔR^{A5I} and pT7-COPΔR^{T7L} plasmids. Expression of the Caf1^{A5I} and Caf1^{T7L} mutants provided *E. coli* with a capsule visible by TEM (see Fig. IV.4a. and Fig. IV.4b.), that had a similar appearance to the wild-type protein. Both the Caf1^{A5I} and Caf1^{T7L} mutants resulted in a flocculent layer and in Caf1 polymers detectable by SDS-PAGE.

In phagocytosis assays, bacteria expressing these mutants still bound poorly to macrophages but were engulfed at high levels (see Fig. IV.2c.), similarly to cells expressing the RGDS mutant, demonstrating that these single amino acid substitutions abrogate Caf1's ability to prevent the phagocytosis of bound cells. This result was surprising, as the experiments were conducted at 37°C, far below the reduced melting temperature of the proteins ~82°C. (Peters et al. 2019)

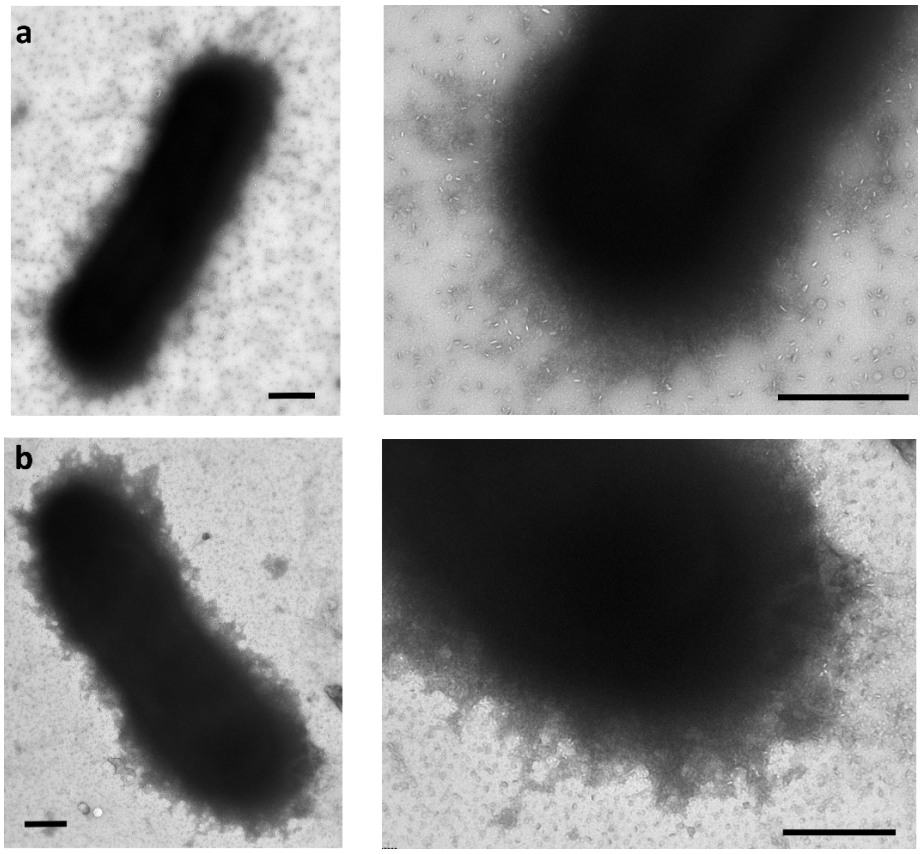

Fig. IV.4. Expression of *caf1*^{A5I} and *caf1*^{T7L} results in capsule formation. Transmission electron micrographs of *E. coli* transformed with pT7-COPΔR^{A5I} a. and pT7-COPΔR^{T7L} b. All scale bars represent 500 nm.

• Lower stability Caf1 polymers are not recognised by macrophages

To determine whether the loss of protective ability demonstrated by these mutant polymers was caused by an increase in their affinity for macrophage receptors, we performed a phagocytosis assay using polystyrene beads coated in Caf1 proteins, rather than bacteria. As these beads lack the macrophage recognition sites present

on the bacterial outer membrane, any increase in the ability of macrophages to engulf beads coated with the mutant proteins over beads coated with the wild-type protein will be caused by increases in the ability of the macrophages to recognise and bind to the proteins.

Beads coated with Caf1^{WT} were not readily phagocytosed (see Fig. IV.5a. and Fig. IV.5f.), in contrast to the beads coated with Caf1^{RGDS} where the majority of the beads were engulfed (see Fig. IV.5b. and Fig. IV.5f.). As expected, beads coated with the low affinity Caf1^{RGES} protein were engulfed at a similar low level to the Caf1^{WT} coated beads (see Fig. IV.5c. and Fig. IV.5f.). The lower stability Caf1^{A5I} and Caf1^{T7L} coated beads were also not readily phagocytosed (see Fig. IV.5d., Fig. IV.5e. and Fig. IV.5f.), and were internalised at levels similar to the Caf1^{WT}.

To provide further evidence that the lower stability mutants were not more readily recognised by macrophage receptors than the wild-type protein, a 2D cell adhesion assay was conducted, where plastic surfaces were coated with Caf1 polymers and the number of HeLa cells or macrophages that had adhered to the surface after 24 h were observed.

For the HeLa cells, large numbers of cells could be seen to adhere to the uncoated and Caf1^{RGDS} coated surfaces, whilst the Caf1^{WT}, Caf1^{RGES}, Caf1^{A5I} and Caf1^{T7L} coated surfaces supported the attachment of much fewer cells.

For the macrophages, a similar pattern was observed, although the Caf1^{A5I} and Caf1^{T7L} coated surfaces supported the attachment of an intermediate number of cells, much fewer than the uncoated and Caf1^{RGDS} surfaces but more than the Caf1^{WT} and Caf1^{RGES} coated surfaces. Together, these results show that, similar to Caf1^{WT} and unlike the Caf1^{RGDS}, the Caf1^{A5I} and Caf1^{T7L} proteins are not easily recognised by macrophages, hence the lack of protective ability observed in the phagocytosis assay with the bacteria must come from another property of these proteins.

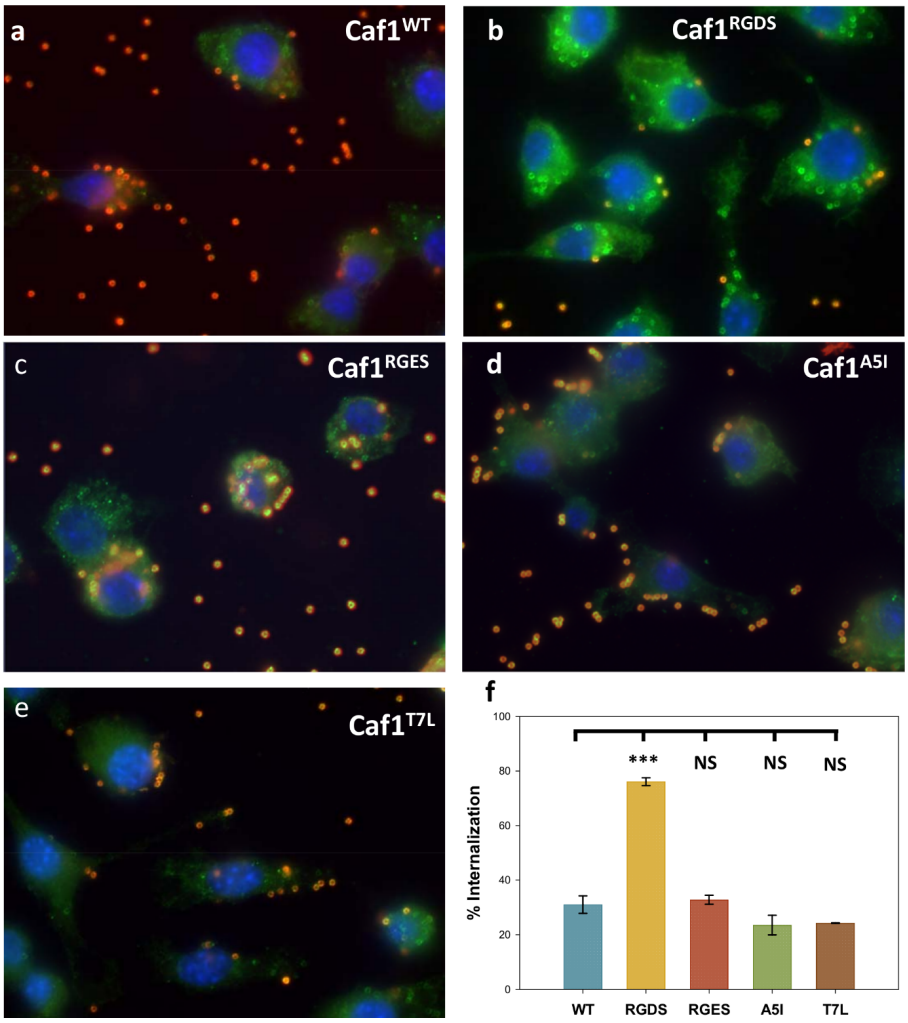

Fig. IV.5. Polystyrene beads coated with lower stability Caf1 mutants show no increase in phagocytosis levels over wild-type Caf1. a.-e. Polystyrene beads were coated with purified Caf1 polymers and incubated with J774.A1 macrophages for 2 h before fixation. Non-phagocytosed Beads were visualized by incubation with a mouse anti-Caf1 antibody, followed by a goat anti-mouse Alexa Fluor 555 antibody, that fluoresces red. Phagocytosed beads were visualized following permeabilization with Triton X-100 by probing with the mouse anti-Caf1 antibody, followed by a goat anti-mouse Alexa Fluor 488 antibody, which fluoresces green. The percentage of internalized beads (**f**) was determined by comparing the number of external (red) beads to the total number of beads (green). Error bars represent the standard deviation of three independent biological replicates. Data were analysed by one way ANOVA with a Holm-Sidak post-hoc test. NS – Not significant, *** - P<0.01. Images were taken with a Zeiss Axioskop Epifluorescence microscope with a 100x oil objective.

• Mechanical stability of Caf1 proteins

As macrophages are known to exert forces on their targets during phagocytosis (Kress et al. 2007; Vonna et al. 2007; Vorselen et al. 2020), and the N-terminal donor strand of Caf1 is important for polymer stability (Peters et al. 2019; Yu et al. 2012), we hypothesized that the mechanical stability of Caf1 might be an important property in determining its protective ability, and that our substitutions in this strand may affect this stability. Therefore, we determined the mechanostability of wild-type Caf1, Caf1^{A5I} and Caf1^{T7L} using single molecule force spectroscopy (SMFS), a technique we had previously used for another chaperone usher protein (Alonso-Caballero et al. 2018). Briefly, we constructed a polyprotein in which a circularly permuted *caf1* subunit (cpCaf1, where the N-terminal donor strand is placed on the C-terminus after a flexible linker, completing the Ig-like fold, (see Fig. IV.6a.) was bracketed with two tandem I91 domains from the cardiac protein titin, that are used as a mechanical fingerprint on account of their well-known properties (Alonso-Caballero et al. 2018). The final constructs ($I91_2$-cpCaf1-$I91_2$, $I91_2$-cpCaf1^{A5I}-$I91_2$, $I91_2$-cpCaf1^{T7L}-$I91_2$) terminate with a cysteine to facilitate adhesion to the gold surface. (see Fig. IV.6b.) The structure and thermostability of the cpCaf1 (Chalton et al. 2006) and similar self-complemented subunits (Yu et al. 2012) have been characterised previously and match those of polymeric Caf1.

In the SMFS experiments a cantilever tip, with a single protein absorbed, retracts at a constant speed of 400 nm/s. With the protein captured between the tip and the gold surface, the force exerted triggers the unfolding of the protein, which can be monitored as a force-extension peak. (see Fig. IV.6c., Fig. IV.6d. and Fig. IV.6e.) In our polyprotein, we first observed the unfolding of the I91 domains at a typical force of around 200 pN with an increment in contour length of 28 nm. We subsequently observed a higher peak of 54-55 nm that we attribute to cpCaf1, which unfolds at a force of 394 ± 40 pN. (see Fig. IV.6c.) This value is very high compared to other proteins, which typically unfold at forces between 25-250 pN (Bustamante et al. 2004), but similar to other CU proteins, such as the Fim proteins, which have unfolding forces within the range of 350-530 pN (Alonso-Caballero et al. 2018). In comparison, cpCaf1^{A5I} and cpCaf1^{T7L} unfold at forces of 318 ± 21 pN and 310 ± 30

pN respectively. (see Fig. IV.6d., Fig. IV.6e. and Fig. IV.6f.) Therefore, the point mutations caused a drop in mechanostability of approximately 20%. Together with the results of the phagocytosis assay, these data indicate that the mechanostability of Caf1 is not only essential for its anti-phagocytic capability but that its magnitude is surprisingly close to the minimal effective value.

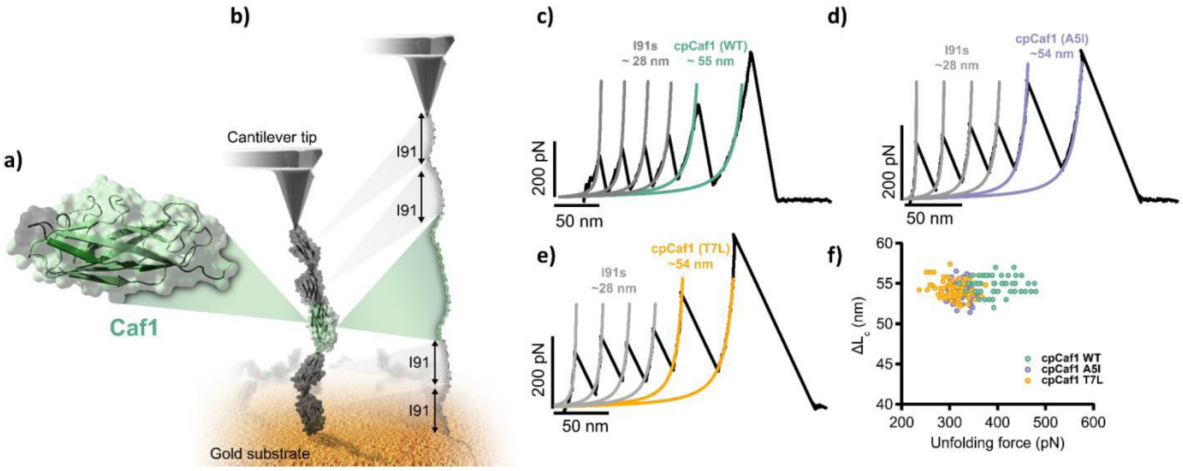

Fig. V.6. Mechanical stability of Caf1 mutants. a. Close up view of a self-complemented Caf1 (cpCaf1) monomer. The gene encoding this monomer was inserted in the middle of 4x I91 protein domains from titin to produce the $I91_2$-cpCaf1-$I91_2$ construct. b. The $I91_2$-cpCaf1-$I91_2$protein was attached to a gold substrate at one end and to a cantilever tip on the other. When a tensile force is applied to Caf1 it elongates until breaking point at which it is completely unfolded. c.-e. Force unfolding curves of $I91_2$-cpCaf1^{WT}-$I91_2$, $I91_2$-cpCaf1^{A5I}-$I91_2$ and $I91_2$-cpCaf1^{T7L}-$I91_2$. Coloured lines represent fits of the worm-like chain model to the data. f. Plot of extension vs. unfolding force for $I91_2$-cpCaf1^{WT}-$I91_2$ (green), $I91_2$-cpCaf1^{A5I}-$I91_2$ (purple) and $I91_2$-cpCaf1^{T7L}-$I91_2$ (yellow). Individual unfolding experiment are shown as individual data points coloured according to the protein used.

Discussion

Although Caf1 was known to protect bacteria from phagocytosis, the specific molecular requirements had not been defined (Du, Rosqvist, and Forsberg 2002).

Here, we have conclusively demonstrated that the anti-phagocytic activity of Caf1 is dependent on three factors: its low affinity for cells in general, its lack of specific ligands for critical macrophage receptors and its high mechanical stability.

• Determinants of anti-phagocytic activity: Low binding to cell surfaces

Compared to uncoated, control, E. coli, far fewer Caf1 coated bacteria were found associated (surface bound or engulfed) with macrophages. Thus Caf1 coated surfaces interact weakly with cells in general, a phenomenon also observed previously for a range of cell types(Du, Rosqvist, and Forsberg 2002). Furthermore, bacteria expressing Caf1^{RGDS} showed no increase in attachment to macrophages, revealing that even a dense coverage of integrin ligands cannot reverse the fundamental non-stick phenotype. This behaviour may be explained in simple molecular terms since Caf1 also demonstrates a notable resistance to self-aggregation (Soliakov et al. 2010) and even at high concentrations the long polymers do not gel but behave as a viscous liquid (Ulusu et al. 2017). This is reminiscent of highly hydrated polymers such a polyethylene glycol which are used to artificially reduce cell surface interactions. Coupled to this Caf1 has a pI of 4.5 giving it a net negative charge at physiological pH which will repel both other Caf1 polymers and cell surfaces which are generally negatively charged too. These parameters could explain the low association of any Caf1 coated cells to macrophages in our assays.

• Determinants of anti-phagocytic activity: Low affinity for macrophage receptors

Macrophage integrins are critical receptors which, when activated by specific ligand binding, initiate the signalling pathways which drive engulfment. Ligands of the $\alpha_M\beta_2$

integrins include bacterial LPS which promotes recognition and engulfment of Gram negative bacteria such as *E coli* whilst $\alpha_5\beta_1$ integrins bind the RGDS motifs of fibronectin and vitronectin (Proctor 1987; Wright and Meyer 1985; Kao et al. 2001) to enable macrophages to either eliminate apoptotic cells or migrate to sites of infection to increase their bactericidal activity (Clark, Dvorak, and Colvin 1981; Proctor 1987). The addition of RGDS to Caf1 allows the macrophages to phagocytose the bacteria attached to their surface. This effect is specific, as this reversal was not observed when the highly similar but inactive RGES sequence was inserted instead. Furthermore, polystyrene beads coated in $Caf1^{RGDS}$ can be recognised and engulfed by macrophages, but beads coated with $Caf1^{WT}$ or $Caf1^{RGES}$ cannot. $Caf1^{RGDS}$ coated plastic surfaces also support the adhesion of both macrophages and HeLa cells, whereas $Caf1^{WT}$ and $Caf1^{RGES}$ do not. In summary, these data suggest that Caf1 lacks the molecular signals that promote engulfment and, by also masking the organism's own PAMPs (such as LPS), prevents receptor recognition, allowing bacteria to escape phagocytosis. In future Caf1 could be used as a platform to discover other sequence motifs that play roles in engulfment.

• Determinants of anti-phagocytic activity: Mechanical Strength

We show here that Caf1 exhibits a high mechanical stability, in accordance with its fold and homology to other stable fimbriae, and that single amino acid substitutions in the N-terminal donor strand of Caf1 reduce this mechanostability by approximately 80-90 pN (20%). Such substitutions were known to lower the thermodynamic stability of the subunit-subunit interface, causing a drop in melting temperature (Yu et al. 2012), but the effect on mechanostability was unknown. Crucially, SDS-PAGE analysis and TEM images revealed that, despite their lower stability, the mutant proteins still form SDS-resistant polymers, which coat the bacterium. Additionally, we have shown that the $Caf1^{A5I}$ polymers formed are long, as they can be purified using a 500 kDa molecular weight cut-off filter (corresponding to a minimum of 32 subunits with a length of >190 nm (Peters et al. 2019)). However, whilst the ~20% reduction in Caf1 mechanostability does not affect the polymer's structure, it entirely

suppressed Caf1 mediated protection from phagocytosis. Polystyrene beads coated in the Caf1^{A5I} and Caf1^{T7L} were not phagocytosed at levels any higher than Caf1^{WT} and HeLa cells adhered to these proteins at similarly low levels to Caf1^{WT}, indicating that these proteins are not recognised by the macrophages any more readily than the wild-type. Since the loss of its anti-phagocytic behaviour is not due to incomplete Caf1 polymer formation, spontaneous polymer breakdown, increased recognition by macrophage receptors or shedding of the Caf1 coat, it must be related to the mechanics of the macrophage interface.

• Role of macrophage contractile forces in the anti-phagocytic mechanism of Caf1

One potential mechanism through which this process could occur is through disruption of the Caf1 coat by force applied by the macrophage. (Flannagan et al. 2010; Kress et al. 2007; Barger, Gauthier, and Krendel 2020) (see Fig. IV.7.) The force could be generated as an engaged bacterium attempts to move away from a macrophage (either by Brownian motion or bacterial motility), or as receptors bound to the bacterial surface apply stretching forces on account of the increase in membrane tension which accompanies stages after cup formation (Barger, Gauthier, and Krendel 2020). Wild-type Caf1 capsules could resist such forces, and allow bacteria to escape phagocytosis, whilst weaker capsules such as A5I could be disrupted, exposing bacterial surface PAMPs and facilitating engulfment. In favour of this hypothesis, bacteria coated with the lower stability Caf1 mutants are readily engulfed by macrophages, whereas polystyrene beads that are similarly coated and have no PAMPs, are not. Furthermore, HeLa cells do not readily adhere to surfaces coated with the lower stability Caf1 mutants, but macrophages show slightly increased levels of adhesion in these conditions compared to Caf1^{WT} and Caf1^{RGES} coated surfaces, though not as high as those found on uncoated plastic and Caf1^{RGDS} coated surfaces. It is possible that the macrophages are able to disrupt the lower stability coatings and adhere to the plastic surfaces beneath, resulting in their intermediate level of adhesion.

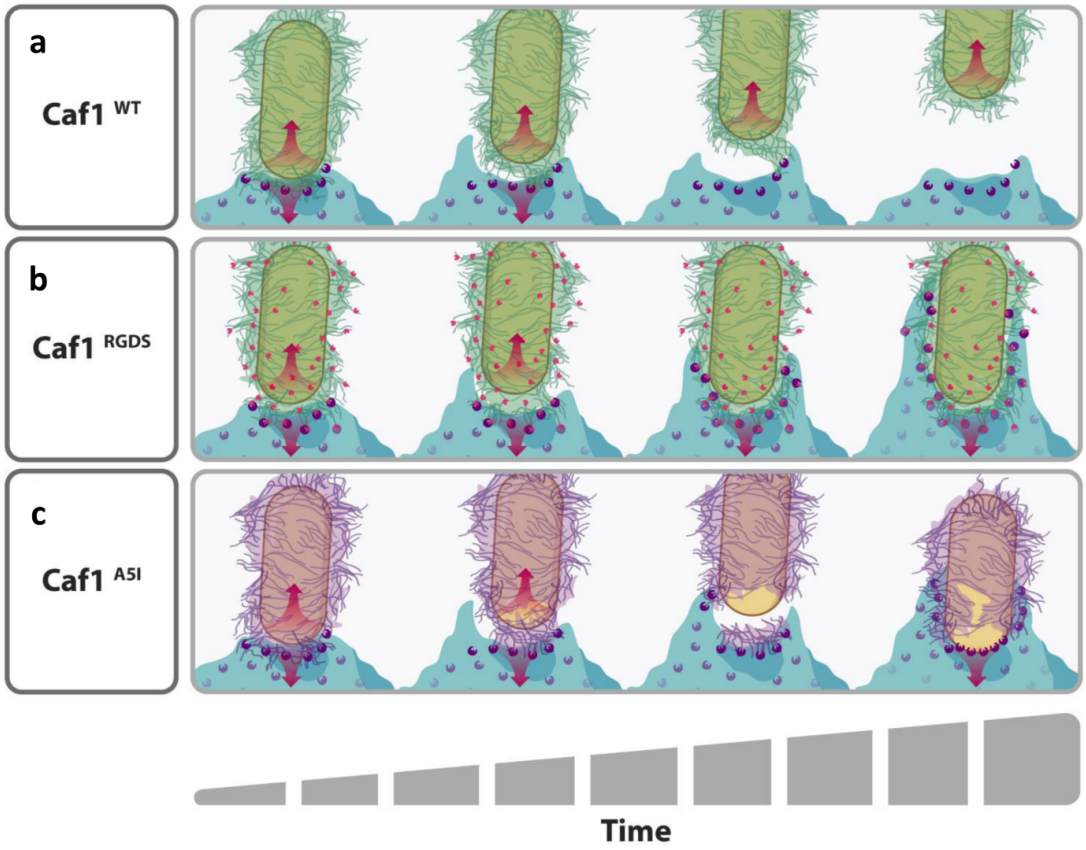

Fig. IV.7. Potential mechanism for Caf1 mediated bacterial escape from phagocytosis. The Caf1 coat (green) of an encapsulated *E. coli* cell (tan) on the surface of a macrophage (light blue) is engaged by macrophage receptors (purple). The macrophage exerts a force on the bacteria (downwards red arrow). Brownian motion and bacterial motility provide forces in the opposing direction (red upwards arrow). a. The Caf1 coat is mechanically strong and so does not break. The receptor-Caf1 interaction is weak and releases under the strain, allowing the bacterium to escape phagocytosis. In b., the RGDS mutation (pink dots) is incorporated into Caf1. This allows the macrophage receptors to bind with higher affinity to the Caf1 coat, so that the bacterium can no longer escape phagocytosis and is pulled towards the macrophage, resulting in further receptor engagement and clustering, and the formation of a phagocytic cup. In c., the A5I mutation reduces the mechanical strength of the Caf1 coat. Therefore, when the macrophage exerts a force on the coat, it experiences a strain and breaks to reveals the surface of the bacterium (tan). This is readily recognised by the macrophage and allows the bacteria to be phagocytosed.

Previous studies measuring the forces that can be generated by macrophages have produced a range of values, from the pN to the nN scale (Kress et al. 2007; El-Kirat-Chatel and Dufrêne 2016; Vonna et al. 2007; Flannagan et al. 2010; Trichet et al.

2012; Labernadie et al. 2014). We observe that a drop in Caf1 mechanostability from ~400 to ~320 pN is enough to reverse its anti-phagocytic activity. Providing that Caf1 has, like most proteins (Taverna and Goldstein 2002; DePristo, Weinreich, and Hartl 2005), evolved a stability only marginally higher than necessary for its function, it would appear that the stretching force exerted by the macrophage on *individual* molecules of Caf1 is within this range. Furthermore, is not inconceivable that the low adherence and high stability have co evolved to a point where the imparted force, limited by a lack of adhesion, can be resisted by a sufficiently strong polymer. As the macrophage likely exerts this force on several Caf1 molecules at once during attachment, the overall force exerted by the macrophage on the bacterium would be expected to be on the nN scale. Caf1 mutagenesis coupled with SFMS thus directly reports the mechanical stresses that occur during phagocytosis adding a new method to probe this important area of cell mechanics (Jain, Moeller, and Vogel 2019).

Methods

Plasmids and cloning. pGEM-T (Promega) was used as the basis for all subsequent plasmids. Caf1 and its mutants were expressed from the pT7-COP and pT7-COPΔR plasmids (Al-Jawdah et al. 2019; Peters et al. 2019), which contain T7-dependent transcriptional units comprising either the full *caf1* operon (*caf1R, caf1M, caf1A and caf1)* or the operon where *caf1R* has been deleted (*caf1M, caf1A, caf1),* which we have observed results in higher levels of Caf1 expression (Peters et al. 2019). $Caf1^{L5RGDS}$, $Caf1^{L5RGES}$, $Caf1^{A5I}$ and $Caf1^{T7L}$ mutants were cloned using the sequence and ligation independent cloning (SLIC) method (Li and Elledge 2007) with pT7-COPΔR as a template, where primer and mutant protein sequences are displayed in Chapter II: Materials and methods pT7-COPΔCaf1 and pT7-COPΔRΔCaf1 were generated through the substitution of codon 4 for a stop codon, i.e. the wild-type sequence, MKKISS, was mutated to MKK-stop, hence causing a knock-out of the gene through premature truncation of translation.

$I91_2$-cpCaf1-$I91_2$ was synthesised as a double stranded DNA insert by GeneArt (ThermoFisher Scientific), and ligated into a linear pQE80L plasmid by the SLIC method (Li and Elledge 2007). $I91_2$-cpCaf1^{A5I}-$I91_2$ and $I91_2$-cpCaf1^{T7L}-$I91_2$ were then generated from this plasmid by PCR mutagenesis using the SLIC method (Li and Elledge 2007). Primer and protein sequences are shown in Chapter II: Materials and methods.

Protein expression. *E. coli* BL21(DE3) cells (NEB) were transformed with the relevant plasmid and grown in 5 mL Terrific Broth (TB) cultures supplemented with 100 μg/mL ampicillin at 35°C for 22 h in order to express Caf1 proteins. For expression of the $I91_2$-cpCaf1-$I91_2$ constructs, *E. coli* BL21(DE3) cells were transformed with pQE80L plasmids containing the relevant coding sequences. Single colonies were then used to inoculate 500 mL of lysogeny broth (LB) medium. The cultures were grown at 37°C until the OD_{600} value was ~0.6, at which time IPTG was added to the culture to a final concentration of 1 mM in order to induce protein expression. Cultures were then grown for a further 3.5 h at 37°C, before centrifugation at 4424 x g for 15 min at 4°C. Cell pellets were resuspended in phosphate buffered saline (PBS) then centrifuged at 2367 x g for 10 min at 4°C. The cell pellets were then stored at -20°C.

Protein purification. Caf1 polymers for coating surfaces and beads were produced as described previously(Dura et al. 2018; Ulusu et al. 2017; Peters et al. 2019). For proteins that were used for SMFS experiments, frozen cell pellets were resuspended in loading buffer (50 mM Tris pH 7.4, 150 mM NaCl, 20 mM imidazole) supplemented with protease inhibitors (100 μg/mL AEBSF, 100 μg/mL Benzamide, 0.5 μg/mL Aprotinin, 1 μg/mL. Pepstatin and 1 μg/mL Leupeptin). Cells were lysed using a OneShot cell disruptor operated at 20 kPSI of pressure. The lysate was then clarified by centrifugation at 43667 x g for 30 min, then 39191 x g for 20 min at 4°C. 4 mL of Nickel-NTA resin in a gravity flow column was equilibrated in loading buffer before application of the lysate to the resin. Bound proteins were washed with 3 column volumes of loading buffer before elution with a solution containing 50 mM Tris pH 7.4, 150 mM NaCl and 500 mM imidazole. Fractions were analysed for protein

content by SDS-PAGE, then relevant fractions pooled and applied to a ProteoSEC S75 column (Generon), pre-equilibrated in PBS. Elution fractions were analysed by SDS-PAGE, and fractions containing the $I91_2$-cpCaf1-$I91_2$ proteins pooled and concentrated using Vivaspin 6 30 kDa molecular weight cut-off centrifugal concentrators (Sartorius). The concentration of the final samples was determined using UV absorbance at 280 nm and samples were flash frozen using liquid nitrogen for storage.

Transmission electron microscopy. Cultures of transformed BL21(DE3) *E. coli* (NEB) were grown in TB media supplemented with antibiotic for 24 h at 35°C. Carbon coated copper electron microscopy grids were glow discharged, then incubated with 20 μL of culture for 5 min. The bacteria were then fixed by a 5 min incubation with 20 μL 2% glutaraldehyde. The grid was then washed 1-2 times with 20 μL water, before a 30 s incubation in 20 μL 2% uranyl acetate for negative staining. Grids were then visualised using a Hitachi HT7800 120kV transmission electron microscope (EM Research Services, Newcastle University). Images were recorded in tagged image file format (TIFF).

Coating of polystyrene beads. 100 µL of 1 μm diameter Fluroesbrite® PolyFluor® 511 polystyrene beads (Polysciences) was centrifuged at 5000 x g and resuspended in 100 µL 50 mM sodium acetate buffer, pH 5.0. Caf1 proteins were diluted to 0.4 mg/mL in the same buffer and added to the beads in a 1:1 ratio. The solutions were incubated on a roller for ~ 16 h at 4˚C, centrifuged at 5000 x g, resuspended in the 200 µL fresh sodium acetate buffer, before centrifuging again at 5000 x g and resuspending in 200 µL fresh sodium acetate buffer. This resulted in a solution of 2.275 x 10^{10} beads/mL, and successful protein coating was determined by dot blot using a mouse anti-Caf1 antibody (Stratech) at a 1/1000 dilution and a goat anti-mouse alkaline phosphatase conjugated secondary antibody (Proteintech) also at a 1/1000 dilution.

Phagocytosis assay. J774.A1 (mouse macrophage-like; ATCC_TIB-67) cells were seeded (~1.1x10^5) in Dulbecco's Modified Eagle's Media (DMEM) supplemented

with 10% fetal calf serum (FCS) on glass coverslips 2 days prior to infection to obtain 60-70% confluence on the infection day. *E. coli* cultures were grown overnight in Lysogeny Broth (LB) media (with antibiotic when appropriate) prior to determining the OD_{600} value and calculating the volume for a Multiplicity of Infection (MOI) of 100:1 (bacteria to J774.A1 macrophage). Thirty minutes prior to infection, the macrophages were washed (37°C PBS) and incubated in DMEM only. Once inoculated, for all strains apart from EPEC and Cfm-14, macrophages were centrifuged for 5 min at 500 x g, 37°C and incubated for 1 h. Macrophages were then washed (37°C PBS) and incubated in DMEM containing chloramphenicol (bacterial protein synthesis inhibitor; 25 µg/ml final concentration) for 1 h (EPEC or Cfm) and 2hrs (for other strains) to promote bacterial uptake. Finally, the cells were washed twice (ice cold PBS) and fixed by incubating 20 min with PBS containing 2.5% para-formaldehyde (PFA; Santa Cruz Biotechnology), then stored at 4°C.

The percentage of bacterial internalisation was determined as previously described (Quitard et al. 2006). Briefly, extracellular bacteria were labelled by incubating 30 min (at RT) with 1/100 rabbit anti-*E. coli* all serotypes antibodies (Abcam) diluted in PBS. Following three washes with PBS, the cells were incubated for 30 min with 1/100 diluted goat anti-rabbit Alexa-555 conjugated secondary antibodies (Molecular Probes). The cells were then washed three more times with PBS. All cell-associated bacteria were labelled by incubating with the same primary antibody (PBS containing 1% Triton X-100, which makes macrophage membrane permeable to antibodies) followed by goat anti-rabbit Alexa-488 conjugated secondary antibodies (Molecular Probes), at a 1/100 dilution. The dye 4'6-diamidino-2-phenylinodole (DAPI - fluoresces blue) was routinely added in final antibody incubations to detect bacterial and host DNA. Coverslips were placed onto FluorSave reagent (Calbiochem) on glass slides (Thermo Scientific) for phase contrast/fluorescent microscopy examination (Zeiss Axioskop Epifluorescence microscope).

Fifty macrophages were randomly selected to count the number of extracellular and total-cell associated bacteria enabling the percentage internalisation to be calculated. These studies were undertaken in a semi-blind manner i.e. samples were placed in a withheld order until all counting was complete, and the percentage of internalisation calculated.

Phagocytosis assays involving polystyrene beads were performed similarly, with the following differences. Cells were incubated for 2 h with 10 µL of the coated polystyrene beads, before fixation. Extracellular beads were labelled by incubating 30 min at room temperature with a mouse anti-Caf1 antibody (Gene Tex) diluted 1/50 in PBS. Following three washes (PBS), the cells were incubated 30 min with 1/100 goat anti-mouse Alexa-555 conjugated secondary antibodies (Invitrogen-Molecular Probes). The cells were then washed again (3 x with PBS) with all cell-associated beads labelled by incubating with the same primary antibody diluted 1/50 in PBS containing 1% Triton X-100 to permeabilise the cells. This treatment was followed by 1/100 goat anti-mouse Alexa-488 conjugated secondary antibodies (Invitrogen- Molecular Probes). Percentage internalisation of the beads was then calculated in the same way as for the bacteria.

Adhesion Assay. 1 mL solutions of 1 mg/mL of $Caf1^{WT}$, $Caf1^{RGDS}$, $Caf1^{RGES}$, $Caf1^{A5I}$ and $Caf1^{T7L}$ proteins in water were added to wells of a 24-well plastic plate (Corning), which was then incubated at -80°C for 1 h, before freeze drying for 24 h. 1 mL of DMEM containing 10% FCS, Penicillin-Streptomycin (Sigma-Aldrich) and 1 x 10^5 J774.A1 (mouse macrophage-like; ATCC_TIB-67) or Hela cells (ATCC-CCL-2) were added to the coated wells, as well as an uncoated well, and then incubated for 24 h at 37°C. Pictures were taken using an EVOS bright-field imaging system (Thermo Fisher).

Single molecule force spectroscopy. Single-molecule force spectroscopy experiments were carried out using a commercial atomic force spectroscope (Luigs and Neumann). The cantilevers used in the experiments were calibrated using the equipartition theorem and they had typical spring constant of around 6 pN/nm (Bruker OBL-10). Proteins were incubated for ten minutes over custom made gold surfaces at a concentration of 0.1-1.0 g/L. The buffer used was HEPES 10 mM pH 7.0, NaCl 150 mM and 1 mM EDTA. Force-extension experiments were performed at 400 nm/s. The traces obtained were collected and analyzed with a custom-written code using the worm-like chain model for polymer elasticity. All the figures were generated using Igor Pro (Wavemetrics) and Adobe Illustrator (Adobe).

Data Availability

The data that support the findings of this study are available from the corresponding author upon reasonable request.

Acknowledgements

The authors would like to thank Dr. Kathryn White and Dr. Tracey Davey of the Newcastle Electron Microscopy Services team for technical assistance. This work was funded by the Industrial Biotechnology Catalyst (Innovate UK, BBSRC, EPSRC) award number BB/M018318/1, to support the translation, development and commercialisation of innovative Industrial Biotechnology processes. Equipment funded by Wellcome Trust grant 056232 was used in this study. The funding agencies had no involvement in the acquisition and analysis of the data, or in the writing of the manuscript.

Author Contributions

DTP: Conceptualisation, Investigation, Writing – Original Draft, Writing – Review and Editing, Visualisation

AR: Investigation, Formal Analysis, Writing – Review and Editing, Visualisation

AAC: Investigation, Formal Analysis,

AM: Investigation, Formal Analysis, Writing – Review and Editing, Visualisation

HW: Resources, Writing – Review and Editing

BK: Resources, Supervision, Writing – Review and Editing, Funding Acquisition

RPJ: Conceptualisation, Resources, Supervision, Writing – Original Draft, Writing – Review and Editing, Project Administration, Funding Acquisition

JHL: Conceptualisation, Supervision, Writing – Original Draft, Writing – Review and Editing, Project Administration, Funding Acquisition.

Chapter V:

High throughput search of small molecules for controlling the mechanical stability of proteins

Antonio Reifs[1], Alba Fernandez-Calvo[1], Borja Alonso-Lerma[1], Jörg Schönfelder[1], David Franco[2], Mariano Ortega-Muñoz[3], David De Sancho[4,5], Eider San Sebastian[6,*] & Raul Perez-Jimenez[1,6,*]

1. *CIC nanoGUNE BRTA, Tolosa Hiribidea 76, 20018 San Sebastian, Spain.*
2. *Glaxosmithkline (GSK Vaccines), Rue de l'Institut 89, 1330 Rixensart, Belgium.*
3. *Department of Organic Chemistry, Faculty of Science, University of Granada, 18071 Granada, Spain.*
4. *Applied chemistry Department, Faculty of Chemistry, University of the Basque Country (UPV/EHU), Manuel Lardizabal Ibilbidea 3, 20018 San Sebastian, Spain.*
5. *Donostia International Physics Center (DIPC), Manuel Lardizabal Ibilbidea 4, 20018 San Sebastian, Spain.*
6. *Applied Chemistry Department, Faculty of Chemistry, University of the Basque (UPV/EHU), Manuel Lardizabal Ibilbidea 3, 20018 San Sebastian, Spain.*
7. *Ikerbasque Foundation for Science, Plaza Euskadi 5, 48009 Bilbao, Spain.*

*Corresponding Authors

Protein mechanical stability determines the function of a myriad of proteins, especially proteins from the extracellular matrix. Failure to maintain protein mechanical stability may result in diseases and disorders such as cancer, cardiomyopathies, or muscular dystrophy. Thus, developing mutation-free approaches to enhance and control the mechanical stability of proteins using pharmacology-based methods, may have important implications in drug development and discovery. Here, we present the first approach that employs computational High-Throughput Virtual Screening (HTVS) and Molecular Docking to search for small-molecules in chemical libraries that function as mechano-regulators of the stability of human CD4. Using single-molecule force spectroscopy we probe that these small-molecules can increase the mechanical stability of CD4D1D2 domains over 4-fold also modifying the mechanical integrity of the tandem. Our experiments demonstrate that chemical libraries are a source of mechanoactive molecules and that drug discovery approaches provide the foundation of a new type of molecular function, i.e., mechanoregulation, paving the way towards mechanopharmacology.

Introduction

Numerous proteins in the cell withstand mechanical loads while performing their function (Schonfelder et al. 2018; Gupta, Toptygin, and Kaiser 2020; Seifert and Gräter 2013; Vogel and Sheetz 2006). This is especially significant for cell-surface proteins located in the extracellular matrix, which are essential for the communication between cells in the extracellular milieu (Dufrene and Pelling 2013; Klotzsch et al. 2015; Yusko and Asbury 2014). Reacting to mechanical force through conformational changes is crucial for these cell-surface proteins, translating a physical signal into an intracellular signaling process (Lim, Jang, and Kim 2018; Pines et al. 2012; del Rio et al. 2009), or establishing physical connection with other cells (Pannekoek, de Rooij, and Gloerich 2019). Over 1400 cell-surface proteins compose the human surfaceome, including integrins, adhesion molecules (ICAM) and CD molecules (Bausch-Fluck et al. 2015), which highlights the importance of protein mechanics in the cell. Similarly, viruses and bacteria use their own surface proteins to establish anchoring with cell-surface molecules to initiate infection (Gordon and Wang 2019). Again, the mechanical stability of these protein-protein interaction plays a crucial role in the success of the infection process (Alonso-Caballero et al. 2018; Alegre-Cebollada, Badilla, and Fernandez 2010), implying an important function of mechanical force in viral entry and bacterial adhesion(Perez-Jimenez et al. 2014; Wiegand et al. 2020; Mathelie-Guinlet et al. 2020). In fact, it is known that perturbating such interaction may result in avoidance of infection (Spaulding et al. 2018).

In the past years, efforts have been made towards designing protocols to control the mechanostability of proteins. For instance, an elegant work by Rivas et al, demonstrated that blocking the formation of isopeptide bonds in S*treptococcus pyogenes* pilus proteins, it is possible to interfere with the pili formation (Rivas-Pardo et al. 2018), which may result in the modification of the adhesion capabilities of the bacterium. Also, it is well-known that mutations in strategic locations show effectiveness in altering the mechanical stability of proteins (Perez-Jimenez et al. 2006; Li et al. 2000); nevertheless, mutations are irreversible and most often go in the destabilizing direction. Other studies have demonstrated that antibody binding or metal chelation can also alter the mechanical stability of proteins (Perez-Jimenez et al. 2014; Hu and Li 2014). Altogether, these studies have provided a wealth of information regarding protein mechanics in biological systems, however, introducing mutations, using antibodies or metal ions may have some complications for practical implementation as mechano-modulators.

Here, we propose a mutation-free approach to alter protein mechano-stability utilizing small molecules. Our technology combines High-Throughput Virtual Screening (HTVS) of compound libraries, molecular docking, and single-molecule Atomic Force Spectroscopy (smAFS). HTVS allows searching thousands of compounds from virtual chemical libraries similar to procedures commonly utilized in drug discovery (Cerqueira et al. 2009; Irwin and Shoichet 2016; Lavecchia and Di Giovanni 2013). The molecular docking allows targeting specific regions that can even be selected to alter the mechanics of a protein. We apply this approach to CD4 protein, a coreceptor present in T lymphocytes membrane, which is involved on antigen recognition, but also, it is the primary receptor of HIV-1. We have identified three small-molecules that in smAFS experiments, probe their ability to modify and enhance CD4 mechanical stability alone or combined, thus acting as surface-protein mechanical regulators (SUPROMERs). We propose these SUPROMER molecules as a prove of concept of mechano-active molecules discovered by means of a drug discovery pharmacology-based approach, bringing the possibility of a new class of mechano-drugs. We propose that SUPROMERs might be useful molecules not only to alter the mechanical stability of cell-surface protein, but also that of any protein whose function relies on its mechanical integrity. Thus, SUPROMERs may be useful to interfere with any protein-protein interaction process that occurs with the intervention of forces, such as those happening between microbes and host cells or cell-cell interaction.

Results

• High-Throughput Virtual Screening (HTVS) of a compound library.

Our initial step focused on the search of small-molecules capable of binding regions of CD4 that can potentially influence the mechanical stability of the molecule. We designed a virtual screening search of commercially available small-molecules available in the ZINC chemical library (https://zinc.docking.org/), using Glide software from Schrödinger Suite (Friesner et al. 2004), that docks molecules in the structure of CD4 (pdb:1WIP). We restricted the search and docking to domains D1 and D2 of CD4 by creating three partially overlapping grids that cover the whole structure. (see Fig. V.1.) The first grid focussed on D1, another one D2 and a third

one focussing on the interface of D1D2. This strategy derives from our previous knowledge on the mechanical stability of CD4 domains(Perez-Jimenez et al. 2014), from which we know that the continuous β-strand shared by domains D1 and D2 and the interface between these domains play a crucial role in the mechanical integrity of the tandem(Perez-Jimenez et al. 2014). In fact, it was demonstrated that an antibody named Ibalizumab (commercialized as Trogarzo) that precisely binds the D1D2 interface (Freeman et al. 2010), has a strong mechanical effect on the stability of CD4 D1D2 (Perez-Jimenez et al. 2014). Thus, the interface between the domains is a clear target in our search.

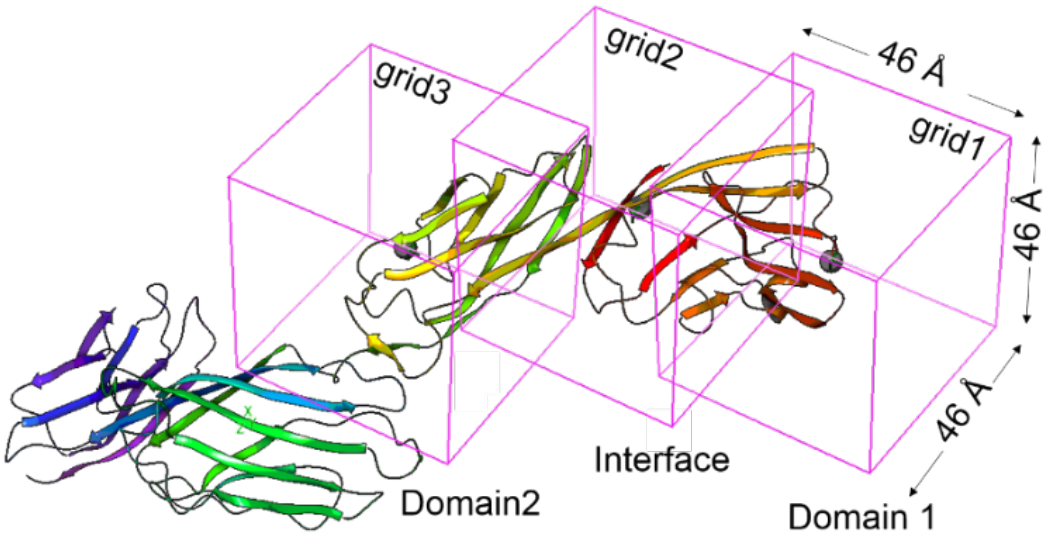

Fig. V.1. View of the outer boxes of grids 1, 2 and 3 generated with the Glide grid generation module. To properly map domains 1 and 2 of CD4 in 1WIP, as well as their interface. Grey spheres represent CA atoms of residues SER23, LEU95 and VAL146, where grids 1, 2 and 3 where centered, respectively.

We then followed a multistep approach to retain molecules with at least one with binding energy below a given threshold of -5 kcal/mol. This resulted in 1549 compounds with binding energies below that threshold established in the HTVS phase. (see Fig. V.2.) depicts a schematic representation of the search protocol which is described in the Methods section. Subsequent re-docking of the selected compounds using the Standard Precision level of Glide (SP mode), which performs a harder torsional refinement and sampling of the conformations, promoted the number of compounds of interest to be narrowed down to 82. The latter

displayed a binding energy (docking score) with values below -5 kcal/mol for at least one of the three grids under study.

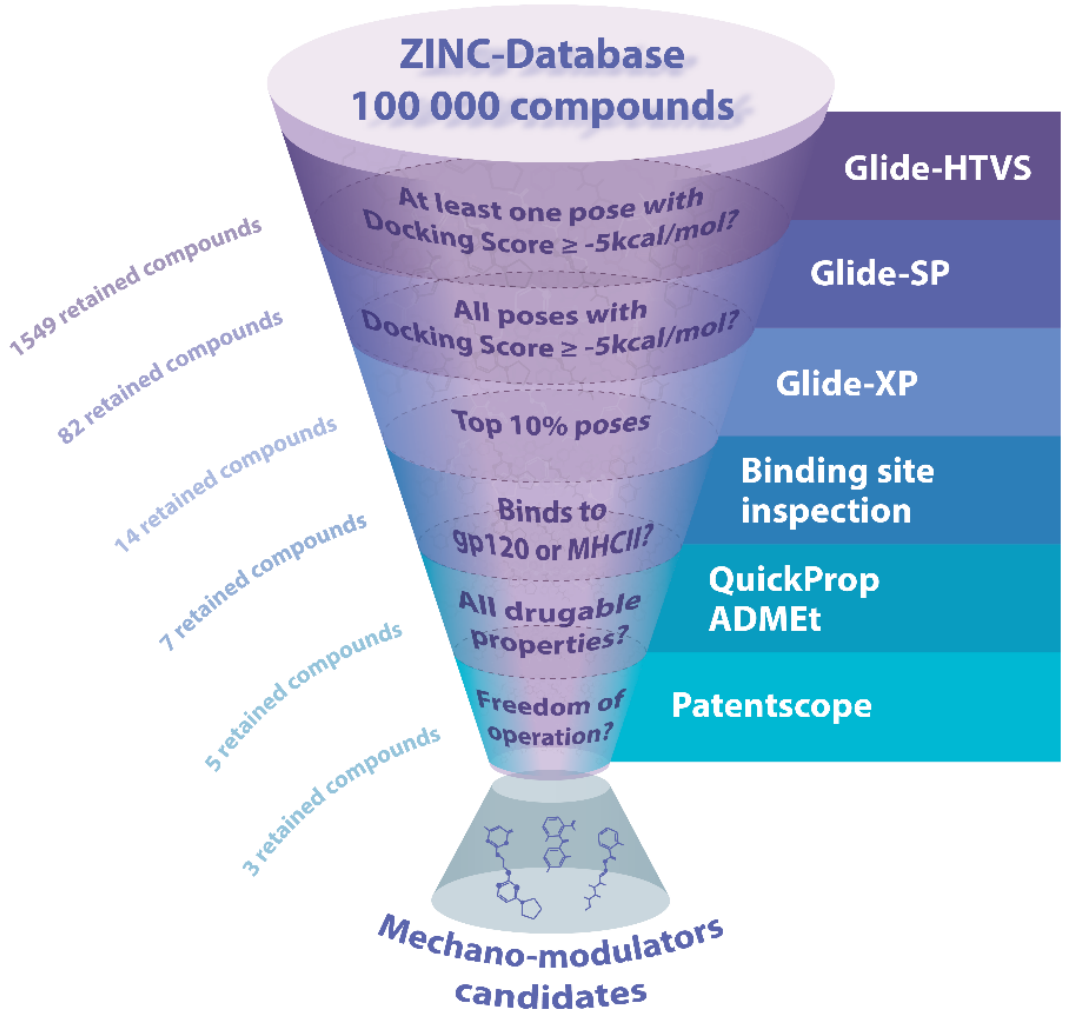

Fig. V.2. Workflow used to identify protein mechano-modulators. The key properties of an ideal mechano-modulator were established as follows: should display a strong binding to the problem protein, to achieve this we make use of Glide-HTVS, Glide-SP and Glide-XP; should not interfere with the protein binding site or any relevant epitope/active site, depending on the problem protein; should have optimal ADMEt properties; and should enjoy of a complete freedom of operation at the industrial property level.

A final Extra precision (XP level of Glide) docking procedure of the compounds selected so-far, to penalize ligands that do not fit well to the receptor conformation, filtered out all but 14 compounds. Subsequent binding site analysis excluded ligand/poses interfering with forbidden binding sites (FBS). FBS were defined in the CD4 structure, resides 35-52, 55-60 defined as MHC class II binding epitope (see Fig. V.3.) (Wang et al. 2001), retaining 8 compounds. A QuickProp ADMEt analysis retained 5 compounds of which three enjoy freedom of operation.

In summary, three were the compounds from the ZINC lead-like subset of compounds that fulfilled all the filtering criteria established in the present study. These potential mechanical regulators of CD4 (ZINC65466948, ZINC00481608 and ZINC05514670 in ZINC database) will be referred to as SUPROMER 1, 2 and 3, (see Fig. V.4.) respectively (acronym for SUrface PROtein MEchanical Regulator). The structures of the SUPROMERs are shown in Fig. V.4a. SUPROMERs were obtained either by direct purchase or by chemical synthesis.

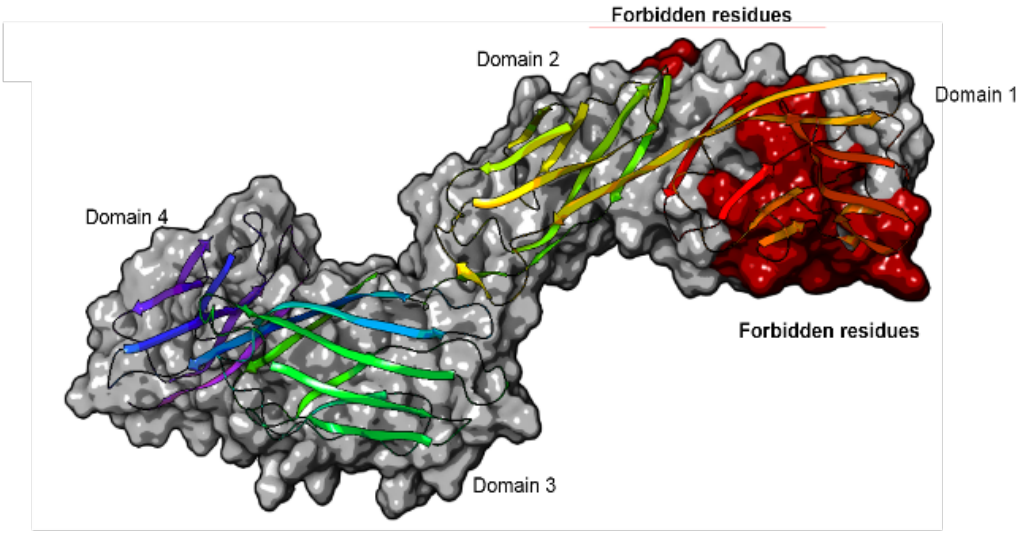

Fig. V.3. Forbidden binding sites. CD4 (full length) surface and carton representation, where residues implicated in gp120 and/or MHCII binding ("Forbidden residues") are indicated in red.

- **Binding and interaction of SUPROMERs with CD4D1D2.**

An analysis of the binding energetics, binding sites, and binding modes of SUPROMERs to CD4 revealed that these compounds can bind to distinct regions of the receptor with different affinities; (see Fig. V.4b.) however, some of these regions are similar for the three small-molecules.

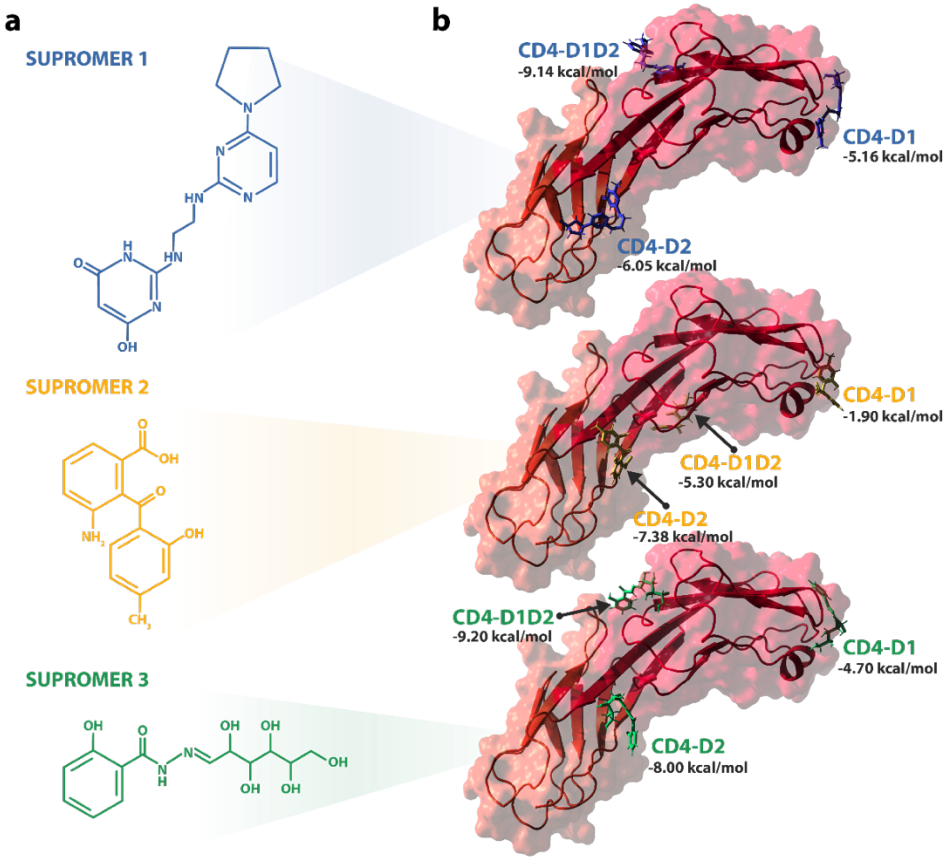

Fig. V.4. Structural interaction of SUPROMERs and CD4 domains. a. Chemical structure of SUPROMER 1 (ZINC65466948), SUPROMER 2 (ZINC0048160) and SUPROMER 3 (ZINC05514670) b. Surface and cartoon representation of CD4 domains 1 and 2. In stick representation appear all the poses derived from the XP docking procedure of (top) SUPROMER 1, (middle) SUPROMER 2, and (bottom) SUPROMER 3.

SUPROMER 1 may preferentially bind to the interface between domain 1 and domain 2, with a GScore of -9.14 kcal/mol, but can also bind D1 and D2 with GScore of 5.16 and 6.05 kcal/mol, respectively.

SUPROMER 2 may preferentially bind to domain 2, with a scoring energy of -7.38 kcal/mol. It also binds close to the interface between D1 and D2 with GScore value -5.30 kcal/mol but in the opposite side that that of SUPROMER 1.

Finally, SUPROMER 3 binds the interface between domain 1 and 2 in the back side of the tandem with GScore value of -9.20 kcal/mol but can also bind D2 with GScore value of -8.0 kcal/mol and weakly to D1.

In addition, as observed in Fig. V.5., SUPROMERs establish key interaction with residues in CD4, mostly charged and polar residues indicating the electrostatic nature of the interactions. Interestingly, the interaction of SUPROMER 3 near the interface between D1 and D2 involves residues Ser79 and Glu77 in D1, which have been also shown to be important in the interaction of Ibalizumab and CD4(Freeman et al. 2010). Nevertheless, given the considerable smaller size of the SUPROMER with respect to Trograzo, we do not expect many interacting residues to be common between both molecules.

Moreover, we were surprised to see that some of the SUPROMERs poses bind very similar locations in CD4 domains, e.g., SUPROMER 1 and 3 in the three grids, or poses in D1 and D2, which highlight these regions as potential druggable sites (see Fig. V.6.)

For informative purposes on the translational potential, we have run a prediction of multiple physically significant descriptors and pharmaceutically relevant properties (ADME descriptors) of single conformers of SUPROMERs using QikProp software.

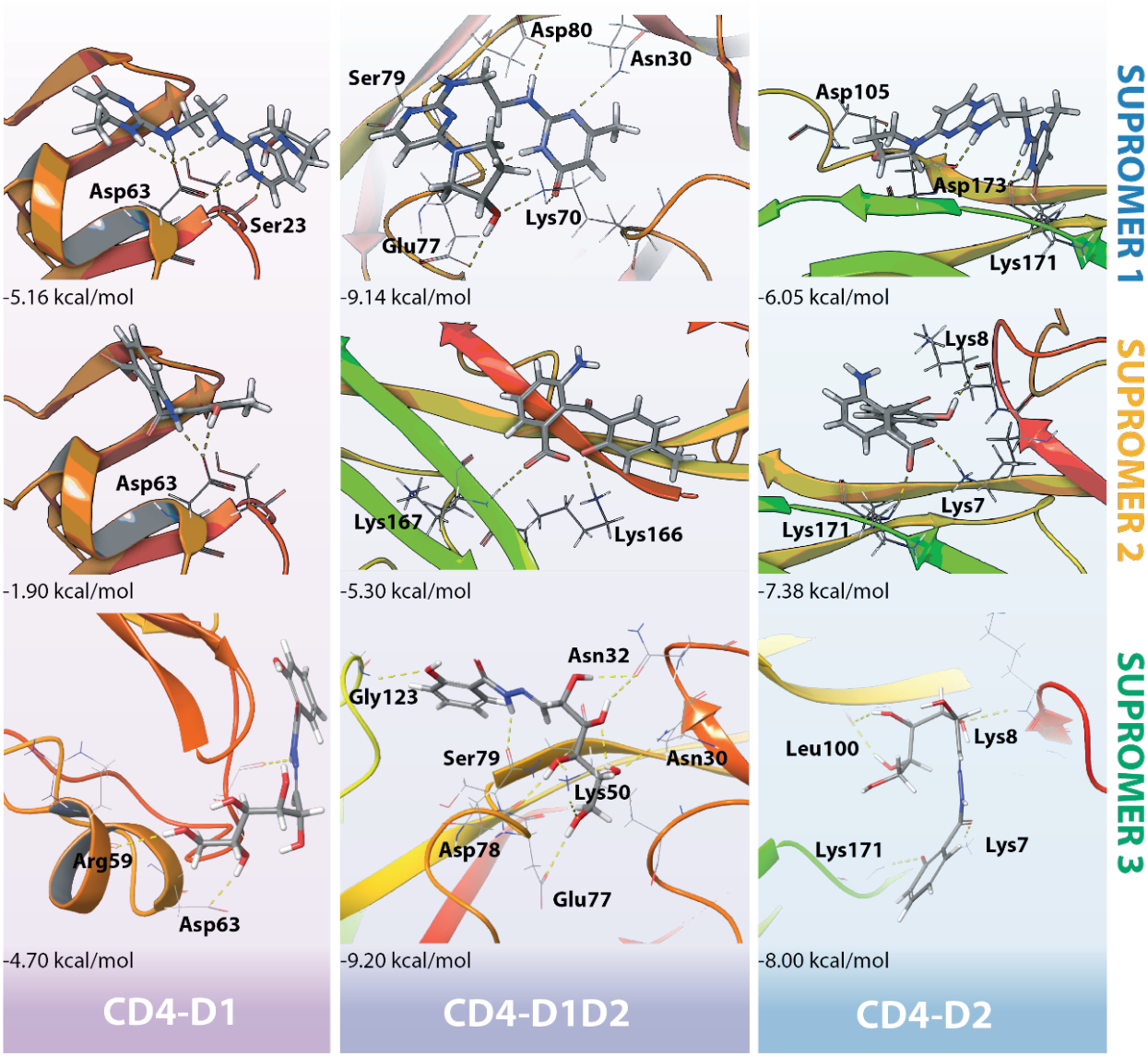

FigV.5. Detailed interaction of SUPROMERs and residues in CD4 domains. SUPROMER 1 (top) SUPROMER 2 (middle) and SUPROMER 3 (bottom) most efficient binding modes to domain 1 tip (left), domains 1 and 2 interface (middle) and domain 2 (right). XP GScore values (kcal/mol) are indicated in bold below each pose. H-bonds established between each molecule and key residues in CD4 domains are indicated with dashed lines.

The ADME descriptors were compared with those of 95% of known drugs. As observed, SUPROMER 1 and 2 have optimal properties with respect to their drugability.

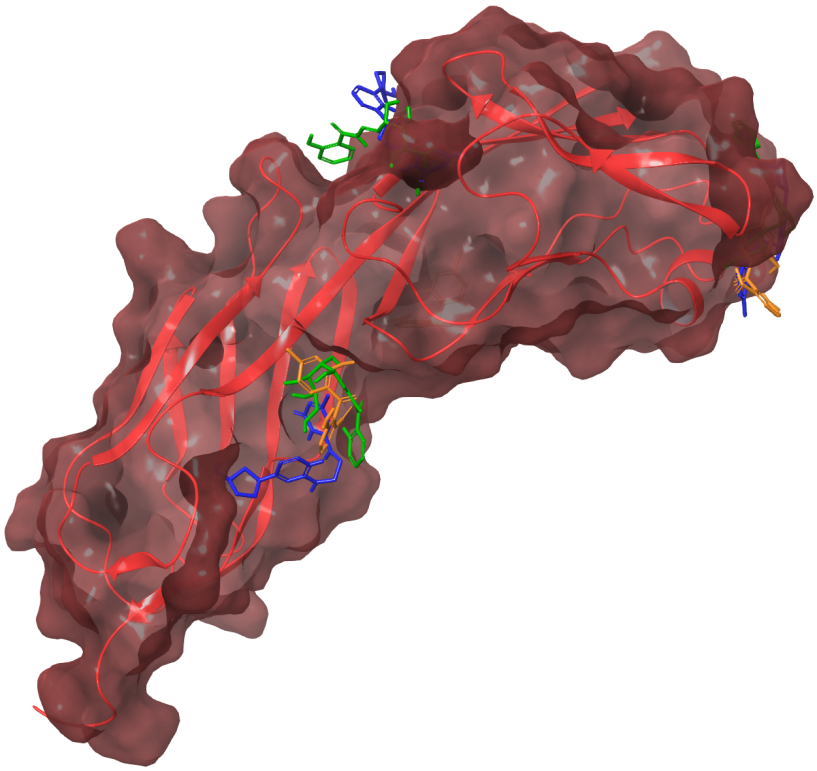

Fig. V.6. Representation of CD4D1D2 structure with the three SUPROMERs bound to it in their best pose. The three locations are the same for all of them.

In this line, an analysis of the Lipinskis rule of five(Lipinski 2004) (if # stars =0 fulfills all the rules) implies that SUPROMER 1 and 2 have properties like 95% of those drugs found in the market, which suggest that the search process provides small molecules that are even potential drugs. For instance, Human Oral absorption value equal to 3, implies that these two drugs may likely be good candidates to be orally administered in *in vivo* preclinical and clinical tests. SUPROMER 3, with 6 H-bond donors and # stars =1 is still an excellent oral candidate. We have also carried a standard test of the cytotoxicity on HEK293 cells of the different SUPROMERs and

compared it with that of Ibalizumab at different concentrations. Very similar levels of cell viability were obtained with all SUPROMERs and Ibalizumab. (see Fig. V.7.)

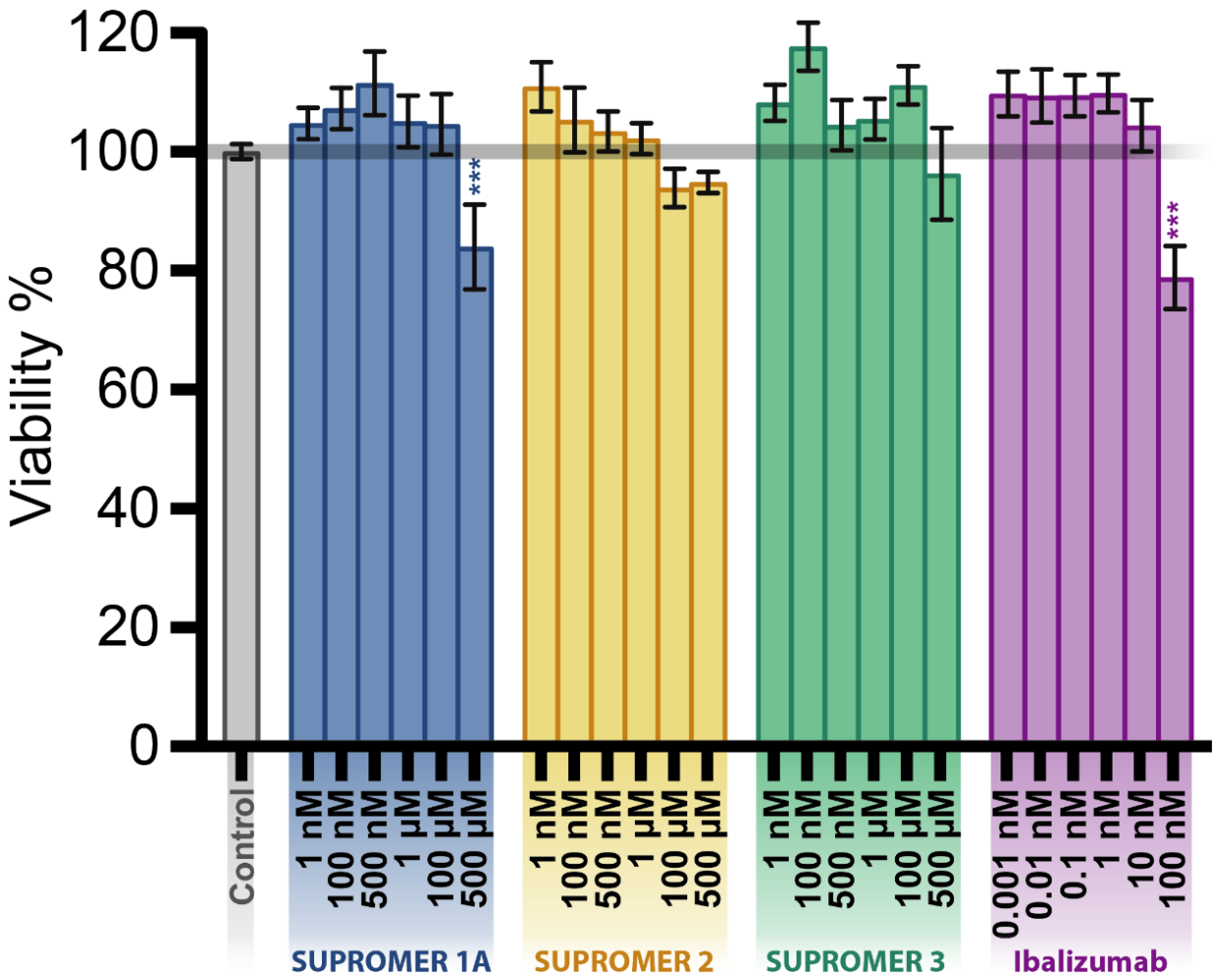

Fig. V.7. Cytotoxicity assay using HEK 293 cells. In absence (grey) as a control and presence of increasing concentrations of SUPROMERs and Ibalizumab. The difference of viability percentage between control and cells in presence of 500 μM of Supromer 1A and 100 nM of Ibalizumab are considered to be extremely statistically.

- **Single-molecule atomic force spectroscopy of SUPROMER molecules.**

To test the mechanical effect of SUPROMER effectors on CD4 domains we used smAFS. We first designed a polyprotein composed of CD4, domains D1 and D2, flanked by handles of two-domains I91 subunits from human cardiac titin, resulting the polyprotein $(I91)_2CD4D1D2(I91)_2$ to which we apply a calibrated mechanical force. (see FigV.8a.) We have successfully used this construct before to probe the effect of force on CD4(Perez-Jimenez et al. 2014). These four I91 subunits are used as a mechanical fingerprint, due to the well-known properties of this subdomain in smAFS systems and have been used to study the mechanics of many other proteins(Alonso-Caballero et al. 2018; del Rio et al. 2009). For the smAFS experiments, we chose the so-called force-ramp mode, in which the force applied to the polyprotein is ramped up at a constant speed of 33 $pN \cdot s^{-1}$. Force-ramp experimental data is characterized by a typical ramped staircase, in which each step represents the unfolding process of one subdomain from the polyprotein construct. (see FigV.8b.) In the case of the polyprotein used here, we identify 4 equal steps from I91 domains. We have measured an initial unfolding force of 128 ± 5 pN (mean ± SEM). This initial unfolding force represents the average minimum force at which I91 domains start unfolding. For these domains we determine step size of 24.9 ± 2.6 nm (mean ± SD) which is in accordance with the size expected at the loading rate that we applied(Perez-Jimenez et al. 2014). (see FigV.9.)

We also identify one or two additional steps corresponding to our protein of interest CD4D1D2. In the case of CD4D1D2 alone, we mostly observe two unfolding steps, although we also observed the unfolding of the tandem in a single step, which means that both domains are being unfolded simultaneously. We determine an average initial unfolding force of 81 ± 6 pN. In the case of two-step unfolding of the tandem, we measure step size of 7.4 ± 1.4 nm and 13.5 ± 0.9 nm for D1 and D2, respectively. (see Fig. V.8b.) In the case of the one step unfolding, the step size observed is 22.4 ± 1.4 nm, which is the sum of the two domains. These values are consistent with those reported before by us(Perez-Jimenez et al. 2014).

To determine the ability of the SUPROMERs molecules to alter the mechanics of CD4 domains we perform the smAFS experiment in the presence of SUPROMER in a ratio 1:5, protein:SUPROMER. Starting with SUPROMER 1, we observe the same step size but with a significant shift in the number of events for each one, with the peak corresponding to one step unfolding, at 20.6 ± 1.0 nm nm, as the more

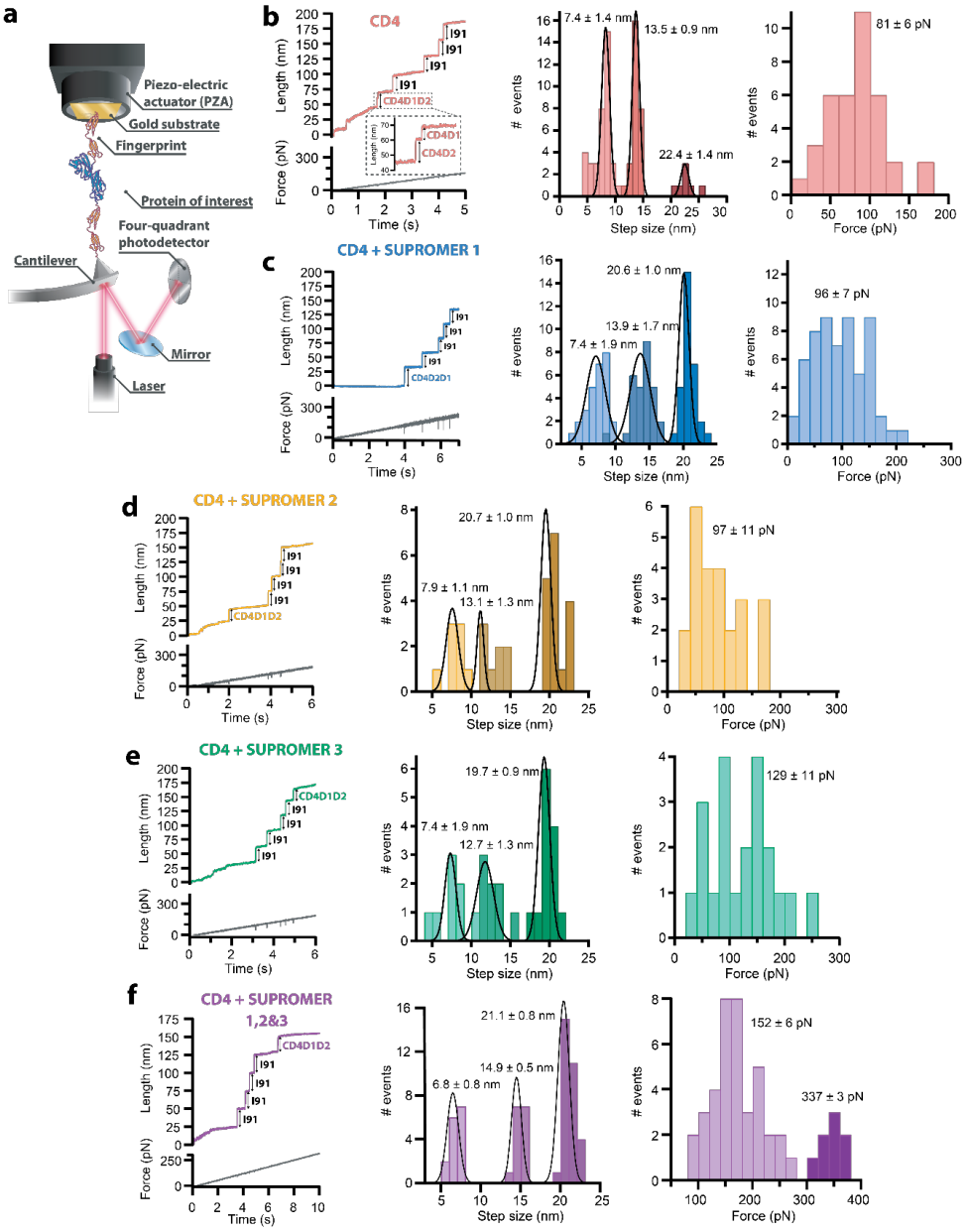

Fig. V.8. smAFS experiments of SUPROMERS and CD4 in force-ramp mode. a. Representation of the $(I91)_2$-CD4D1D2-$(I91)_2$ polyprotein construct on an smAFS set-up. The I91 modules are used as molecular fingerprint. The polyprotein is attached to a gold substrate in one end and a cantilever in the other end. b. Typical force-ramp trace of $(I91)_2$-CD4D1D2-$(I91)_2$ polyprotein and histogram of step size and initial unfolding force (n=37). c. trace and histograms in the presence of SUPROMER 1 (n=56), d. SUPROMER 2 (n=29), e. SUPROMER 3 (n=29) and f. the three SUPROMERs together (n=46). Different colors have been used to identify each combination.

prominent one. (see Fig. V.8c.) We also observe a slight increment in the initial unfolding force with respect to CD4D1D2 alone, being this force 95 ± 7 pN. (see Fig. V.8c.)

In the case of SUPROMER 2 we measure a very similar step size with distribution with initial unfolding force of 97 ± 11 pN. (see Fig. V.8d.) and for SUPROMER 3, similar step size but in this case the increment in initial unfolding force is quite significant at 129 ± 11 pN. (see Fig. V.8e.) However, the most substantial increment in force occurs with the combined action of the three SUPROMERs by which the initial unfolding force shows two populations, one peaking at 152 ± 6 pN, (see Fig. V.8f.) which is similar to the mechanical effect of Ibalizumab(Perez-Jimenez et al. 2014), and a second population with higher average unfolding force of 336 ± 3 pN, which represents an increment of over four-fold with respect to CD4D1D2 alone. We believe that this is probably the result of different combinations of SUPROMERs in the mix. Initial unfolding forces for all three SUPROMERs are summarized in. Fig. V.10.

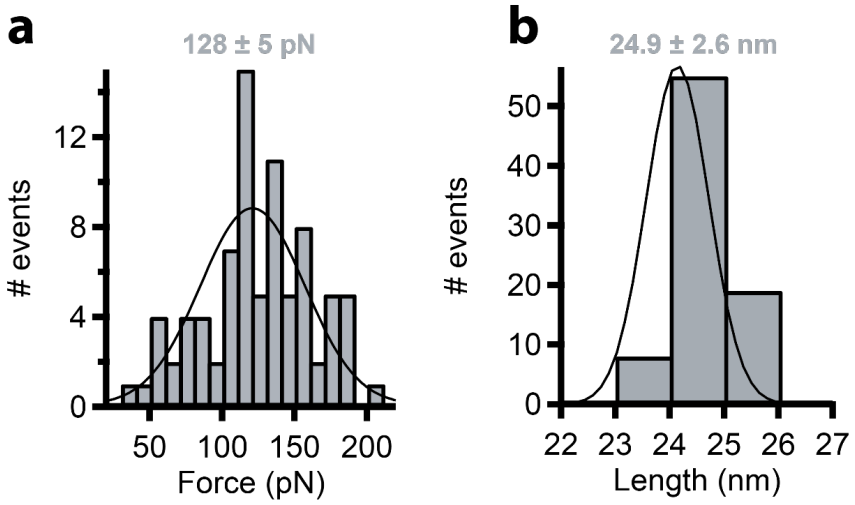

Fig. V.9. a. Histogram of initial unfolding force of I91 (n = 82) we measured an unfolding force of 128 ± 4.5 pN. b. Histogram of step size for the unfolding of I91(n = 82) The unfolding of I91 Domain was measured at 24.9 ± 2.6 nm.

Interestingly, if we consider the pulling speed in the force-damp experiments, we can estimate the mechanical unfolding lifetime increment of the tandem CD4D1D2 upon SUPROMER binding. For such calculation we take as zero reference value the unfolding of CD4D1D2 alone. The binding of SUPROMERs increase the lifetime of

the folded domains, a fraction of a second for SUPROMERs 1 and 2, up to several seconds for SUPROMERs 1,2 and 3 together right axis in Fig. V.10a.

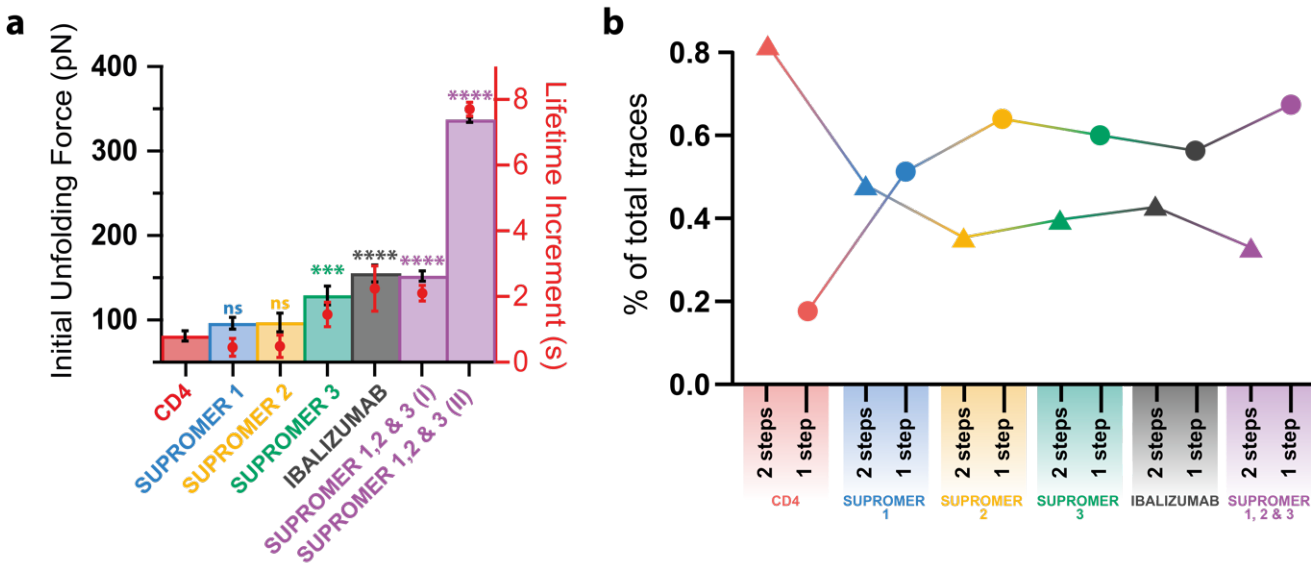

Fig. V.10. Mechanical stability and unfolding of CD4D1D2 and SUPROMER. a. Comparison of initial unfolding forces for CD4D1D2 domains in the presence of each SUPROMER, Ibalizumab and combination of all SUPROMERs. The difference of initial unfolding force between CD4 and CD4 in presence of SUPROMER 3, Ibalizumab and SUPROMER 1, 2 and 3 are statistically significant with a P value of 0.0004, 0.0001 and 0.0001, respectively. Right axis in red represents the mechanical unfolding lifetime increment of the tandem CD4D1D2 upon SURPOMERs binding. b. Fraction of unfolding events for CD4D1 and D2 domains in one (triangles) or two steps (circles) for each combination of CD4D1D2 and SUPROMERs.

A clear effect that we observed is that with the binding of every SUPROMER, CD4D1D2 changes its unfolding pattern from two steps to just one. As shown in Fig. V.10b. in the case of CD4D1D2, about 80% of the traces show two-step unfolding and following a regular pattern in which D2 unfolds first. In the presence of SUPROMER 1, about 50% of the traces show one-step unfolding of about 21 nm. This percentage increases to over 60% for SUPROMERs 2 and 3, which is even more than the observed effect for Ibalizumab. Interestingly, the more drastic shift is observed when combining the three SUPROMERs molecules with a proportion of one versus two steps of about 65% to 35%. (see Fig. V.10b.) This alteration in the mechanical unfolding clearly proves the effect of the SUPROMERs molecules in the mechanical integrity of the tandem. By avoiding the two-step unfolding, the small-

molecules are stabilizing the structure, likely reinforcing the β-strand network that connects both domains. Considering that the three SUPROMERs molecules seem to bind with elevated Gscore in the region connecting D1 and D2, these results are somehow expected.

Discussion

In the past decades, High-throughput Screening (HTS) techniques have become the gold standard approach to drug discovery, not only in research but also in the pharmaceutical industry. Additionally, the implementation of computational methods for structure-based virtual screening and molecular docking has boosted the capability of screening methods(Gerhold and Schwartz 2016; Gao et al. 2022; Sianati et al. 2019). These methods mostly utilize protein structures where small molecules, peptides or ligands are docked to high affinity serving as initial step for further design or even experimental testing of alterations in a particular molecular process. This procedure can be applied to chemical libraries of compounds, providing a protocol for rapid testing of many molecules, thus considered a High-throughput Virtual Screening (HTVS). In the present study, we apply a HTVS approach to search for small molecules that serve as mechano-regulators of CD4 domains, named SUPROMERs. To the best of our knowledge, this is the first protocol aimed to find small molecules that alter the mechanical properties of a protein. We thus, demonstrate that a highly developed drug-discovery approach can be repurposed for a new functionality, which is mechanoregulation.

The identified SUPROMER molecules alter the mechanical properties of CD4 making the tandem D1D2 of CD4 to behave as a single unit, which means that structural integrity of the protein is reinforced. This is demonstrated by the unfolding of the tandem as a single step. One of the SUPROMERs, increases the mechanical strength of the tandem over 50%, however, the combined action of the three molecules renders a CD4D1D2 tandem with a highly increased mechanical stability, with numerous unfolding events reaching over 330 pN. We believe that such increment is the results of high affinity interaction, especially in the intermediate region holding both domains, where a long β-strand is shared between the two domains. In fact, the three SUPROMERs show docking poses in that region, as demonstrated in. Fig. V.5. Interestingly, only two residues of the D1D2 tandem, Ser79 and Asn30, are common to the interaction of the three SUPROMERs, with

suggests that the combined interaction may entail double or even triple binding with no competition. This could result in the large increment in mechanical stability that we observe.

Our results represent a proof of concept of the possibility of searching molecules that act as mechano-regulators. This is important because controlling the mechanical stability of proteins may have important implications. It is well known that numerous diseases are related to structural changes in proteins that may results from mechanical perturbations. These changes may be introduced by mutations and therefore are not easily corrigible. A good example could be mutations that cause mechanical alterations in cardiac proteins, generating hypertrophic cardiomyopathies(Poole 2022). Similarly, other mutations relating mechanical stability of proteins and disease have been identified (Lewis and Grandl 2021) . However, other biological processes such as protein transport across membrane pathways or nuclear pores(Richardson, Kotevski, and Poole 2021; Stewart et al. 2021; Alonso-Caballero et al. 2018; Kefauver, Ward, and Patapoutian 2020), the mechanoactivation of ion channels (Gerhold and Schwartz 2016), (Kefauver, Ward, and Patapoutian 2020; Martinac and Poole 2018) or cancer cell development (Wirtz, Konstantopoulos, and Searson 2011; Yankaskas et al. 2021), are associated to protein mechanics. Therefore, having a protocol that employs the same approaches as drug discovery techniques to alter protein mechanical stability makes this approach very interesting in many disciplines related to cell and molecular biology.

In our case, we have chosen CD4 as potential target for protein mechanical stabilization. The intended idea was to find small molecules whose docking pose had a high Gscore and therefore are candidate to stabilize the protein. From over 100,000 compounds we found only three molecules with high enough affinity, but our search criteria were purposely strict, akin to conditions used for drug discovery. Thus, our intention of creating a pharmacology-based approach has been successful in terms of mechanical stabilization of CD4 domains. Whether our SUPROMERs molecules may have an inhibitory effect of HIV-1 such as the case of Trozargo, is an open question that is beyond the initial scope of this work; however, we hypothesize that these molecules may be a good starting point for developing potential small-molecule inhibitors of HIV-1, as they may restrict the molecular interactions of CD4 and gp120 binding, but also avoid conformational alterations in CD4. Also, in this initial analysis, only domains D1 and D2 have been studied. Including D3 and D4 might be of interest for further development of mechano-modulators for inhibiting HIV-1 entry. In fact, conformational changes in the interface between domains D2 and D3 has been suggested to play a role during infection.

Finally, it is important to mention that this approach could also be used to decrease the mechanical stability of proteins. Thus, targeting regions that serve as anchoring point of mechanical elements may create a binding competition that results in diminished stability. An example could be the β-strand complementation that occurs between protein modules of bacterial adhesin molecules such as microbial surface components recognizing adhesive matrix molecules (MSCRAMM) or bacterial pili. This type of interaction between domains is extremely strong and the main responsible for the success of many bacterial infections (Alonso-Caballero et al. 2018; Murthy et al. 2018).

We conclude that the many possibilities of mechanoregulators as molecules that modify the mechanical stability of proteins in a controlled manner, opens new possibilities in experimental protein studies, as virtually any protein could be the subject of a search of such molecules. The approach is simple, it is well established, and mostly requires knowledge about the mechanical properties and structure of the protein under study. Hence, we demonstrate that protein mechanics brings new molecular interactions and functionalities for drug discovery approaches not considered before, thus expanding the applicability of these techniques.

Methods

Rational identification of CD4 surface receptor mechanical regulators: compound selection criteria: A virtual screening protocol was set up to identify small molecules with the ability to modify the mechanical properties of CD4. In this sense, the key properties of an ideal CD4 mechano-modulator were established in this work as follows: i) should display a strong (at least nanomolar) binding to CD4, ii) should not compete directly with MHCII or gp120 binding to CD4; iii) should have optimal ADMEt properties; and iv) should enjoy of a complete freedom of operation at the industrial property level. In addition, the commercial availability and price of the compounds identified were also considered.

Receptor preparation: To quantify the binding affinity of known molecules to CD4, the following procedure was followed: The structure of residues 1-178 of the human T-Cell surface glycoprotein CD4 was downloaded from the protein data bank (PDB ID: 1WIP) and prepared with the Protein Preparation Wizard of Schrödinger suite.

The pre-processing was carried out with default methods and H-bond refinement was carried out with default pH value 7. Three distinct Glide Grid files with an enclosing box of ca. 46 Å were created using the above-mentioned structure, centered on Ser23, Leu95 and Val146, respectively, which properly cover CD4-D1, CD4-D2 and the CD4-D1D2 interface, respectively.

Ligand preparation and docking: Molecules (ligands) to be screened were downloaded from the ZINC Database, a free database of commercially available compounds for virtual screening. Approximately 100.000 compounds of the lead-like subset of the ZINC databasewere prepared for docking using LigPrep 5, with the OPLS_2005 force field. To set the ionization and tautomerization state of compounds at a pH range of 6–8, Epik v16207 was used, with a maximum number of 4 generated structures. The binding affinity of 100000 lead-like prepared compounds was estimated through a three steps docking protocol summarized as follows: a) a High Throughput Virtual Screening (HTVS) Glide procedure of all the compounds and a subsequent filtering-off of those that did not display a single pose with a binding affinity (docking score) above a predefined lower-limit value of -5 kcal/mol; b) an Standard Precision (SP) level Glide docking procedure applied to those compounds overcoming the HTVS filter and a subsequent selection of those compounds displaying consistent binding affinities (docking scores) above -5 kcal/mol in all their poses for at least one site; c) an extra precision (XP) Glide docking and selection of top binders (10%).

Forbidden binding sites: The compounds overcoming the mentioned energy barriers, we subjected to a second analysis focused on the identification of their binding regions, aimed at discarding drug-candidates that would competitively interfere with either MHCII or gp120 binding. In this line, two distinct regions with "forbidden residues" were defined in the CD4 structure, a region defined by residues 35-52, 55-60 and 164-165 (MHCII binding epitope) and a region around residues 29, 35, 43-47 and 59 in D1 tip (gp120 binding epitope). First region, MHCII, is related to natural function of CD4, therefore no interaction of SUPROMERs is desired. In the case of gp120, potential future experiments using viral elements would not interact with SUPROMERs molecules thus focusing only on mechanical effects.

Final selection criteria: The ADMEt properties of the non-competitive and efficient CD4 binders identified so far, were estimated using the Quick prop module of the

Schrödinger software (Schrödinger Release 2017–4: Canvas, Schrödinger, LLC, New York, NY, 2017). Also, the conclusions derived from a deep analysis of the patentability of these compounds, their market price and availability were key to select the final molecules to be tested as novel CD4 mechano-modulators.

Protein expression: Gene encoding $(I91)_2$-CD4D1D2-$(I91)_2$ chimeric polyprotein construct was designed and optimized for expression in E. coli (Life Technologies). Here two additional cysteine residues were added in the C-terminus, which helps for sample immobilization on the gold surface. Standard DNA manipulation protocols were used to clone the construct into the pQE80L expression plasmid (Quiagen). C41 strand competent cells E. coli (Novagen) were used for protein expression. Transformed competent cells were grown in 750mL of LB media at 37°C until an OD600 of around 0.6 was reached. Then protein expression was introduced by 1mM of IPTG and further incubation at room temperature for 4 hours. Cells were then centrifuged, and a gentle cell lysis protocol was used to avoid damage to the expressed polyproteins. The sample was then purified first by HisTag affinity chromatography using a gravity column filled with HisPur Cobalt resin (Thermo Fisher) and second by size exclusion chromatography using a Superdex 200 HR column (GE Healthcare). The final elution buffer was HEPES 10mM pH 7.0, NaCL 150mM and EDTA 1 mM. The sample was further concentrated using ultrafiltration Amicon 3k filters (Millipore). The final protein concentration was estimated to be around 1 mg mL-1 using a Nanodrop (Thermo Scientific). Then the samples were snap frozen in liquid nitrogen and stored at -80°C.

Single molecule force spectroscopy: All single-molecule force spectroscopy force ramp experiments were performed on an Atomic Force Spectrometer AFS-1 (Luigs Neumann). Biolever cantilevers from Olympus/Bruker were used with a spring constant of around 6 pN nm^{-1}. The spring constant was measured before each experiment using the equipartition theorem within a software built-in procedure. Data was recorded between 0.5 to 4 kHz for the force ramp measurements. For experiments the force was ramped at 33pN·s^{-1} until 485 pN (starting from 10 pN pushing $F < 0$). At this point it was holder to this force for 5 seconds to ensure the I91 subdomain unfoldings. All AFM experiments were carried out at room-temperature (~24 °C) in HEPES buffer at pH 7.0. Typically, 40 μl of the protein sample (~μM concentration) was left around 20 minutes for adsorption on a fresh gold coated surface, using gold evaporation (Oerlikon UNIVX350). After the adsorption time the sample was then rinsed of the gold surface by the HEPES buffer to remove unbounded protein sample just before starting the measurements. In the

experiments in presence of different SUPROMER these molecules were added to the HEPES buffer in a ratio 1:5 (protein:SUPROMER)

Cytotoxicity assay: After two weeks of TZM lb passage, our cell cultures were ready to try a cytotoxicity assay using our SUPROMER. We used a colorimetric assay using MTT, which measures the metabolic activity by a reduction that takes place in the mitochondria of viable cells. In those cells, this reactive change its color from yellow to purple, measured at 590 nm. To do that, our cell culture was grown in a P96 well plate. When cell coverage was optimum, the assay began. Every well was treated with different concentrations of SUPROMER and Ibalizumab, After the convenient incubation time, media from every well was discarded, and a 100 ml of a mixture of FBS-free media and MTT solution (ratio 1:1) was added to every well, we let incubate at 37ºC for 3 hours. After incubation, 150 ml of MTT solvent was added to each well, incubated, wrapped in foil, and shaken on an orbital shaker at RT for 15 minutes. Finally, absorbance at 590nm of each well was measured in Victor equipment.

Data availability

Data supporting the findings of this study are available from the corresponding author upon request.

Acknowledgements

This work has been supported by grants PID2019-109087RB-I00 to R.P.-J. from Spanish Ministry of Science and Innovation. This project has received funding from the European Union's Horizon 2020 research and innovation program under grant agreement No 964764 to R.P.-J. Financial support to DDS comes from Eusko Jaurlaritza (Basque Government) through the project IT1254-19, Grants RYC-2016-19590 and PID2021-127907NB-I00 from the Spanish Ministry of Science and Innovation through the Office of Science Research (MINECO/FEDER).

Competing financial interest

The Authors declare no competing Financial Interests

Author Contributions

R. P.-J. conceived the project. R. P.-J and E. SS. designed research. E. SS. performed HTVS and identification of SUPROMERs A. R., A. F.-C., B. A.-L., J. S., carried out all experimental measurements including protein and sample preparation. A. R., A. F-C., J. S, and R. P.-J. performed data analysis. M. O-M performed chemical synthesis of SUPROMERs. D. F. provided antibody samples and helpful ideas on CD4 nanomechanics. A. R., E. SS. and D. DS. performed structural analysis. A. R., E. SS and R. P.-J. wrote the manuscript and all authors contributed to revising and editing the manuscript.

Chapter VI:
Nanomechanics of microbial infection, from single molecule to single bacterium

Antonio Reifs[1], Alba Fernandez Calvo[1], Pablo Rodriguez-Jimenez[2], Ylenia Jalabera[1], Concepcion Jimenez-Lopez[2], and Raul Perez-Jimenez[1,3,*]

1. *CIC nanoGUNE BRTA, Tolosa Hiribidea 76, 20018 San Sebastian, Spain.*
2. *Departamento de Microbiologia, Universidad de Granada, Campus de Fuentenueva S/N, 18002 Granada, Spain.*
3. *Ikerbasque Foundation for Science, Plaza Euskadi 5, 48009 Bilbao, Spain.*

*Corresponding Authors

Microbial infections are one the leading cause of death worldwide. Bacteria causing diseases such as pneumonia, tuberculosis, and cholera are some of the major threats. There is an increasing concern in relation to bacterial infections due to the virulence and resistance to antibiotics of many bacterial strains, such as Methicillin-resistant *Staphylococcus aureus* (MRSA). Hence, the fight against this type of infections requires new avenues of research for the development of novel treatments, which will involve innovative approaches such as nanotechnology and biotechnology. Here, we investigate the mechanical stability of protein FnBPA, an MSCRAMM (Microbial Surface Components Recognizing Adhesive Matrix Molecules) from *Staphylococcus aureus* that, as a first stage in its infection process, attaches to Human Fibronectin. We examine its mechanical stability using single-molecule atomic force microscopy, but we go further by connecting single-molecule to single-bacterium, creating a novel technique which combines microscopy with magnetic tweezers, generating a magnetic field that controls the movement of our desired magnetic-like bacteria, and measuring the force applied to the bacteria at any given time. This technique opens a door to researchers to examine the strength of a bacterium's attachment and how to modulate it to prevent bacterial infection.

Introduction

Infections caused by microorganisms, such as pneumonia, tuberculosis, and cholera, continue to be a primary cause of death on a global scale. (Bearman and Wenzel 2005) The increasing virulence and antibiotic resistance observed in numerous bacterial strains, including Methicillin-resistant Staphylococcus aureus (MRSA), which causes thousands of fatalities annually, (Klein, Smith, and Laxminarayan 2007; Whitby, McLaws, and Berry 2001) is of particular concern. This worldwide issue necessitates new research and the creation of novel treatments. The inadequacy of traditional cell and molecular biology approaches in combating microbial infections has necessitated the development of novel techniques such as nanotechnology and biotechnology. In this context, the emerging discipline of mechanomedicine offers potential solutions by examining how mechanical forces influence the behavior of cells and proteins, particularly in relation to disease. (Naruse 2018)

Proteins in the extracellular matrix, which are subject to mechanical forces, mediate cellular interactions. (Chiquet 1999; Meng et al. 2011) For instance, bacterial infections depend on the adhesion of virulence factors known as adhesins, which are cell-wall-anchored (CWA) proteins that facilitate the attachment of bacteria to target organisms. (Geoghegan and Foster 2017; Foster et al. 2014) Endocarditis, an infection of the interior lining of the heart primarily caused by gram-positive bacteria such as Staphylococcus aureus, coagulase-negative Staphylococcus, and Streptococci and Enterococci species, is an example of a bacterial infection. (Asgeirsson, Thalme, and Weiland 2018) Endocarditis has a high global incidence and mortality rate, and its removal frequently necessitates surgery due to antibiotic resistance, especially in the case of MRSA. Additionally, these microorganisms are able to infect cardiac devices. (Asgeirsson et al. 2018)

Bacteria must travel through the circulation and attach to heart valves using adhesins in order to cause endocarditis. MSCRAMM (Microbial Surface Components Recognizing Adhesive Matrix Molecules) refers to a particular class of CWA proteins implicated in endocarditis. (Foster et al. 2014) The MSCRAMMs fibronectin binding A (FnBPA) and clumping factor A (ClfA) (Herman-Bausier et al. 2018) are among

the most important. These virulence factors are multidomain proteins; FnBPA contains intrinsically disordered fibronectin binding repeats (FnBRs). FnBRs form antiparallel strands along a triple β-strand, using a tandem β-zipper mechanism to connect multiple Fibronectin type I domains. (Josse, Laurent, and Diot 2017; Lower et al. 2011)

In this work, we investigated Staphylococcus aureus attachment through FnBPA using single-molecule and single-cell techniques. Atomic Force Microscopy (AFM) was used to investigate the molecular mechanics of adhesion by engineering protein constructs that enable precise determination of the protein interactions involved in bacterial attachment. In order to transition to the cellular level, we developed a novel technique developed involving magnetic beads attached to individual bacteria. This method enables the generation of magnetic-like bacteria,(Yan et al. 2012) allowing for the control of their adhesion by applying a magnetic field with a magnetic tweezers apparatus (Tanase, Biais, and Sheetz 2007) while imaging with bright field or fluorescence microscopy. By applying calibrated forces, we can determine each bacterium's adhesion strength.

Using AFS and magnetic tweezers, we examined the MSCRAMMs of pathogenic strains at the single-molecule and single-cell levels, respectively. The objective is to establish a relationship between the strength of their adhesins and their ability to cause infection, casting light on the mechanics of bacterial adhesion and its role in pathogenesis.

Results

- ### Single-molecule atomic force spectroscopy of FnBPA attachment to Fibronectin

For our AFM studies, we engineered a polyprotein in which the protein fibronectin-binding repeat 1 (FnBR1) is linked via the sequence (GGGSGGGS) to the human

protein fibronectin type I subdomains 2-5 (FnI 2-5) (PDB code: 2CG7 and 1FBR)(Bingham et al. 2008), as depicted in Fig. VI.1.

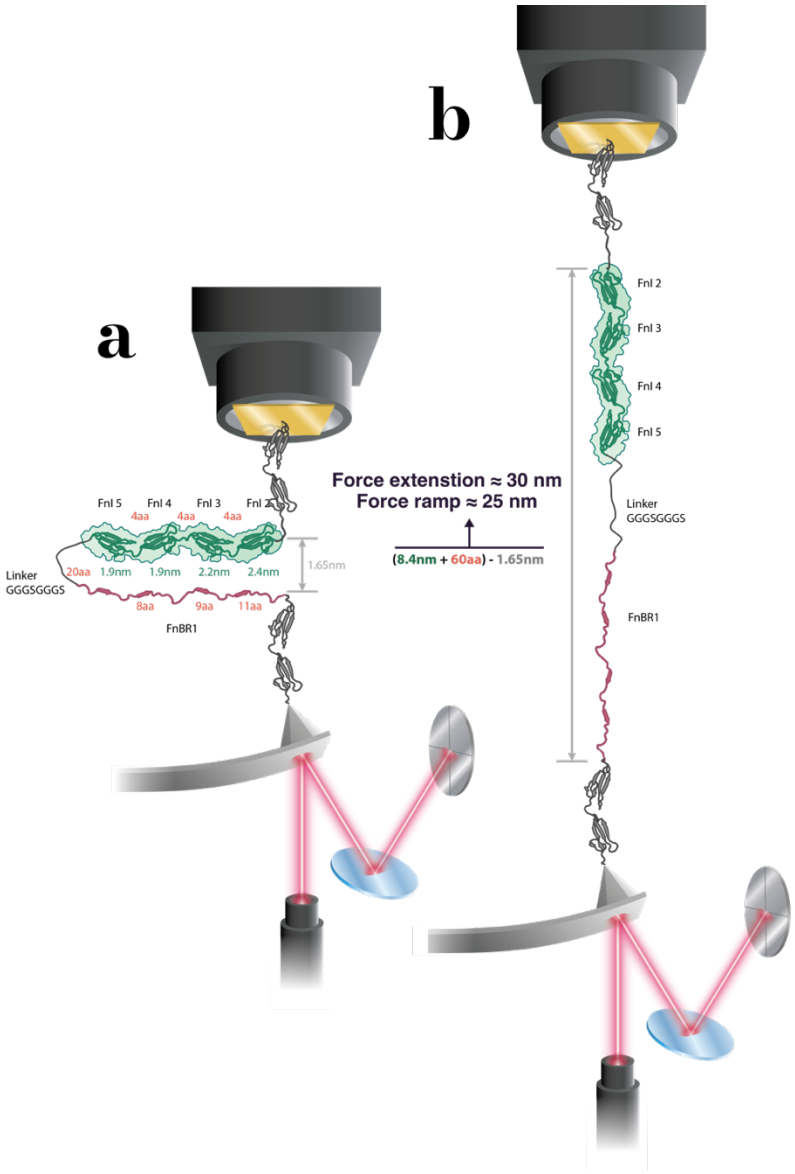

Fig. VI.1. Construct for single-molecule force experiments. a. Representation of the polyprotein $(I91)_2$-FnI2-5-linker-FnBR1-$(I91)_2$ with the zipper folded between both proteins. b. When the setup applies force to our polyprotein the first event consists of the rupture of the zipper bonding which is weaker than any unfolding event, the extension increment due to this event is approximately 30nm.

$(I91)_2$-FnI2-5-linker-FnBR1-$(I91)_2$ is the construct formed by sandwiching our construct between two pairs of I91 domains of human cardiac titin. When a polyprotein is subjected to mechanical force, the I91 domains serve as mechanical handles. (see Fig. VI.1.) Importantly, the mechanical properties of I91, such as unfolding force and contour length (ΔLc), are well characterized and can be distinguished using force spectroscopy.(Peters et al. 2022; Manteca et al. 2017)

Thus, I91 functions as a molecular fingerprint for adequate trace selection when it is difficult to identify the protein's mechanical properties. This is especially crucial in the case of the zipper rupture between FnI2-5 and FnBR1 due to its low mechanical resistance, which may result in a featureless signal under force.

First, we conducted force-extension experiments in which our polyprotein was extended at a constant rate of 40 nm s^{-1}. In these experiments, the unfolding of the molecule typically produces a sawtooth pattern because the unfolding of each domain consists of a stage of increasing force while the domain resists the applied tension, followed by a sudden drop in the registered force due to the process of unfolding. The analysis with the worm like chain (WLC) model reveals a mechanical stability of approximately in the range of 119±9 pN, although it is dependent on the unfolding speed, and a ΔLc of 28±1 nm, which is consistent with what is described in the literature.(Perez-Jimenez et al. 2006) (see FigVI.2.) In contrast, there is no discernible sawtooth pattern for the vast majority of zipper ruptures. This indicates that zipper rupture has a very low mechanical resistance and unfolds at very low forces, so it is practically undetectable during force-extension experiments.

We conducted force-ramp experiments to better understand the mechanical zipper rupture between FnI2-5 and FnBR1. Due to the intervention of a feedback loop that compensates for changes within a sub 1 ms time interval, this method provides precise control over the applied force. Thus, this protocol makes it possible to scan a wide spectrum of unfolding forces while controlling the applied force. The force protocol begins by applying a 10 pN force to the cantilever against the gold substrate. The cantilever is then slowly pulled away from the protein at a loading rate of 10 pN s^{-1}, providing sufficient resolution to detect the zipper rupture at low forces but also at high forces, sufficient to unfold FnI2-5 and I91.

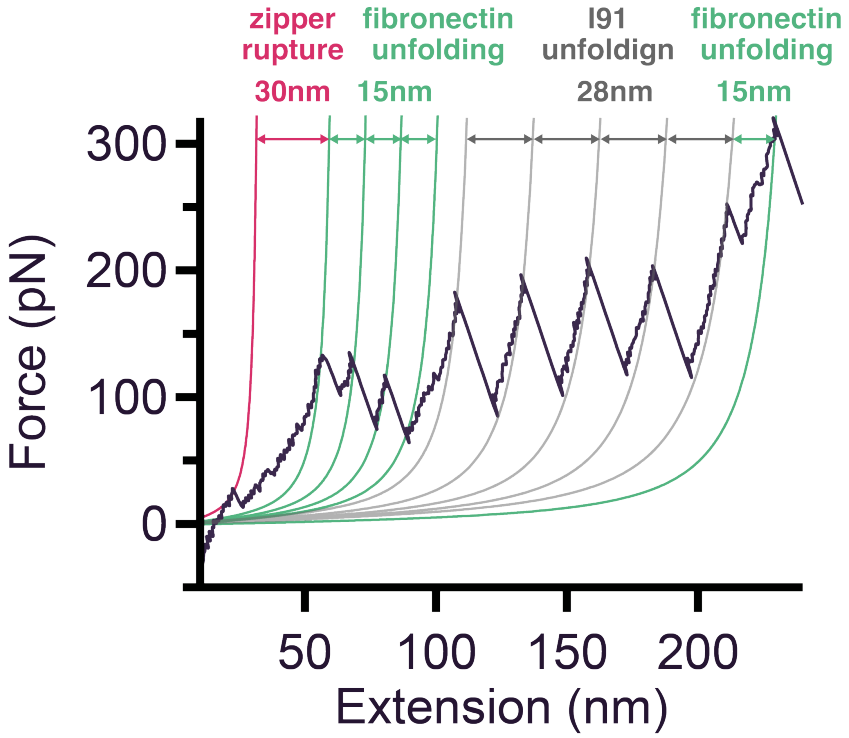

Fig. V.2. Single-molecule force-extension experiments. Force-extension trace including the characteristic sawtooth pattern for the titin domains, and the initial featureless signal for zipper rupture. Stretching is conducted at a speed of 40 nm s^{-1}.

This type of experiment typically detects discrete steps with force-dependent length extensions for two-state proteins, which can be explained by models of polymer elasticity such as the Worm-like chain or freely-jointed chain. (Oberhauser et al. 2001) At forces below 60 pN, we observed a sigmoidal pattern for zipper rupture. (see FigVI.3. and FigVI.4.) Followed by the step events corresponding to FnI2-5 with an extension of 13 nm and titin unfolding with an extension of 24nm. The initial change in extension corresponds to the expected extension of 26 nm for zipper rupture in this range of force, indicating that this sigmoidal behavior corresponds to the rupture.

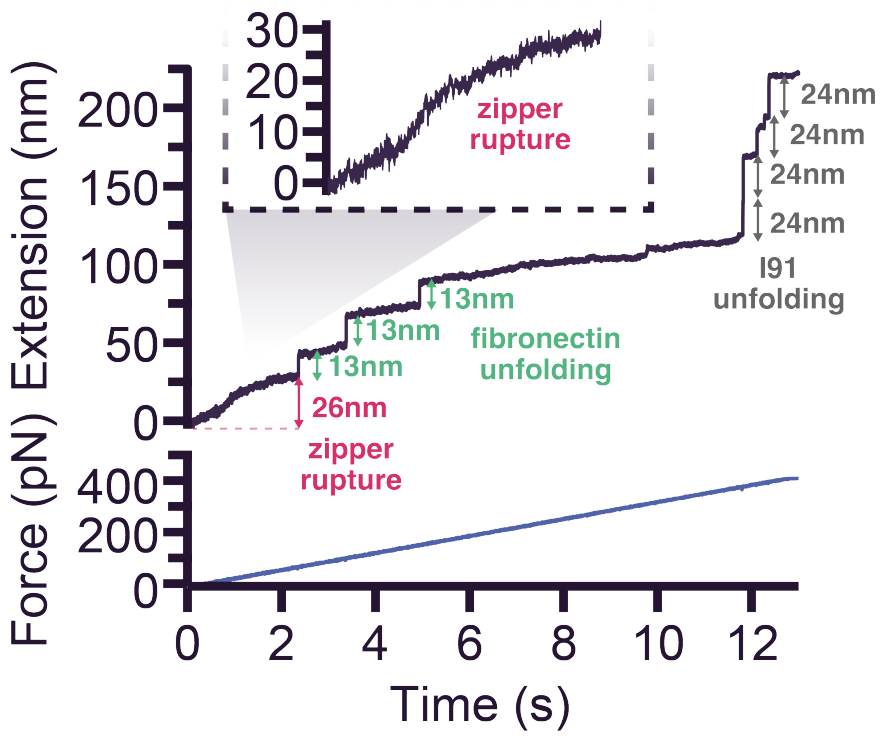

FigVI.3. Single-molecule force-ramp experiments. Time series for the measured extension (top) and force (bottom) in a force ramp experiment at 10 pN/s. The inset highlights the signal corresponding zipper rupture.

The sigmoidal curves that we report have been observed in the smFS literature before. (Reifs et al. 2023) In Fig. VI.4. we show the average of several traces, from whose derivative we estimate a mid-unfolding force F1/2 for this zipper rupture between FnI2-5 and FnBR1 of 6 pN. Which is consistent with the unfolding force for beta zippers observed in the literature. (Rohs, Etchebest, and Lavery 1999; Brockwell et al. 2003)

In the literature, the binding of these proteins has been investigated using a different force vector, which allows the study of this rupture in a shear mode, which surprisingly reveals rupture forces on the order of 1nN. (Geoghegan and Dufrêne 2018)

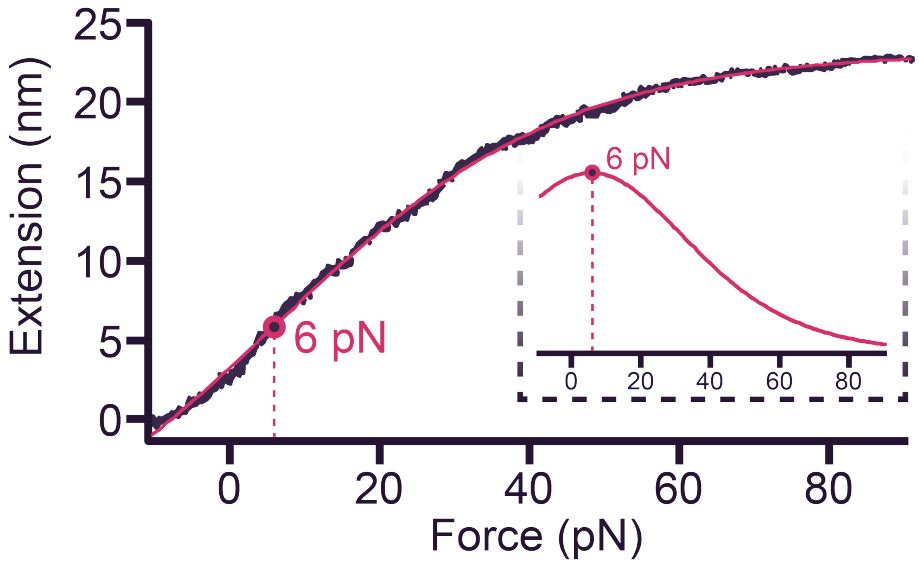

Fig. VI.4. Mid unfolding force of zipper rupture. Average force extension curve from multiple traces for zipper rupture between FnI2-5 and FnBR1 (n=25). The inset is the first derivative of the sigmoidal fit.

- ## Magnetic like-bacteria obtention

In order to transition to the cellular level, a novel technique involving magnetic beads attached to an individual bacterium was utilized. This method permits the production of magnetic-like bacteria, these bacteria can be controlled by a magnetic field generated by a magnetic tweezers apparatus while all the process is recorded thanks to bright field or fluorescence microscopy. (see Fig. VI.5.)

In order to produce magnetic-like bacteria Dynabeads M-270 previously functionalized with the human protein fibronectin was used. These magnetic beads were incubated with the bacteria SH1000 + FnBPA, which specifically bonded to this magnetic bead via the studied attachment.

To verify this hypothesis, a modest experiment was conducted which consist on measuring the colony forming units (CFU) of two different bacteria: SH1000,

staphylococcus aureus strain which lacked MSCRAMMS genes, and SH1000 + FnBPA, which contained a plasmid that included the FnBPA gene.

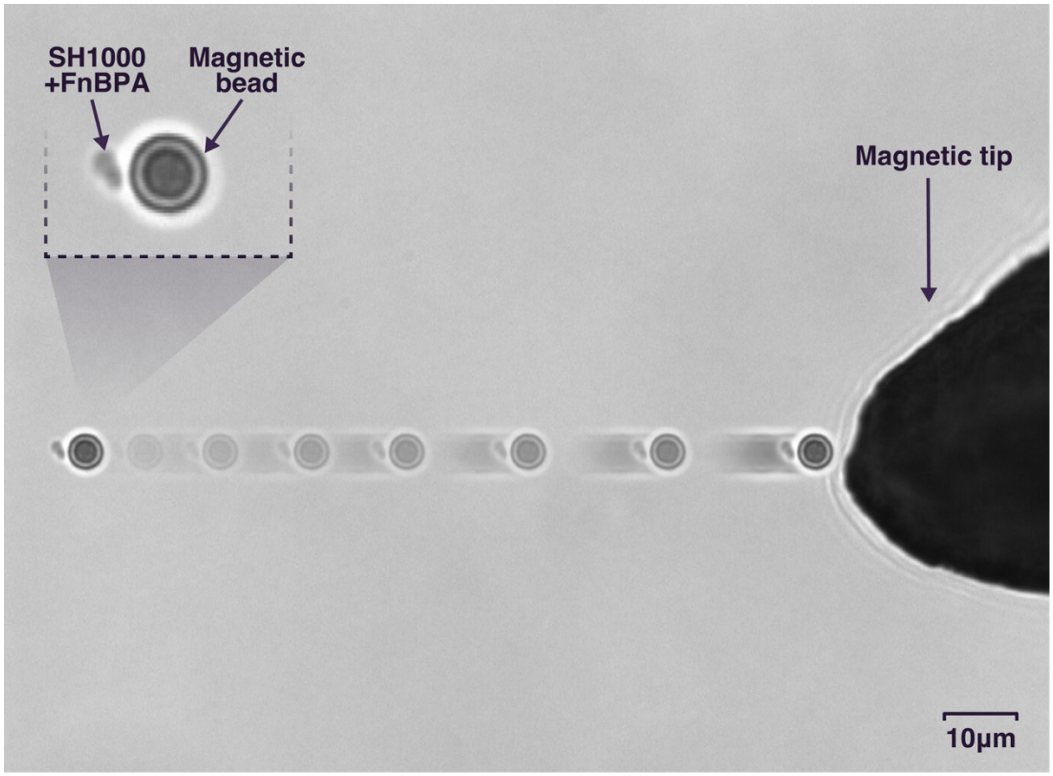

Fig. VI.5. Magnetic tweezers apparatus. An actual image of our magnetic tweezers apparatus, the image illustrates the magnetic-like bacterium trajectory to the magnetic tip. The inset shows the attachment of the bacteria SH1000 + FnBPA to the Dynabead M-270.

Both cultures were grown to an optical density of 0.2, which is optimal for FnBPA gene expression,(Saravia-Otten et al. 1997) and then their CFU were measured before and after an incubation step with Dynabeads M-270 (0.5 mg) in order to calculate the recovery percentage in both cases, which was 15.7% in the case of SH1000 + FnBPA and 1.1% in the case of SH1000. This demonstrates that the

attachment of the bacteria to the magnetic bead is specific and is due to the binding of FnBPA to the human fibronectin present in the magnetic bead surface.

To test our magnetic tweezers apparatus, we designed an experiment in which magnetic-like bacteria are exposed to a protocol of magnetic pulses consisting of cycles of 1.4s at 2.5V applied to the magnetic tip (electromagnet) and a quenching time of 1.4s as well. The magnetic-like bacteria's movement was recorded, and its velocity is depicted in Figure VI.6. in addition to the applied voltage protocol. As can be seen, both protocols precisely overlap, with the bacteria's movement being null when no voltage is applied to the tip. This demonstrates that the movement of the magnetic-like bacteria is caused exclusively by the magnetic field generated by the magnetic tip.

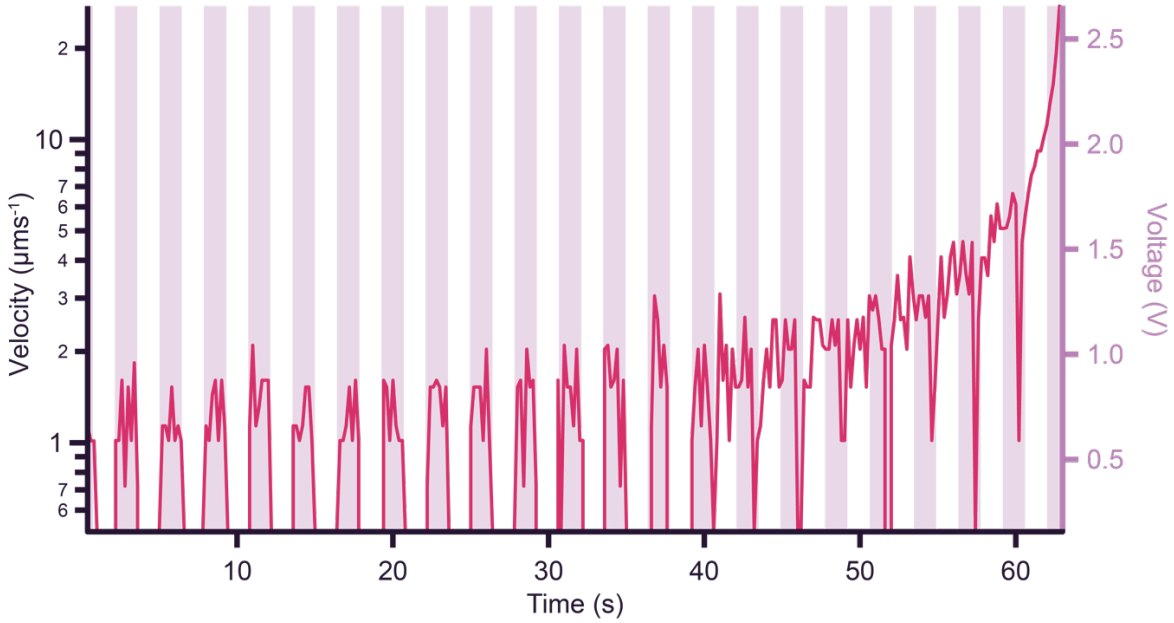

Fig. VI.6. Testing our magnetic-like bacteria. This graph shows the magnetic-like bacteria velocity when a voltage pulse protocol is applied to the electromagnet.

• Magnetic tweezers calibration using magnetic-like bacteria

To calibrate the magnetic tip, which is, after all, an electromagnet to which we can apply controlled voltages, we must be able to translate the voltages that we apply into the corresponding force applied to our magnetic-like bacterium. To accomplish this, magnetic-like bacterium trajectories were recorded across the entire voltage range (0.1V-2.5V). Using Stokes' Law (Tanase et al. 2007; Ramms et al. 2013) Equation VI.1 and the velocity of the bacterium's trajectory, it is possible to calculate the drag force or, equivalently, the magnetic force applied to it.

$$Drag\ Force = 6 \cdot \pi \cdot r \cdot \mu_{abs} \cdot v \quad \text{(VI.1)}$$

Stokes law. Being r, magnetic bead radius, $\mu_{abs,}$ absolute viscosity, and v, the velocity of magnetic bead

Knowing the magnetic force applied to our bacteria at each point of its trajectory and also its distance from the magnetic tip, Fig. VI.7. was elaborated, which shows the relationship between magnetic force and distance from the tip as a function of the applied voltage.

But a phenomenon was observed when working at closer distances to the magnetic tip, and hence higher values of magnetic force. The error of this calibration increased and the trend was not obvious. This is due to two main factors, the low obturation velocity of the cam inserted in the confocal microscopy, and the precision of bead tracking during this faster portion of the trajectory. We chose to skew these calibration curves between 40 and 110 μm from the magnetic tip for this purpose. (see Fig. VI.7. and Fig. VI.8.)

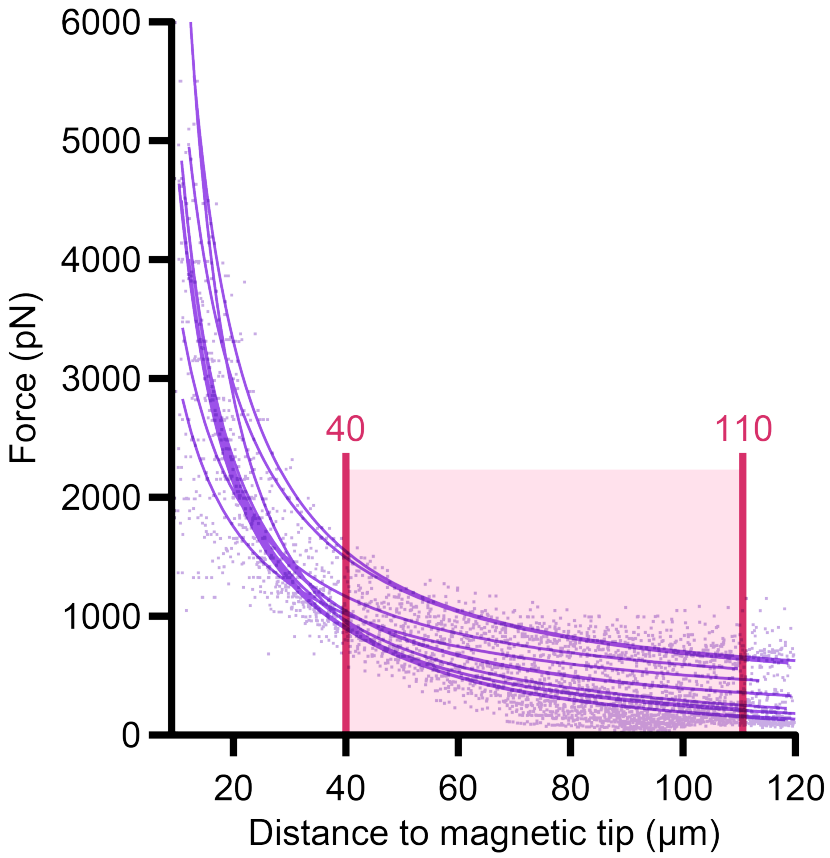

Fig. VI.7. First approach to calibration curves. This graph shows the relationship of magnetic force applied to the magnetic-like bacteria depending on its distance to the magnetic tip.

In the range of 40-110 μm the trend of our calibration curves is clear, increasing the magnetic force applied proportionally when the applied voltage increase. Reaching values of force of 1.6 nN at a maximum voltage in distances to the magnetic tip close to 40 μm. This is the functional window of our apparatus, within which we can precisely calculate the magnetic force applied to our magnetic-like bacteria. (see Fig. VI.8.)

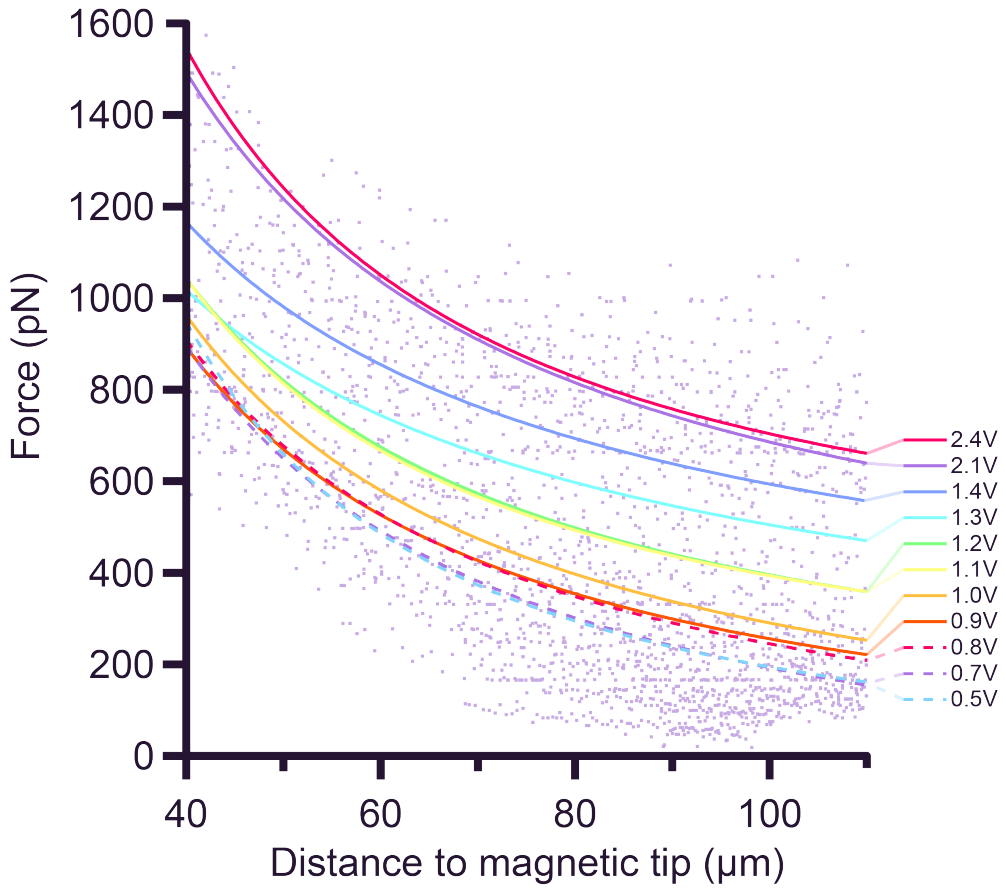

Fig. VI.8. Calibration curves of magnetic force at different voltages. This graph shows the magnetic force applied to the magnetic-like bacteria at different voltages depending on the distance to the magnetic tip. Lines represent represents the fit of our data to power function meanwhile points is our original data set

- ## Single bacterium attachment measurements

Now that we have everything that we require to carry out actual measurements of bacterial attachment, we will measure the adhesion force of our magnetic-like bacteria as well as the Dynabead, checking the adhesion force of our samples to a surface that does not include its protein target, we had use BSA as a negative control.

To accomplish this, we will subject our samples to a voltage ramp applied to the electromagnet in which the voltage increases from 0 to 2.5V in 20s, measuring the voltage value and the distance between the sample and the magnetic tip and using our calibration curves, aceasily they detach force can be determined.

The attachment force of the magnetic-like bacteria was 248±27 pN, whereas that of the Dynabeads was 215±27 pN. According to t-test, in which the two-tailed P value equals 0.5455 by conventional criteria, there is no statistically significant difference. Indicating that there is no specific bond between the samples and the BSA-functionalized surface, as expected.

When we applied the same protocol explained above to human fibronectin-functionalized glass slides, we observed two distinct behaviors: one in which the bacteria detached at the same force values as our negative control, (no attachment) and another in which we were unable to detach the bacteria.

Our SH1000 + FnBPA bacteria are attached to the glass slide surface functionalized with human fibronectin and to the magnetic bead which is also functionalized with human fibronectin via the same specific binding. Both interactions are identical and stronger than the point forces that our apparatus can achieve.(Prystopiuk et al. 2018) (see Fig. VI.9.)

In order to solve this, we have applied a continuous force protocol at maximum voltage, but we are unable to conduct this experiment properly due to technical issues. When we apply maximum voltage to the magnetic tip, there is a drift that makes accurate measurement impossible. So, we have to resolve these technical issues in order to perform the detachment measurements properly.

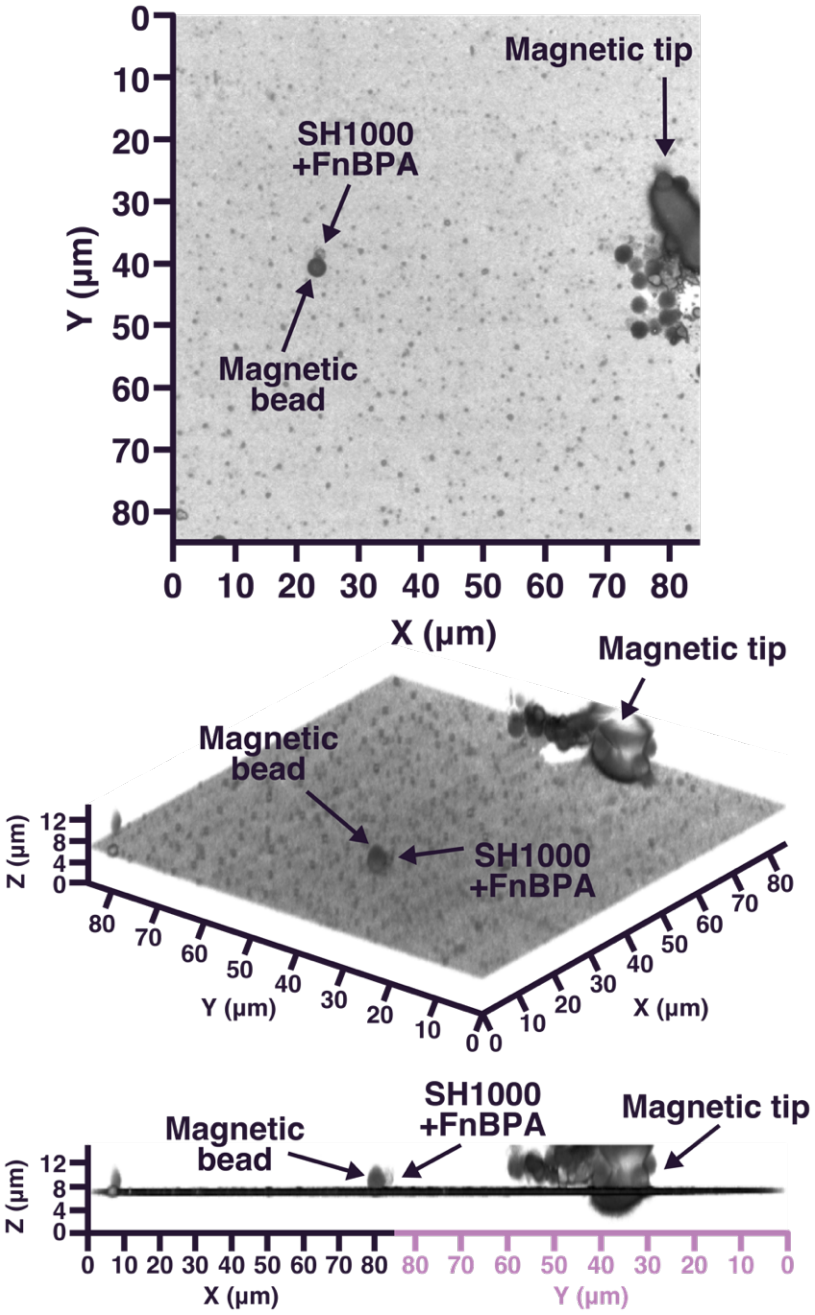

Fig. VI.9. Magnetic-like bacteria attachment. Our SH1000 + FnBPA bacteria are attached by the same specific binding to the glass slide surface functionalized with human fibronectin, and also to the magnetic bead which it is also functionalized with human fibronectin.

Discussion

In the past decades, single-molecule force experiments have suffered a huge development but their connection with the single cell is not a very transited way. Very relevant information could be obtained from this type of connections, especially in the bacterial attachment and bacterial infection process nowadays it is become more relevant than ever, the increase of bacteria resistance to antibiotics is alarming and the development of new strategies to overcome these resistances is crucial. So, for this reason, we believe that this new methodology could shed light on infection processes and the finding of new anti-attachment strategies in order to avoid bacterial infections.

Our results pave the way to study the single bacterium attachment force, first, we must solve the technical issues with the magnetic tweezers apparatus in order to actually measure the detachment force, but when these issues will be overcome these results will open a door to find peptides or small molecules using High-throughput Screening (HTS) techniques to find mechano-regulators able to modulate bacterial attachment, altering the mechanochemistry attachment of the proteins making them weaker, thus potentially preventing infections. We have developed this methodology in previous works. Chapter V: High Throughput search of small molecules for controlling the mechanical stability of proteins, present in this thesis.

The idea of controlling the nanomechanics of bacterial attachment proteins as a way of fighting infections can lead to a novel class of treatments. Our final results, when technical issues will be solved will contribute to establishing a new research area of mechanopharmacology, which aims to undertake one of the major challenges of our society, fighting against microbial infections.

Methods

Protein expression and purification. Gene encoding $(I91)_2$-FnI2-5-linker-FnBR1-$(I91)_2$ chimeric polyprotein construct was designed and optimized for expression in E. coli (Life Technologies). Here two additional cysteine residues were added in the C-terminus, which helps for sample immobilization on the gold surface. Standard DNA manipulation protocols were used to clone the construct into the pQE80L expression plasmid (Qiagen). C41 strand competent cells E. coli (Novagen) were used for protein expression. Transformed competent cells were grown in 1L of LB media at 37°C until an OD600 of around 0.6 was reached. Then protein expression was introduced by 1mM of IPTG and further incubation at 37°C for 4 hours. Cells were then centrifuged, and a gentle cell lysis protocol was used to avoid damage to the expressed polyproteins. The sample was then purified first by HisTag affinity chromatography using a gravity column filled with HisPur Cobalt resin (Thermo Fisher Scientific) and second by size exclusion chromatography using a Superdex 200 HR column (GE Healthcare). The final elution buffer was HEPES 10mM pH 7.0, NaCL 150mM and EDTA 1 mM. The sample was further concentrated using ultrafiltration Amicon 3k filters (Millipore). The final protein concentration was estimated to be around 1 mg mL^{-1} using a Nanodrop (Thermo Scientific). Then the samples were snap-frozen in liquid nitrogen and stored at -80°C.

Single molecule force spectroscopy: All single-molecule force spectroscopy force ramp experiments were performed on an Atomic Force Spectrometer AFS-1 (Luigs Neumann). Biolever cantilevers from Olympus/Bruker were used with a spring constant of around 6 pN nm^{-1}. The spring constant was measured before each experiment using the equipartition theorem within a software built-in procedure. Data was recorded between 0.5 to 4 kHz for the force ramp measurements. For force-extension experiments, the elongation was done at a constant velocity of 40 nm s^{-1}. For force-ramps experiments the force was ramped at 10pN·s^{-1} until 485 pN (starting from 10 pN pushing $F < 0$). At this point it was holder to this force for 5 seconds to ensure the I91 subdomain unfoldings. All AFM experiments were carried out at room-temperature (~24 °C) in HEPES buffer at pH 7.0. Typically, 40 μl of the protein sample (~μM concentration) was left around 20 minutes for adsorption on a fresh gold coated surface, using gold evaporation (Oerlikon UNIVX350). After the

adsorption time the sample was then rinsed of the gold surface by the HEPES buffer to remove unbounded protein sample just before starting the measurements.

Dynabeads M-270 functionalization: In order to prepare and functionalize magnetic beads (Dynabeads M-270; Invitrogen) with human fibronectin protein, several steps are required. Initially, 5 mg of magnetic beads should be washed with PBS using a magnetic rack for efficient pelleting. Following the washing step, the beads need to be incubated in a MES solution containing 0.1M EDC and 0.7M NHS for one hour at 20ºC. Once the incubation is completed, the magnetic beads should be washed twice with pH 6.5 PBS. Subsequently, 150-250 µg of the desired protein, human fibronectin, should be added to the beads, which are then incubated overnight at 20ºC. To terminate the functionalization process, a saturated solution of glycine (20 mg) is introduced and left for 30 minutes. The functionalized magnetic beads are then washed twice with PBS before being resuspended in 1 mL PBS for further use.

Magnetic-like bacteria production: To bind our functionalized magnetic beads with human fibronectin to Staphylococcus aureus SH1000 + FnBPA bacteria, we start by growing the bacteria until they reach an O.D. of 0.2. Once the desired O.D. is achieved, we mix 1 mL of the bacteria with 100 µL of functionalized magnetic beads (0.5 mg) and incubate the mixture at room temperature with gentle agitation for a maximum of 2 minutes. Care should be taken to avoid extended incubation to prevent nonspecific binding. The goal is to bind the bacteria to the bead through FnBPA present on the bacteria's cell wall and human fibronectin protein on the bead's surface. The mixture is then washed three times with PBS, taking care to pipet slowly to preserve the bacteria-bead bond. Finally, the bacteria and magnetic bead tandem are resuspended in 1 mL of PBS, resulting in magnetically responsive bacteria.

Glass slide functionalization: In order to prepare the adequate surface needed for further we must begin by depositing the peptide onto the surface of a NHS-glass slide (24x74mm) and allowing it to incubate overnight in a water-saturated atmosphere. The slide is then washed twice with PBS (phosphate-buffered saline) followed by a wash with PBS-T (PBS with Tween-20 0.5%). Next, the coverslip is

blocked with 10% BSA (bovine serum albumin) in PBS-T for a duration of 2 hours. After the blocking step, the slide is washed three times with PBS-T.

Magnetic tip calibration: To prepare the sample for measurement, a glass slide (24x74mm) and a gasket (Sigma Aldrich) are used as the sample holder. The gasket is pressed onto the slide after applying vacuum grease to the bottom. For force calibration, the same magnetic beads (Dynabeads M-270; Invitrogen) used in experiments are employed.

To initiate magnetic tip force calibration, the magnetic tip is installed in the confocal microscope LSM 710. A high viscosity reference liquid called DMPS Dimethylpolysiloxane is used. The DMPS is mixed with dynabeads inside the gasket. The gasket is then inserted into the sample holder. The objectives used was 63X and 100X, focusing on the magnetic beads. The tip is adjusted up or down to be in the same focus as the beads.

The calibration process begins by starting the Time Series brightfield acquisition and applying a desired voltage. Over time, the bead approaches and reaches the tip. The acquisition of Time Series images is then stopped, and the images are saved. The saved .lsm file can be analyzed using ImageJ software with the Nano Tracking plugin to estimate the coordinates and distances traveled by the magnetic beads towards the tip.

In the analysis, conversion pixel-µm factors, absolute viscosity, magnetic bead radius, and sampling time are taken into account. Matlab files are executed to estimate the drift of the tip, calculate bead velocity, and derive the distance between the bead and the tip. Using Stokes' equation, the force is calculated based on velocity and viscosity. The distance and force vectors are saved as, and a force-distance curve is plotted. The curve is fitted with a power equation.

The measurements are performed in triplicate for the range of voltages applied by the magnetic tip. A standard curve is constructed to correlate magnetic tip voltage, distance, and force. This standard curve allows the determination of the magnetic

force applied to the sample during actual measurements of bacteria attachment forces.

Attachment force measurements: The methodology to measure bacterial attachment force consist of sandwiched our studied bacteria between the magnetic bead and the glass slide. That is, SH1000 + FnBPA bacteria are attached to the glass slide surface functionalized with human fibronectin and to the magnetic bead which is also functionalized with human fibronectin via the same specific binding. Breaking the attachment can occur either by detaching the bacteria-magnetic bead tandem from the glass slide or by separating the bacteria from the magnetic bead. Both scenarios yield valid results.

Once we focus on a magnetic bead with a bacterium attached, we apply a ramp protocol to the magnetic tip. The voltage applied to the tip increases linearly with time (from 0 to 2.5V in 20s) while recording the process. By noting the precise moment when the bacteria detach from either the glass surface or the magnetic bead, we can calculate the applied voltage. Using the distance between the magnetic-like bacteria and the magnetic tip, we extrapolate the magnetic force applied to the bacteria using the established standard curve.

Data availability

Data supporting the findings of this study are available from the corresponding author upon reasonable request.

Acknowledgements

This work has been supported by grants PID2019-109087RB-I00 to R.P.-J. and PGC2018-099321-B-I00 to DD from Spanish Ministry of Science and Innovation. This project has received funding from the European Union's Horizon 2020 research and innovation programme under grant agreement No 964764 to R.P.-J. A. R. is the recipient of a doctorate fellow from Spanish Ministry of Science and Innovation.

Competing financial interest

The authors declare no competing financial interest.

Author Contributions

R.P.-J., A.R. conceived the project and designed research. A.R., A.F-C., P.R.J cloned the protein and performed smFS experiments. A.R., and P.R-J. analysed smFS experiments. A.R. and A.F-C. developed the magnetic tweezers apparatus. All authors contributed to writing and revising the manuscript.

Chapter VII:
Discussion

In the present thesis I have studied the mechanics of four proteins using smFS by AFM. I have studied very labile proteins such as the Engrailed Homeodomain (EnHD) and highly resistant proteins such as Caf1, uncovering the molecular aspects behind such different mechanical behavior. The AFM technique provides access to a wide range of mechanical force, from a few pN to nN, which cannot be easily matched by any SMFS technique in use today. I have demonstrated that the range of cooperativity and mechanical resistance that can be studied by this technique extends from the most labile fast-folding proteins to the most resistant ones, allowing us to study protein mechanics across the entire biologically relevant protein mechanics spectrum.

The present work demonstrates that the AFM technique can be used to capture and study labile proteins such as EnHD. I have observed a novel mechanical unfolding behavior captured as sigmoid signature when extending the protein at a controlled starting force of a few pN, which I interpret as multiple events of protein folding and unfolding. This has allowed me to investigate features such as the plasticity of transition state mechanics, a characteristic EnHD protein feature that defined its low cooperativity. In the opposite spectrum, I have been able to study the high cooperativity of the highly resistant protein Caf1.

The AFM technique permits the investigation of physical phenomena, such as the downhill folding of fast-folding proteins. Nevertheless, I have also studied the mechanical properties of other systems and related them to biological processes, such as the viral and bacterial infection processes. In the two systems presented in this thesis, CD4 and Caf1, I have observed that the battle between pathogens and hosts has undergone a process of evolution and adaptation of the protein's mechanical properties to overcome the host's defense systems and, in turn, defend itself against the virulence of pathogens. And in most scenarios, the differences that suppose the victory and the proliferation of the pathogenic organism are due to minimal modification that entails subtle differences.

In this thesis, I propose that the infection process of viral and bacterial infection is a purely mechanical process or one in which protein mechanics plays a significant role. Pathogens must first adhere to a cell and an organism in order to infect it. Alternatively, in order to defend the organism against a microbial infection, the immune system must interact with the pathogen via processes such as phagocytosis, which have a crucial mechanical significance.

For a virus or bacterium to adhere to the surface of its target cell, it must interact with its surface proteins and withstand the mechanical forces to which it is exposed in its environment, such as the Brownian movements of the medium or the flows of blood and other fluids shear forces. Proteins have been shaped to resist these mechanical stresses likely by small margins. It is reasonable to assume that when a variant capable of resisting these mechanical interactions emerged, it would proliferate relative to the rest of its congeners, thus allowing a better adaptation.

On the other hand, the case of pathogens surviving the immune system can provide us with a different perspective on the mechanical nature of evolution that certain organisms may have undergone. For example, *Yersinia pestis* has developed polymers that protect it from phagocytosis by macrophages. This is because these polymers are non-adhesive and resistant to mechanical stress. And once more, this resistance is just marginal in order to evade the phagocytosis process of the macrophage, as I have observed that point mutations that reduce their mechanical stability by only 20% are sufficient to turn this evasion ineffective.

For these reasons, I have centered the following steps of this thesis on the modulation of the mechanical stability of proteins, instead of the modification of their genetic sequence and structure, which has already been extensively studied. I have developed a search strategy for small molecules with mechano-regulatory capability. This methodology allows us to search for molecules that could potentially be used in vivo to regulate the folding and unfolding mechanics and dynamics of already

expressed and functional proteins. I have used methodologies such as high-throughput screening and molecular docking, which are commonly employed by the pharmaceutical industry in the search for and development of new drugs. To the best of my knowledge, this is the first of approach that using drug-discovery approaches, targets the mechanical stability of proteins.

Knowing the mechanical properties of proteins involved in infection processes and potentially being able to intervene them, would allow us to approach therapies against infections from a mechanical perspective, advancing the concept of mechanopharmacology and allowing the treatment of antibiotic-resistant bacteria. As it is well-known, the rise of antibiotic-resistant bacteria is alarming, and the development of alternative or combined therapies to replace antibiotics is becoming increasingly important.

I have demonstrated the utility of this methodology by identifying three molecules that modulate the mechanical stability of the CD4 protein, doubling its stability. It has been reported that the monoclonal antibody Ibalizumab prevents the entry of the HIV virus due to a stabilization of the CD4 protein, (Perez-Jimenez et al. 2014) it prevents its unfolding by the virus, a crucial step in the mechanism of virus entry. Whether these three molecules have a similar effect on viral entry is an open question beyond the scope of this thesis, but it certainly opens a new line of research.

I have focused the last efforts of this thesis on the development of a technique that allows us to quantitatively measure the adhesion force of bacteria at the level of a single cell, allowing us to study all these infection processes not only at the molecular level but also at the cellular level. Once this technique has been completed, I will be able to determine the precise binding forces of various pathogens to their target cells and, combined with the previously described method, search for mechano-regulators that will allow us to modulate these interactions and thereby prevent bacterial adhesion.

This thesis studies protein mechanics across its entire spectrum and not just their physical properties, but also opening the frontiers that connect protein physics with biological processes and developing useful methodologies for controlling the mechanics of proteins in biologically relevant systems connected to diseases.

Bibliography

Alberts, B., Johnson A, and Lewis J. 2002. ‘Analyzing Protein Structure and Function’. Molecular Biology of the Cell.
Abraham, Mark James, Teemu Murtola, Roland Schulz, Szilárd Páll, Jeremy C. Smith, Berk Hess, and Erik Lindahl. 2015. 'GROMACS: High performance molecular simulations through multi-level parallelism from laptops to supercomputers', SoftwareX, 1-2: 19-25.
Al-Jawdah, Abdulmajeed D., Iglika G. Ivanova, Helen Waller, Neil D. Perkins, Jeremy H. Lakey, and Daniel T. Peters. 2019. 'Induction of the immunoprotective coat of Yersinia pestis at body temperature is mediated by the Caf1R transcription factor', BMC Microbiology, 19: 68.
Alegre-Cebollada, J., C. L. Badilla, and J. M. Fernandez. 2010. 'Isopeptide bonds block the mechanical extension of pili in pathogenic Streptococcus pyogenes', J Biol Chem, 285: 11235-42.
Alonso-Caballero, A., J. Schonfelder, S. Poly, F. Corsetti, D. De Sancho, E. Artacho, and R. Perez-Jimenez. 2018. 'Mechanical architecture and folding of E. coli type 1 pilus domains', Nat Commun, 9: 2758.
Alonso-Caballero, Alvaro, Daniel J. Echelman, Rafael Tapia-Rojo, Shubhasis Haldar, Edward C. Eckels, and Julio M. Fernandez. 2021. ‘Protein Folding Modulates the Chemical Reactivity of a Gram-Positive Adhesin’. Nature Chemistry 13(2). doi: 10.1038/s41557-020-00586-x.
Alonso-Caballero, Alvaro, Rafael Tapia-Rojo, Carmen L. Badilla, and Julio M. Fernandez. 2021. ‘Magnetic Tweezers Meets AFM: Ultra-Stable Protein Dynamics across the Force Spectrum’. BioRxiv.
Anfinsen, Christian B. 1973. ‘Principles That Govern the Folding of Protein Chains’. Science 181(4096):223–30. doi: 10.1126/SCIENCE.181.4096.223/ASSET/1A648F0F-E322-4108-98DD-B0857103738D/ASSETS/SCIENCE.181.4096.223.FP.PNG.
Asgeirsson, Hilmir, Anders Thalme, and Ola Weiland. 2018. ‘Staphylococcus Aureus Bacteraemia and Endocarditis–Epidemiology and Outcome: A Review’. Infectious Diseases 50(3).
Ashkin, A., J. M. Dziedzic, J. E. Bjorkholm, and Steven Chu. 2016. ‘Observation of a Single-Beam Gradient Force Optical Trap for Dielectric Particles’. in Optical Angular Momentum.
Bai, Yawen, John S. Milne, Leland Mayne, and S. Walter Englander. 1993. ‘Primary Structure Effects on Peptide Group Hydrogen Exchange’. Proteins: Structure, Function, and Bioinformatics 17(1). doi: 10.1002/prot.340170110.
Bakk, Audun, Johan S. Høye, Alex Hansen, Kim Sneppen, and Mogens H. Jensen. 2000. ‘Pathways in Two-State Protein Folding’. Biophysical Journal 79(5). doi: 10.1016/S0006-3495(00)76510-6.
Balkwill, D. L., D. Maratea, and R. P. Blakemore. 1980. ‘Ultrastructure of a Magnetotactic Spirillum’. Journal of Bacteriology 141(3). doi: 10.1128/jb.141.3.1399-1408.1980.

Bär, Julia, Yannes Popp, Michael Bucher, and Marina Mikhaylova. 2022. 'Direct and Indirect Effects of Tubulin Post-Translational Modifications on Microtubule Stability: Insights and Regulations'. Biochimica et Biophysica Acta - Molecular Cell Research 1869(6).
Barger, Sarah R., Nils C. Gauthier, and Mira Krendel. 2020. 'Squeezing in a Meal: Myosin Functions in Phagocytosis', Trends in Cell Biology, 30: 157-67.
Bartlett, A. I., S. E. Radford-Nature structural & molecular biology, and undefined 2009. n.d. 'An Expanding Arsenal of Experimental Methods Yields an Explosion of Insights into Protein Folding Mechanisms'. Nature.Com.
Bausch-Fluck, D., A. Hofmann, T. Bock, A. P. Frei, F. Cerciello, A. Jacobs, H. Moest, U. Omasits, R. L. Gundry, C. Yoon, R. Schiess, A. Schmidt, P. Mirkowska, A. Hartlova, J. E. Van Eyk, J. P. Bourquin, R. Aebersold, K. R. Boheler, P. Zandstra, and B. Wollscheid. 2015. 'A mass spectrometric-derived cell surface protein atlas', PLoS One, 10: e0121314.
Bearman, Gonzalo M. L., and Richard P. Wenzel. 2005. 'Bacteremias: A Leading Cause of Death'. Archives of Medical Research 36(6):646–59. doi: 10.1016/J.ARCMED.2005.02.005.
Beedle, Amy E. M., Ainhoa Lezamiz, Guillaume Stirnemann, and Sergi Garcia-Manyes. 2015. 'The Mechanochemistry of Copper Reports on the Directionality of Unfolding in Model Cupredoxin Proteins'. Nature Communications 6. doi: 10.1038/ncomms8894.
Bell, George I. 1978. 'Models for the Specific Adhesion of Cells to Cells', Science, 200: 618-27.
Bingham, Richard J., Enrique Rudiñ O-Piñ Era † ‡, Nicola A. G. Meenan, Ulrich Schwarz-Linek, Johan P. Turkenburg, Magnus Hö, Elspeth F. Garman, and Jennifer R. Potts. 2008. Sciences of the USA 12254-12258 PNAS. Vol. 105.
Binnig, G., C. F. Quate' ', Edward L. Gi, and Ch Gerber. n.d. Atomic Force Microscope.
Binnig, G., C. H. Gerber, E. Stoll, T. R. Albrecht, and C. F. Quate. 1987. Atomic Resolution with Atomic Force Microscope. Vol. 3.
Bloom, Jesse D., and Frances H. Arnold. 2009. 'In the Light of Directed Evolution: Pathways of Adaptive Protein Evolution.' Proceedings of the National Academy of Sciences of the United States of America 106 Suppl 1.
Bondos, Sarah E., A. Keith Dunker, and Vladimir N. Uversky. 2022. 'Intrinsically Disordered Proteins Play Diverse Roles in Cell Signaling'. Cell Communication and Signaling 20(1).
Brockwell, David J., and Sheena E. Radford. 2007. 'Intermediates: Ubiquitous Species on Folding Energy Landscapes?' Current Opinion in Structural Biology 17(1).
Brockwell, David J., Emanuele Paci, Rebecca C. Zinober, Godfrey S. Beddard, Peter D. Olmsted, D. Alastair Smith, Richard N. Perham, and Sheena E. Radford. 2003. 'Pulling Geometry Defines the Mechanical Resistance of a β-Sheet Protein'. Nature Structural Biology 10(9):731–37. doi: 10.1038/nsb968.
Brucale, Marco, Benjamin Schuler, and Bruno Samorì. 2014. 'Single-Molecule Studies of Intrinsically Disordered Proteins'. Chemical Reviews 114(6).

Bryngelson, Joseph D., José Nelson Onuchic, Nicholas D. Socci, and Peter G. Wolynes. 1995. 'Funnels, Pathways, and the Energy Landscape of Protein Folding: A Synthesis'. Proteins: Structure, Function, and Bioinformatics 21(3). doi: 10.1002/prot.340210302.
Bustamante, C., L. Alexander, K. Maciuba, and C. M. Kaiser. 2020. 'Single-Molecule Studies of Protein Folding with Optical Tweezers', Annu Rev Biochem, 89: 443-70.
Bustamante, Carlos, Yann R. Chemla, Nancy R. Forde, and David Izhaky. 2004. 'Mechanical Processes in Biochemistry', Annual Review of Biochemistry, 73: 705-48.
C.N., Pace. 1986. 'Determination and Analysis of Urea and Guanidine Hydrochloride Denaturation Curves'. Methods in Enzymology 131(539).
Cao, Yi, and Hongbin Li. 2008. 'How Do Chemical Denaturants Affect the Mechanical Folding and Unfolding of Proteins?' Journal of Molecular Biology 375(1). doi: 10.1016/j.jmb.2007.10.024.
Carlos Bustamante, Steven B Smith, Jan Liphardt, and Doug Smith. 2000. 'Single-Molecule Studies of DNA Mechanics'. Current Opinion in Structural Biology 10(3):279–85.
Carrion-Vazquez, M., A. F. Oberhauser, S. B. Fowler, P. E. Marszalek, S. E. Broedel, J. Clarke, and J. M. Fernandez. 1999. 'Mechanical and chemical unfolding of a single protein: A comparison', Proceedings of the National Academy of Sciences, 96: 3694-99.
Carrion-Vazquez, Mariano, Andres F. Oberhauser, Thomas E. Fisher, Piotr E. Marszalek, Hongbin Li, and Julio M. Fernandez. 2000. 'Mechanical Design of Proteins Studied by Single-Molecule Force Spectroscopy and Protein Engineering'. Progress in Biophysics and Molecular Biology 74(1–2).
Cavanaugh, Dan C., and Raymond Randall. 1959. 'The Role of Multiplication of Pasteurella Pestis in Mononuclear Phagocytes in the Pathogenesis of Flea-Borne Plague', The Journal of Immunology, 83: 348.
Cerqueira, N. M., S. F. Sousa, P. A. Fernandes, and M. J. Ramos. 2009. 'Virtual screening of compound libraries', Methods Mol Biol, 572: 57-70.
Chalton, David A., Julie A. Musson, Helen Flick-Smith, Nicola Walker, Alistair McGregor, Heather K. Lamb, E. Diane Williamson, Julie Miller, John H. Robinson, and Jeremy H. Lakey. 2006. 'Immunogenicity of a Yersinia pestis Vaccine Antigen Monomerized by Circular Permutation', Infection and Immunity, 74: 6624.
Checkley, Mary Ann, Benjamin G. Luttge, and Eric O. Freed. 2011. 'HIV-1 Envelope Glycoprotein Biosynthesis, Trafficking, and Incorporation'. Journal of Molecular Biology 410(4).
Chiquet, Matthias. 1999. 'Regulation of Extracellular Matrix Gene Expression by Mechanical Stress'. Matrix Biology 18(5):417–26. doi: 10.1016/S0945-053X(99)00039-6.
Chu, Steven, J. E. Bjorkholm, A. Ashkin, and A. Cable. 1986. 'Experimental Observation of Optically Trapped Atoms'. Physical Review Letters 57(3). doi: 10.1103/PhysRevLett.57.314.

Clark, R. A., H. F. Dvorak, and R. B. Colvin. 1981. 'Fibronectin in delayed-type hypersensitivity skin reactions: associations with vessel permeability and endothelial cell activation', The Journal of Immunology, 126: 787.
Connor, Michael G., Amanda R. Pulsifer, Donghoon Chung, Eric C. Rouchka, Brian K. Ceresa, and Matthew B. Lawrenz. 2018. 'Yersinia pestis Targets the Host Endosome Recycling Pathway during the Biogenesis of the Yersinia Containing Vacuole To Avoid Killing by Macrophages', mBio, 9: e01800-17.
Cossio, Pilar, Gerhard Hummer, and Attila Szabo. 2015. 'On artifacts in single-molecule force spectroscopy', Proceedings of the National Academy of Sciences of the United States of America, 112: 14248-53.
De Sancho, David, Jörg Schönfelder, Robert B. Best, Raul Perez-Jimenez, and Victor Muñoz. 2018. 'Instrumental Effects in the Dynamics of an Ultrafast Folding Protein under Mechanical Force', The Journal of Physical Chemistry B: acs.jpcb.8b05975-acs.jpcb.8b75.
Del Rio, Armando, Raul Perez-Jimenez, Ruchuan Liu, Pere Roca-Cusachs, Julio M. Fernandez, and Michael P. Sheetz. 2009. ‘Stretching Single Talin Rod Molecules Activates Vinculin Binding’. Science 323(5914). doi: 10.1126/science.1162912.
DePristo, Mark A., Daniel M. Weinreich, and Daniel L. Hartl. 2005. 'Missense meanderings in sequence space: a biophysical view of protein evolution', Nature Reviews Genetics, 6: 678-87.
Dill, Ken A., and Justin L. MacCallum. 2012. ‘The Protein-Folding Problem, 50 Years On’. Science 338(6110):1042–46. doi: 10.1126/SCIENCE.1219021.
Du, Yidong, Roland Rosqvist, and Åke Forsberg. 2002. ‘Role of Fraction 1 Antigen of Yersinia Pestis in Inhibition of Phagocytosis’. Infection and Immunity 70(3). doi: 10.1128/IAI.70.3.1453-1460.2002.
Dufrene, Y. F., and A. E. Pelling. 2013. 'Force nanoscopy of cell mechanics and cell adhesion', Nanoscale, 5: 4094-104.
Dura, Gema, Helen Waller, Piergiorgio Gentile, Jeremy H. Lakey, and David A. Fulton. 2018. 'Tuneable hydrogels of Caf1 protein fibers', Materials Science and Engineering: C, 93: 88-95.
Dyer, R. Brian. 2007. ‘Ultrafast and Downhill Protein Folding’. Current Opinion in Structural Biology 17(1).
Edwards, D. T., J. K. Faulk, A. W. Sanders, M. S. Bull, R. Walder, M. A. LeBlanc, M. C. Sousa, and T. T. Perkins. 2015. 'Optimizing 1-mus-Resolution Single-Molecule Force Spectroscopy on a Commercial Atomic Force Microscope', Nano Lett, 15: 7091-8.
Edwards, D. T., M. A. LeBlanc, and T. T. Perkins. 2021a. 'Modulation of a protein-folding landscape revealed by AFM-based force spectroscopy notwithstanding instrumental limitations', Proc Natl Acad Sci U S A, 118.

Edwards, Devin T., Jaevyn K. Faulk, Marc-André LeBlanc, and Thomas T. Perkins. 2017. 'Force Spectroscopy with 9- μ s Resolution and Sub-pN Stability by Tailoring AFM Cantilever Geometry', Biophysical Journal, 113: 2595-600.
El-Kirat-Chatel, Sofiane, and Yves F. Dufrêne. 2016. 'Nanoscale adhesion forces between the fungal pathogen Candida albicans and macrophages', Nanoscale Horizons, 1: 69-74.
Englander, S. Walter, and Leland Mayne. 2014. 'The Nature of Protein Folding Pathways'. Proceedings of the National Academy of Sciences of the United States of America 111(45):15873–80.
Erickson, H. P. 1994. 'Reversible Unfolding of Fibronectin Type III and Immunoglobulin Domains Provides the Structural Basis for Stretch and Elasticity of Titin and Fibronectin'. Proceedings of the National Academy of Sciences of the United States of America 91(21). doi: 10.1073/pnas.91.21.10114.
Fällman, M., K. Andersson, S. Håkansson, K. E. Magnusson, O. Stendahl, and H. Wolf-Watz. 1995. 'Yersinia pseudotuberculosis inhibits Fc receptor-mediated phagocytosis in J774 cells', Infection and Immunity, 63: 3117.
Fan, Jiyu, Ailing Fu, and Le Zhang. 2019. 'Progress in Molecular Docking'. Quantitative Biology 7(2).
Ferreiro, Diego U., Joseph A. Hegler, Elizabeth A. Komives, and Peter G. Wolynes. 2007. 'Localizing Frustration in Native Proteins and Protein Assemblies'. Proceedings of the National Academy of Sciences of the United States of America 104(50). doi: 10.1073/pnas.0709915104.
Finlay, B. Brett, and Grant McFadden. 2006. 'Anti-Immunology: Evasion of the Host Immune System by Bacterial and Viral Pathogens', Cell, 124: 767-82.
Flannagan, Ronald S., Rene E. Harrison, Christopher M. Yip, Khuloud Jaqaman, and Sergio Grinstein. 2010. 'Dynamic macrophage "probing" is required for the efficient capture of phagocytic targets', The Journal of Cell Biology, 191: 1205.
Flannagan, Ronald S., Valentin Jaumouillé, and Sergio Grinstein. 2012. 'The Cell Biology of Phagocytosis', Annual Review of Pathology: Mechanisms of Disease, 7: 61-98.
Floudas, C. A., H. K. Fung, S. R. McAllister, M. Mönnigmann, and R. Rajgaria. 2006. 'Advances in Protein Structure Prediction and de Novo Protein Design: A Review'. Chemical Engineering Science 61(3). doi: 10.1016/j.ces.2005.04.009.
Foster, Timothy J., Joan A. Geoghegan, Vannakambadi K. Ganesh, and Magnus Höök. 2014. 'Adhesion, Invasion and Evasion: The Many Functions of the Surface Proteins of Staphylococcus Aureus'. Nature Reviews Microbiology 12(1).
Freeman, M. M., M. S. Seaman, S. Rits-Volloch, X. Hong, C. Y. Kao, D. D. Ho, and B. Chen. 2010. 'Crystal structure of HIV-1 primary receptor CD4 in complex with a potent antiviral antibody', Structure, 18: 1632-41.

Friesner, R. A., J. L. Banks, R. B. Murphy, T. A. Halgren, J. J. Klicic, D. T. Mainz, M. P. Repasky, E. H. Knoll, M. Shelley, J. K. Perry, D. E. Shaw, P. Francis, and P. S. Shenkin. 2004. 'Glide: a new approach for rapid, accurate docking and scoring. 1. Method and assessment of docking accuracy', J Med Chem, 47: 1739-49.
Fukuto, Hana S., and James B. Bliska. 2014. 'Editorial: Yersinia pestis survives in neutrophils and sends a PS to macrophages: bon appétit!', Journal of leukocyte biology, 95: 383-85.
Gao, W., H. Hasan, D. E. Anderson, and W. Lee. 2022. 'The Role of Mechanically-Activated Ion Channels Piezo1, Piezo2, and TRPV4 in Chondrocyte Mechanotransduction and Mechano-Therapeutics for Osteoarthritis', Front Cell Dev Biol, 10: 885224.
Garcia-Manyes, Sergi, Jasna Brujić, Carmen L. Badilla, and Julio M. Fernández. 2007. 'Force-Clamp Spectroscopy of Single-Protein Monomers Reveals the Individual Unfolding and Folding Pathways of I27 and Ubiquitin'. Biophysical Journal 93(7). doi: 10.1529/biophysj.107.104422.
Garcia-Mira, Maria M., Mourad Sadqi, Niels Fischer, Jose M. Sanchez-Ruiz, and Victor Muñoz. 2002. 'Experimental Identification of Downhill Protein Folding'. Science 298(5601):2191–95. doi: 10.1126/science.1077809.
Gefen, Amit. 2010. 'Effects of Virus Size and Cell Stiffness on Forces, Work, and Pressures Driving Membrane Invagination in a Receptor-Mediated Endocytosis'. Journal of Biomechanical Engineering 132(8). doi: 10.1115/1.4001888.
Geoghegan, Joan A., and Timothy J. Foster. 2017. 'Cell Wall-Anchored Surface Proteins of Staphylococcus Aureus: Many Proteins, Multiple Functions'. in Current Topics in Microbiology and Immunology. Vol. 409.
Geoghegan, Joan A., and Yves F. Dufrêne. 2018. 'Mechanomicrobiology: How Mechanical Forces Activate Staphylococcus Aureus Adhesion'. Trends in Microbiology 26(8).
Gerhold, Kristin A., and Martin A. Schwartz. 2016. 'Ion Channels in Endothelial Responses to Fluid Shear Stress', Physiology, 31: 359-69.
Ghosh, Kingshuk, S. Banu Ozkan, and Ken A. Dill. 2007. 'The Ultimate Speed Limit to Protein Folding Is Conformational Searching'. Journal of the American Chemical Society 129(39). doi: 10.1021/ja066785b.
Gillespie, Daniel T. 1977. 'Exact stochastic simulation of coupled chemical reactions', The Journal of Physical Chemistry, 81: 2340-61.
Gorby, Y. A., T. J. Beveridge, and R. P. Blakemore. 1988. 'Characterization of the Bacterial Magnetosome Membrane.' Journal of Bacteriology 170(2). doi: 10.1128/jb.170.2.834-841.1988.
Gordon, Siamon. 2016. 'Phagocytosis: An Immunobiologic Process', Immunity, 44: 463-75.
Gordon, Vernita D., and Liyun Wang. 2019. 'Bacterial mechanosensing: the force will be with you, always', Journal of Cell Science, 132: jcs227694.

Gosse, Charlie, and Vincent Croquette. 2002. 'Magnetic Tweezers: Micromanipulation and Force Measurement at the Molecular Level'. Biophysical Journal 82(6). doi: 10.1016/S0006-3495(02)75672-5.
Greene, Warner C. 2007. 'A History of AIDS: Looking Back to See Ahead'. European Journal of Immunology 37(SUPPL. 1). doi: 10.1002/eji.200737441.
Grosdent, Nadine, Isabelle Maridonneau-Parini, Marie-Paule Sory, and Guy R. Cornelis. 2002. 'Role of Yops and Adhesins in Resistance of Yersinia enterocolitica to Phagocytosis', Infection and Immunity, 70: 4165.
Grützner, Anika, Sergi Garcia-Manyes, Sebastian Kötter, Carmen L. Badilla, Julio M. Fernandez, and Wolfgang A. Linke. 2009. 'Modulation of Titin-Based Stiffness by Disulfide Bonding in the Cardiac Titin N2-B Unique Sequence'. Biophysical Journal 97(3). doi: 10.1016/j.bpj.2009.05.037.
Guedes, Isabella A., Camila S. de Magalhães, and Laurent E. Dardenne. 2014. 'Receptor-Ligand Molecular Docking'. Biophysical Reviews 6(1).
Guinn, Emily J., Wayne S. Kontur, Oleg V. Tsodikov, Irina Shkel, and M. Thomas Record. 2013. 'Probing the protein-folding mechanism using denaturant and temperature effects on rate constants', Proceedings of the National Academy of Sciences, 110: 16784-89.
Gupta, R., D. Toptygin, and C. M. Kaiser. 2020. 'The SecA motor generates mechanical force during protein translocation', Nat Commun, 11: 3802.
Haldar, Shubhasis, Rafael Tapia-Rojo, Edward C. Eckels, Jessica Valle-Orero, and Julio M. Fernandez. 2017. 'Trigger Factor Chaperone Acts as a Mechanical Foldase'. Nature Communications 8(1). doi: 10.1038/s41467-017-00771-6.
Haqqani, Aiman A., and John C. Tilton. 2013. 'Entry Inhibitors and Their Use in the Treatment of HIV-1 Infection'. Antiviral Research 98(2).
Harris, Reed J., Steven M. CHAMOW, Timothy J. GREGORY, and Michael W. SPELLMAN. 1990. 'Characterization of a Soluble Form of Human CD4: Peptide Analyses Confirm the Expected Amino Acid Sequence, Identify Glycosylation Sites and Demonstrate the Presence of Three Disulfide Bonds'. European Journal of Biochemistry 188(2). doi: 10.1111/j.1432-1033.1990.tb15402.x.
Hartl, F. Ulrich. 2009. 'Chaperone-assisted Protein Folding in Health and Disease'. The FASEB Journal 23(S1). doi: 10.1096/fasebj.23.1_supplement.195.1.
Herman-Bausier, Philippe, Cristina Labate, Aisling M. Towell, Sylvie Derclaye, Joan A. Geoghegan, and Yves F. Dufrêne. 2018. 'Staphylococcus Aureus Clumping Factor A Is a Force-Sensitive Molecular Switch That Activates Bacterial Adhesion'. Proceedings of the National Academy of Sciences of the United States of America 115(21). doi: 10.1073/pnas.1718104115.
Hersel, Ulrich, Claudia Dahmen, and Horst Kessler. 2003. 'RGD modified polymers: biomaterials for stimulated cell adhesion and beyond', Biomaterials, 24: 4385-415.

Hinterdorfer, Peter, and Yves F. Dufrêne. 2006. ‘Detection and Localization of Single Molecular Recognition Events Using Atomic Force Microscopy’. Nature Methods 3(5).
Hoffmann, Toni, and Lorna Dougan. 2012. ‘Single Molecule Force Spectroscopy Using Polyproteins’. Chemical Society Reviews 41(14). doi: 10.1039/c2cs35033e.
Hoffmann, Toni, Katarzyna M. Tych, Megan L. Hughes, David J. Brockwell, and Lorna Dougan. 2013. ‘Towards Design Principles for Determining the Mechanical Stability of Proteins’. Physical Chemistry Chemical Physics 15(38).
Hu, Wei, Yong Zhang, Panyu Fei, Tongtong Zhang, Danmei Yao, Yufei Gao, Jia Liu, Hui Chen, Qiao Lu, Tenny Mudianto, Xinrui Zhang, Chuxuan Xiao, Yang Ye, Qiming Sun, Jing Zhang, Qi Xie, Pei Hui Wang, Jun Wang, Zhenhai Li, Jizhong Lou, and Wei Chen. 2021. ‘Mechanical Activation of Spike Fosters SARS-CoV-2 Viral Infection’. Cell Research 31(10). doi: 10.1038/s41422-021-00558-x.
Hu, Xiaotang, and Hongbin Li. 2014. 'Force spectroscopy studies on protein–ligand interactions: A single protein mechanics perspective', FEBS Letters, 588: 3613-20.
Huang, Wenmao, Shimin Le, Yuze Sun, Dennis Jingxiong Lin, Mingxi Yao, Yi Shi, and Jie Yan. 2022. ‘Mechanical Stabilization of a Bacterial Adhesion Complex’. Journal of the American Chemical Society 144(37). doi: 10.1021/jacs.2c03961.
Infante, Elvira, Andrew Stannard, Stephanie J. Board, Palma Rico-Lastres, Elena Rostkova, Amy E. M. Beedle, Ainhoa Lezamiz, Yong Jian Wang, Samuel Gulaidi Breen, Fani Panagaki, Vinoth Sundar Rajan, Catherine Shanahan, Pere Roca-Cusachs, and Sergi Garcia-Manyes. 2019. ‘The Mechanical Stability of Proteins Regulates Their Translocation Rate into the Cell Nucleus’. Nature Physics 15(9). doi: 10.1038/s41567-019-0551-3.
Irwin, J. J., and B. K. Shoichet. 2016. 'Docking Screens for Novel Ligands Conferring New Biology', J Med Chem, 59: 4103-20.
Jabalera, Y., M. Montalban-Lopez, J. J. Vinuesa-Rodriguez, G. R. Iglesias, M. Maqueda, and C. Jimenez-Lopez. 2021. ‘Antibacterial Directed Chemotherapy Using AS-48 Peptide Immobilized on Biomimetic Magnetic Nanoparticles Combined with Magnetic Hyperthermia’. International Journal of Biological Macromolecules 189. doi: 10.1016/j.ijbiomac.2021.08.110.
Jabalera, Ylenia, Antonia Fernández-Vivas, Guillermo R. Iglesias, Ángel V. Delgado, and Concepcion Jimenez-Lopez. 2019. ‘Magnetoliposomes of Mixed Biomimetic and Inorganic Magnetic Nanoparticles as Enhanced Hyperthermia Agents’. Colloids and Surfaces B: Biointerfaces 183. doi: 10.1016/j.colsurfb.2019.110435.
Jabalera, Ylenia, Francesca Oltolina, Ana Peigneux, Alberto Sola-Leyva, Maria P. Carrasco-Jiménez, Maria Prat, Concepcion Jimenez-Lopez, and Guillermo R. Iglesias. 2020. ‘Nanoformulation Design Including MamC-Mediated Biomimetic Nanoparticles Allows the Simultaneous Application of Targeted Drug Delivery and Magnetic Hyperthermia’. Polymers 12(8). doi: 10.3390/POLYM12081832.

Jain, Nikhil, Jens Moeller, and Viola Vogel. 2019. 'Mechanobiology of Macrophages: How Physical Factors Coregulate Macrophage Plasticity and Phagocytosis', Annual Review of Biomedical Engineering, 21: 267-97.
Josse, Jérôme, Frédéric Laurent, and Alan Diot. 2017. 'Staphylococcal Adhesion and Host Cell Invasion: Fibronectin-Binding and Other Mechanisms'. Frontiers in Microbiology 8(DEC).
Jumper, John, Richard Evans, Alexander Pritzel, Tim Green, Michael Figurnov, Olaf Ronneberger, Kathryn Tunyasuvunakool, Russ Bates, Augustin Žídek, Anna Potapenko, Alex Bridgland, Clemens Meyer, Simon A. A. Kohl, Andrew J. Ballard, Andrew Cowie, Bernardino Romera-Paredes, Stanislav Nikolov, Rishub Jain, Jonas Adler, Trevor Back, Stig Petersen, David Reiman, Ellen Clancy, Michal Zielinski, Martin Steinegger, Michalina Pacholska, Tamas Berghammer, Sebastian Bodenstein, David Silver, Oriol Vinyals, Andrew W. Senior, Koray Kavukcuoglu, Pushmeet Kohli, and Demis Hassabis. 2021. 'Highly Accurate Protein Structure Prediction with AlphaFold'. Nature 596(7873):583–89. doi: 10.1038/s41586-021-03819-2.
Kao, Weiyuan John, Damian Lee, Jason C. Schense, and Jeffrey A. Hubbell. 2001. 'Fibronectin modulates macrophage adhesion and FBGC formation: The role of RGD, PHSRN, and PRRARV domains', Journal of Biomedical Materials Research, 55: 79-88.
Ke, Yi Yu, Mohane Selvaraj Coumar, Hui Yi Shiao, Wen Chieh Wang, Chieh Wen Chen, Jen Shin Song, Chun Hwa Chen, Wen Hsing Lin, Szu Huei Wu, John T. A. Hsu, Chung Ming Chang, and Hsing Pang Hsieh. 2014. 'Ligand Efficiency Based Approach for Efficient Virtual Screening of Compound Libraries'. European Journal of Medicinal Chemistry 83. doi: 10.1016/j.ejmech.2014.06.029.
Kefauver, J. M., A. B. Ward, and A. Patapoutian. 2020. 'Discoveries in structure and physiology of mechanically activated ion channels', Nature, 587: 567-76.
Kendrew JC. 1961. The Three-Dimensional Structure of a Protein Molecule.
Khoury, George A., James Smadbeck, Chris A. Kieslich, and Christodoulos A. Floudas. 2014. 'Protein Folding and de Novo Protein Design for Biotechnological Applications'. Trends in Biotechnology 32(2).
Klein, Eili, David L. Smith, and Ramanan Laxminarayan. 2007. 'Hospitalizations and Deaths Caused by Methicillin-Resistant Staphylococcus Aureus, United States, 1999-2005'. Emerging Infectious Diseases 13(12). doi: 10.3201/eid1312.070629.
Klotzsch, Enrico, Johannes Stiegler, Eldad Ben-Ishay, and Katharina Gaus. 2015. 'Do mechanical forces contribute to nanoscale membrane organisation in T cells?', Biochimica et Biophysica Acta (BBA) - Molecular Cell Research, 1853: 822-29.
Komeili, Arash, Hojatollah Vali, Terrance J. Beveridge, and Dianne K. Newman. 2004. 'Magnetosome Vesicles Are Present before Magnetite Formation, and MamA Is Required for Their Activation'. Proceedings of the National Academy of Sciences of the United States of America 101(11). doi: 10.1073/pnas.0400391101.

Kornberg, Thomas B. 1993. THE JOURNAL OF B I O L ~ ~ I C A L CHEMISTRY Understanding the Homeodomain*. Vol. 268.
Kress, Holger, Ernst H. K. Stelzer, Daniela Holzer, Folma Buss, Gareth Griffiths, and Alexander Rohrbach. 2007. 'Filopodia act as phagocytic tentacles and pull with discrete steps and a load-dependent velocity', Proceedings of the National Academy of Sciences, 104: 11633.
Krupyanko, Vladimir I. 2000. 'Experimental Biochemistry, by R.L. Switzer and L.F. Garrity, (Third Edition). W.H. Freeman and Company, New York, 1999, ISBN 0-7167-3300-5'. Process Biochemistry 36(4). doi: 10.1016/s0032-9592(00)00214-4.
Kuhlman, Brian, and Philip Bradley. 2019. 'Advances in Protein Structure Prediction and Design'. Nature Reviews Molecular Cell Biology 20(11):681–97.
Labernadie, Anna, Anaïs Bouissou, Patrick Delobelle, Stéphanie Balor, Raphael Voituriez, Amsha Proag, Isabelle Fourquaux, Christophe Thibault, Christophe Vieu, Renaud Poincloux, Guillaume M. Charrière, and Isabelle Maridonneau-Parini. 2014. 'Protrusion force microscopy reveals oscillatory force generation and mechanosensing activity of human macrophage podosomes', Nature Communications, 5: 5343.
Lang, Matthew J., Charles L. Asbury, Joshua W. Shaevitz, and Steven M. Block. 2002. 'An Automated Two-Dimensional Optical Force Clamp for Single Molecule Studies'. Biophysical Journal 83(1). doi: 10.1016/S0006-3495(02)75185-0.
Lavecchia, A., and C. Giovanni. 2013. 'Virtual Screening Strategies in Drug Discovery: A Critical Review'. Current Medicinal Chemistry 20(23). doi: 10.2174/09298673113209990001.
Lewis, A. H., and J. Grandl. 2021. 'Stretch and poke stimulation for characterizing mechanically activated ion channels', Methods Enzymol, 654: 225-53.
Li, Bei, and Ruifu Yang. 2008. 'Interaction between Yersinia pestis and the host immune system', Infection and Immunity, 76: 1804-11.
Li, Chaohong, and Qingbo Xu. 2007. 'Mechanical Stress-Initiated Signal Transduction in Vascular Smooth Muscle Cells in Vitro and in Vivo'. Cellular Signalling 19(5).
Li, H., M. Carrion-Vazquez, A. F. Oberhauser, P. E. Marszalek, and J. M. Fernandez. 2000. 'Point mutations alter the mechanical stability of immunoglobulin modules', Nat Struct Biol, 7: 1117-20.
Li, Mamie Z., and Stephen J. Elledge. 2007. 'Harnessing homologous recombination in vitro to generate recombinant DNA via SLIC', Nature Methods, 4: 251.
Lim, C. G., J. Jang, and C. Kim. 2018. 'Cellular machinery for sensing mechanical force', BMB Rep, 51: 623-29.
Lindorff-Larsen, Kresten, Stefano Piana, Ron O. Dror, and David E. Shaw. 2011. 'How fast-folding proteins fold', Science (New York, N.Y.), 334: 517-20.

Lipinski, Christopher A. 2004. 'Lead- and drug-like compounds: the rule-of-five revolution', Drug Discovery Today: Technologies, 1: 337-41.
Lower, Steven K., Supaporn Lamlertthon, Nadia N. Casillas-Ituarte, Roberto D. Lins, Ruchirej Yongsunthon, Eric S. Taylor, Alex C. DiBartola, Catherine Edmonson, Lauren M. McIntyre, L. Barth Reller, Yok Ai Que, Robert Ros, Brian H. Lower, and Vance G. Fowler. 2011. 'Polymorphisms in Fibronectin Binding Protein A of Staphylococcus Aureus Are Associated with Infection of Cardiovascular Devices'. Proceedings of the National Academy of Sciences of the United States of America 108(45). doi: 10.1073/pnas.1109071108.
Manteca, A., J. Schonfelder, A. Alonso-Caballero, M. J. Fertin, N. Barruetabena, B. F. Faria, E. Herrero-Galan, J. Alegre-Cebollada, D. De Sancho, and R. Perez-Jimenez. 2017. 'Mechanochemical evolution of the giant muscle protein titin as inferred from resurrected proteins', Nat Struct Mol Biol, 24: 652-57.
Marszalek, Plotr E., Hui Lu, Hongbin Li, Mariano Carrion-Vazquez, Andres F. Oberhauser, Klaus Schulten, and Julio M. Fernandez. 1999. 'Mechanical Unfolding Intermediates in Titin Modules'. Nature 402(6757). doi: 10.1038/47083.
Martinac, B., and K. Poole. 2018. 'Mechanically activated ion channels', Int J Biochem Cell Biol, 97: 104-07.
Mathelie-Guinlet, M., F. Viela, G. Pietrocola, P. Speziale, D. Alsteens, and Y. F. Dufrene. 2020. 'Force-clamp spectroscopy identifies a catch bond mechanism in a Gram-positive pathogen', Nat Commun, 11: 5431.
Mayne, Leland, and S. Walter Englander. 2000. 'Two-State vs. Multistate Protein Unfolding Studied by Optical Melting and Hydrogen Exchange'. Protein Science 9(10). doi: 10.1110/ps.9.10.1873.
Mayor, U., C. M. Johnson, V. Daggett, and A. R. Fersht. 2000. 'Protein folding and unfolding in microseconds to nanoseconds by experiment and simulation', Proc Natl Acad Sci U S A, 97: 13518-22.
Mayor, U., N. R. Guydosh, C. M. Johnson, J. G. Grossmann, S. Sato, G. S. Jas, S. M. V. Freund, D. O. V. Alonso, V. Daggett, and A. R. Fersht. 2003. 'The complete folding pathway of a protein from nanosecons to microseconds', Nature, 421: 863-67.
Mayor, Ugo, Christopher M. Johnson, Valerie Daggett, and Alan R. Fersht. 2000. 'Protein Folding and Unfolding in Microseconds to Nanoseconds by Experiment and Simulation'. Proceedings of the National Academy of Sciences of the United States of America 97(25). doi: 10.1073/pnas.250473497.
McGibbon, R. T., K. A. Beauchamp, M. P. Harrigan, C. Klein, J. M. Swails, C. X. Hernandez, C. R. Schwantes, L. P. Wang, T. J. Lane, and V. S. Pande. 2015. 'MDTraj: A Modern Open Library for the Analysis of Molecular Dynamics Trajectories', Biophys J, 109: 1528-32.
Meng, Fanjie, Thomas M. Suchyna, Elena Lazakovitch, Richard M. Gronostajski, and Frederick Sachs. 2011. 'Real Time FRET Based Detection of Mechanical Stress in Cytoskeletal

and Extracellular Matrix Proteins'. Cellular and Molecular Bioengineering 4(2). doi: 10.1007/s12195-010-0140-0.
Michel Grandbois, Martin Beyer, Matthias Rief, Hauke Clausen-Schaumann, and Hermann E. Gaub. 1999. 'How Strong Is a Covalent Bond?' Science 283(5408):1727–30.
Miller, Julie, E. Diane Williamson, Jeremy H. Lakey, Martin J. Pearce, Steven M. Jones, and Richard W. Titball. 1998. 'Macromolecular organisation of recombinant Yersinia pestis F1 antigen and the effect of structure on immunogenicity', FEMS Immunology & Medical Microbiology, 21: 213-21.
Moffitt, Jeffrey R., Yann R. Chemla, Steven B. Smith, and Carlos Bustamante. 2008. 'Recent Advances in Optical Tweezers'. Annual Review of Biochemistry 77.
Mok, K. Hun, Lars T. Kuhn, Martin Goez, Iain J. Day, Jasper C. Lin, Niels H. Andersen, and P. J. Hore. 2007. 'A Pre-Existing Hydrophobic Collapse in the Unfolded State of an Ultrafast Folding Protein'. Nature 447(7140). doi: 10.1038/nature05728.
Müller, Daniel J., and Yves F. Dufrêne. 2008. Atomic Force Microscopy as a Multifunctional Molecular Toolbox in Nanobiotechnology. Vol. 3.
Muñoz, Victor, and Michele Cerminara. 2016. 'When Fast Is Better: Protein Folding Fundamentals and Mechanisms from Ultrafast Approaches'. Biochemical Journal 473(17).
Murthy, S. E., A. E. Dubin, T. Whitwam, S. Jojoa-Cruz, S. M. Cahalan, S. A. R. Mousavi, A. B. Ward, and A. Patapoutian. 2018. 'OSCA/TMEM63 are an Evolutionarily Conserved Family of Mechanically Activated Ion Channels', Elife, 7.
Naganathan, A. N., U. Doshi, and V. Munoz. 2007. 'Protein Folding Kinetics: Barrier Effects in Chemical and Thermal Denaturation Experiments', Journal of the American Chemical Society: 2283-87.
Naganathan, Athi N., Jose M. Sanchez-Ruiz, and Victor Muñoz. 2005. 'Direct Measurement of Barrier Heights in Protein Folding', Journal of the American Chemical Society, 127: 17970-71.
Nam, G. M., and D. E. Makarov. 2016. 'Extracting intrinsic dynamic parameters of biomolecular folding from single-molecule force spectroscopy experiments', Protein Sci, 25: 123-34.
Naruse, Keiji. 2018. 'Mechanomedicine'. Biophysical Reviews 10(5).
Nelson, David L., and Michael M. Cox. 2017. 'Lehninger Principles of Biochemistry SEVENTH EDITION'. Journal of Craniofacial Surgery 22(6).
Neuman, Keir C., and Attila Nagy. 2008. 'Single-Molecule Force Spectroscopy: Optical Tweezers, Magnetic Tweezers and Atomic Force Microscopy'. Nature Methods 5(6).
Noé, Frank, Gianni De Fabritiis, and Cecilia Clementi. 2020. 'Machine Learning for Protein Folding and Dynamics'. Current Opinion in Structural Biology 60:77–84.

Noel, J. K., M. Levi, M. Raghunathan, H. Lammert, R. L. Hayes, J. N. Onuchic, and P. C. Whitford. 2016. 'SMOG 2: A Versatile Software Package for Generating Structure-Based Models', PLoS Comput Biol, 12: e1004794.
O'Neill, Eoghan, Clarissa Pozzi, Patrick Houston, Hilary Humphreys, D. Ashley Robinson, Anthony Loughman, Timothy J. Foster, and James P. O'Gara. 2008. 'A Novel Staphylococcus Aureus Biofilm Phenotype Mediated by the Fibronectin-Binding Proteins, FnBPA and FnBPB'. Journal of Bacteriology 190(11). doi: 10.1128/JB.00167-08.
Oberhauser, A. F., P. K. Hansma, M. Carrion-Vazquez, and J. M. Fernandez. 2001. 'Stepwise unfolding of titin under force-clamp atomic force microscopy', Proc Natl Acad Sci U S A, 98: 468-72.
Onuchic, José Nelson, Zaida Luthey-Schulten, and Peter G. Wolynes. 1997. 'Theory of Protein Folding: The Energy Landscape Perspective'. Annual Review of Physical Chemistry 48(1). doi: 10.1146/annurev.physchem.48.1.545.
Paci, Emanuele, and Martin Karplus. 2000. Unfolding Proteins by External Forces and Temperature: The Importance of Topology and Energetics. Vol. 97.
Pannekoek, W. J., J. de Rooij, and M. Gloerich. 2019. 'Force transduction by cadherin adhesions in morphogenesis', F1000Res, 8.
Park, Eunyong, and Tom A. Rapoport. 2012. 'Mechanisms of Sec61SecY-Mediated Protein Translocation across Membranes'. Annual Review of Biophysics 41(1).
Peigneux, Ana, Jose D. Puentes-Pardo, Alejandro B. Rodríguez-Navarro, Maxwell T. Hincke, and Concepción Jimenez-Lopez. 2020. 'Development and Characterization of Magnetic Eggshell Membranes for Lead Removal from Wastewater'. Ecotoxicology and Environmental Safety 192. doi: 10.1016/j.ecoenv.2020.110307.
Perales-Calvo, J., D. Giganti, G. Stirnemann, and S. Garcia-Manyes. 2018. 'The force-dependent mechanism of DnaK-mediated mechanical folding', Sci Adv, 4: eaaq0243.
Perez-Jimenez, R., S. Garcia-Manyes, S. R. Ainavarapu, and J. M. Fernandez. 2006. 'Mechanical Unfolding Pathways of the Enhanced Yellow Fluorescent Protein Revealed by Single Molecule Force Spectroscopy'. J Biol Chem 281(52):40010–14. doi: 10.1074/jbc.M609890200.
Perez-Jimenez, Raul, Alvaro Alonso-Caballero, Ronen Berkovich, David Franco, Ming Wei Chen, Patricia Richard, Carmen L. Badilla, and Julio M. Fernandez. 2014. 'Probing the Effect of Force on HIV-1 Receptor CD4'. ACS Nano 8(10). doi: 10.1021/nn503557w.
Perry, Robert D., and Jacqueline D. Fetherston. 1997. 'Yersinia Pestis - Etiologic Agent of Plague'. Clinical Microbiology Reviews 10(1).
Peters, D. T., A. Reifs, A. Alonso-Caballero, A. Madkour, H. Waller, B. Kenny, R. Perez-Jimenez, and J. H. Lakey. 2022. 'Unraveling the molecular determinants of the anti-phagocytic protein cloak of plague bacteria', PLoS Pathog, 18: e1010447.

Peters, Daniel T., Helen Waller, Mark A. Birch, and Jeremy H. Lakey. 2019. 'Engineered mosaic protein polymers; a simple route to multifunctional biomaterials', Journal of Biological Engineering, 13: 54.
Pines, M., R. Das, S. J. Ellis, A. Morin, S. Czerniecki, L. Yuan, M. Klose, D. Coombs, and G. Tanentzapf. 2012. 'Mechanical force regulates integrin turnover in Drosophila in vivo', Nat Cell Biol, 14: 935-43.
Poole, K. 2022. 'The Diverse Physiological Functions of Mechanically Activated Ion Channels in Mammals', Annu Rev Physiol, 84: 307-29.
Popa, Ionel, Ronen Berkovich, Jorge Alegre-Cebollada, Carmen L. Badilla, Jaime Andrés Rivas-Pardo, Yukinori Taniguchi, Masaru Kawakami, and Julio M. Fernandez. 2013. 'Nanomechanics of HaloTag Tethers'. Journal of the American Chemical Society 135(34):12762–71. doi: 10.1021/ja4056382.
Proctor, Richard A. 1987. 'Fibronectin: An Enhancer of Phagocyte Function', Reviews of Infectious Diseases, 9: S412-S19.
Prystopiuk, Valeria, Cécile Feuillie, Philippe Herman-Bausier, Felipe Viela, David Alsteens, Giampiero Pietrocola, Pietro Speziale, and Yves F. Dufrêne. 2018. 'Mechanical Forces Guiding Staphylococcus Aureus Cellular Invasion'. ACS Nano 12(4):3609–22. doi: 10.1021/acsnano.8b00716.
Pujol, Céline, and James B. Bliska. 2005. 'Turning Yersinia pathogenesis outside in: subversion of macrophage function by intracellular yersiniae', Clinical Immunology, 114: 216-26.
Quitard, Sabine, Paul Dean, Marc Maresca, and Brendan Kenny. 2006. 'The enteropathogenic Escherichia coli EspF effector molecule inhibits PI-3 kinase-mediated uptake independently of mitochondrial targeting', Cellular Microbiology, 8: 972-81.
Ramms, Lena, Gloria Fabris, Reinhard Windoffer, Nicole Schwarz, Ronald Springer, Chen Zhou, Jaroslav Lazar, Simone Stiefel, Nils Hersch, Uwe Schnakenberg, Thomas M. Magin, Rudolf E. Leube, Rudolf Merkel, and Bernd Hoffmann. 2013. 'Keratins as the Main Component for the Mechanical Integrity of Keratinocytes'. Proceedings of the National Academy of Sciences of the United States of America 110(46):18513–18. doi: 10.1073/pnas.1313491110.
Ray, M., M. Acharyya, and N. Chatterjee. 2001. 'Expression of Engrailed and Wingless Genes in the Imaginal Discs of Drosophila Melanogaster-D. Simulans Hybrids'. Entomon (spl.):159–63.
Reifs, Antonio, Irene Ruiz Ortiz, Amaia Ochandorena Saa, Jörg Schönfelder, David De Sancho, Victor Muñoz, and Raul Perez-Jimenez. 2023. 'Compliant Mechanical Response of the Ultrafast Folding Protein EnHD under Force'. Communications Physics 6(1). doi: 10.1038/s42005-022-01125-5.

Religa, T. L., C. M. Johnson, D. M. Vu, S. H. Brewer, R. B. Dyer, and A. R. Fersht. 2007. 'The helix turn helix motif as an ultrafast independently folding domain: The pathway of folding of Engrailed homeodomain', Proceedings of the National Academy of Sciences, 104: 9272-77.
Religa, Tomasz L., Christopher M. Johnson, Dung M. Vu, Scott H. Brewer, R. Brian Dyer, and Alan R. Fersht. 2007. 'The Helix-Turn-Helix Motif as an Ultrafast Independently Folding Domain: The Pathway of Folding of Engrailed Homeodomain'. Proceedings of the National Academy of Sciences of the United States of America 104(22). doi: 10.1073/pnas.0703434104.
Richardson, J., A. Kotevski, and K. Poole. 2021. 'From stretch to deflection: the importance of context in the activation of mammalian, mechanically activated ion channels', FEBS J.
Rief, Matthias, Jaime Pascual, Matti Saraste, and Hermann E. Gaub. 1999. 'Single Molecule Force Spectroscopy of Spectrin Repeats: Low Unfolding Forces in Helix Bundles'. Journal of Molecular Biology 286(2). doi: 10.1006/jmbi.1998.2466.
Rief, Matthias, Mathias Gautel, Filipp Oesterhelt, Julio M. Fernandez, and Hermann E. Gaub. 1997. 'Reversible Unfolding of Individual Titin Immunoglobulin Domains by AFM'. Science 276(5315). doi: 10.1126/science.276.5315.1109.
Rivas-Pardo, J. A., C. L. Badilla, R. Tapia-Rojo, A. Alonso-Caballero, and J. M. Fernandez. 2018. 'Molecular strategy for blocking isopeptide bond formation in nascent pilin proteins', Proc Natl Acad Sci U S A, 115: 9222-27.
Rohs, Remo, Catherine Etchebest, and Richard Lavery. 1999. 'Unraveling Proteins: A Molecular Mechanics Study'. Biophysical Journal 76(5):2760–68. doi: 10.1016/S0006-3495(99)77429-1.
Roque, Ana I., Andrei Soliakov, Mark A. Birch, Sion R. Philips, Deepan S. H. Shah, and Jeremy H. Lakey. 2014. 'Reversible Non-Stick Behaviour of a Bacterial Protein Polymer Provides a Tuneable Molecular Mimic for Cell and Tissue Engineering', Advanced Materials, 26: 2704-09.
Runco, Lisa M., Selina Myrczek, James B. Bliska, and David G. Thanassi. 2008. 'Biogenesis of the Fraction 1 Capsule and Analysis of the Ultrastructure of Yersinia pestis', Journal of Bacteriology, 190: 3381.
Sacquin-Mora, Sophie, Émilie Laforet, and Richard Lavery. 2007. 'Locating the Active Sites of Enzymes Using Mechanical Properties'. Proteins: Structure, Function and Genetics 67(2). doi: 10.1002/prot.21353.
Saravia-Otten, Patricia, Hans-Peter Mu¨ller, Mu¨ Mu¨ller, † And, and Staffan Arvidson. 1997. Transcription of Staphylococcus Aureus Fibronectin Binding Protein Genes Is Negatively Regulated by Agr and an Agr-Independent Mechanism. Vol. 179.
Schlierf, M., H. Li, and J. M. Fernandez. 2004. 'The unfolding kinetics of ubiquitin captured with single-molecule force-clamp techniques', Proc Natl Acad Sci U S A, 101: 7299-304.

Schneck, Emanuel, Dominik Horinek, and Roland R. Netz. 2013. ‘Insight into the Molecular Mechanisms of Protein Stabilizing Osmolytes from Global Force-Field Variations’. Journal of Physical Chemistry B 117(28):8310–21. doi: 10.1021/jp400790f.
Schönfelder, J., A. Alonso-Caballero, D. De Sancho, and R. Perez-Jimenez. 2018a. ‘The Life of Proteins under Mechanical Force’. Chem Soc Rev 47(10):3558–73. doi: 10.1039/c7cs00820a.
Schönfelder, Jörg, David De Sancho, and Raul Perez-Jimenez. 2016. 'The power of force: Insights into the protein folding process using single-molecule force spectroscopy', Journal of Molecular Biology, 428: 4245-57.
Schönfelder, Jörg, David De Sancho, Ronen Berkovich, Robert B. Best, Victor Muñoz, and Raul Perez-Jimenez. 2018. ‘Reversible Two-State Folding of the Ultrafast Protein GpW under Mechanical Force’. Communications Chemistry 1(1). doi: 10.1038/s42004-018-0060-9.
Schönfelder, Jörg, Raul Perez-Jimenez, and Victor Muñoz. 2016. 'A simple two-state protein unfolds mechanically via multiple heterogeneous pathways at single-molecule resolution', Nature communications, 7: 11777-77.
Schüpbach, Jörg, Mikulas Popovic, Raymond V. Gilden, Matthew A. Gonda, M. G. Sarngadharan, and Robert C. Gallo. 1984. ‘Serological Analysis of a Subgroup of Human T-Lymphotropic Retroviruses (HTLV-III) Associated with AIDS’. Science 224(4648). doi: 10.1126/science.6200937.
Seifert, Christian, and Frauke Gräter. 2013. 'Protein mechanics: How force regulates molecular function', Biochimica et Biophysica Acta (BBA) - General Subjects, 1830: 4762-68.
Shtilerman, Mark, George H. Lorimer, and S. Walter Englander. 1999. ‘Chaperonin Function: Folding by Forced Unfolding’. Science 284(5415). doi: 10.1126/science.284.5415.822.
Sianati, S., A. Kurumlian, E. Bailey, and K. Poole. 2019. 'Analysis of Mechanically Activated Ion Channels at the Cell-Substrate Interface: Combining Pillar Arrays and Whole-Cell Patch-Clamp', Front Bioeng Biotechnol, 7: 47.
Simon, Horst H., Sandrine Thuret, and Lavinia Alberi. 2004. ‘Midbrain Dopaminergic Neurons: Control of Their Cell Fate by the Engrailed Transcription Factors’. Cell and Tissue Research 318(1):53–61.
Singh, Surinder M., Swati Bandi, Dinen D. Shah, Geoffrey Armstrong, and Krishna M. G. Mallela. 2014. ‘Missense Mutation Lys18Asn in Dystrophin That Triggers X-Linked Dilated Cardiomyopathy Decreases Protein Stability, Increases Protein Unfolding, and Perturbs Protein Structure, but Does Not Affect Protein Function’. PLoS ONE 9(10). doi: 10.1371/journal.pone.0110439.
Soliakov, Andrei, J. Robin Harris, Allan Watkinson, and Jeremy H. Lakey. 2010. 'The structure of Yersinia pestis Caf1 polymer in free and adjuvant bound states', Vaccine, 28: 5746-54.

Solís, Christopher, and Brenda Russell. 2021. ‘Striated Muscle Proteins Are Regulated Both by Mechanical Deformation and by Chemical Post-Translational Modification’. Biophysical Reviews 13(5).
Spaulding, C. N., H. L. th Schreiber, W. Zheng, K. W. Dodson, J. E. Hazen, M. S. Conover, F. Wang, P. Svenmarker, A. Luna-Rico, O. Francetic, M. Andersson, S. Hultgren, and E. H. Egelman. 2018. 'Functional role of the type 1 pilus rod structure in mediating host-pathogen interactions', Elife, 7.
Speziale, Pietro, and Giampiero Pietrocola. 2020. ‘The Multivalent Role of Fibronectin-Binding Proteins A and B (FnBPA and FnBPB) of Staphylococcus Aureus in Host Infections’. Frontiers in Microbiology 11.
Spinner, Justin L., Seth Winfree, Tregei Starr, Jeffrey G. Shannon, Vinod Nair, Olivia Steele-Mortimer, and B. Joseph Hinnebusch. 2014. 'Yersinia pestis survival and replication within human neutrophil phagosomes and uptake of infected neutrophils by macrophages', Journal of leukocyte biology, 95: 389-98.
Stefan Walter, and Johannes Buchner. 2002. Protein Folding and Molecular Chaperones. doi: https://doi.org/10.1002/1521-3773(20020402)41:7<1098::AID-ANIE1098>3.0.CO;2-9.
Stewart, T. A., K. Hughes, A. J. Stevenson, N. Marino, A. L. Ju, M. Morehead, and F. M. Davis. 2021. 'Mammary mechanobiology - investigating roles for mechanically activated ion channels in lactation and involution', J Cell Sci, 134.
Stollar, Elliott J., Ugo Mayor, Simon C. Lovell, Luca Federici, Stefan M. V. Freund, Alan R. Fersht, and Ben F. Luisi. 2003. ‘Crystal Structures of Engrailed Homeodomain Mutants: Implications for Stability and Dynamics’. Journal of Biological Chemistry 278(44):43699–708. doi: 10.1074/jbc.M308029200.
Strick, T. R., M. N. Dessinges, G. Charvin, N. H. Dekker, J. F. Allemand, D. Bensimon, and V. Croquette. 2003. ‘Stretching of Macromolecules and Proteins’. Reports on Progress in Physics 66(1). doi: 10.1088/0034-4885/66/1/201.
Sullivan, David C., and Irwin D. Kuntz. 2002. ‘Protein Folding as Biased Conformational Diffusion’. Journal of Physical Chemistry B 106(12). doi: 10.1021/jp012911g.
Svoboda, Karel, and Steven M. Block. 1994. ‘Biological Applications of Optical Forces’. Annual Review of Biophysics and Biomolecular Structure 23.
Swanson, Joel A. 2008. 'Shaping cups into phagosomes and macropinosomes', Nature Reviews Molecular Cell Biology, 9: 639.
Tanase, Monica, Nicolas Biais, and Michael Sheetz. 2007. ‘Magnetic Tweezers in Cell Biology’. Methods in Cell Biology 83:473–93. doi: 10.1016/S0091-679X(07)83020-2.
Tapia-Rojo, Rafael, Edward C. Eckels, and Julio M. Fernández. 2019. 'Ephemeral states in protein folding under force captured with a magnetic tweezers design', Proceedings of the National Academy of Sciences, 116: 7873-78.

Taverna, Darin M., and Richard A. Goldstein. 2002. 'Why are proteins marginally stable?', Proteins: Structure, Function, and Bioinformatics, 46: 105-09.
Tinoco, Ignacio, and Carlos Bustamante. 2002. 'The Effect of Force on Thermodynamics and Kinetics of Single Molecule Reactions'. Biophysical Chemistry 101–102. doi: 10.1016/S0301-4622(02)00177-1.
Tokuriki, Nobuhiko, and Dan S. Tawfik. 2009. 'Stability Effects of Mutations and Protein Evolvability'. Current Opinion in Structural Biology 19(5).
Traub, Oren, and Bradford C. Berk. 1998. 'Laminar Shear Stress: Mechanisms by Which Endothelial Cells Transduce an Atheroprotective Force'. Arteriosclerosis, Thrombosis, and Vascular Biology 18(5).
Trichet, Léa, Jimmy Le Digabel, Rhoda J. Hawkins, Sri Ram Krishna Vedula, Mukund Gupta, Claire Ribrault, Pascal Hersen, Raphaël Voituriez, and Benoît Ladoux. 2012. 'Evidence of a large-scale mechanosensing mechanism for cellular adaptation to substrate stiffness', Proceedings of the National Academy of Sciences, 109: 6933.
Uebe, René, and Dirk Schüler. 2016. 'Magnetosome Biogenesis in Magnetotactic Bacteria'. Nature Reviews Microbiology 14(10).
Ulusu, Yakup, Gema Dura, Helen Waller, Matthew J. Benning, David A. Fulton, Jeremy H. Lakey, and Daniel T. Peters. 2017. 'Thermal Stability and Rheological Properties of the "non-Stick" Caf1 Biomaterial'. Biomedical Materials (Bristol) 12(5). doi: 10.1088/1748-605X/aa7a89.
Van Mierlo, Carlo P. M., and Elles Steensma. 2000. Protein Folding and Stability Investigated by Fluorescence, Circular Dichroism (CD), and Nuclear Magnetic Resonance (NMR) Spectroscopy: The Flavodoxin Story. Vol. 79.
Voelz, Vincent A., and Ken A. Dill. 2007. 'Exploring Zipping and Assembly as a Protein Folding Principle'. Proteins: Structure, Function and Genetics 66(4). doi: 10.1002/prot.21234.
Vogel, V., and M. Sheetz. 2006. 'Local force and geometry sensing regulate cell functions', Nat Rev Mol Cell Biol, 7: 265-75.
Von Pawel-Rammingen, Ulrich, Maxim V. Telepnev, Gudula Schmidt, Klaus Aktories, Hans Wolf-Watz, and Roland Rosqvist. 2000. 'GAP activity of the Yersinia YopE cytotoxin specifically targets the Rho pathway: a mechanism for disruption of actin microfilament structure', Molecular Microbiology, 36: 737-48.
Vonna, L., A. Wiedemann, M. Aepfelbacher, and E. Sackmann. 2007. 'Micromechanics of filopodia mediated capture of pathogens by macrophages', European Biophysics Journal, 36: 145-51.
Vorselen, Daan, Yifan Wang, Miguel M. de Jesus, Pavak K. Shah, Matthew J. Footer, Morgan Huse, Wei Cai, and Julie A. Theriot. 2020. 'Microparticle traction force microscopy reveals subcellular force exertion patterns in immune cell–target interactions', Nature Communications, 11: 20.

Walder, Robert, Marc André Leblanc, William J. Van Patten, Devin T. Edwards, Jacob A. Greenberg, Ayush Adhikari, Stephen R. Okoniewski, Ruby May A. Sullan, David Rabuka, Marcelo C. Sousa, and Thomas T. Perkins. 2017. 'Rapid Characterization of a Mechanically Labile α-Helical Protein Enabled by Efficient Site-Specific Bioconjugation', Journal of the American Chemical Society, 139: 9867-75.
Wang, Jia-huai, Rob Meijers, Yi Xiong, Jin-huan Liu, Toshiko Sakihama, Rongguang Zhang, Andrzej Joachimiak, and Ellis L. Reinherz. 2001. 'Crystal structure of the human CD4 N-terminal two-domain fragment complexed to a class II MHC molecule', Proceedings of the National Academy of Sciences, 98: 10799-804.
Wang, Xuefeng, and Taekjip Ha. 2013. 'Defining Single Molecular Forces Required to Activate Integrin and Notch Signaling'. Science 340(6135). doi: 10.1126/science.1231041.
West, Daniel K., David J. Brockwell, Peter D. Olmsted, Sheena E. Radford, and Emanuele Paci. 2006. 'Mechanical Resistance of Proteins Explained Using Simple Molecular Models'. Biophysical Journal 90(1). doi: 10.1529/biophysj.105.071035.
Westby, Michael, and Angus G. Dalgleish. 1998. 'Chapter 27 Genetics and Molecular Biology of AIDS Virus'. Principles of Medical Biology 9(C). doi: 10.1016/S1569-2582(97)80011-6.
Whitby, M., M. L. McLaws, and G. Berry. 2001. 'Risk of Death from Methicillin-Resistant Staphylococcus Aureus Bacteraemia: A Meta-Analysis'. Medical Journal of Australia 175(5).
Whitford, P. C., J. K. Noel, S. Gosavi, A. Schug, K. Y. Sanbonmatsu, and J. N. Onuchic. 2009. 'An all-atom structure-based potential for proteins: bridging minimal models with all-atom empirical forcefields', Proteins, 75: 430-41.
Wiegand, Tina, Marta Fratini, Felix Frey, Klaus Yserentant, Yang Liu, Eva Weber, Kornelia Galior, Julia Ohmes, Felix Braun, Dirk-Peter Herten, Steeve Boulant, Ulrich S. Schwarz, Khalid Salaita, E. Ada Cavalcanti-Adam, and Joachim P. Spatz. 2020. 'Forces during cellular uptake of viruses and nanoparticles at the ventral side', Nature Communications, 11: 32.
Wilen, Craig B., John C. Tilton, and Robert W. Doms. 2012. 'HIV: Cell Binding and Entry'. Cold Spring Harbor Perspectives in Medicine 2(8). doi: 10.1101/cshperspect.a006866.
Wirtz, Denis, Konstantinos Konstantopoulos, and Peter C. Searson. 2011. 'The physics of cancer: the role of physical interactions and mechanical forces in metastasis', Nature Reviews Cancer, 11: 512-22.
Wooley, John C., and Yuzhen Ye. 2007. 'A Historical Perspective and Overview of Protein Structure Prediction'. in Computational Methods for Protein Structure Prediction and Modeling.
Wright, S. D., and B. C. Meyer. 1985. 'Fibronectin receptor of human macrophages recognizes the sequence Arg-Gly-Asp-Ser', The Journal of Experimental Medicine, 162: 762.
Wu, Chun, and Joan Emma Shea. 2010. 'On the Origins of the Weak Folding Cooperativity of a Designed Bβα Ultrafast Protein FSD-1'. PLoS Computational Biology 6(11). doi: 10.1371/journal.pcbi.1000998.

Wyatt, R., P. D. Kwong, E. Desjardins, R. W. Sweet, J. Robinson, W. A. Hendrickson, and J. G. Sodroski. 1998. 'The Antigenic Structure of the HIV Gp120 Envelope Glycoprotein'. Nature 393(6686). doi: 10.1038/31514.

Yamazaki, Tsutomu, Issei Komuro, and Yoshio Yazaki. 1996. 'Molecular Aspects of Mechanical Stress-Induced Cardiac Hypertrophy'. Molecular and Cellular Biochemistry 163–164. doi: 10.1007/BF00408658.

Yan, Lei, Shuang Zhang, Peng Chen, Hetao Liu, Huanhuan Yin, and Hongyu Li. 2012. 'Magnetotactic Bacteria, Magnetosomes and Their Application'. Microbiological Research 167(9).

Yankaskas, Christopher L., Kaustav Bera, Konstantin Stoletov, Selma A. Serra, Julia Carrillo-Garcia, Soontorn Tuntithavornwat, Panagiotis Mistriotis, John D. Lewis, Miguel A. Valverde, and Konstantinos Konstantopoulos. 2021. 'The fluid shear stress sensor TRPM7 regulates tumor cell intravasation', Science Advances, 7: eabh3457.

Yin, Yiyuan, Xin Xiang Wang, and Roy A. Mariuzza. 2012. 'Crystal Structure of a Complete Ternary Complex of T-Cell Receptor, Peptide-MHC, and CD4'. Proceedings of the National Academy of Sciences of the United States of America 109(14). doi: 10.1073/pnas.1118801109.

Yu, Xiao Di, Laura J. Fooks, Elham Moslehi-Mohebi, Vladimir M. Tischenko, Gelareh Askarieh, Stefan D. Knight, Sheila MacIntyre, and Anton V. Zavialov. 2012. 'Large Is Fast, Small Is Tight: Determinants of Speed and Affinity in Subunit Capture by a Periplasmic Chaperone', Journal of Molecular Biology, 417: 294-308.

Yusko, Erik C., and Charles L. Asbury. 2014. 'Force is a signal that cells cannot ignore', Molecular Biology of the Cell, 25: 3717-25.

Zavialov, A. V., N. V. Batchikova, T. Korpela, L. E. Petrovskaya, V. G. Korobko, J. Kersley, S. MacIntyre, and V. P. Zav'yalov. 2001. 'Secretion of recombinant proteins via the chaperone/usher pathway in Escherichia coli', Applied and environmental microbiology, 67: 1805-14.

Zavialov, Anton V., Jenny Berglund, Alexander F. Pudney, Laura J. Fooks, Tara M. Ibrahim, Sheila MacIntyre, and Stefan D. Knight. 2003. 'Structure and Biogenesis of the Capsular F1 Antigen from Yersinia pestis: Preserved Folding Energy Drives Fiber Formation', Cell, 113: 587-96.

Zavialov, Anton V., Natalia V. Batchikova, Timo Korpela, Lada E. Petrovskaya, Vyacheslav G. Korobko, Joanne Kersley, Sheila MacIntyre, and Vladimir P. ZaV'Yalov. 2001. 'Secretion of Recombinant Proteins via the Chaperone/Usher Pathway in Escherichia Coli'. Applied and Environmental Microbiology 67(4). doi: 10.1128/AEM.67.4.1805-1814.2001.

Zhu, Y., D. O. Alonso, K. Maki, C. Y. Huang, S. J. Lahr, V. Daggett, H. Roder, W. F. DeGrado, and F. Gai. 2003. 'Ultrafast folding of alpha3D: a de novo designed three-helix bundle protein', Proc Natl Acad Sci U S A, 100: 15486-91.

Zoldak, G., J. Stigler, B. Pelz, H. Li, and M. Rief. 2013. 'Ultrafast folding kinetics and cooperativity of villin headpiece in single-molecule force spectroscopy', Proc Natl Acad Sci U S A, 110: 18156-61.
Zou, Y., Y. Hu, B. Metzler, and Q. Xu. 1998. 'Signal Transduction in Arteriosclerosis: Mechanical Stress-Activated MAP Kinases in Vascular Smooth Muscle Cells (Review).' International Journal of Molecular Medicine 1(5).
Zwanzig, Robert. 1997. 'Two-State Models of Protein Folding Kinetics'. Proceedings of the National Academy of Sciences of the United States of America 94(1). doi: 10.1073/pnas.94.1.148.

Reagents, Buffers, Instruments, and sequences appendix

Reagents:

I. E. coli XL1-Blue: (Agilent) https://www.agilent.com/en/product/mutagenesis-cloning/competent-cells-competent-cell-supplies/competent-cells-for-routine-cloning/xl1-blue-competent-cells-233099

II. E. coli C41: (Sigma) https://www.sigmaaldrich.com/GB/en/product/sigma/cmc0017

III. Mix & Go! Transformation Kit: (Zymo Research) https://www.zymoresearch.com/products/mix-and-go-e-coli-transformation-kit

IV. SOC media: (Invitrogen) https://www.fishersci.es/shop/products/invitrogen-s-o-c-ready-to-use-medium/11528896

V. Carbenicillin disodium salt: (Fisher) https://www.fishersci.es/shop/products/gibco-carbenicillin-disodium-salt/11568616

VI. GeneJET miniprep kit: (ThermoFisher) https://www.thermofisher.com/order/catalog/product/K0503?SID=srch-srp-K0503

VII. IPTG: (Sigma) https://www.sigmaaldrich.com/GB/en/substance/iptg23830367931

VIII. Laemmli sample buffer: (Bio-rad) https://www.bio-rad.com/es-es/sku/1610747-4x-laemmli-sample-buffer?ID=1610747

IX. Tris-Glycine-SDS, 10x Solution: (Fisher) https://www.fishersci.com/shop/products/tris-glycine-sds-10x-solution-electrophoresis-fisher-bioreagents-2/p-29189

X. Coomassie Blue: (Thermo Scientific) https://www.thermofisher.com/order/catalog/product/20278

XI. Protease inhibitor: (Millipore) https://www.merckmillipore.com/ES/es/product/Protease-Inhibitor-Cocktail-Set-III-EDTA-Free-Calbiochem,EMD_BIO-539134

XII. Syringe filter 0.8 mm: (Sartorius) https://www.ddbiolab.com/frontoffice/article/150492

XIII. Syringe filter 0.45 mm: (Agilent) https://www.agilent.com/en/product/sample-preparation/filtration/syringe-filters?gclid=CjwKCAjwrqqSBhBbEiwAlQeqGmcnj8-6OJOdok3ulbVQkekNrsj_c10_ofiHEQ372th52NNiC-NpJBoCkT8QAvD_BwE&gclsrc=aw.ds

XIV. Syringe filter 0.22 mm: (Sartorius) https://www.sigmaaldrich.com/GB/en/product/supelco/16534k?gclid=CjwKCAjwrqqSBhBbEiwAlQeqGqgdPnD85OaSohyZDAUUJDkmymM-zwoc8UaCSzcaQYqlZ5bscOjt1BoCxEAQAvD_BwE

XV. HisPur Cobalt Resin: (Thermo scientific) https://www.merckmillipore.com/ES/es/product/Protease-Inhibitor-Cocktail-Set-III-EDTA-Free-Calbiochem,EMD_BIO-539134

XVI. HisPur Nickel Resin: (Thermo scientific) https://www.thermofisher.com/order/catalog/product/25215?SID=srch-srp-25215

XVII. Imidazole: (Sigma) https://www.sigmaaldrich.com/GB/en/product/sigma/i5513

XVIII. Hydrogen peroxide 100 volumenes > 30% w/v: (Fisher) https://www.fishersci.es/shop/products/hydrogen-peroxide-30-w-v-100-volumes-extra-pure-slr-2/10687022

XIX. Instruments:

XX. Electrophoresis system: (Bio-rad) https://www.bio-rad.com/es-es/category/second-dimension-mini-format-electrophoresis-systems?ID=1d552427-b697-4946-9486-a8724a0d1fcd

XXI. Nanodrop 2000L spectrophotometer: (Thermo scientific) https://www.thermofisher.com/order/catalog/product/ND-2000

XXII. Centrifuge 5910R: (Eppendorf) https://online-shop.eppendorf.es/ES-es/Centrifugacion-44533/Centrifugas-multiproposito-1007184/Centrifuge-5910Ri-PF-963296.html

XXIII. Centrifuge high-speed Sorvall Lynx 6000: (Thermofisher) https://www.thermofisher.com/order/catalog/product/75006590

XXIV. Gel Documentation System XR+: (Bio-rad) https://www.bio-rad.com/es-es/product/gel-doc-xr-gel-documentation-system?ID=O494WJE8Z

XXV. AKTA pure fast protein liquid chromatography (FPLC): (GE Healthcare) https://www.cytivalifesciences.com/en/us/shop/chromatography/chromatography-systems/akta-pure-p-05844

XXVI. HiLoad 16/600 Superdex 200pg: (Cytiva) https://www.sigmaaldrich.com/GB/en/product/sigma/ge28989335

Buffers:

XXVII. Extraction Buffer: (pH 7, Sodium phosphate 50 mM and NaCl 300 mM)

XXVIII. Elution Buffer: (pH 7, Sodium phosphate 50 mM, NaCl 300 mM and Imidazole 500mM)

XXIX. Running buffer: (Tris-Glycine-SDS 1x)

XXX. Staining buffer: (

XXXI. Washing buffer: (80% Milli-Q water, 10% Ethanol, 10% Acetic acid v/v)

XXXII. HEPES Buffer: (pH 7.2, NaCl 150 mM and EDTA 1 mM)

Sequences appendix:

- **I91$_2$-CD4-I91$_2$**

LIEVEKPLYGVEVFVGETAHFEIELSEPDVHGQWKLKGQPLTASPDCE
IIEDGKKHILILHNCQLGMTGEVSFQAANAKSAANLKVKELIEVEKPL
YGVEVFVGETAHFEIELSEPDVHGQWKLKGQPLTASPDCEIIEDGKKH
ILILHNCQLGMTGEVSFQAANAKSAANLKVKERSRSGSSKKVVLGKKG
DTVELTCTASQKKSIQFHWKNSNQIKILGNQGSFLTKGPSKLNDRADS
RRSLWDQGNFPLIIKNLKIEDSDTYICEVEDQKEEVQLLVFGLTANSD
THLLQGQSLTLTLESPPGSSPSVQCRSPRGKNIQGGKTLSVSQLELQD
SGTWTCTVLQNQKKVEFKIDIVVLAFQKASSRSLIEVEKPLYGVEVFV
GETAHFEIELSEPDVHGQWKLKGQPLTASPDCEIIEDGKKHILILHNC
QLGMTGEVSFQAANAKSAANLKVKELIEVEKPLYGVEVFVGETAHFEI
ELSEPDVHGQWKLKGQPLTASPDCEIIEDGKKHILILHNCQLGMTGEV
SFQAANAKSAANLKVKERS

- **I91$_2$-Caf1WT-I91$_2$**

MRGSHHHHHHGSLIEVEKPLYGVEVFVGETAHFEIELSEPDVHGQWKL
KGQPLAASPDCEIIEDGKKHILILHNCQLGMTGEVSFQAANTKSAANL
KVKELRSLIEVEKPLYGVEVFVGETAHFEIELSEPDVHGQWKLKGQPL
AASPDCEIIEDGKKHILILHNCQLGMTGEVSFQAANTKSAANLKVKEL
RSPARITLTYKEGAPITIMDNGNIDTELLVGTLTLGGYKTGTTSTSVN
FTDAAGDPMYLTFTSQDGNNHQFTTKVIGKDSRDFDISPKVNGENLVG
DDVVLATGSQDFFVRSIGSKGGKLAAGKYTDAVTVTVSTGSGNGADLT
ASTTATATLVERSLIEVEKPLYGVEVFVGETAHFEIELSEPDVHGQWK
LKGQPLAASPDCEIIEDGKKHILILHNCQLGMTGEVSFQAANTKSAAN
LKVKELRSLIEVEKPLYGVEVFVGETAHFEIELSEPDVHGQWKLKGQP
LAASPDCEIIEDGKKHILILHNCQLGMTGEVSFQAANTKSAANLKVKE
LCC

- **I91$_2$-Caf1A5I-I91$_2$**

MRGSHHHHHHGSLIEVEKPLYGVEVFVGETAHFEIELSEPDVHGQWKL
KGQPLAASPDCEIIEDGKKHILILHNCQLGMTGEVSFQAANTKSAANL
KVKELRSLIEVEKPLYGVEVFVGETAHFEIELSEPDVHGQWKLKGQPL
AASPDCEIIEDGKKHILILHNCQLGMTGEVSFQAANTKSAANLKVKEL
RSPARITLTYKEGAPITIMDNGNIDTELLVGTLTLGGYKTGTTSTSVN
FTDAAGDPMYLTFTSQDGNNHQFTTKVIGKDSRDFDISPKVNGENLVG
DDVVLATGSQDFFVRSIGSKGGKLAAGKYTDAVTVTVSTGSGNGADLT
ASTTATATLVERSLIEVEKPLYGVEVFVGETAHFEIELSEPDVHGQWK
LKGQPLAASPDCEIIEDGKKHILILHNCQLGMTGEVSFQAANTKSAAN
LKVKELRSLIEVEKPLYGVEVFVGETAHFEIELSEPDVHGQWKLKGQP
LAASPDCEIIEDGKKHILILHNCQLGMTGEVSFQAANTKSAANLKVKE
LCC

- **I91$_2$-Caf1T7L-I91$_2$**

MRGSHHHHHHGSLIEVEKPLYGVEVFVGETAHFEIELSEPDVHGQWKL
KGQPLAASPDCEIIEDGKKHILILHNCQLGMTGEVSFQAANTKSAANL
KVKELRSLIEVEKPLYGVEVFVGETAHFEIELSEPDVHGQWKLKGQPL
AASPDCEIIEDGKKHILILHNCQLGMTGEVSFQAANTKSAANLKVKEL
RSPARITLTYKEGAPITIMDNGNIDTELLVGTLTLGGYKTGTTSTSVN
FTDAAGDPMYLTFTSQDGNNHQFTTKVIGKDSRDFDISPKVNGENLVG
DDVVLATGSQDFFVRSIGSKGGKLAAGKYTDAVTVTVSTGSGNGADLT
IS**T**TATATLVERSLIEVEKPLYGVEVFVGETAHFEIELSEPDVHGQWK
LKGQPLAASPDCEIIEDGKKHILILHNCQLGMTGEVSFQAANTKSAAN
LKVKELRSLIEVEKPLYGVEVFVGETAHFEIELSEPDVHGQWKLKGQP
LAASPDCEIIEDGKKHILILHNCQLGMTGEVSFQAANTKSAANLKVKE
LCC

- **I91$_2$-EnHD-I91$_2$**

LIEVEKPLYGVEVFVGETAHFEIELSEPDVHGQWKLKGQPLAASPDCE
IIEDGKKHILILHNCQLGMTGEVSFQAANTKSAANLKVKELSSLIEVE
KPLYGVEVFVGETAHFEIELSEPDVHGQWKLKGQPLAASPDCEIIEDG
KKHILILHNCQLGMTGEVSFQAANTKSAANLKVKELRPRTAFSSEQLA
RLKREFNENRYLTERRRQQLSSELGLNEAQIKIWFQNKRAKISSLIEV
EKPLYGVEVFVGETAHFEIELSEPDVHGQWKLKGQPLAASPDCEIIED
GKKHILILHNCQLGMTGEVSFQAANTKSAANLKVKELSSLIEVEKPLY
GVEVFVGETAHFEIELSEPDVHGQWKLKGQPLAASPDCEIIEDGKKHI
LILHNCQLGMTGEVSFQAANTKSAANLKVKELSSCC

- **I91$_2$-FnI(2-5)-FnBR1-I91$_2$**

LIEVEKPLYGVEVFVGETAHFEIELSEPDVHGQWKLKGQPLTASPDCE
IIEDGKKHILILHNCQLGMTGEVSFQAANAKSAANLKVKELLIEVEKP
LYGVEVFVGETAHFEIELSEPDVHGQWKLKGQPLTASPDCEIIEDGKK
HILILHNCQLGMTGEVSFQAANAKSAANLKVKELRSRSAEETCFDKYT
GNTYRVGDTYERPKDSMIWDCTCIGAGRGRISCTIANRCHEGGQSYKI
GDTWRRPHETGGYMLECVCLGNGKGEWTCKPIAEKCFDHAAGTSYVVG
ETWEKPYQGWMMVDCTCLGEGSGRITCTSRNRCNDQDTRTSYRIGDTW
SKKDNRGNLLQCICTGNGRGEWKCERHTSGGGSGGGSnekngpiiqnn
kfeykedtiketltgqydknlvttveeeydsRSLIEVEKPLYGVEVFV
GETAHFEIELSEPDVHGQWKLKGQPLTASPDCEIIEDGKKHILILHNC
QLGMTGEVSFQAANAKSAANLKVKELLIEVEKPLYGVEVFVGETAHFE
IELSEPDVHGQWKLKGQPLTASPDCEIIEDGKKHILILHNCQLGMTGE
VSFQAANAKSAANLKVKELSSCC

List of abbreviations

AFM	Atomic force microscopy
AFS	Atomic force spectroscopy
AIDS	acquired immunodeficiency syndrome
AmpR	Ampicillin resistance gene
Caf1	capsular antigen fraction 1
ClfA	Clumping factor A
CmR	Chloramphenicol resistance gene
CWA	Cell wall anchored proteins
DTS	Distance to transition state
En-1	Engrailed-1
En-2	Engrailed-2
EnHD	Engrailed Homeodomain
FBS	Forbidden binding sites
FBRs	Fibronectin binding repeats
FC	Force clamp
FJC	Freely-jointed chain
FnBPA	Fibronectin binding protein A
FnBPB	Fibronectin binding protein B
FR	Force ramp
FRET	Föster resonance energy transfer
FX	Force extension
HIV-1	Human immunodeficiency virus-1
HTVS	High-throughput virtual screening
IPTG	Isopropyl-β-D-thiogalactoside
MCS	Multiple cloning site
MHC	Mayor histocompatibility complex
MRSA	Methicillin-resistant *Staphylococcus aureus*
MSCRAMM	Microbial surface recognizing adhesive matrix
MT	Magnetic tweezers
OT	Optical tweezers
PD	Photodetector
PZA	Piezoelectric actuator
SMFS	Single-molecule force spectroscopy
SUPROMER	Surface-protein mechanical regulators

T3SS	Type III secretion system
WLC	Worm-like chain
Yop	*Yersinia* outer membrane protein

Acknowledgment

Deseo comenzar expresando mi agradecimiento a aquellos organismos que han financiado mis estudios de doctorado. En segundo lugar, quiero agradecer a Txema Pitarke y a CIC nanoGUNE por haberme brindado la oportunidad de realizar mi preparación doctoral.

Darle las gracias a mi director Raúl Pérez Jiménez por haberme otorgado el privilegio de realizar mi tesis en un proyecto tan interesante, el cual me ha permitido aprender y crecer como investigador.

a mi codirector, David de Sancho, le debo un reconocimiento especial. por toda su ayuda en el desarrollo de la tesis, así como todo su apoyo en relación a la ilustración científica, tema que sabe que me apasiona y el cual me ha ayudado a desarrollar y crecer.

No puedo olvidar a Jörg, quien en el breve pero intenso tiempo que compartimos, sembró los cimientos más sólidos sobre los cuales he edificado mi crecimiento y aprendizaje a lo largo de mi formación.

Y ahora, mis más sinceros agradecimientos se dirigen a Leire, Borja, Ane y Alba, quienes han sido mis pilares inquebrantables. Sin su apoyo constante en los momentos de alegría y desafío, nada de lo que he logrado sería posible. Sois "mi piña", siempre ahí para brindarme vuestro apoyo emocional y científico. Siempre llevaré vuestros nombres grabados en mi corazón, allá donde la vida me lleve.

A mi familia, a mis padres y a mi hermana, les debo un reconocimiento eterno. Han sido los pilares que me han dado fuerzas para convertirme en la persona que soy hoy y en la que seré en el futuro. Os admiro y os quiero de forma ilimitada.

Y finalmente, quiero dirigirme a mi corazón, a ti, Tony. Mi gratitud hacia ti es inmensurable. Día tras día, has sido mi apoyo incondicional en este viaje. Tu ayuda, tu paciencia y tu presencia constante han sido mi roca en los momentos más turbulentos. Sigamos construyendo nuestro futuro juntos, apoyándonos mutuamente en cada paso del camino.

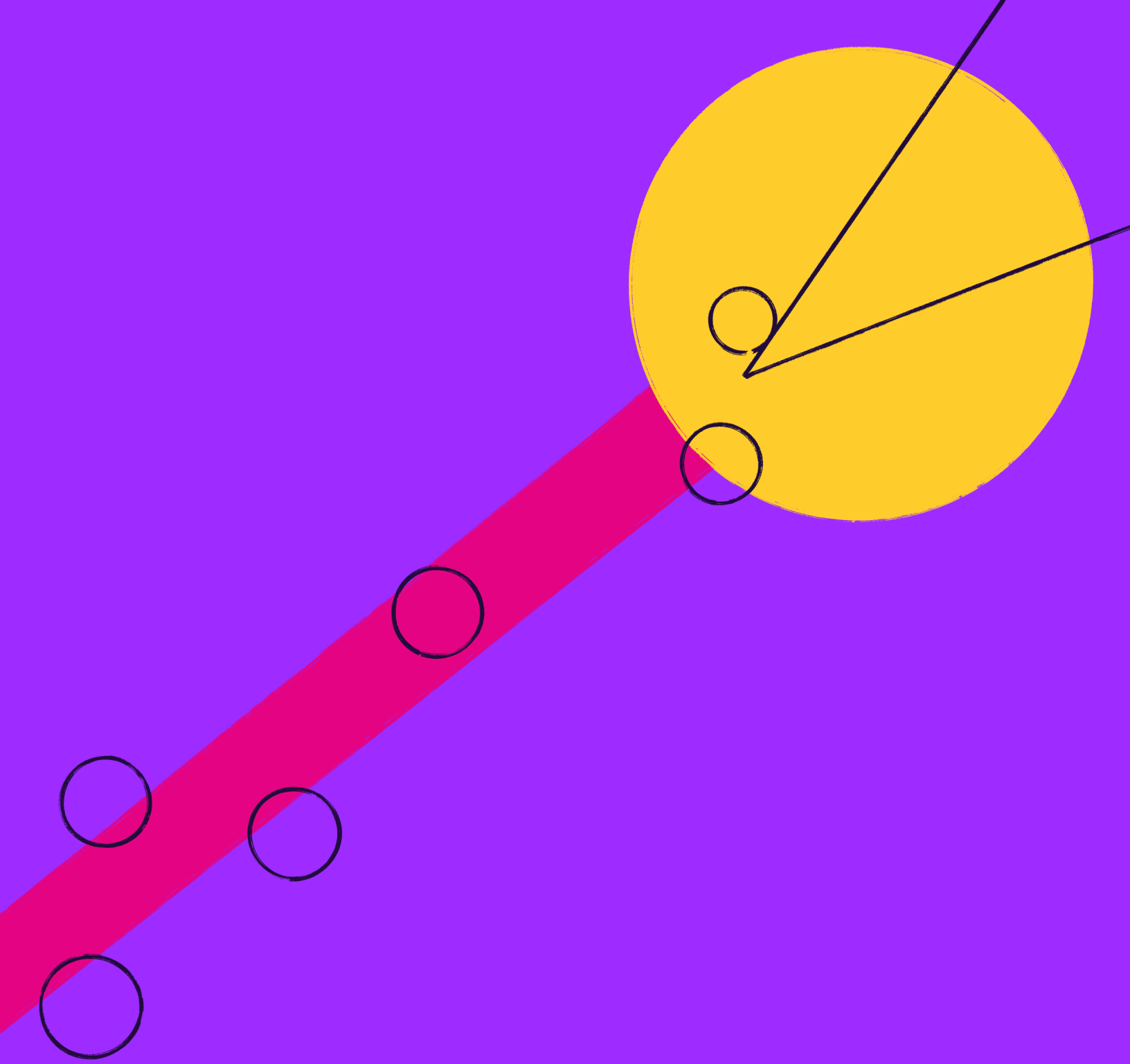

CIC nanoGUNE

nanoscience cooperative research center